UNIVERSITY OF CALIFORNIA
RIVERSIDE

Understanding the Bestowing of Enantioselectivity to Heterogeneous Catalysts via the Addition of Chiral Modifiers

A Dissertation submitted in partial satisfaction
of the requirements for the degree of

Doctor of Philosophy

in

Chemistry

by

Zihao Wang

June 2023

Dissertation Committee:
Dr. Francisco Zaera, Chairperson
Dr. Ludwig Bartels
Dr. Chia-En Angelina Chang

The Dissertation of Zihao Wang is approved:

_____

_____

_____

Committee Chairperson

University of California, Riverside

ACKNOWLEDGEMENTS

First and foremost, I wish to express my deepest gratitude to Professor Francisco Zaera for his firm support, invaluable instruction, and insightful feedback throughout my Ph.D. journey. I vividly recall our inaugural meeting, during which his recommendation to the chemistry department's admission committee at UCR facilitated my acceptance into his research group. Professor Zaera's profound knowledge in surface chemistry has left an indelible impression on me. His mentorship has been crucial in honing my research abilities and fostering my academic career. Moreover, his continuous encouragement to pursue my genuine interests and his respect for our ideas have been truly inspiring. His assistance in presenting my work at the 27th North American Catalysis Society Meeting was invaluable in expanding my perspectives and professional network. I consider myself exceptionally fortunate to have had him as my advisor, and the memories and lessons gained from his mentorship will forever be cherished.

Further, my deep appreciation extends to Professor Ludwig Bartels and Professor Chia-En Angelina Chang for serving as my committee members during my second-year research evaluation, qualifying exam, and final defense. Their invaluable feedback and suggestions have substantially improved my work.

I would also like to acknowledge the expert support provided by several individuals during my research. At the UCR Analytical Chemistry Instrumentation Facility, Dr. Jie Zhou's assistance with GC-MS tests and data analysis was indispensable.

I am grateful to Dr. Lingchao Zhu for training me in the use of transmission IR and NMR instruments, and to David Lyons from the Environmental Science Research Laboratory for his assistance with IPC-OES tests and data processing. Additionally, I want to thank our collaborators, Professor Noboru Takeuchi, Héctor Noé Fernández-Escamilla, and Jonathan Guerrero-Sánchez from the Centro de Nanociencias y Nanotecnología, Universidad Nacional Autónoma de México. Their quantum mechanics calculations provided valuable insights, facilitating our understanding of the isotope exchange pathway.

I must express my gratitude to Kristen Herbert and Gary Qin from the Graduate Writing Center at UCR for their invaluable assistance in polishing my dissertation.

Furthermore, I am thankful for the supportive and collaborative environment created by my lab colleagues. Special recognition goes to Dr. Ilkeun Lee, whose vast knowledge and lab experience have been invaluable. His support in various aspects of lab management has facilitated a well-structured and safe working environment. In addition, I also appreciate the contributions of our postdoctoral members and all lab members, Yufei Ni, Tongxin Han, Mohammed Alam, Ameer Siddique, Yihan Zhou, and Hyeonkyeong (Elly) Lee, for their collective support. I am especially grateful to Yufei Ni for his exceptional guidance during the early stages of my project.

Lastly, I wish to express my heartfelt thanks to my friends for their invaluable support and encouragement throughout my PhD journey. Special mention goes to Fei Ji, Zongbo Li, and Siwen (Ellen) Wang for their unwavering companionship and invaluable counsel. I am also grateful to my friends, Ge Sun, Zuyang Ye, Lei Yang, Yuan Qin, Junyi

Chen, and others for their kind words and gestures, which have kept me motivated even during the most challenging times. I am truly honored to have you as part of this journey.

COPYRIGHT ACKNOWLEDGEMENT

Part of the work in Chapter 3 has been published in ACS catalysis (DOI: 10.1021/acscatal.2c01627). The theoretical calculations in the published paper were performed by our collaborators: Professor Noboru Takeuchi, Héctor Noé Fernández-Escamilla, and Jonathan Guerrero-Sánchez from Centro de Nanociencias y Nanotecnología, Universidad Nacional Autónoma de México.

The Figure 2.1, Figure 2.4, Figure 3.1, Figure 7.1 and Table 3.1 have been adapted or reprinted from the following publications with permission from the copyright owner via RightsLink as listed below.

Figure 2.1: Zaera, F., Probing liquid/solid interfaces at the molecular level. *Chemical Reviews*, **2012** 112(5), pp.2920-2986.

Figure 2.4: Sing, K.S., Reporting physisorption data for gas/solid systems with special reference to the determination of surface area and porosity (Recommendations 1984). *Pure and Applied Chemistry*, **1985** 57(4), pp.603-619.

Figure 3.1 Zaera, F.. Designing sites in heterogeneous catalysis: are we reaching selectivities competitive with those of homogeneous catalysts?. *Chemical Reviews*, **2022** 122(9), pp.8594-8757.

Figure 7.1 Tamura, M., Hayashigami, N., Nakayama, A., Nakagawa, Y. and Tomishige, K., Heterogeneous enantioselective hydrogenation of ketones by 2-Amino-2′-hydroxy-1, 1′-binaphthyl-Modified CeO_2-supported Ir nanoclusters. *ACS Catalysis*, **2021** *12*(2), pp.868-876

Table 3.1 Ni, Y., Gordon, A.D., Tanicala, F. and Zaera, F., Correlation between chiral modifier adsorption and enantioselectivity in hydrogenation catalysis. *Angewandte Chemie*, **2017** 129(27), pp.8071-8074.

DEDICATION

I dedicate this dissertation to my family, whose love, support, and encouragement have been a bedrock throughout my academic journey. Their role in this accomplishment is indispensable and I am deeply grateful.

To my parents

Zhike Wang and **Rong Yan**

I owe a debt of gratitude for the profound love and sacrifices that have facilitated my pursuit of my dreams. You are the individuals who have cared for me the most and I remain eternally grateful for your unwavering support.

To my sister

Xun Wang

Your role as a beacon of inspiration, your unwavering support in challenging times, and your consistent motivation have been invaluable to my journey. Thank you for being there, cheering me on, and providing a guiding light when necessary.

ABSTRACT OF THE DISSERTATION

Understanding the Bestowing of Enantioselectivity to Heterogeneous Catalysts via the Addition of Chiral Modifiers

by

Zihao Wang

Doctor of Philosophy, Graduate Program in Chemistry
University of California, Riverside, June 2023
Dr. Francisco Zaera, Chairperson

The synthesis of enantiopure compounds in pharmaceuticals is a critical area given the various enantiomers of many drugs behave differently in the human body. One promising way to introduce enantioselectivity into heterogeneous catalysis is to add a small quantity of chiral modifiers in reaction mixtures. However, a gap in knowledge persists concerning the molecular-level understanding of the interaction between these chiral modifiers and reactants on solid catalyst surfaces. This research utilizes an *in-situ* infrared (IR) spectroscopy to monitor the adsorption behavior of chiral modifiers on solid surfaces from liquid solutions, drawing the correlations between adsorption mode and enantioselectivity in asymmetric hydrogenations.

Adsorption behavior of 1-(1-naphthyl) ethylamine (1-NEA) from solution on Pt surfaces was studied via kinetic catalytic measurements, IR spectroscopy, and theoretical calculations. The research revealed that 1-NEA can undergo H−D exchange with D_2 in solutions, mediated by Pt-supported catalysts. This reaction was general, observed with r- and s-1-NEA, r- and s-2-NEA, and cinchonine, on both Pt/SiO_2 and Pt/Al_2O_3 catalysts.

NEA adsorption and protonation through the amine N atom provide a mechanism explaining how the NEA molecule bestows enantioselectivity to Pt hydrogenation catalysts.

Adsorption studies were also conducted with different types of chiral modifiers. It was found that both the naphthyl ring and amine group are crucial for adsorption on Pt surfaces. No adsorption evidence was observed with hydroxyl group functionalized molecules and molecules with a benzene ring.

The kinetic measurements were made on the hydrogenation of ethyl pyruvate, catalyzed by chiral molecules modified Pt-supported catalysts, showed that chiral NEA molecules contributed to enantioselectivity, albeit not as effectively as cinchona alkaloids. Attempts to enhance enantioselectivity through the modification of Pt-supported catalysts with silylation agents yielded no significant increase.

This research provides a comprehensive study of different chiral modifiers' adsorption behaviors on Pt-supported catalysts at solid/liquid interfaces and their catalytic performance in enantioselectivity on ethyl pyruvate hydrogenations. This not only aids in understanding the adsorption nature of chiral modifiers on Pt surfaces but also assists in the design of a more efficient heterogeneous enantioselective catalysis.

Table of Contents

List of Figures

List of Tables

Chapter 1

Introduction and Overview

1.1 What is Chirality?

In chemistry, a molecule is chiral if it cannot be superimposed onto its mirror image by transition and rotation[1-2]. Chiral molecules are most commonly seen with organic compounds as they usually have one or more carbon atoms with four different substituents. For each of these carbon centers, there are two different possible arrangements within the tetrahedral geometry, which are so-called enantiomers. As shown in the Figure 1.1, for example, the two enantiomers of naproxen, named as (*S*)-(+)-naproxen and (*R*)-(−)-naproxen respectively, are mirror images of each other, which are non-superposable.

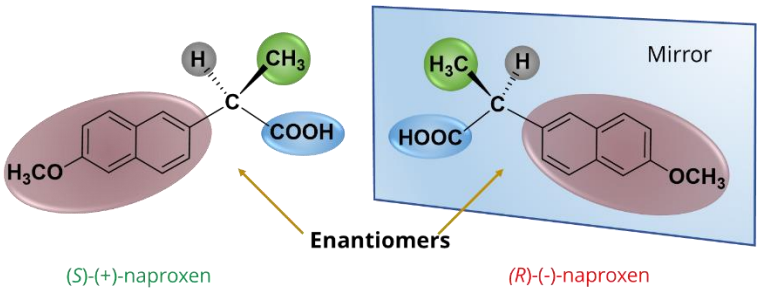

Figure 1.1 The molecular chirality illustrated through the two mirror-image enantiomers of naproxen.

The two enantiomers usually have identical chemical and physical properties, except that they often have opposite optical behaviors, which was originally observed by

Louis Pasteur in 1848[3]. Pasteur found that tartrates derived from wine fermentation are optically active, meaning the tartrates can rotate the plane of polarized light; in contrast, it was found the paratartrates are optically inactive, which behave differently. The reason why paratartrates are not rotating the plane of polarized light is that it contains the same amount of right-handed and left-handed crystals, which is called a racemic mixture. In other words, the racemic mixtures are optically inactive. Thus, Pasteur discovered the existence of molecular asymmetry, the foundation of stereochemistry.

1.2 Why Should We Care About Enantiomers?

In pharmaceuticals, many drug molecules possess at least one chiral center, producing different enantiomers. It has been proven that the enantiomers of chiral pharmaceuticals can behave very differently in the human body[4]. For example, (*S*)-naproxen can treat arthritis pain, while (*R*)-naproxen may cause liver poisoning[5]. Therefore, it is crucial to consider the presence of enantiomers in the discovery and development of drugs, as well as in other areas of chemistry where the biological activities, pharmacological effects, and toxicity profiles are related. It has been reported[6] that half or more of the top selling drugs in the market, such as Lipitor, Plavix, Nexium, Singulair, and Seretide, are enantiopure.

1.3 Ways to Manufacture Enantiopure Compounds

There are several ways to manufacture enantiopure compounds, including the separation of racemic mixtures via the chiral chromatographic columns, and the combination of these mixtures with other chiral compounds, which usually involve the

use of chiral starting materials, chiral reagents, or chiral catalysts to control the stereochemistry of the final product. Some typical examples are discussed in the following section.

1.3.1 Chromatographic Separation

One of the most common ways for manufacturing enantiopure compounds is through enantiomeric resolution, which involves the separations of racemic mixtures into their individual enantiomers through different technologies like crystallization[7], chiral capillary electrophoresis[8], or, the most common, chromatography[9-10]. Enantioselective chromatography uses chiral stationary phase to separate enantiomers, because one of the enantiomers binds more strongly with stationary phase compared to the other, leading to separation. While chiral resolution remains an important tool for the separation and analysis of enantiomers, there are still some shortcomings[11], such as the limited availability of chiral stationary phases, time consuming, high cost, difficulties in scale-up.

1.3.2 Enantioselective Biocatalysis

Biocatalysis has emerged as a promising method for manufacturing enantiopure compounds.[12] The use of enzymes for synthesizing enantiopure compounds has been a well-established manufacturing process in the pharmaceutical industry[13]. It has been shown that enzymes can be highly selective in catalyzing reactions, allowing for the production of enantiopure compounds with high efficiency and selectivity. The racemic separation of amino acids via the acylase method is one of the successful applications of

using isolated enzymes[14]. Additionally, biocatalytic processes are often environmentally friendly and can be conducted under mild conditions, which makes it a more sustainable option for industrial production. However, the use of enzymes and other biocatalysts can be limited by the availability of substrate scope and potential instability, as well as long-time and high-cost of biocatalytic processes[15].

1.3.3 Homogeneous Enantioselective Catalysis

Over the years, the most versatile and studied enantioselective catalysis is homogeneous metal complexes[16-17]. Many efforts have been made with the chiral complex in asymmetric reactions. The 2001 Nobel Prize in chemistry was awarded to William S. Knowles, Ryoji Noyori, and K. Barry Sharpless for their outstanding research in the field of asymmetric synthesis[18]. A variety of transition metals, such as Rh, Ir, Pd, are widely used in the asymmetric hydrogenations of unsaturated ketones and imines[19-20]. Even though the homogenous catalysis displayed higher activity and enantioselectivity compared to the heterogeneous catalysis, there are still some limitations to consider. The most difficult problems in catalysis are separation and reuse of chiral catalysts since the chiral complexes are typically dissolved in the reaction mixture.

1.3.4 Heterogeneous Enantioselective Catalysis

One common way to bestow chirality on heterogeneous catalysts is to modify the achiral solid surface with chiral regents. For example, self-assembled monolayers (SAMs) have been commonly used for modification on metal surfaces[21-22]. In addition,

the immobilizations of homogeneous catalysts onto the heterogeneous catalysts have been extensively developed, and this is aimed to overcome problems of recycling and separation while taking advantages of high enantioselectivity with homogeneous catalysts. Four typical strategies including adsorption[23-24], encapsulation[25-26], covalent tethering[27-28] and electrostatic interaction[29] have been developed, however, only a limited number of developments have shown the stable immobilized catalysts that are capable of re-use.

The most promising solution so far is adsorption of chiral modifiers onto solid surfaces from liquid solutions. In our group, many efforts have been developed to explore the chiral adsorption and reactivity at the liquid/solid interfaces[30-34]. The premise is that chiral modifiers may co-adsorb with reactants on the surface of the catalysts and then modify the local environments to favor a specific reaction pathway. However, only two families of reactions have been proven successful in doing this: one is the hydrogenation of β-keto esters on nickel catalysts modified with tartaric acid[35-36], and the other is the hydrogenation of α-keto esters modified with cinchona alkaloids catalyzed by Pt-based catalysts[37-39].

Regrettably, despite their potential usefulness, both families have shown limited practical applicability. The complexity of the liquid/solid systems has restricted the generalization to other reactants or catalysts. Moreover, the systems are highly sensitive to variations in reactants, catalysts, modifiers, solvents, and/or reaction conditions, and predicting these effects remains challenging. To overcome these limitations and further advance this field, a molecular-level understanding of the mechanism occurring at the

liquid/solid interfaces is required. Such an understanding would enable the design of new chiral catalytic processes from the first principles.

1.4 Probing Liquid/Solid Interfaces at the Molecular Level

Over the years, a good number of spectroscopic techniques have been developed or adapted for probing the liquid/solid interfaces at the molecular level[31] .

The most promising solution is to use analytical techniques based on electromagnetic radiation, for example, infrared, visible, UV, and X-ray radiation. Among them, infrared (IR) absorption spectroscopy techniques are the most commonly used and could provide the detailed vibrational modes of molecules at the liquid/solid interfaces. One negative aspect of this solution is that IR is not intrinsically a surface-sensitive technique, there are still challenges in distinguishing the adsorbates occurring at the interface from the molecules in bulk solutions. However, several approaches, such as the use of polarized light and/or attenuated reflection, are used to address these problems. In particular, the *in-situ* attenuated total reflectance infrared spectroscopy (*in-situ* ATR-IR)[40-41] and *in-situ* reflection absorption infrared spectroscopy (*in-situ* RAIRS)[42] in our laboratory have been successfully used for detecting the adsorbates in solution on Pt supported powder catalysts, and on flat Pt surfaces. The former was the most commonly used technique in this study, though more details will be provided in Chapter 2.

Vibrational information can also be collected by visible and UV-vis via the Raman Spectroscopy, however, more intense light is required to obtain significant sample signals, leading to possible damage to the samples. Other UV-vis and acoustic

techniques, such as UV-vis absorption spectroscopy[43], surface plasmon resonance[44], and quartz crystal microbalance (QCM), have been developed to characterize the reactions at liquid/solid interfaces. The applications are usually in a specific area that is not related to our research. For example, the QCM was mainly used in biochemical systems involving proteins, antibodies, etc[45-46].

Additionally, the use of intense and tunable X-ray based techniques for probing chemical and biological systems, such as X-ray absorption (XAS) and X-ray emission (XES) spectroscopies[47], have gained a lot of attention recently due to the advantage of penetrating deep into liquid, and even solid phases, making it more feasible to extract both electronic and structural data. However, the use of synchrotron radiation is expensive and hard to implement. Moreover, not many studies with the use of this technique especially those involving liquid/solid interfaces were reported.

Some microscopies are also applicable to probe liquid/solid interfaces, as they provide spatial information on heterogeneous interfaces. For example, scanning tunneling microscopy (STM) is a useful technique to obtain images of liquid/solid interfaces with atomic-scale resolution. Most published work focused on supramolecular self-assembled monolayers[48-49]. The STM sample needs to be conductive, which could be difficult for some liquid/solid interfaces. Additionally, STM images can provide information on the topography and electronic structure of the sample. The data of chemical composition or bonding at the interfaces will not be collected.

1.5 Research Directions

The two main directions of this research are proposed as illustrated in Figure 1.2. As discussed above, the main challenge in modification with chiral modifiers is the complexity of catalytic systems occurring at liquid/solid interfaces in realistic environments. Unlike well-controlled environments, realistic environments where solvents and supported catalysts are present are quite sensitive to various parameters such as the catalysts, support materials, solvents, and concentrations that are selected. Therefore, one direction would be to explore the adsorption behavior of different chiral modifiers on Pt supported catalysts at liquid/solid interfaces. The other direction would be to examine the catalytic performance of chiral modifiers in asymmetric hydrogenations. The primary goal is to find the correlation between adsorption mode and catalytic behavior by combining adsorption and kinetic studies. The details of each direction of this study are described below.

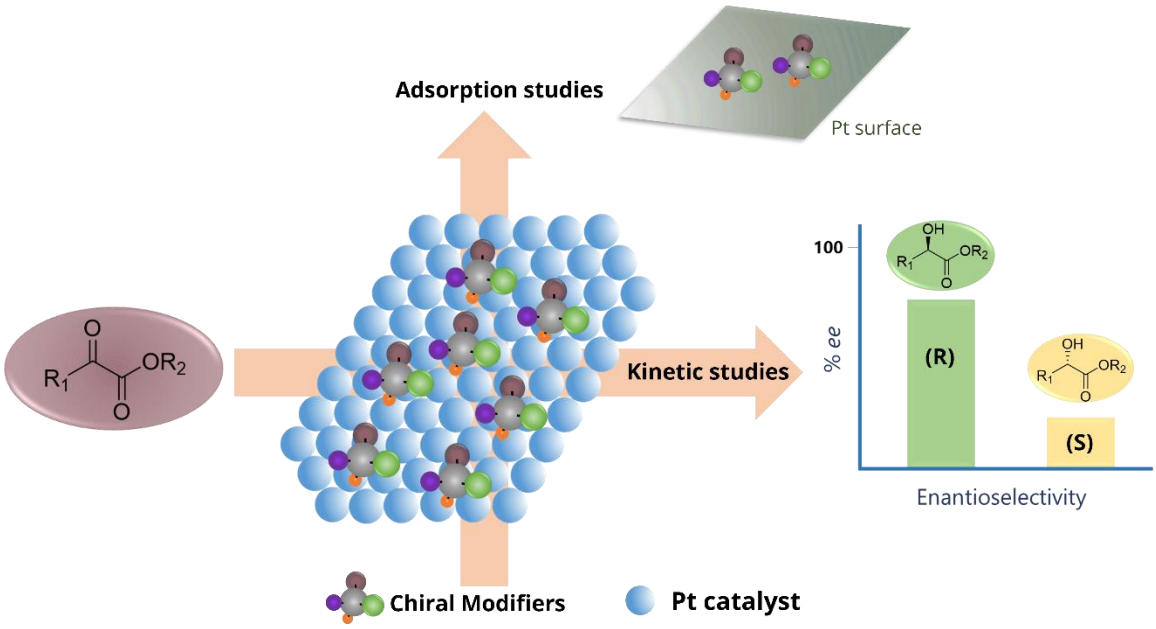

Figure 1.2 The illustration of two directions of this research.

Adsorption Behavior on Pt Surfaces at Liquid/Solid Interfaces

In our group's aforementioned study[40], we found that adsorption mode of 1-NEA molecules would bind to Pt surfaces through the amine group and not through aromatic ring as commonly believed[50-52]. In addition, the NEA adsorption might require a breaking of the N−H bond, which, however, was proposed but not proven. In this regard, the characterizations of the N−H bond dissociation are designed through different techniques. The *in-situ* ATR-IR tests with 1-NEA solutions will be performed in the presence of Pt catalysts while bubbling D_2, and this is aimed to detect the N−D vibrational mode. The ^{1}H-NMR and GC-MS will also be used to characterize the H−D exchange process. The theoretical calculations from our collaborators are expected to help explain the experimentally observed results.

To expand the chiral modifiers to a larger family, different types of molecules are proposed for study as shown in Figure 1.3. The oxygen-based modifiers, such as 1-(-naphthyl) ethanol (1-NE), will be explored and compared to the NEA molecules. Another comparison will be made between the biaryl compounds, such as 1,1'-Bi(2-naphthol) (BINOL) and 1,1'-Bi(2-naphthylamine). In this regard, the purpose is to explore the role of the hydroxyl group and the amine group on adsorption behavior.

Another aim is to explore the adsorption behavior of chiral amino acids, such as 3-(1-naphthyl)-L-alanine (1-NLA), and terpinen-4-ol. It was found that molecules, such as terpinen-4-ol, could direct enantioselectivity, which is different from what the traditional cinchona alkaloids and NEA molecules do to add enantioselectivity. In studying terpinen-4-ol, our aim is to explore a different way in enantioselective heterogeneous catalysis.

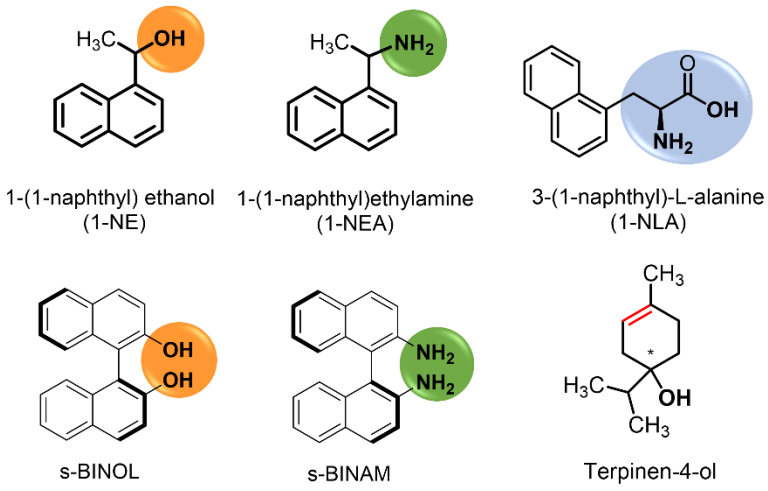

Figure 1.3 Proposed molecules for exploring the adsorption behavior.

The effect of the functionality position, the solvent, and the catalysts supports will be investigated as well. The purpose is to find the correlation between the adsorption behavior and these parameters. Additionally, we expect to determine the minimum requirement of the functionalities for adsorption on Pt surfaces.

Catalytic Performance on Pt Supported Catalysts

Kinetic measurements will be performed with the hydrogenation of α-keto esters catalyzed by Pt/SiO_2 or Pt/Al_2O_3 catalysts using the chiral modifiers investigated, as illustrated in Figure 1.4.

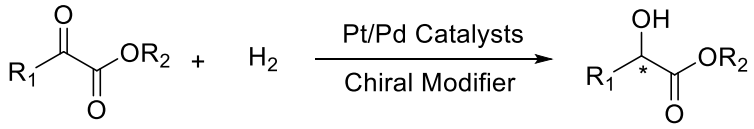

Figure 1.4 Illustration of hydrogenation of α-ketone esters.

Modifier concentration, solvents and types of Pt or Pd catalysts will be explored regarding the dependence of activity and enantioselectivity, given that these parameters have been proven to be critical for the optimization of enantioselectivity. We propose that this effect will be directly identifiable from the IR spectroscopic results.

Lastly, the modification of Pt catalysts with different silylation agents is designed to improve enantioselectivity. The silylated catalysts are expected to degrade the conversion rate but promote enantioselectivity.

Chapter 2

Experimental Techniques and Characterizations

2.1 Infrared Spectroscopy Techniques for Adsorption Studies

2.1.1 *In-Situ* Attenuated Total Reflection Infrared Spectroscopy (*In-Situ* ATR-IR)

The adsorption behavior of chiral modifiers on Pt/SiO_2 or Pt/Al_2O_3 catalysts in the presence of solvents were measured by *in-situ* attenuated total reflection infrared spectroscopy (*In-situ* ATR-IR), as illustrated in Figure 2.1.

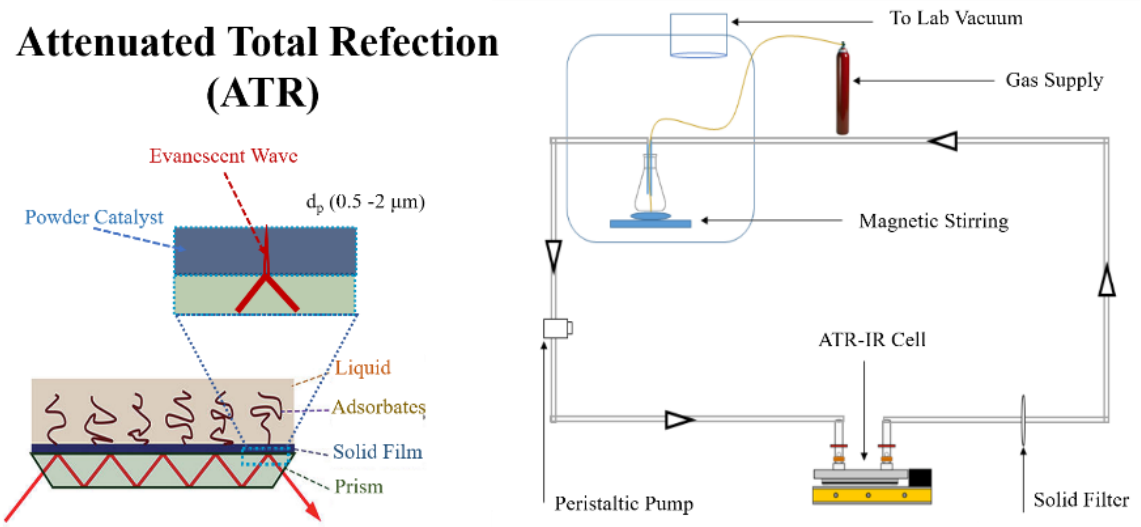

Figure 2.1 Schematic illustration of ATR cell (left) and the setup (right). The left figure is adapted with permission from reference 31, Copyright 2012 American Chemical Society.

The commercial multiple-reflection ATR accessory was purchased from Pike Technologies and was equipped with a Ge crystal (45º, 80×10×4 mm). The powder catalysts, Pt/SiO_2 or Pt/Al_2O_3, in the form of a thin film were evenly dispersed on the surface of the prism. The IR beam impinged on the crystal at a certain angle upon which the total internal reflection of light would occur. The angle was determined by the difference in refractive index between the crystal and the catalysts above it. Although the light was totally reflected, the generated evanescent wave tended to penetrate into the other side of the interface. The depth of penetration, usually between 0.5 and 2 μm, depended on the wavelength, the angle of incidence, and the relevant indices of refraction. The absorption of light from the evanescence wave by the chemical system can be detected and then collected as it exited the crystal.

Typically, 5 mg of powder Pt catalysts were evenly dispersed on the surface of the ATR-IR cell prism, then the cell was purged with the pure solvent (CCl_4, for example). The catalysts were preconditioned by bubbling either H_2 (for typical adsorption tests) or D_2 (for H-D exchange experiments) gas for 60 min, after which a background spectrum of the pure solvent was collected. Then the ATR-IR cell was exposed to a solution of chiral modifier (1 mM r-1-NEA/CCl_4, for example), the spectra were collected every 30 minutes until the intensity of the peaks did not change anymore. At the end, the cell was flushed with pure solvent again for about 30 minutes, and additional spectra were collected to see if the sample peaks could decrease or disappear. All of the spectra were obtained by adding 256 scans taken with 4 cm^{-1} resolution and were ratioed against the pure solvent reference spectrum collected at the beginning of the experiment.

2.1.2 Transmission Infrared (IR)

The transmission infrared (IR) spectra of pure solid or liquid chiral molecules were acquired using the Nicolet iS50 FTIR spectrometer. This spectrometer was equipped with a built-in diamond attenuated total reflectance (ATR) module and offered both transmission and ATR modes. For the measurements, the solid or liquid samples were placed directly on the diamond crystal, allowing for easy collection of spectra. The spectra range spanned from 4000 to 400 cm^{-1}, with a resolution of 0.09 cm^{-1} and a scan time of 256 units.

2.2 Synthesis and Characterizations of Pt Catalysts

2.2.1 Synthesis of Pt Supported Catalysts

The experimental procedures for synthesizing 1 wt% Pt/SiO_2 and 1 wt% Pt/Al_2O_3 are described below. The synthesis process utilized the simple wet-impregnation method. The supports used were commercial silica gel and commercial γ-Al_2O_3, and their basic information of them is provided in Table 2.1.

Table 2.1 Basic information of the commercial silica gel and gamma Al_2O_3

Name	**Silica gel**	**γ-Al_2O_3**
Grade	high-purity grade	99.97 % purity
Particle size	200-400 mesh, 40-75 μm	3 Micron APS powder
Pore size	0.75 cm^3/g pore volume, 60 Å	N/A
Surface area	500 m^2/g	80-120 m^2/g

Synthesis of 1 wt% Pt/SiO_2:

1. The first step involved determining the water saturated adsorption capacity of commercial SiO_2. Approximately 1.0 g of SiO_2 was measured into a beaker, and deionized water was added drop by drop with continuous stirring until saturation of SiO_2 was achieved. The quantity of water added corresponded to the amount of solution required for preparation.
2. The Pt solution was prepared by dissolving the necessary quantity of $H_2PtCl_6 \cdot 6H_2O$ in deionized water.
3. The solution was gradually added drop by drop to a sample of 0.5 g SiO_2 while stirring.
4. The resulting mixture was stored overnight at room temperature and subsequently dried in an oven at approximately 80 °C for 12.0 hours.
5. Prior to catalyst utilization, the sample was subjected to calcination with H_2 gas at 350 °C for 3.0 hours.

Synthesis of 1 wt% Pt/Al_2O_3:

The experimental procedures for synthesizing 1 wt% Pt/Al_2O_3 catalysts were similar to those used for synthesizing 1 wt% Pt/SiO_2. In this case, commercial γ-Al_2O_3 was employed as the support.

2.2.2 Transmission Electron Microscopy (TEM)

Transmission electron microscopy (TEM) is a highly valuable tool for investigating catalysts at the nanoscale, providing detailed information regarding their morphology, crystal structure, and elemental composition. This technique plays a critical role in understanding the catalytic properties of these materials.

TEM samples were typically prepared by dispersing approximately 2 mg of Pt catalysts in approximately 5 mL ethanol or another volatile solvent within a vial. The resulting mixture was sonicated until a uniform slurry was formed. Subsequently, several drops of mixture were transferred onto a TEM copper grid (Formvar/Carbon on 400 Mesh Copper). The sample was considered ready for analysis once it had completely dried.

The characterization of both homemade and commercial Pt catalysts was performed using a FEI Titan Themis 300 scanning transmission electron microscope. This instrument was equipped with Schottky X-FEG, HT 60 to 300 kV constant power lenses, offering a resolution of 2.0 Å point with 5.4 mm gap.

Figure 2.2 and Figure 2.3 present the TEM images of both commercial and homemade Pt supported catalysts. The Pt nanoparticles were uniformly dispersed on the SiO_2 and Al_2O_3 supports. Furthermore, the average sizes of Pt nanoparticles were determined and provided. As illustrated in Figure 2.2, the size of Pt nanoparticles in the homemade Pt/SiO_2 was approximately 2.0 nm, slightly smaller than the commercial Pt/SiO_2 catalysts (~2.6 nm). A similar trend was observed in the case of the Pt/Al_2O_3 catalysts. As indicated in Figure 2.3, the size of Pt nanoparticles in the commercial Pt/Al_2O_3 was approximately 2.6 nm, while in the homemade Pt/Al_2O_3 catalysts, it was approximately 2.2 nm.

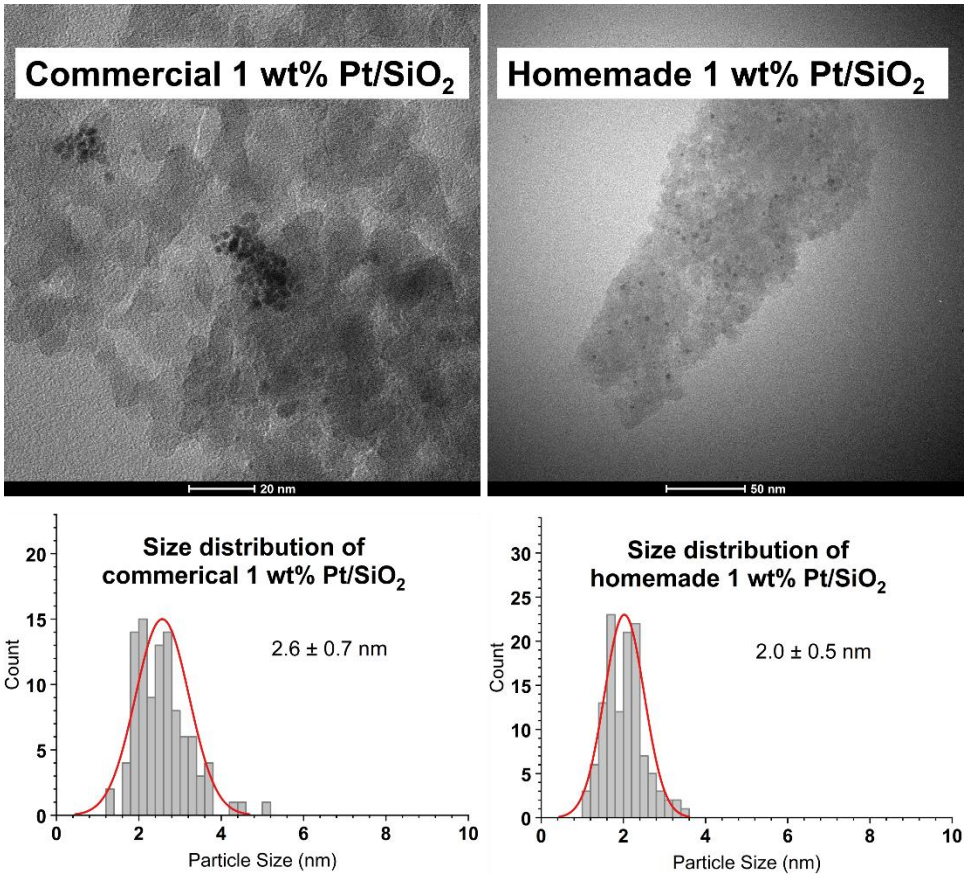

Figure 2.2 TEM images and size distribution of commercial and homemade 1 wt% Pt/SiO_2 catalysts.

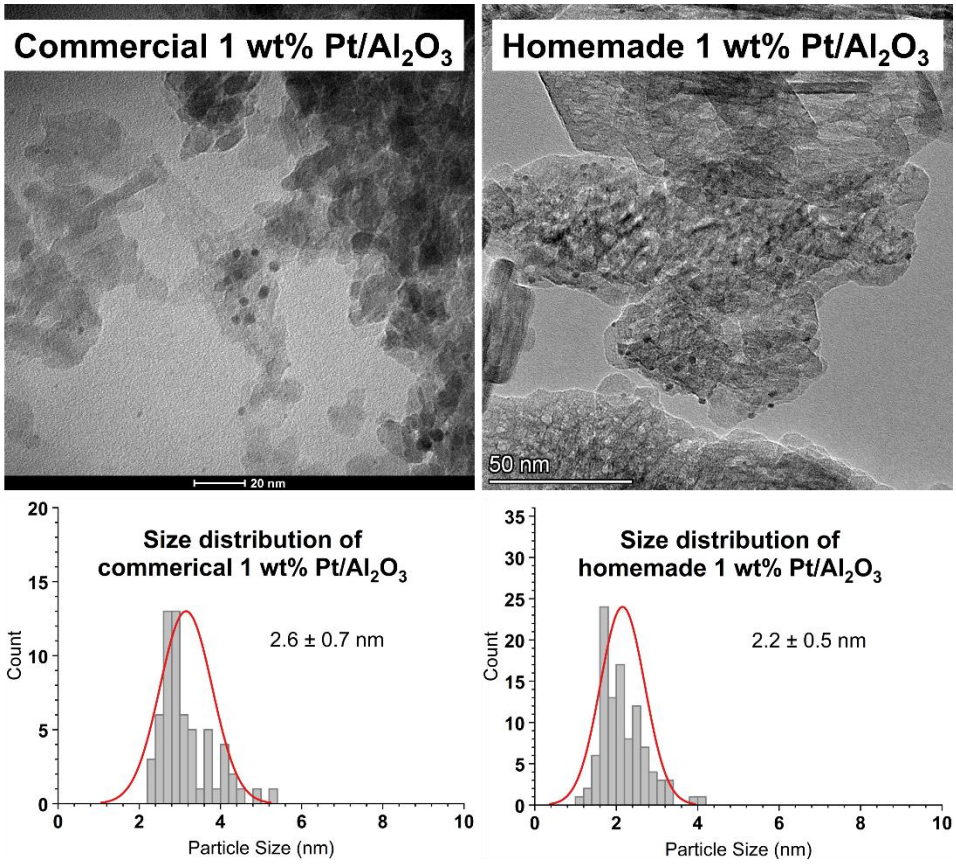

Figure 2.3 TEM images and size distribution of commercial and homemade 1 wt% Pt/Al_2O_3 catalysts.

2.2.3 Specific Surface Properties Characterization (BET)

The specific surface properties of Pt catalysts, including surface area, pore size and pore volume, were determined using the NOVA 2000e series surface area analyzer manufactured by Quantachrome Instruments in our laboratory.

The Brunauer-Emmett-Teller (BET) theory[53], developed in 1938 by Stephen Brunauer, Paul Emmett, and Edward Teller, is a widely used model in surface chemistry and materials science. It describeS the physical adsorption of gas molecules onto the surface of a solid material.

To characterize the specific surface properties of the Pt supported catalyst, approximately 50 mg sample was weighed and transferred to a 9 mm stem sample cell. The sample was then degassed under vacuum at 160 °C for at least 6 hours to remove any adsorbed gases or moisture. After cooling to room temperature, the analysis was initiated, and the results are presented in Table 2.2.

Table 2.2 BET and ICP-OES results of homemade and commercial Pt catalysts and supports.

Sample	**Surface area (m^2/g)**	**Pore size (nm)**	**Pore volume (cc/g)**	**Pt content by ICP tests**
Silica gel	500	6.0	0.75	N/A
Homemade 1 wt% Pt/SiO_2	419.403	5.982	0.694	0.99 %
Commercial 1 wt% Pt/SiO_2	286.304	13.109	1.195	0.93 %
γ-Al_2O_3*	80-120	N/A	N/A	N/A
Homemade 1 wt% Pt/Al_2O_3	80.598	1.731	0.492	1.10 %
Commercial 1 wt% Pt/Al_2O_3	161.788	10.125	0.529	0.81 %

Figure 2.5 shows the BET properties of homemade and commercial Pt/SiO_2 catalysts. The surface area of homemade Pt/SiO_2 was determined to be 419 m^2/g, while the surface area of commercial Pt/SiO_2 was only around 286 m^2/g. Both values were lower than the theoretical surface area of pure silica gel (500 m^2/g). Furthermore, the two Pt catalysts exhibited different types of hysteresis loops, as indicated in Figure 2.5.

Figure 2.4 illustrates six types of physisorption isotherms and four types of hysteresis loops[54]. The observed hysteresis phenomenon is typically attributed to the

combined effects of thermodynamics and network structures. Based on morphology and connectivity, four distinct pore geometries have been identified. The first type (H1) consists of agglomerates or uniformly arranged spherical particles with cylindrical pore geometry, indicating high pore size uniformity and easy connectivity. The second type (H2) is characterized by narrow-mouthed pores resembling ink bottles with relatively uniform channel-like pores. The third type (H3) comprises aggregates of platelike particles that form slit-like pores. Finally, the fourth type (H4) features narrow, slit-like pores, particles with irregularly shaped internal voids and broad size distribution, and hollow spheres made up of ordered mesoporous silica walls.

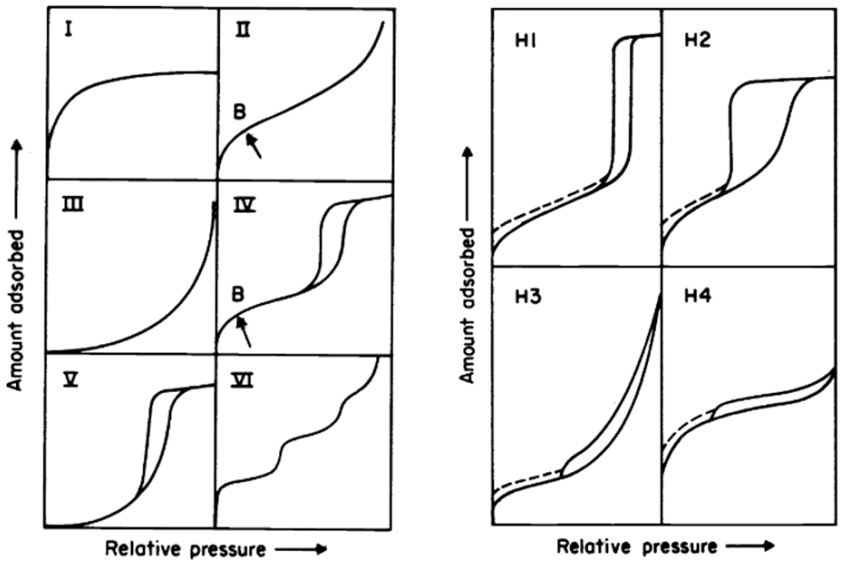

Figure 2.4 Types of physisorption isotherms and hysteresis loops. Adapted with permission from reference 54, Copyright 1985 JUPAC.

As shown in Figure 2.5, the commercial Pt/SiO_2 catalyst displayed the H1 loop of adsorption and desorption isotherm, while the homemade Pt/SiO_2 catalyst exhibited the H2 loop. As discussed earlier, the differences in hysteresis loops account for the significant variations in specific surface areas.

For both commercial and homemade Pt/Al_2O_3 catalysts, noticeable differences in surface area and hysteresis loops were observed. The pure commercial support of γ-Al_2O_3 had a surface area ranging from 80 to 120 m^2/g, similar to the homemade Pt/Al_2O_3 catalyst but considerably lower than the commercial Pt/Al_2O_3.Figure 2.6 shows that the homemade Pt/Al_2O_3 catalyst displayed an H3 type loop, indicating the presence of aggregates of platelike particles forming slit-like pores. This explains the relatively low surface area.

The surface properties of both homemade and commercial Pt supported catalysts were provided for further discussions regarding catalytic performance. In summary, when comparing the homemade and commercial Pt supported catalysts, the commercial Pt/SiO_2 catalysts exhibited larger pores, whereas the commercial Pt/Al_2O_3 catalysts showed a better pore distribution, increased surface area, and higher pore volume.

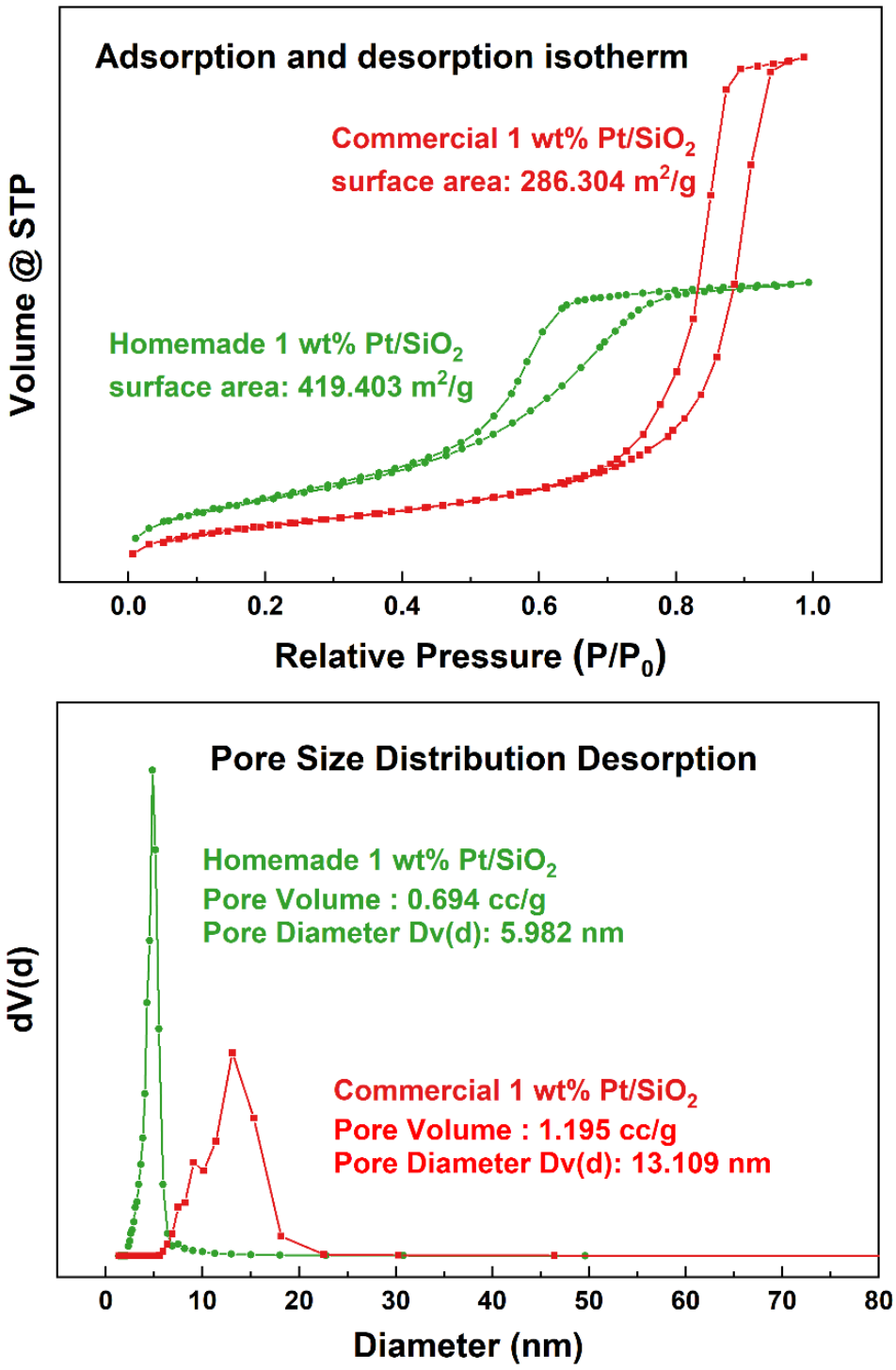

Figure 2.5 The comparison of BET results between commercial and homemade 1 wt% Pt/SiO_2 catalysts.

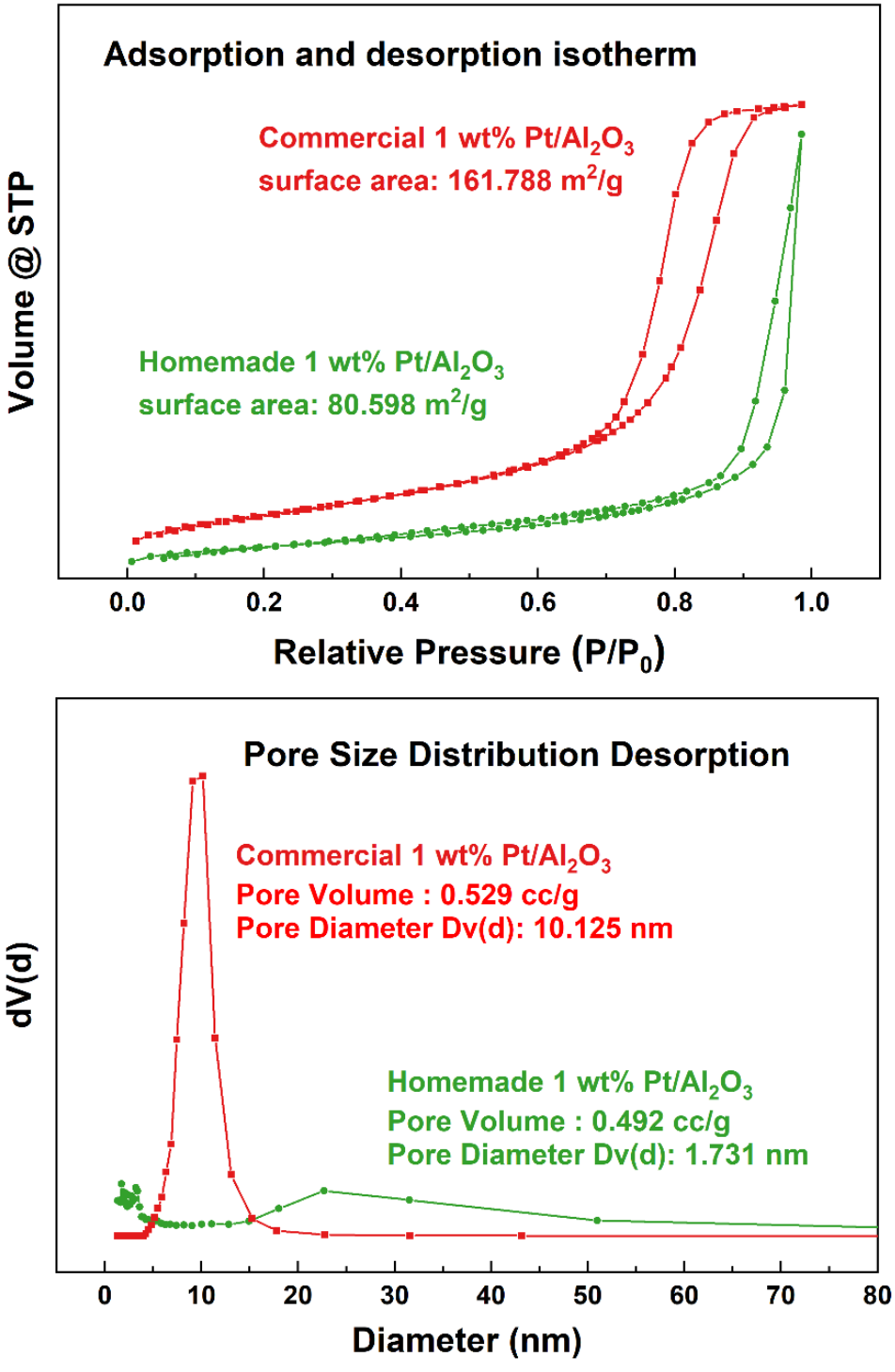

Figure 2.6 The comparison of BET results between commercial and homemade 1 wt% Pt/Al_2O_3 catalysts.

2.2.4 Inductively Coupled Plasma Optical Emission Spectrometry (ICP-OES)

ICP-OES, an analytical technique utilized for detecting trace metals, was employed to determine the amount Pt loading on the catalysts. The Perkin-Elmer Optima 7300DV ICP-OES apparatus was utilized for this purpose. The system incorporates both an SCD detector and an echelle optical system, allowing for simultaneous measurements of all wavelengths within the ultraviolet wavelength (165 to 403 nm) and the visible range (404 to 782 nm).

All four catalysts underwent ICP testing to ascertain the Pt loading amount. As depicted in Table 2.2, the Pt content of commercial 1 wt% Pt/Al_2O_3 catalyst was determined to be 0.81 %, slightly lower than the theoretical value. Conversely, the remaining three Pt catalysts exhibited satisfactory outcomes, with all results falling within the experimental error range. Moreover, despite the absence of Pt nanoparticles in the TEM images of homemade 1 wt% Pt/Al_2O_3 catalyst, the ICP analysis still indicated a Pt loading amount of approximately 1.1 %. This suggests that the Pt nanoparticles might be physically mixed with the γ-Al_2O_3 support, rather than being adsorbed onto the support.

2.2.5 CO Titration by ATR-IR

To assess the Pt active sites for reactions, we conducted CO adsorption experiments using both homemade and commercial Pt catalysts via ATR-IR. The procedure involved dispersing the catalyst onto the ATR-IR surface and subsequently

purging a solution of CO-saturated CCl_4 into the cell. The spectra were collected over time.

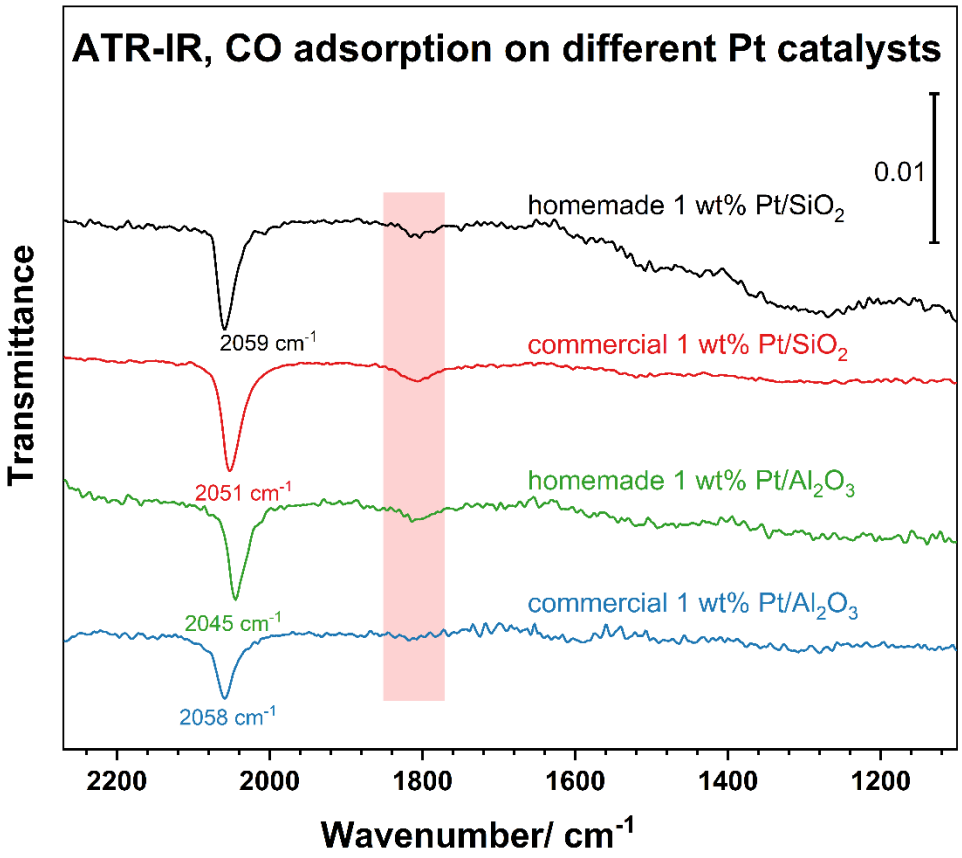

Figure 2.7 ATR-IR spectra of CO adsorption on different Pt supported catalysts.

Figure 2.7 presents the spectra obtained from all four catalysts, each demonstrating a distinct position for the CO peak. The homemade Pt/SiO_2 catalyst exhibited a CO adsorption peak at approximately 2059 cm^{-1} which closely resembled the CO adsorption peak (~2058 cm^{-1}) observed on the commercial Pt/Al_2O_3 catalyst. On the other hand, the CO peaks were observed around 2051 cm^{-1} for commercial Pt/SiO_2 and

around 2045 cm^{-1} for homemade Pt/Al_2O_3. These intense peaks corresponded to CO being linearly bound to Pt single atoms. Additionally, a broad and weak peak emerged at lower wavenumbers (~1800 cm^{-1}), indicative of CO bridging two Pt atoms. This weak peak was also observed in all cases except for the commercial Pt/Al_2O_3 catalyst.

The CO titration experiments not only enabled the identification of active Pt atoms but also provided an explanation for the variation in Pt nanoparticle size, as indicated by TEM images. The peak position proved highly sensitive to coverage and/or surface plane exposure.

2.3 Kinetic Measurements of Ethyl Pyruvate (Et-Py) Hydrogenation

2.3.1 High-Pressure Reactor

The kinetic measurements for the hydrogenation of α-keto esters were conducted using a commercial high-pressure reactor, the Parr 4560 mini bench top reactor. This reactor features a fixed head with a movable vessel. The maximum operating temperature allowed was 225 °C; and the working pressure could reach up to 2000 psig (~138 bar) with the use of a safety rupture disc.

In the specific experimental procedures, the required quantities of reactants, namely ethyl pyruvate (Et-Py), solvent, Pt supported catalysts, and chiral modifiers, were initially added to the stainless steel reactor. Subsequently, the reactor was pressurized with H_2 gas. Samples were collected at 30-minute intervals and then analyzed using gas chromatography (GC).

2.3.2 Gas Chromatography (GC)

Gas chromatography (GC) is a valuable analytical technique used for separating and detecting the components within a sample mixture. The sample collected at various stages of the reaction were analyzed using an Agilent 6890N gas chromatography equipped with a chiral column (Agilent CP-ChiraSil-Dex CB 25m×0.25mm×0.25um). The conversion of the reactant and the enantiomeric excess (*ee*) were calculated and compared under different conditions.

The enantiomeric excess (*ee*) is defined as :

$$ee\% = \frac{|I_R - I_S|}{I_R + I_S} \times 100\%$$

I_R (or I_S) is the area (%) of the respective peak area in the GC output.

Figure 2.8 illustrates an example of the GC results obtained from the hydrogenation reaction of Et-Py in toluene catalyzed by a commercial 1 wt% Pt/Al_2O_3 catalyst without a chiral modifier. The sample was collected after 1.0 hour of reaction. The primary peak at approximately 9.0 minutes corresponded to the solvent, toluene. Following that, the peak at around 10.5 minutes was associated with the reactant, Et-Py molecules. Two products with distinct configurations were observed at approximately 15.3 minutes and 16.0 minutes respectively. The area of the two peaks will be provided and subsequently plugged into the equation, as depicted above, to compute the enantiomeric excess (*ee*) value.

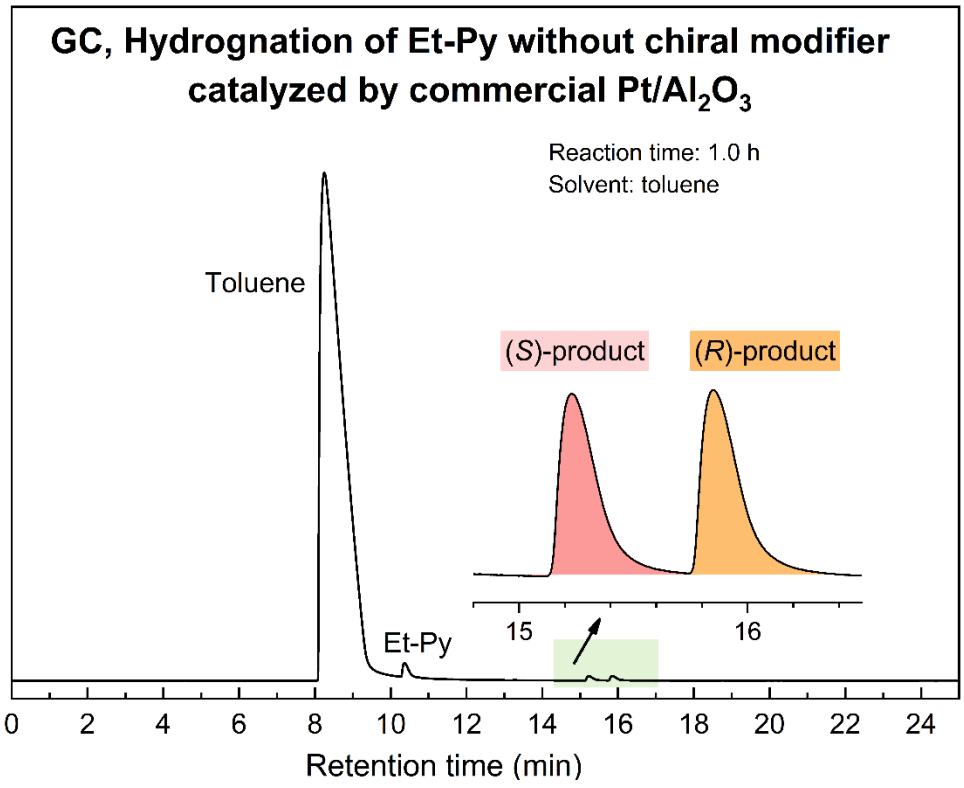

Figure 2.8 GC results of a sample: Et-Py hydrogenation catalyzed by a commercial 1 wt% Pt/Al_2O_3 catalyst in toluene without chiral modifier after 1 hour. An enlarged range of two products is also provided.

2.4 H-D Kinetic Measurements

2.4.1 Proton Nuclear Magnetic Resonance (^{1}H-NMR)

In order to rule out the possible interference from impurities of the solvents during the NEA H-D reactions, the ^{1}H-NMR spectra of the pure solvents were taken. The commercial $CDCl_3$ was used as a solvent for shimming and locking the magnetic field during the NMR characterization of the reaction samples. The CCl_4 was used as a solvent during the H-D exchange experiments. To identify any impurities in the solvents, three types of experiments were carried out. As shown in Figure 2.9, the top trace is the

spectrum of pure commercial $CDCl_3$, the middle one is the spectrum of mixture made by adding CCl_4 directly to $CDCl_3$, the bottom trace is the spectrum of a mixture of pure CCl_4 sealed in a capillary tube and placed inside the larger $CDCl_3$-containing NMR tube.

As a result, small quantities of both $CHCl_3$ and H_2O were detected as shown in the top spectrum of pure $CDCl_3$, the amount is consistent with the those reported by the manufacturer: 99.96 vol% D purity implies an upper limit for $CHCl_3$ of 0.04 vol%, equivalent to a concentration of ~5 mM, and the reported < 0.01 vol% water content amounts to a H_2O concentration of < 2.7 mM.

Virtually no additional signal for either impurity ($CHCl_3$ or H_2O) was seen in experiments where CCl_4 was added. The $H_2O/CHCD_3$ ratio is approximately constant, within experimental error, and the potential excess in the cases with CCl_4, estimated from the extreme values of that ratio, correspond to a maximum water concentration in the CCl_4 solvent of 2-3 mM, an order of magnitude lower than what is needed to provide the total deuterium atoms incorporated in NEA during catalysis (~20 mM). Also, to be noticed is the fact that the position of the water ^{1}H-NMR peak in the case of the CCl_4 sample inside the small tube and the $CDCl_3$ on the outside is the same as for $CDCl_3$ alone, whereas it shifts by ~ 0.01 ppm if CCl_4 is added directly to $CDCl_3$; if there were to be water in the CCl_4 in the dual-tube case, a second peak should have been seen at a lower ppm.

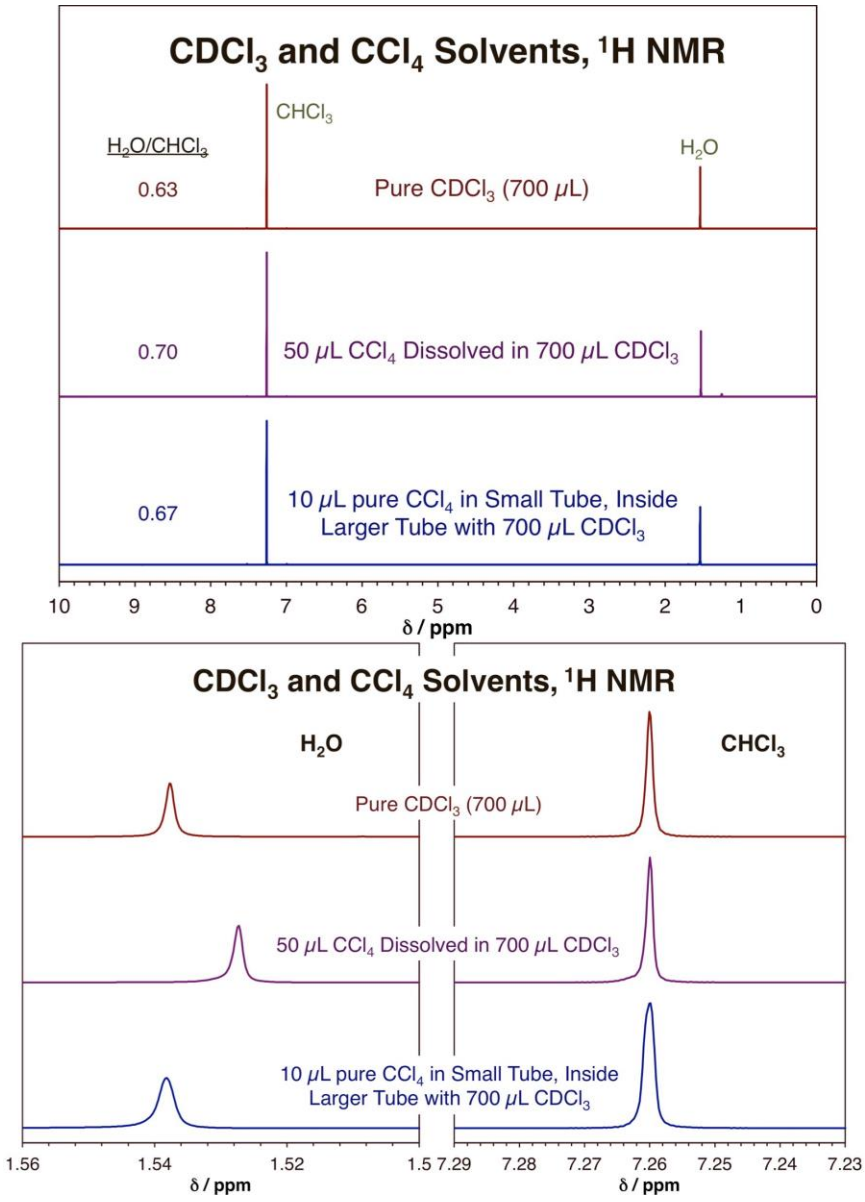

Figure 2.9 ^{1}H-NMR spectra of, from top to bottom: (a) pure $CDCl_3$, as purchased; (b) a solution made by adding CCl_4 directly to $CDCl_3$; and (c) pure CCl_4 sealed in a capillary tube and placed inside the larger $CDCl_3$-containing NMR tube. Expanded versions of the spectra around the water and chloroform peaks are shown in the second row. Reprinted with permission from reference 55, Copyright 2022 American Chemical Society.

It is concluded that the CCl_4 solvent itself does not contain any detectable H_2O. It should be indicated that no water was seen by infrared absorption spectroscopy in any of

the NEA adsorption experiments in this paper either. The fact that CCl_4 does not have measurable amounts of water is critical, because in principle normal water could undergo catalytic H-D exchange with the D_2 gas bubbled during the kinetic experiments reported here, and the resulting D_2O could then undergo H-D exchange with NEA in solution. The absence of H_2O in the CCl_4 solvent allows us to rule out this indirect isotope exchange mechanism.

2.4.2 Gas Chromatography-Mass Spectroscopy (GC-MS)

GC-MS is a highly valuable analytical technique extensively employed in diverse chemical and biochemical applications, including studies involving hydrogen-deuterium (H-D) exchange experiments. In these experiments, GC-MS analysis is typically utilized to separate the components of the reaction mixture and determine the isotopic composition of molecules based on their mass-to-charge ratios. This enables the monitoring of changes over time or under varying reaction conditions, thereby offering valuable insights into the reaction mechanism, kinetics, and energetics.

In the specific experiment conducted, a solution containing a mixture of 20 mM NEA in CCl_4 and 25 mg of Pt catalyst was prepared in a flask. Subsequently, the mixture was exposed to bubbling with D_2 gas, and samples were collected at two-hour intervals for subsequent analysis. The analysis was carried out using an Agilent Technologies 5975 Series MSD apparatus.

Chapter 3

Adsorption and Reactivity of 1-(1-Naphthyl)Ethylamine (1-NEA) on Pt Surfaces in Heterogeneous Catalysis

3.1 Brief Introduction

The previous research on 1-NEA related molecules has been extensively elucidated by Yufei Ni from our group[34, 40]. Comparative adsorption tests with 1-NEA related molecules, as depicted in Figure 3.1, have unequivocally demonstrated that the NEA molecules bind to the Pt catalysts through the primary nitrogen atom rather than the commonly presumed aromatic ring[56-59]. The ATR-IR spectra of various chiral modifiers are presented on the left side of Figure 3.1. Only s-NEA, 1-naphthylmethylamine (NMA), and quinoline exhibited adsorption on the Pt surfaces, while no signs of adsorption were observed with 1-ethylnaphthalene (EtN) or S-N,N-dimethyl-1-(1-naphthyl)-ethylamine (s-DNE).

Despite the presence of aromatic rings in all investigated molecules, only those (NEA and NMA) possessing an NH_2 moiety exhibited significant adsorption uptake on the platinum surfaces. As demonstrated on the right side of Figure 3.1, enantioselectivity in Et-Py hydrogenation reactions was solely detected with NEA and was absent with DNE. Furthermore, the differences in vibrational frequencies observed in the spectra of

NEA adsorbed from solution onto the Pt catalyst, compared to those of pure NEA, suggest a potential break of one of the N−H bonds. Hence, we hypothesized that the adsorption of NEA molecules requires the breaking of one N−H bond. It is plausible that the dissociative adsorption process may be reversible.

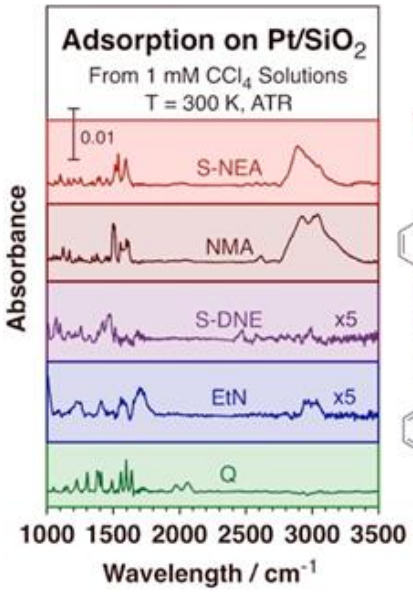

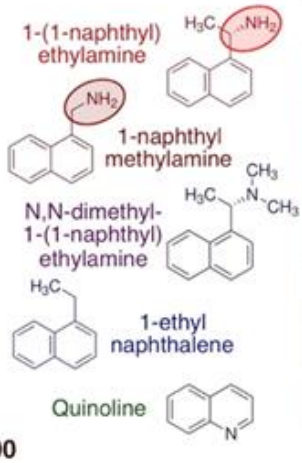

Modifier	Chiral	Ads	ee
No Modifier	No	–	0.2
S-NEA	Yes	Yes	24 (S)
R-NEA	Yes	Yes	29 (R)
Rac-NEA	No	Yes	0.2
NMA	No	Yes	0.7
S-DNE	Yes	No	0.4
EtN	No	No	0.9
Q	No	Yes	0.3

Figure 3.1 Left: ATR-IR spectra of NEA-related compounds on supported Pt catalysts. Right: Corresponding catalytic behavior for the hydrogenation of Et-Py. Reprinted with permission from reference 60. Copyright 2022 American Chemical Society.

In this chapter, both ATR-IR adsorption studies and H−D exchange experiments were conducted to verify our hypothesis. The results corroborated our hypothesis that the amine moiety becomes protonated on the surface during the adsorption process. Moreover, the findings support a model proposing N−bonding adsorption of these amine-based chiral modifiers from solution. To estimate the energetics of the experimentally observed isotope exchange pathway, complementary quantum mechanics calculations

were performed by our collaborators. This particular part of work has been published in ACS Catalysis[55].

In addition to investigating the adsorption mode of NEA molecules on Pt catalysts, further tests were conducted using 1-(2-naphthyl) ethylamine (2-NEA) molecules to explore the influence of amine group position. Additionally, the molecule alpha-methylbenzylamine (MBA) was tested to investigate the effect of aromatic ring size.

3.2 Experimental Details

3.2.1 H−D Exchange Experiments

The H−D exchange kinetic experiments were carried out in a glass flask, for example, 20 mM s-1-NEA ((*S*)-(-)-1-(1-naphthyl)ethylamine, 99 %, Sigma-Aldrich) in CCl_4 (Sigma-Aldrich, 99.9 %) and 25 mg commercial 1 wt % Pt/Al_2O_3 catalyst (Alfa Aesar) were added in a glass flask, and the D_2 gas (Matheson, 99.5 % atom purity) was bubbled into the mixture at atmospheric pressure with magnetic stirring. The reaction was carried out for 8.0 h, 1 mL aliquots were collected every 2.0 h for ^{1}H NMR or GC-MS analysis.

For the ^{1}H NMR tests, the samples were analyzed by using a Bruker Avance NEO 400 spectrometer. The $CDCl_3$ (chloroform-D, 99.96% D, water < 0.01%, Millipore Sigma) was used for shimming and locking the magnetic field during NMR characterization. To avoid any possible H−D exchange

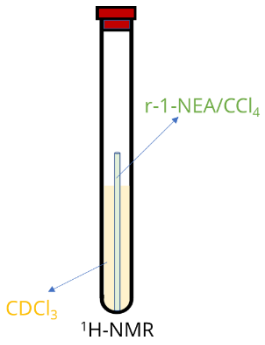

between the NEA molecules and the NMR solvent, $CDCl_3$, the solution of the sample was sealed in a capillary tube and placed inside the larger $CDCl_3$-containing NMR tube, as illustrated in the right figure.

For the GC-MS analysis, the samples were carried out using the Agilent Technologies 5975 Series MSD apparatus.

3.2.2 Theoretical Calculations

For the quantum-mechanics studies, spin-unrestricted first principles calculations were performed based on periodic density functional theory (DFT) as implemented in the Vienna Ab initio simulation package (VASP)[61] with project-augmented waves[62]. For the exchange-correlation (XC) potential, the generalized gradient approximation (GGA) with the Perdew-Burke-Ernzerhof (PBE) functional was employed[63]. Van der Waals interactions were considered using the Grimme D3 method[64]. The electronic states were expanded in plane waves with an energy cutoff of 400 eV. A c(8×4) surface unit cell was used, with four atomic layers and a 15 Å vacuum space added in the z direction, perpendicular to the surface. The bottom layer was fixed during the slab optimization and NEA adsorption. The Brillouin zone integration was done using a k-point grid of 7×7×1 within the c(8×4) cell. The geometric structures were optimized by minimizing the forces on individual atoms with the criterion that all forces on each atom must be smaller than 1×10^{-3} Ry/a.u. Vibrational frequencies were estimated by calculating the second derivative (Hessian matrix) of the potential energy surface using finite differences, and the corresponding intensities were derived from the dynamical dipole moments[65]. Two

atomic layers were used, and atoms were displaced in all directions. The final frequencies were scaled[66-68] to optimize matching with the experimental values as indicated in the text. Reaction pathways and activation energies were calculated by using the nudged elastic band (NEB) method[69-70] within the climbing image scheme, as implemented in VASP. No reoptimization of the transition state structures was attempted as the simplicity of the reaction pathway, mainly involving the diffusion of hydrogen atoms on the surface, suggests that no major surface rearrangements are likely.

Although there are not many previous calculations on these systems that we can compare with (as they depend on the choice of van der Waals interactions), we found that our estimated adsorption energy for the most stable NEA flat geometry (E_{ads}=3.94 eV, using Grimme D3) is close to that reported by Goubert et al. (E_{ads}=3.54 eV, using optB88-vdW)[71]. The effect of the solvent (CCl_4) was briefly evaluated by estimating the energy changes induced by coadsorbing CCl_4 with the flat configuration of NEA. It was found that the effect was minimal as the solvent only weakly physisorbs on the Cu surface.

3.3 Results and Discussions

3.3.1 Adsorption Studies of 1-NEA Molecules on Pt Supported Catalysts

The starting point of my research was to replicate the adsorption tests of 1-NEA molecules on Pt supported catalysts in order to validate the consistency of the data with Yufei's previous work. Figure 3.2 presents the ATR-IR spectra of 1 mM s-1-NEA in CCl_4 on 5 mg commercial 1 wt% Pt/Al_2O_3 catalyst as a function of exposure time. An

enlarged version of figure, focusing on the 1800-1000 cm^{-1} region, is also provided in Figure 3.3.

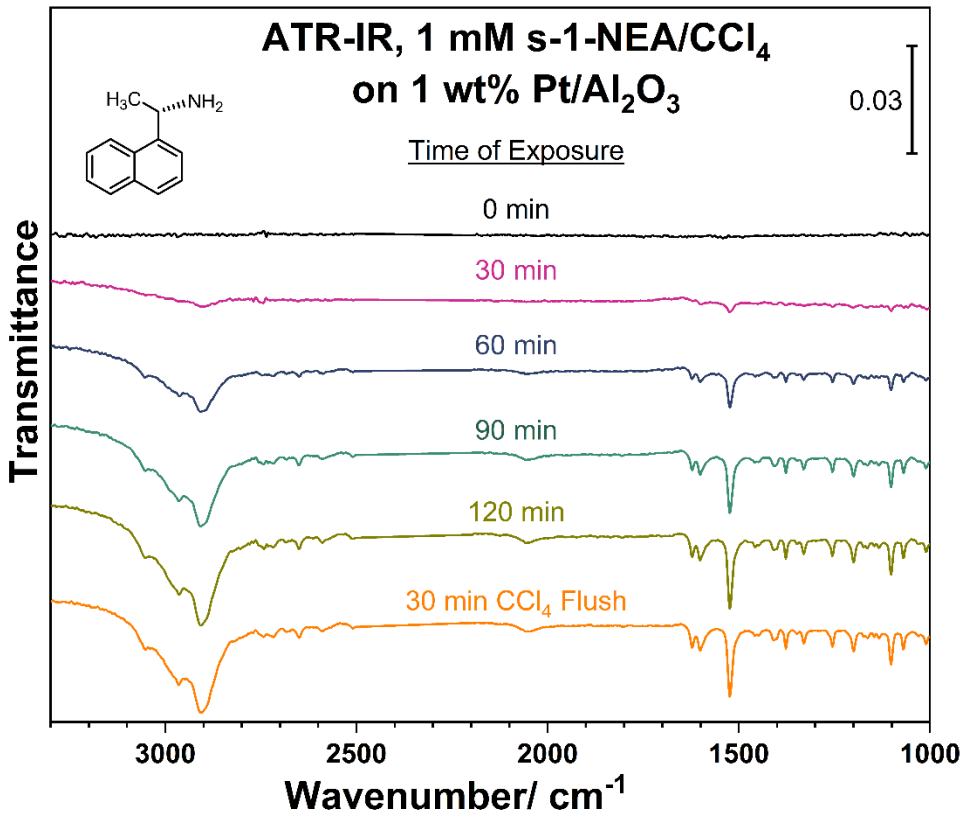

Figure 3.2 ATR-IR spectra of 1 mM s-1-NEA in CCl_4 adsrption on 1 wt% Pt/Al_2O_3 catalyst as a function of exposure time.

Figure 3.2 demonstrates a clear increase in peak intensity with exposure time during the initial 120 minutes, as shown by the peaks. This change in peak intensity indicates a corresponding increase in surface coverage, suggesting higher coverage on Pt surfaces. Furthermore, no notable peak shifts were observed within the 120 minutes exposure time, which is more clearly illustrated in the expanded version displayed in Figure 3.3. The assignment of the IR features to specific vibrational modes of the

adsorbed s-1-NEA and the corresponding adsorption geometry have been previously discussed and reported.

Subsequently, the ATR-IR cell was flushed with pure CCl_4 solvent, and the sample spectrum remained nearly unchanged after 30 minutes of flushing. This observation suggests an irreversible adsorption process.

The obtained results are consistent with previous research, indicating that the data pertaining to 1-NEA can be successfully reproduced.

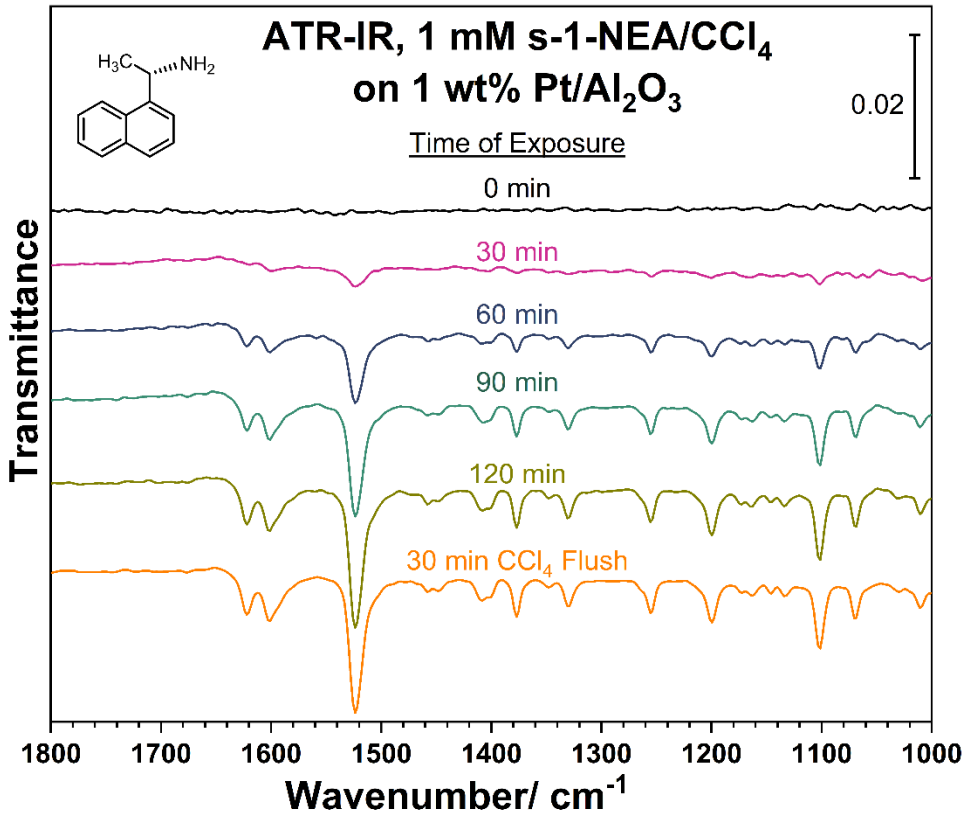

Figure 3.3 ATR-IR spectra, range between 1800-1000 cm^{-1}, of 1 mM s-1-NEA in CCl_4 adsrption on 1 wt% Pt/Al_2O_3 catalyst as a function of exposure time.

Similar experiments were conducted using r-1-NEA. Figure 3.4 presents the ATR-IR spectra of 5 mM r-1-NEA in CCl_4 adsorption on various catalysts. The spectra of 5 mM r-1-NEA on commercial 1 wt% Pt/Al_2O_3 and 1 wt% Pt/SiO_2 did not exhibit significant differences in terms of peak intensity and position. However, these spectra differed notably from the transmission IR spectrum of pure r-1-NEA. These differences further indicate the adsorption of r-1-NEA in CCl_4 on Pt catalysts.

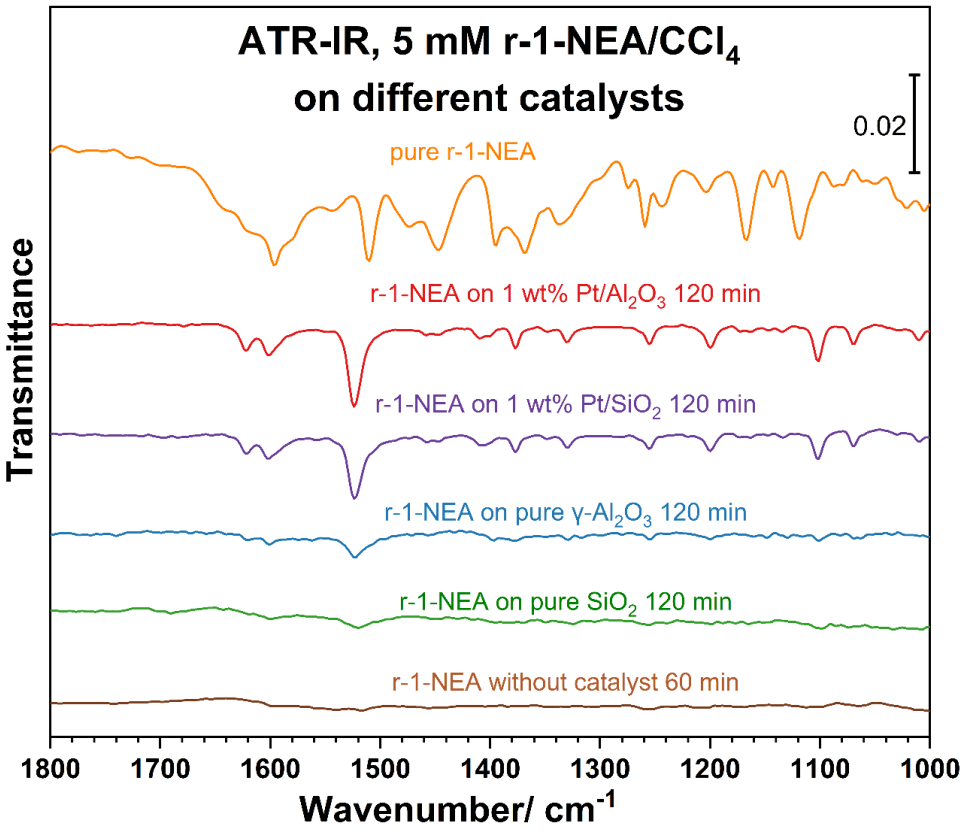

Figure 3.4 ATR-IR spectra of 5 mM r-1-NEA adsorbed from CCl_4 liquid phases onto different catalysts. The transmission IR spectrum is also provided for pure r-1-NEA (top trace, orange).

To account for the potential contribution of the catalyst support, ATR-IR tests were performed pure γ-Al_2O_3 and SiO_2 using 5 mM r-1-NEA in CCl_4. As depicted in Figure 3.4, although some weak sample signals were observed under identical conditions, their contribution from the support was minor compared to the spectra obtained on Pt catalysts. Additionally, a blank test without a catalyst was conducted, revealing no significant sample signals.

The tests conducted on different catalysts strongly suggest that 1-NEA molecules in CCl_4 primarily absorb onto Pt surfaces, while the contribution from the catalyst support is minimal.

3.3.2 Influence of Amine Group Position

The adsorption geometry of chiral modifiers can influence the enantioselectivity behavior observed in asymmetric hydrogenations. Furthermore, the position of the ethylamine group may exhibit varying adsorption geometries on Pt catalysts. This section aims to investigate the impact of ethylamine group's position on the adsorption mode using *in-situ* ATR-IR. We examined the molecule 1-(2-naphthyl)ethylamine (2-NEA) from different perspectives and compared the results with those of 1-NEA molecules. The structure of 1-NEA and 2-NEA is illustrated in Figure 3.5.

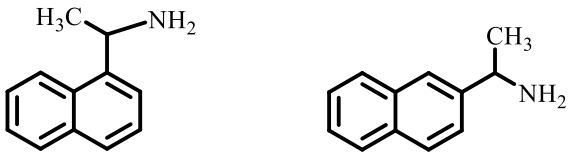

1-(1-naphthyl)ethylamine (1-NEA)

1-(2-naphthyl)ethylamine (2-NEA)

Figure 3.5 Molecular structure of 1-NEA and 2-NEA molecules.

The ATR-IR experiment commenced with a 5 mM r-2-NEA in CCl_4 solution exposed to a 1 wt% Pt/Al_2O_3 catalyst. Figure 3.6 depicts the ATR-IR spectra as a function of exposure time, while Figure 3.7 focused on the specific range between 1800 and 1000 cm^{-1}.

As shown in Figure 3.6, prominent sample peaks were observed, with their intensities increasing over time. Notably, a dominant peak at around 1500 cm^{-1} and a wide, strong peak at a higher wavenumber around 2900 cm^{-1} were observed. After flushing the ATR-IR cell with pure CCl_4 solvent for 30 minutes, the collected spectrum (bottom, Figure 3.6) indicated that the sample peaks persisted without disappearing. These findings suggest that 2-NEA molecules also bind to Pt/Al_2O_3 catalysts in the CCl_4 solution, with the adsorption process appearing to be irreversible.

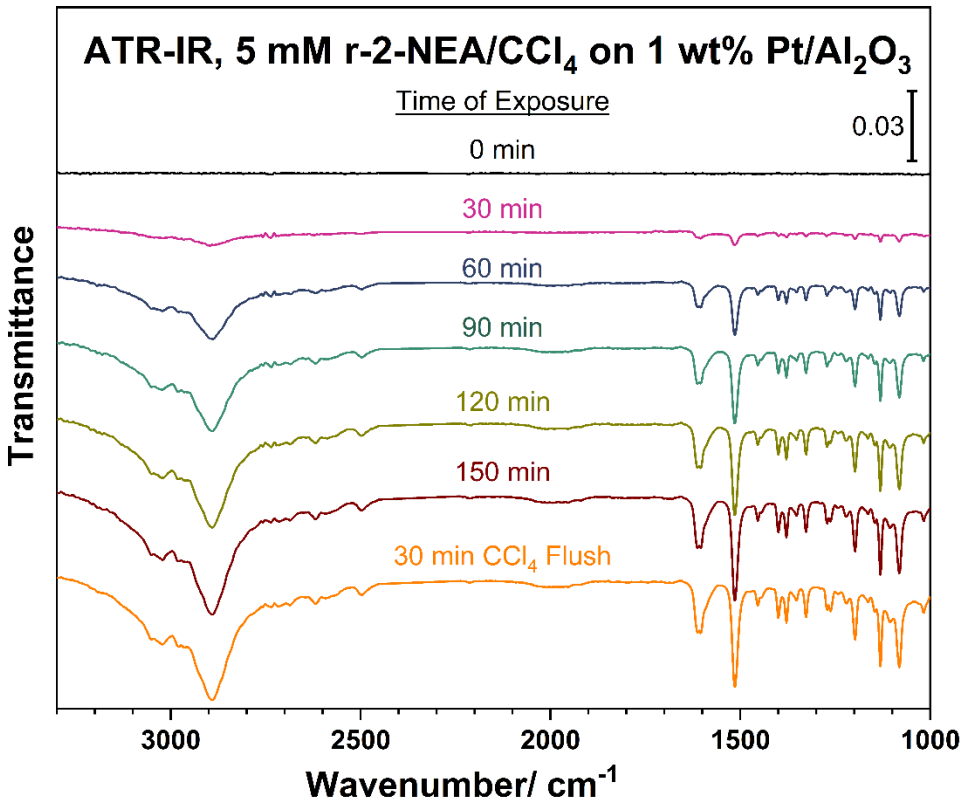

Figure 3.6 ATR-IR spectra of r-2-NEA adsorbed on 1 wt % Pt/Al_2O_3 from a 5 mM CCl_4 solution as a function of the time of exposure of the surface to the liquid.

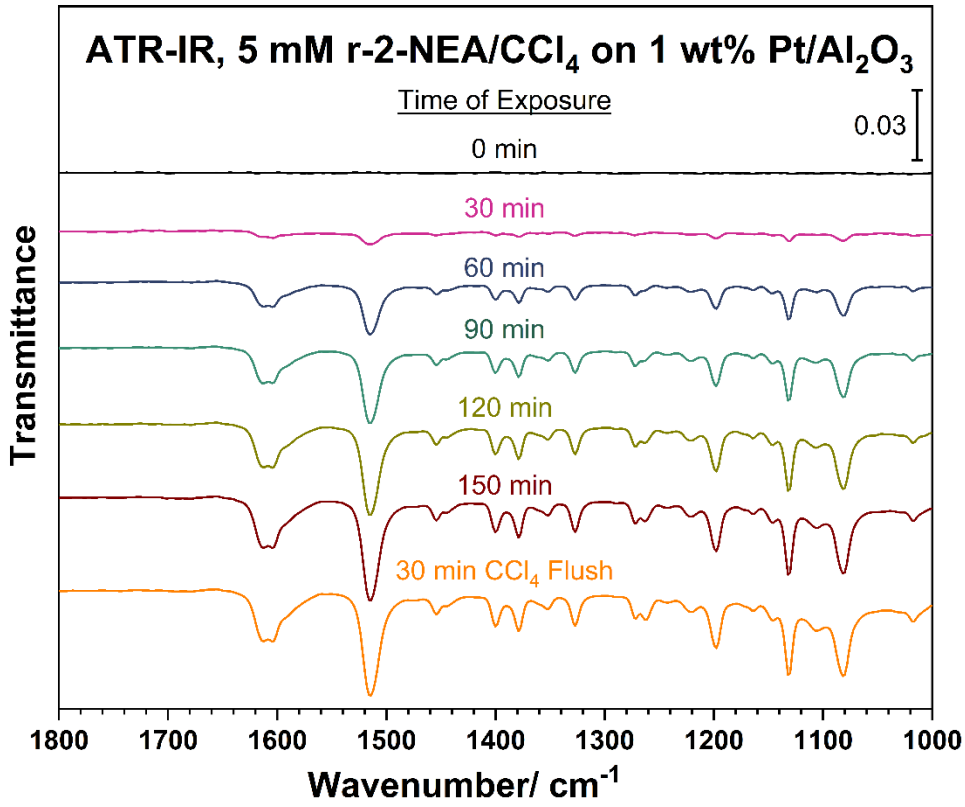

Figure 3.7 ATR-IR spectra, range between 1800-1000 cm^{-1}, of r-2-NEA adsorbed on 1 wt % Pt/Al_2O_3 from a 5 mM CCl_4 solution as a function of exposure time.

The adsorption behavior of 2-NEA appears to be general on both commercial 1 wt% Pt/SiO_2 and Pt/Al_2O_3 catalysts. As shown in Figure 3.8, both enantiomers of 2-NEA (s- and r-2-NEA) exhibit similar behavior on both Pt catalysts. To confirm the binding of 2-NEA molecules to Pt surfaces, blank tests were conducted by collecting spectra of 5 mM r- or s-2-NEA in CCl_4 without Pt catalysts, which revealed no detectable sample signals.

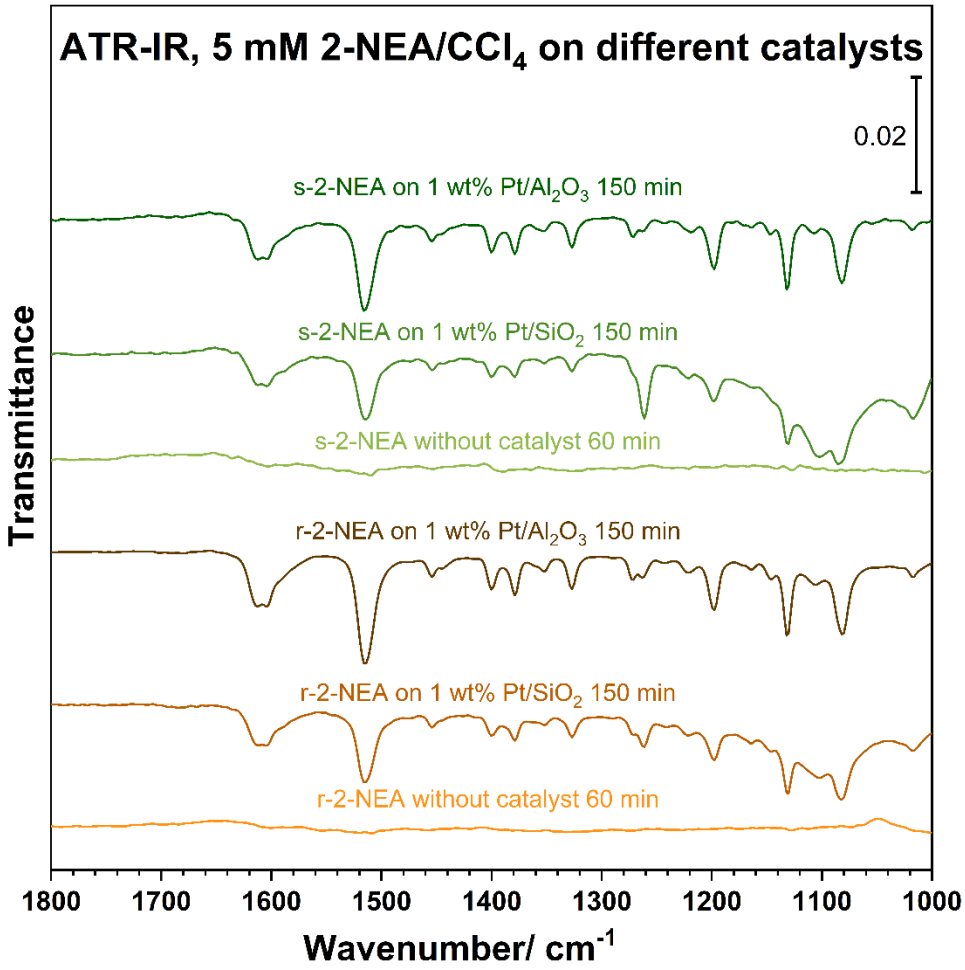

Figure 3.8 ATR-IR spectra of 5 mM r-2-NEA or s-2-NEA in CCl_4 adsorption on 1 wt% Pt catalysts and without catalysts.

Furthermore, in the case of commercial Pt/SiO_2 catalyst, a broad peak around 1100 cm^{-1} was observed in both enantiomers. We attribute this peak to the support of SiO_2 rather than experimental error. To validate this observation, tests with Pt/SiO_2 were performed three times under identical conditions, and the results from all three independent trails were consistent with each other, as summarized in Figure 3.9.

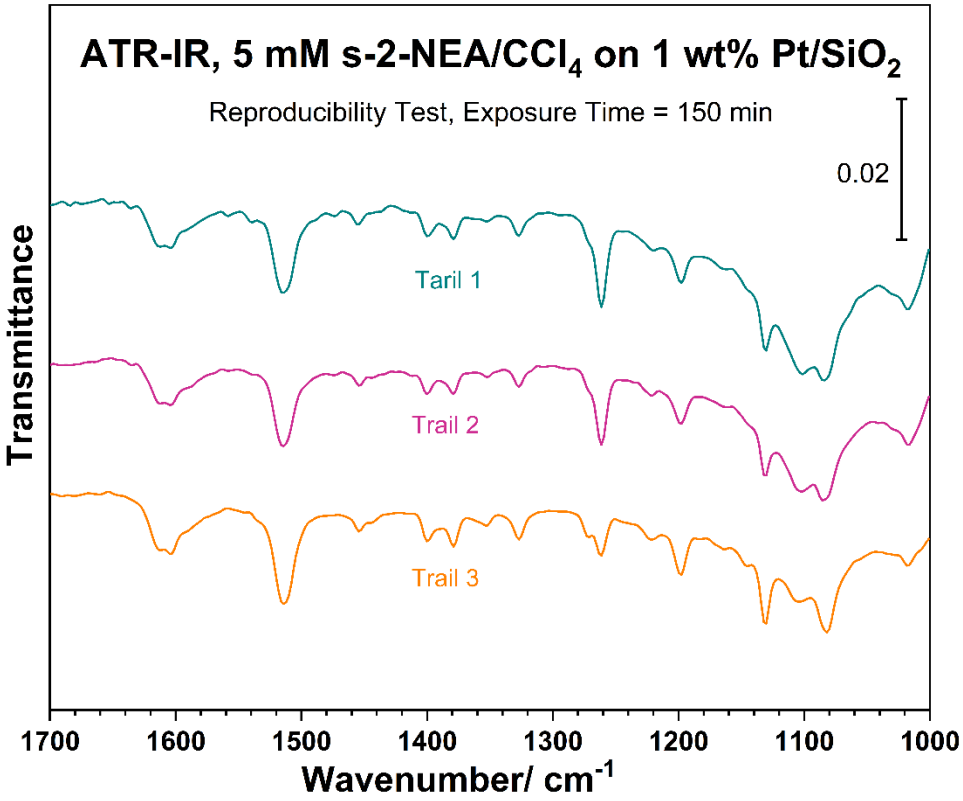

Figure 3.9 ATR-IR spectra of 5 mM s-2-NEA in CCl_4 adsorption on 1 wt% Pt/SiO_2 catalysts. The trail 1, 2 and 3 were three separate tests under the same conditions to check reproducibility.

3.3.3 Comparison Between 1-NEA and 2-NEA

As discussed earlier, 2-NEA molecules exhibit similar behavior to 1-NEA molecules in terms of binding to Pt catalysts in CCl_4 solutions.

Figure 3.10 presents a comparison of the ATR-IR adsorption spectra between 1-NEA and 2-NEA molecules. Several noticeable differences were observed, which may be attributed to variations in adsorption geometry caused by the position of the ethylamine group.

Our research group has previously reported the assignment of peak positions for 1-NEA molecules, and the detailed information can be found in Table 3.1. Considering

the similarity in behavior between both molecules, we believe that both 1-NEA and 2-NEA molecules bind to Pt surfaces through the amine group. The dominant peak for 1-NEA molecules occurs at approximately 1523 cm^{-1} and is assigned to the in-plane stretching mode of C−C from the aromatic ring. In the case of 2-NEA molecules, the dominant peak shifted to a lower wavenumber, around 1513 cm^{-1}. The difference in molecular structure suggests that the angle between the aromatic ring and the Pt surfaces during adsorption via the amine group may vary. This disparity in bond angle could explain the observed peak shift.

Additionally, two distinct peaks were observed for 1-NEA molecules around 1600 cm^{-1}, corresponding to the in-plane symmetric stretching mode of C−C bond from the aromatic ring. These peaks appeared closer together and tended to merge into a wider peak. The differences may be related to the intermolecular interactions within the solution. The position of the ethylamine group could influence the reactivity of these interactions, leading to differences in peak appearance.

Another significant difference was observed in the peak around 1100 cm^{-1}. For 1-NEA molecules, two sharp peaks were detected at approximately 1069 and 1103 cm^{-1}, representing the out-of-plane and in-plane deformation modes of the C−H bond from the aromatic rings, respectively. In the case of 2-NEA, both peaks shifted to higher wavenumbers. Similarly, the peak around 1254 cm^{-1}, corresponding to the in-plane deformation mode of the C−H from the aromatic ring, was observed to shift to a higher wavenumber (~1261 cm^{-1}) in 2-NEA molecules. One possible explanation for these shifts is the difference in steric hindrance between 1-NEA and 2-NEA molecules. In the 1-NEA

molecules, the naphthyl group is attached to the ethylamine chain at the 1-position, resulting in a parallel orientation of the naphthyl group to the ethylamine chain. Conversely, in the 2-NEA molecule, the naphthyl group is attached at the 2-position, leading to a perpendicular orientation of the naphthyl group to the ethylamine chain. This perpendicular orientation in 2-NEA provides more space around the nitrogen atom, resulting in less steric hindrance compared to 1-NEA molecule. Therefore, steric hindrance in 1-NEA molecules could be more significant due to the bulky naphthyl group being closer to the amine group, which could explain the observed peak shifts.

Lastly, despite the significant differences between the 1-NEA and 2-NEA molecules, the disparities between the spectra of 1-NEA and 2-NEA on Pt/SiO_2 and Pt/Al_2O_3 are comparatively minor. Consequently, the support of the Pt catalysts plays a minor role.

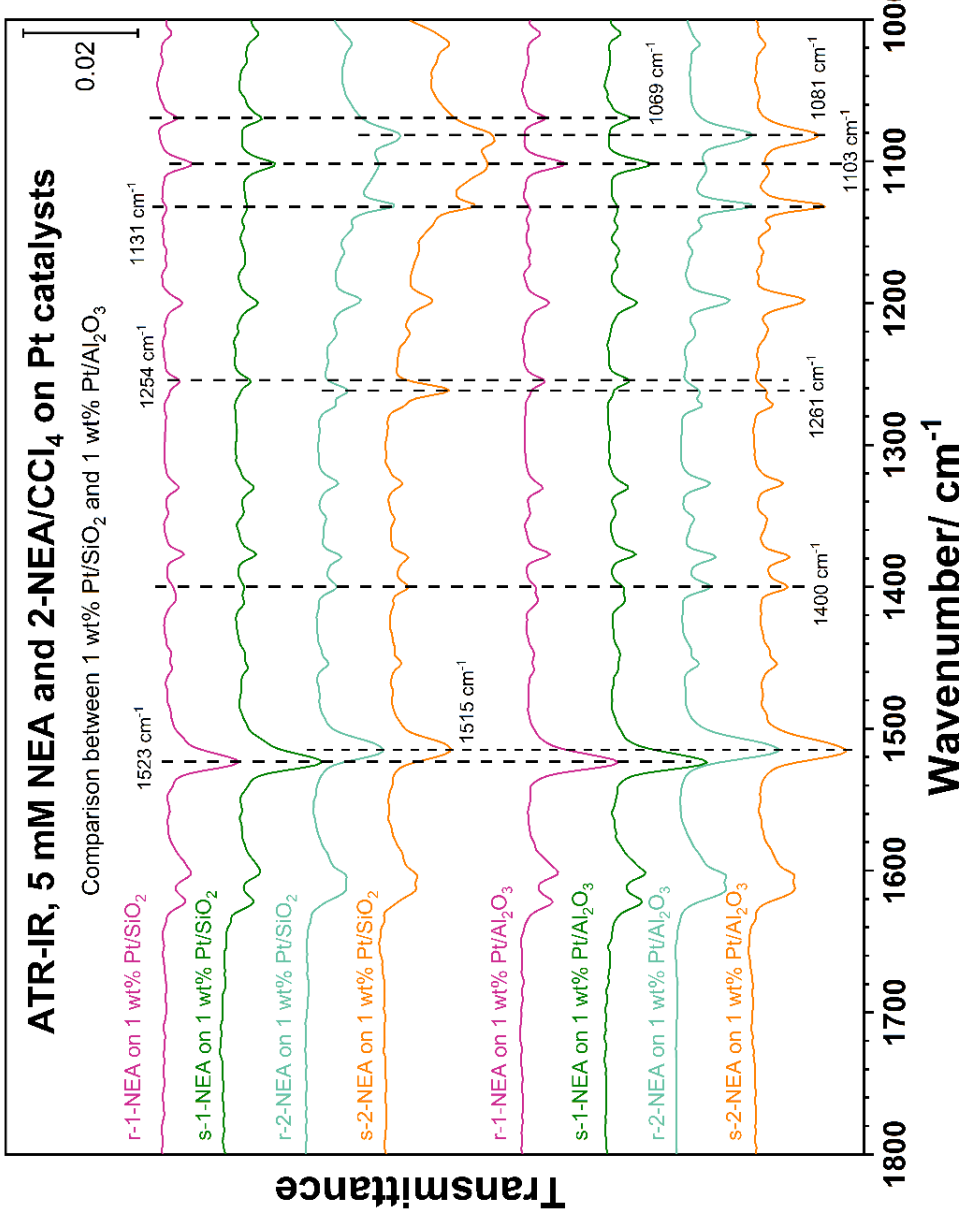

Figure 3.10 ATR-IR of 1-NEA and 2-NEA in CCl_4, both r- and s-configuration chiral molecules, adsorption on 1 wt% Pt supported catalysts

Table 3.1 Assignment of IR peaks for adsorbed 1-NEA. Reprinted with permission from reference 40, Copyright 2017 Angewandte Chemie.

Model	Liquid	Pt/Al_2O_3-CCl_4 Solution	Pt/SiO_2-CCl_4 Solution
$\delta_{oop}(CH)_{ring}$		1101 (s)	1101 (m)
$\delta_{ip}(CH)_{ring}$	1119 (vs)		1119 (sh)
$\delta_{oop}(CH)_{ring}$	1167 (vs)		1163 (m)
$\delta_{ip}(CH)_{ring}$	1204 (m)	1200 (m)	1203 (m), 1217 (sh)
$\delta_{ip}(CH)_{ring}$	1240 (s), 1260 (s)	1256 (m)	1252 (w), 1263 (sh)
$\delta(CH)_{amine}$	1327 (sh), 1339 (m)	1331 (m)	1325 (w), 1344 (m)
$\delta_{sym}(CH_3)_{amine}$	1367 (s)	1377 (m)	1381 (m)
$\nu_{ip}(CC)_{ring, sym}$	1395 (s)	1400 (sh), 1408 (m)	1398 (m)
$\delta_{asym}(CH_3)_{amine}$	1445 (vs)	1447 (w), 1458 (w)	1450 (m), 1461 (sh)
$\nu_{ip}(CC)_{ring}$	1510 (vs)	1524 (vs)	1514 (s), 1539 (vs)
$\nu_{ip}(CC)_{ring, sym}$	1595 (vs)	1601 (s), 1622 (s)	1595 (vs), 1610 (sh)

[a] Values are in cm^{-1} and relative intensities are given in parentheses. Key: very strong (vs), strong (s), medium (m), weak (w), shoulder (sh).

[b] Mode key: deformation (δ), stretching (ν), in-plane (ip), out-of-plane (oop), symmetric (sym), asymmetric (asym).

To further compare 1-NEA and 2-NEA, we examined their adsorption strength on Pt catalysts. The objective was to determine if displacement would occur in the presence of both 1-NEA and 2-NEA molecules.

To test if the 2-NEA molecules can replace the adsorbed 1-NEA molecules, the ATR-IR cell was initially purged with a 5 mM 1-NEA in CCl_4 solution on commercial Pt/SiO_2 catalyst. Once a saturated layer of 1-NEA was achieved, the ATR-IR cell was flushed with a fresh solution of 5 mM r-2-NEA in CCl_4 for approximately 150 minutes. Subsequently, the solution was replaced with a fresh 5 mM r-1-NEA in CCl_4 solution

again, and the cell was finally flushed with pure CCl_4. The results are depicted in Figure 3.11.

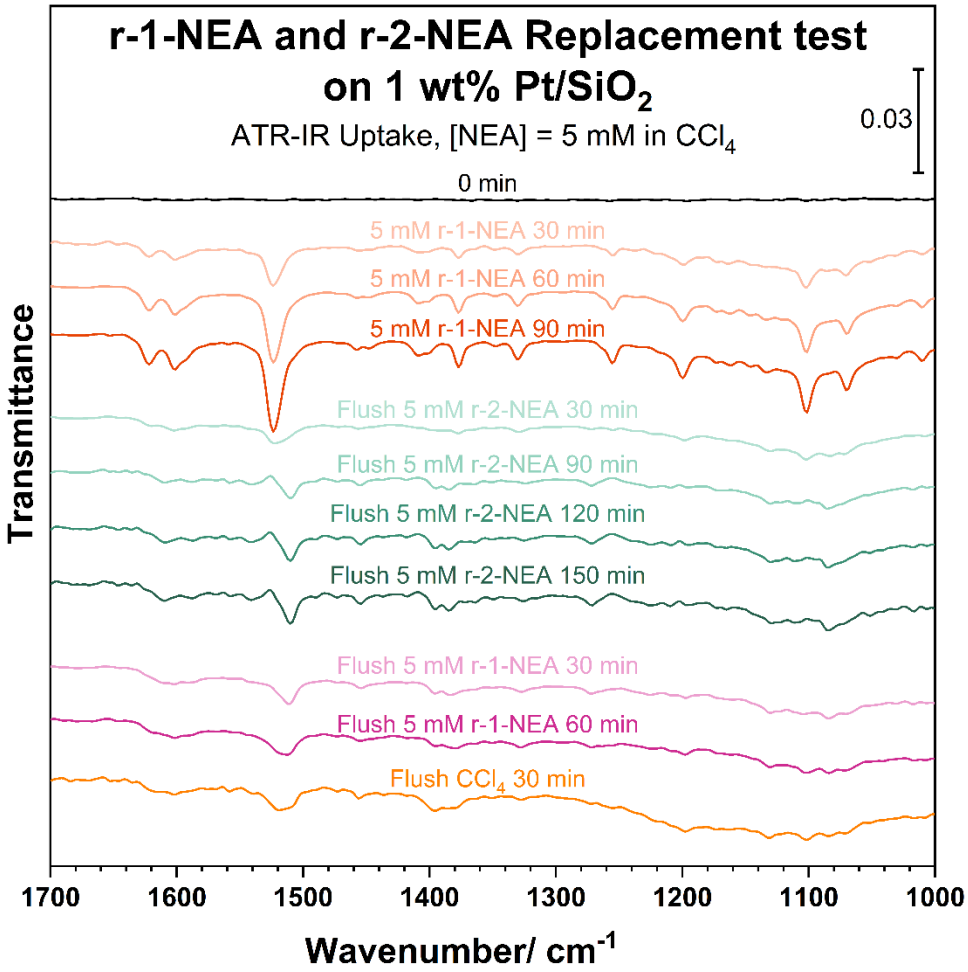

Figure 3.11 ATR-IR spectra of r-1-NEA and r-2-NEA in CCl_4 replacement test on 1 wt% Pt/SiO_2. The ATR-IR cell was first flushed with 5 mM r-1-NEA, followed by a fresh 5 mM r-2-NEA, and then flushed with fresh 5 mM r-1-NEA again. Finally, the cell was flushed with pure CCl_4.

According to Figure 3.11, the absorption of r-1-NEA was observed, and the intensity of sample peaks increased over time due to increasing surface coverage. After approximately 90 minutes, a saturated layer of r-1-NEA on Pt/SiO_2 was obtained. When

the cell was flushed with a fresh 5 mM r-2-NEA in CCl_4 solution, the sample peaks associated with adsorbed r-1-NEA molecules disappeared, and new peaks corresponding to r-2-NEA adsorbed molecules appeared. Even after flushing the ATR-IR cell again with a fresh 5 mM r-1-NEA solution, no significant sample signals related to r-1-NEA molecules were observed. The subsequent flushing tests with pure CCl_4 failed to remove the adsorbed r-2-NEA on Pt/SiO_2 catalysts, indicating the adsorption is irreversible. It appears that the r-2-NEA can replace the adsorbed r-1-NEA molecules on Pt/SiO_2 catalysts.

A similar test was conducted starting with a saturated 2-NEA layer on Pt/SiO_2 catalysts, and the results are shown in Figure 3.12. A 5 mM r-2-NEA in CCl_4 solution was first introduced to the ATR-IR cell with Pt/SiO_2 dispersed on the surface, the spectra were collected until the surface was saturated with r-2-NEA molecules. Then, a fresh solution of 5 mM r-1-NEA in CCl_4 was introduced and flushed into the cell. However, the spectra collected after introducing the r-1-NEA molecules did not show significant IR peaks corresponding to adsorbed r-1-NEA molecules on Pt/SiO_2 surfaces. The sample peaks were still dominated by absorbed r-2-NEA molecules. Furthermore, the flushing test with pure CCl_4 did not remove any of the sample peaks.

In conclusion, it can be inferred that r-2-NEA molecules have the ability to displace the adsorbed r-1-NEA molecules on Pt/SiO_2 catalysts, whereas r-1-NEA does not exhibit the ability to displace adsorbed r-2-NEA molecules from the Pt/SiO_2 catalysts. Thus, the adsorption strength of 2-NEA molecules is stronger than that of 1-NEA molecules.

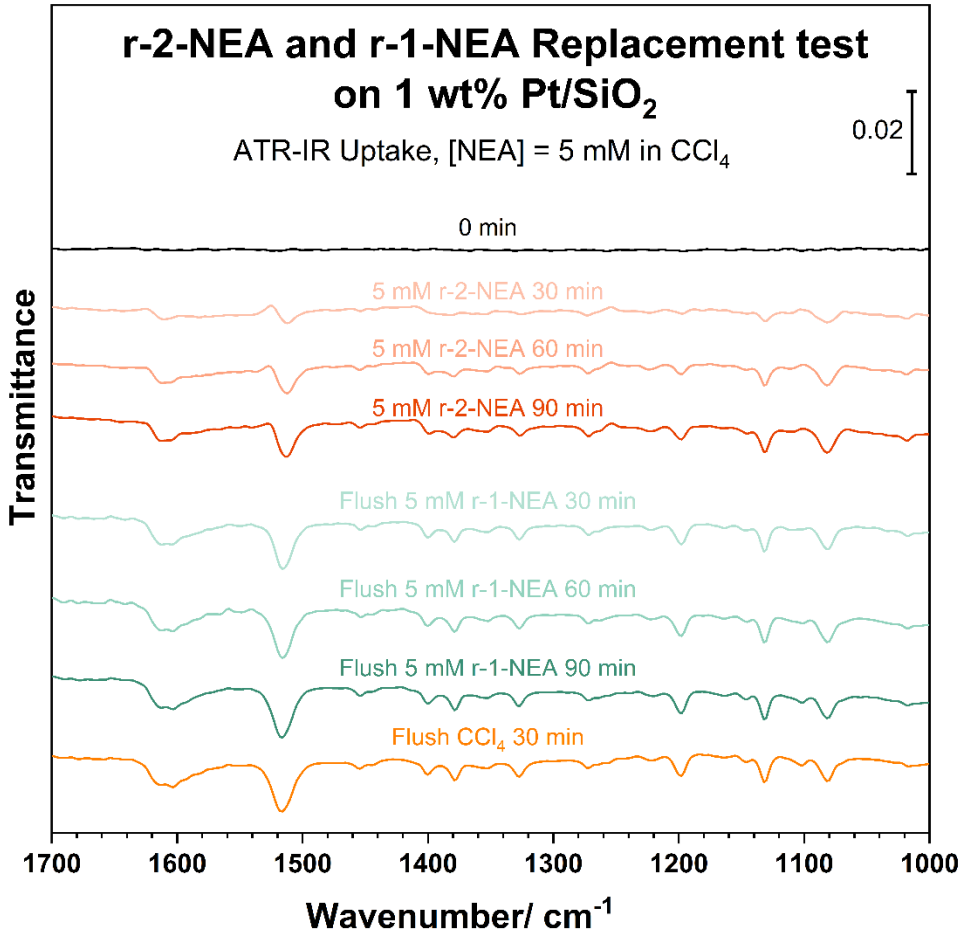

Figure 3.12 ATR-IR spectra of r-1-NEA and r-2-NEA in CCl_4 replacement test on 1 wt% Pt/SiO_2. The ATR-IR cell was first flushed with 5 mM r-2-NEA, followed by a fresh 5 mM r-1-NEA, and then flushed with fresh CCl_4.

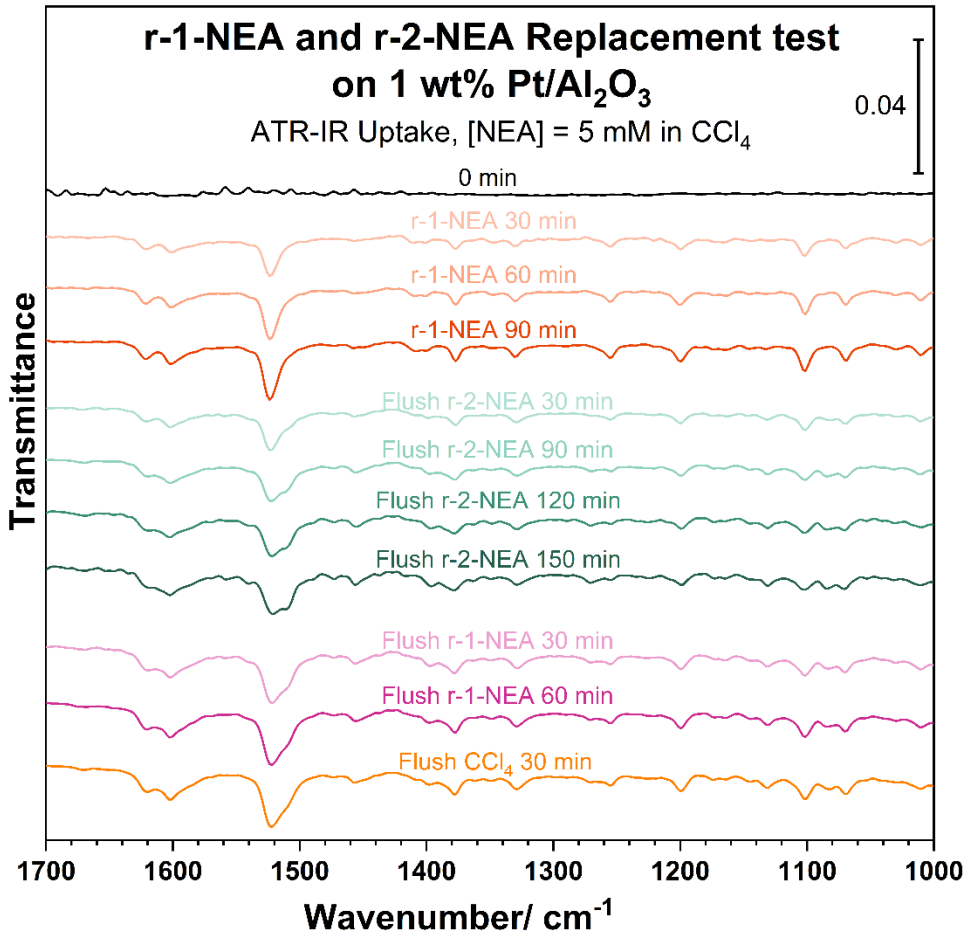

Figure 3.13 ATR-IR spectra of r-1-NEA and r-2-NEA in CCl_4 replacement test on 1 wt% Pt/Al_2O_3. The ATR-IR cell was first flushed with 5 mM r-1-NEA, followed by a fresh 5 mM r-2-NEA, and then flushed with fresh 5 mM r-1-NEA again. Finally, the cell was flushed with pure CCl_4.

The same experiments were conducted for the 1 wt% Pt/Al_2O_3 catalyst, as indicated in Figure 3.13 and Figure 3.14. However, a noticeable difference was observed between the tests on Pt/Al_2O_3 catalysts and Pt/SiO_2 catalysts.

Figure 3.13 demonstrates the formation of a saturated layer of r-1-NEA on Pt/Al_2O_3 catalysts. Even after introducing a fresh solution of 5 mM r-2-NEA, the adsorbed r-1-NEA molecules were not completely displaced. Unlike the case observed in Figure 3.11 for Pt/SiO_2 catalysts, where the introduction of r-2-NEA resulted in the

complete replacement of the adsorbed r-1-NEA molecules. The spectra obtained after introducing r-2-NEA molecules on Pt/Al_2O_3 catalysts appeared to be a combination of both r-1-NEA and r-2-NEA adsorbed species.

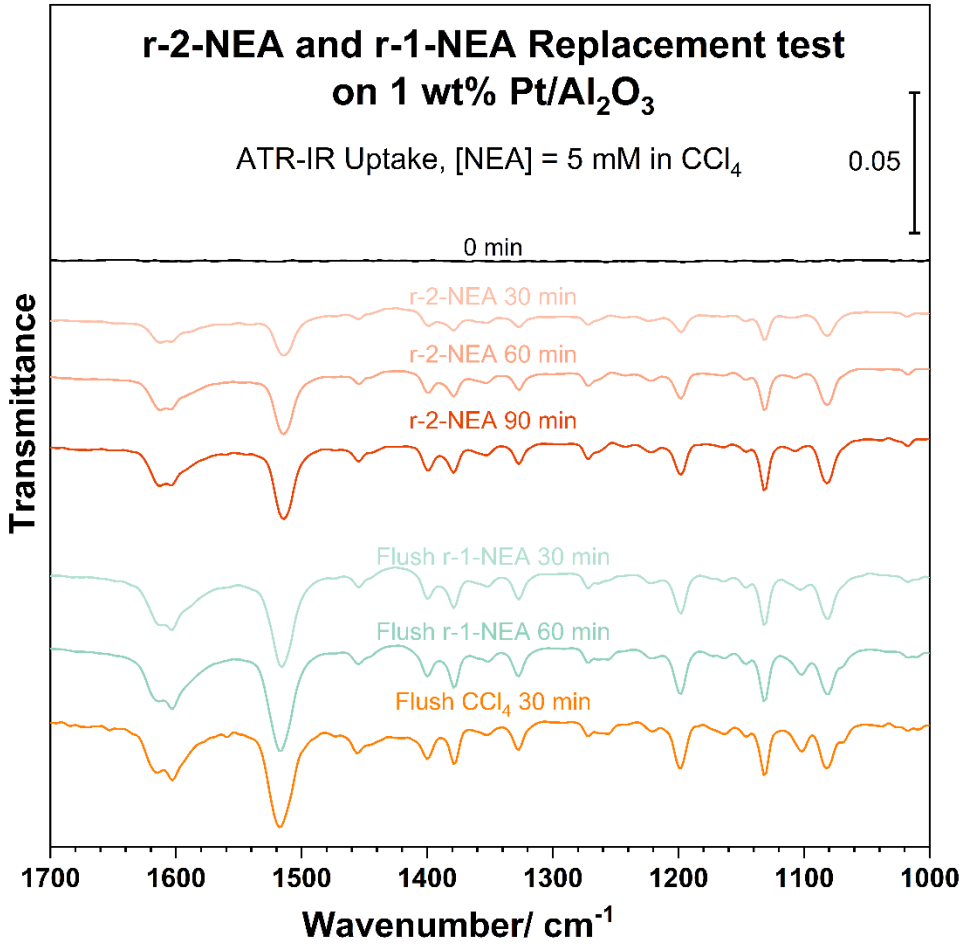

Figure 3.14 ATR-IR spectra of r-1-NEA and r-2-NEA in CCl_4 replacement test on 1 wt% Pt/Al_2O_3. The ATR-IR cell was first flushed with 5 mM r-2-NEA, followed by a fresh 5 mM r-1-NEA, and then flushed with fresh CCl_4.

In contrast, Figure 3.14 clearly indicates that r-1-NEA was unable to displace the adsorbed r-2-NEA on Pt/Al_2O_3 catalysts. The surface of Pt/Al_2O_3 was initially saturated

with r-2-NEA molecules, and no distinct r-1-NEA IR signals were observed upon introducing a fresh r-1-NEA solution.

To summarize, the results suggest that 2-NEA molecules can easily replace the adsorbed 1-NEA molecules on Pt/SiO_2 catalyst. However, it is more challenging for 2-NEA molecules to displace the absorbed 1-NEA molecules on the Pt/Al_2O_3 catalyst. This observation implies that the binding energy of 1-NEA on the Pt/Al_2O_3 catalyst is stronger compared to Pt/SiO_2. Furthermore, the 1-NEA molecules were unable to replace the absorbed 2-NEA on both Pt/Al_2O_3 and Pt/SiO_2 catalysts, indicating that the adsorption of 2-NEA is more stable than that of 1-NEA on Pt catalysts.

3.3.4 Influence of Aromatic Ring Size

Another area of focus in NEA adsorption studies involves examining the impact of the aromatic ring on adsorption. In CCl_4 solutions, both 1-NEA and 2-NEA molecules bind to Pt surfaces primarily through the amine group, which plays a crucial role in the adsorption process. To determine the minimum functional requirements of this group, we conducted a study on the molecule alpha-methylbenzylamine (MBA).

Figure 3.15 illustrates the results obtained from ATR-IR analysis, where various concentrations of s-MBA in CCl_4 solutions (10 mM, 50 mM and 100 mM) were tested in the absence of a catalyst. The intensity of the signals observed in the samples displayed a linear increase with higher concentrations. Notably, the 100 mM s-MBA solution exhibited more prominent IR peaks, particularly in the higher wavenumber range around

3000 cm^{-1}. Furthermore, the spectra collected without catalysts closely resembled the transmission IR spectrum of pure s-MBA (the top trace).

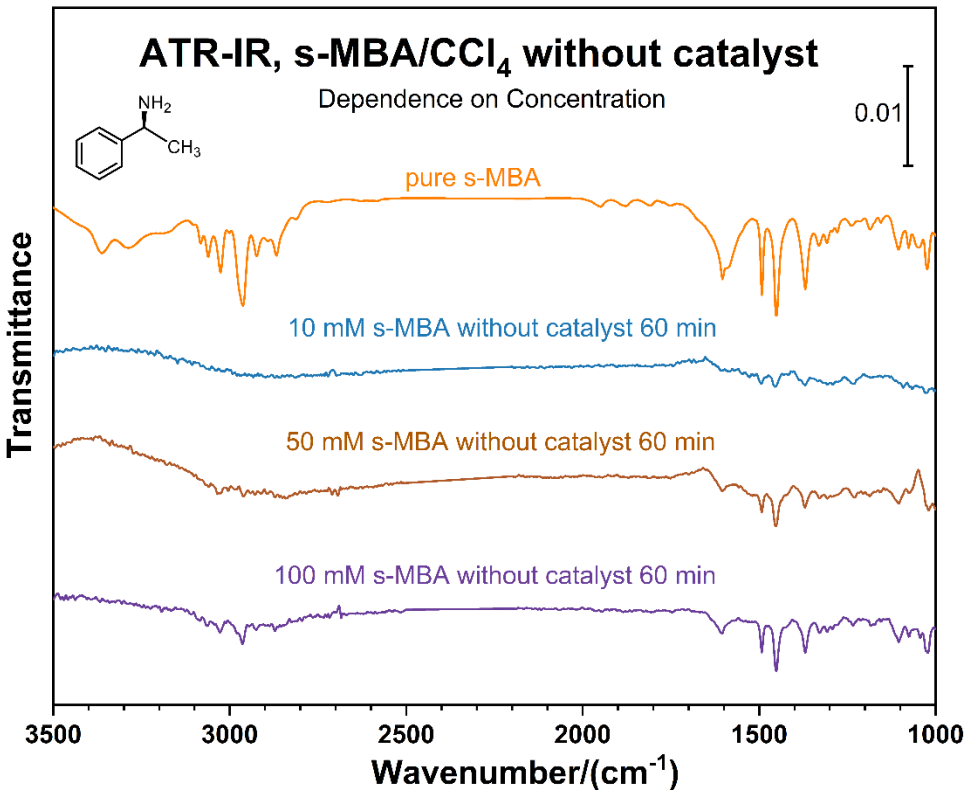

Figure 3.15 ATR-IR spectra of s-MBA in CCl_4 without catalyst as a function of concentration. The top trace is the transmission IR spectrum of pure s-MBA for reference.

In order to investigate whether the behavior of s-MBA differs in the presence of Pt catalysts, a solution of 100 mM s-MBA in CCl_4 was exposed to a 1 wt% Pt/Al_2O_3 catalyst. The ATR-IR spectra were recorded as a function of exposure time, and Figure 3.16 displays these spectra. After 10 minutes of exposure, clear signals from the sample were detected, but the peak intensities did not significantly increase with longer exposure

times. Furthermore, the collected spectra closely resemble the transmission IR spectrum of pure s-MBA, indicating that the observed peaks are associated with the free s-MBA molecules in the CCl_4 solution.

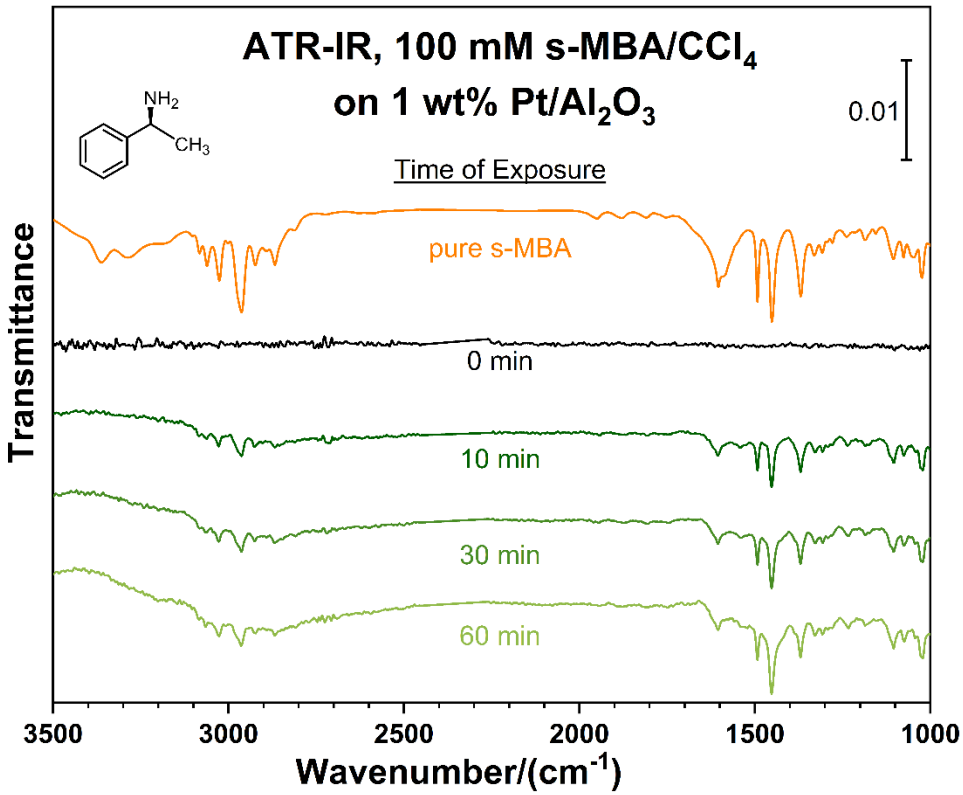

Figure 3.16 ATR-IR spectra of 100 mM s-MBA in CCl_4 adsorption on 1 wt% Pt/Al_2O_3 as a function of exposure time. The reference transmission IR is provided for pure s-MBA (top trace).

Due to the fact that the s-MBA possesses a benzene ring while NEA molecules contain a naphthyl ring, the solubility of s-MBA in CCl_4 is considerably higher. This high solubility poses a challenge in achieving a high surface coverage on Pt catalysts. Therefore, conducting multiple exposures with fresh solutions consecutively might result in a higher surface concentration. Figure 3.17 demonstrates this scenario, where three 100

mM s-MBA in CCl_4 solutions were sequentially introduced into the ATR-IR cell. The spectra were collected after 60 minutes for each solution, and pure CCl_4 was used to flush the cell at the end. However, no distinct differences were observed among the three exposures, and the flushing tests with pure CCl_4 successfully eliminated almost all sample peaks. These results suggest that s-MBA does not bind to Pt/Al_2O_3 catalysts, and the observed sample peaks are attributed to the free molecules in solution.

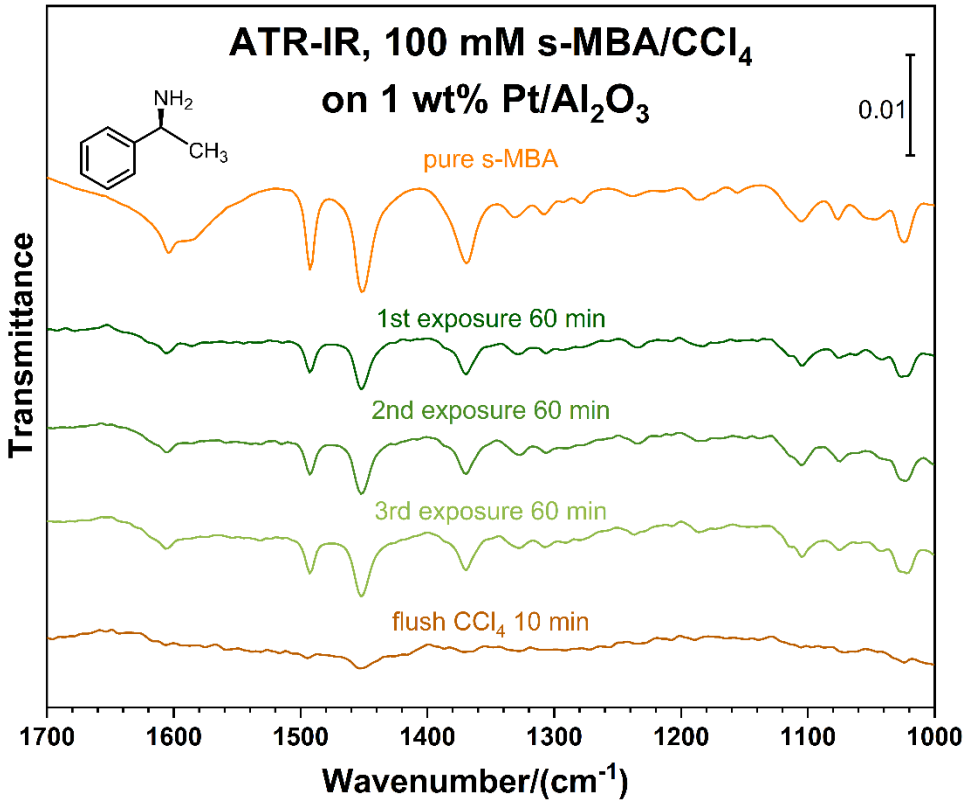

Figure 3.17 ATR-IR spectra of 100 mM s-MBA in CCl_4 adsorption on 1 wt% Pt/Al_2O_3 catalysts with three times exposure. The top trace is the transmission IR spectrum of pure s-MBA for reference.

The same behavior was observed with both 100 mM s- and r-MBA, as well as racemic MBA, in CCl_4 solutions in the presence of Pt/Al_2O_3 catalysts, as depicted in Figure 3.18.

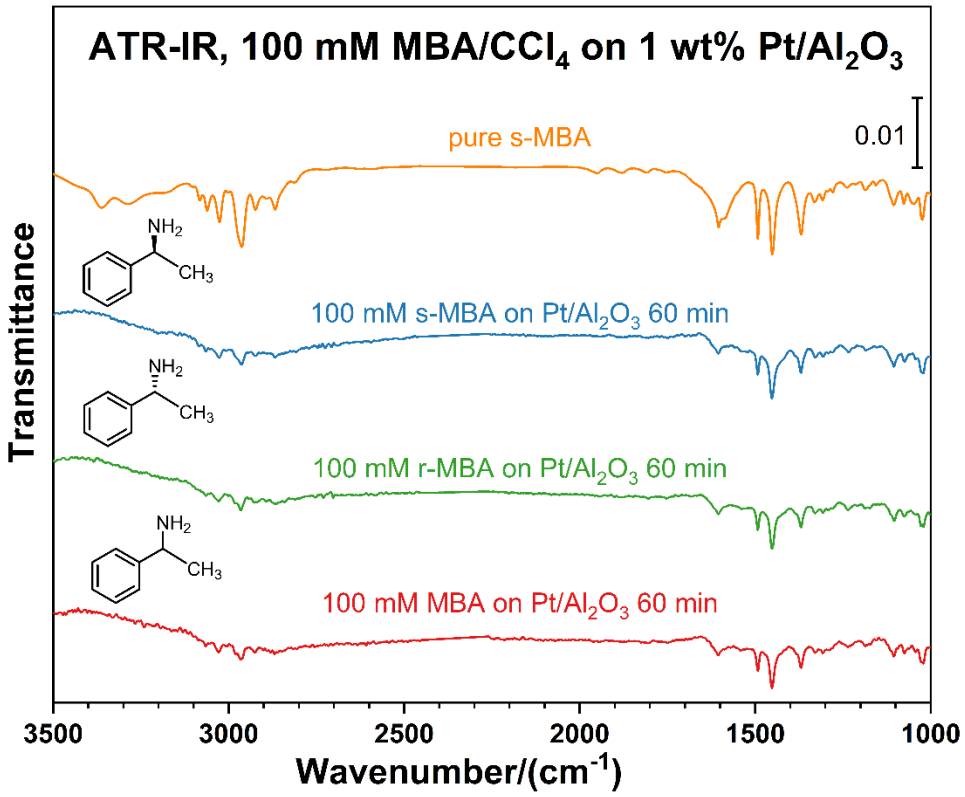

Figure 3.18 ATR-IR spectra of 100 mM s-MBA, r-MBA and MBA in CCl_4 on 1 wt% Pt/Al_2O_3 catalyst. The top trace is the transmission IR spectrum of pure s-MBA for reference.

In addition to testing a 100 mM r-MBA solution, a higher concentration of r-MBA (200 mM in CCl_4) was also examined. Figure 3.19 compares the spectrum collected from this higher concentration to that of the 100 mM r-MBA solution. The sample peaks exhibit greater intensity compared to the 100 mM solution. Furthermore, both spectra resemble the transmission IR spectrum of pure r-MBA (the top trace). No

other noticeable differences in peak positions or relative intensity were observed, suggesting that the sample peaks originate from free molecules in solution. No evidence of adsorption was obtained.

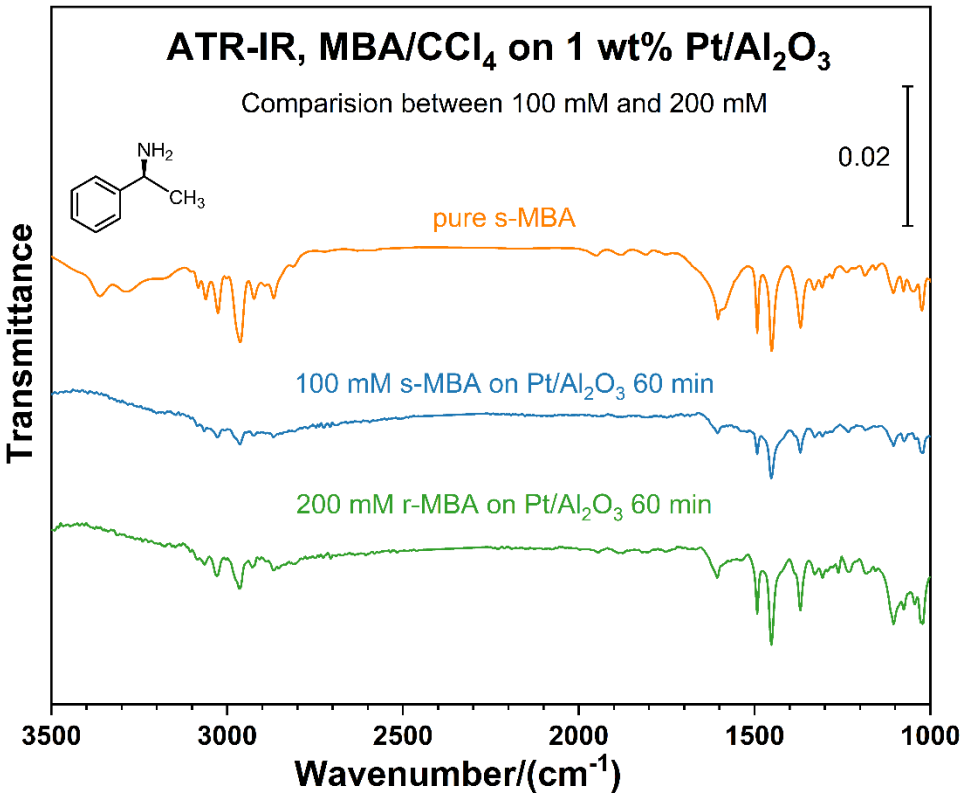

Figure 3.19 ATR-IR spectra of 100 mM and 200 mM r-MBA in CCl_4 on 1 wt% Pt/Al_2O_3 catalyst. The top trace is the transmission IR spectrum of pure s-MBA for reference.

To investigate the impact of solvents on MBA adsorption, two additional solvents, toluene and ethanol, were employed. Figure 3.20 presents the ATR-IR tests conducted with 100 mM and 200 mM s-MBA in toluene, both with and without 1 wt% Pt/Al_2O_3 catalysts. Unfortunately, no evidence of adsorption was observed. The spectra collected with Pt catalysts exhibited similarities to those obtained without a catalyst.

Furthermore, certain peaks, particularly the peak around 1260 cm^{-1}, were attributed to the toluene molecules rather than the MBA molecules.

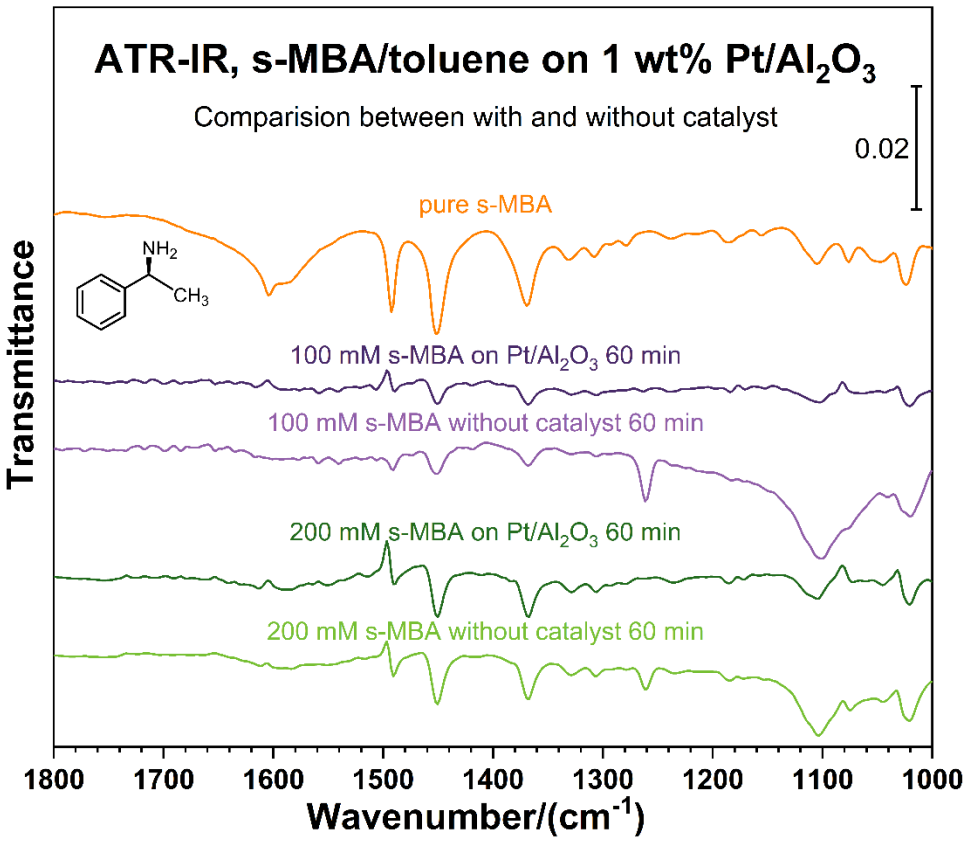

Figure 3.20 ATR-IR spectra of 100 mM and 200 mM s-MBA in toluene on 1 wt% Pt/Al_2O_3 catalyst and without catalyst. The top trace is the transmission IR spectrum of pure s-MBA for reference.

A similar trend was observed when ethanol was used as the solvent, as depicted in Figure 3.21. Both 200 mM and 500 mM s-MBA in ethanol, with and without catalyst, were tested. All the spectra exhibited similar sample peaks, except for differences in intensity. Although there were discrepancies between the ATR-IR spectra and the transmission IR spectrum of pure s-MBA, these differences could be attributed to

molecular interactions in the presence of ethanol. For instance, the peak at 1610 cm^{-1} became broader in the ethanol solution, potentially indicating interactions between s-MBA and ethanol. However, these differences were not caused by the adsorption of s-MBA molecules. Consequently, s-MBA tends to dissolve in ethanol rather than bind to Pt surfaces.

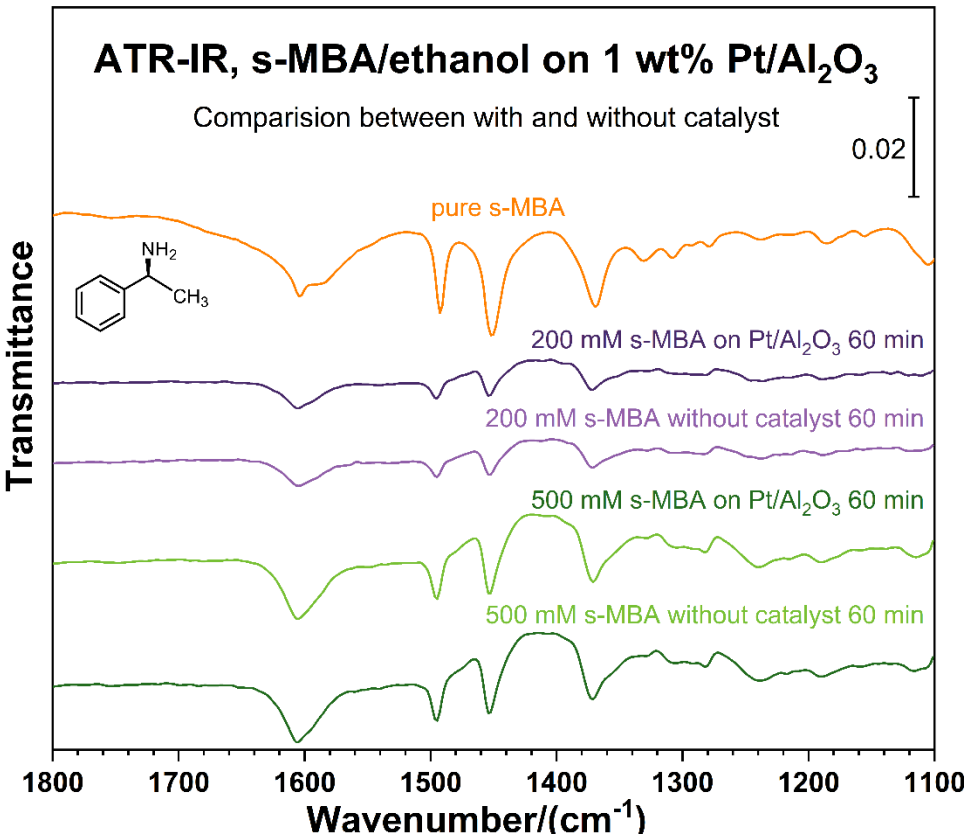

Figure 3.21 ATR-IR spectra of 200 mM and 500 mM s-MBA in ethanol on 1 wt% Pt/Al_2O_3 catalyst and without catalyst. The top trace is the transmission IR spectrum of pure s-MBA for reference.

Previous studies on NEA molecules have suggested that both 1-NEA and 2-NEA molecules bind to Pt surfaces through the amine group in CCl_4 solutions. The position of

the ethylamine group also influenced the adsorption process, as observed from the differences in the ATR-IR adsorption spectra of 1-NEA and 2-NEA. Some peak shifts might be attributed to the position of the ethylamine group. Additionally, the adsorption energy of 2-NEA on Pt catalysts was found to be higher than that of 1-NEA molecules. In contrast, the studies involving MBA molecules did not reveal any evidence of adsorption on Pt catalysts, indicating that the naphthyl ring is crucial for NEA adsorption.

3.3.5 *In-Situ* ATR-IR of 1-NEA and 2-NEA H-D Exchange

In order to further investigate our hypothesis that the adsorption of NEA would involve the breaking of one of the N−H bonds, the molecular details of the adsorption process of 1-NEA on the surface of the Pt catalyst that leads to the H−D exchange reaction were explored by using *in-situ* ATR-IR. In these experiments, the catalyst was dispersed on the top surface of the prism of the ATR cell. Subsequently, the catalyst was exposed to a solution of 1-NEA in CCl_4 while bubbling hydrogen or deuterium gas. The idea by bubbling D_2 gas aimed to determine if any N−D vibrational modes could be detected, as the formation of the N−D bond would indicate dissociation of the amine group. It is interesting to point out that no detectable 1-NEA adsorption was ever seen without prior hydrogen bubbling, an observation consistent with the reported fact that these catalysts need to be preconditioned with hydrogen for the chiral catalysis to be operational[72-74]. In our case, a slow uptake of 1-NEA on the surface was observed over a period of 2-3 h, as already reported by us and others not only with 1-NEA but also with cinchona alkaloids[72, 75-76].

Figure 3.22 contrasts the 1-NEA uptake evolution when using H_2 versus D_2. Pointedly, two new features are seen to grow in the spectra with D_2 not seen with H_2, at 1180 and 2187 cm^{-1} (the corresponding regions of the spectra are expanded in the two right panels of Figure 3.22). These signals, which are easily assigned to N−D deformation (δ_{ND}) and N−D stretching (ν_{ND}) vibrational modes, attest to the formation of new N−D bonds in the adsorbed 1-NEA.

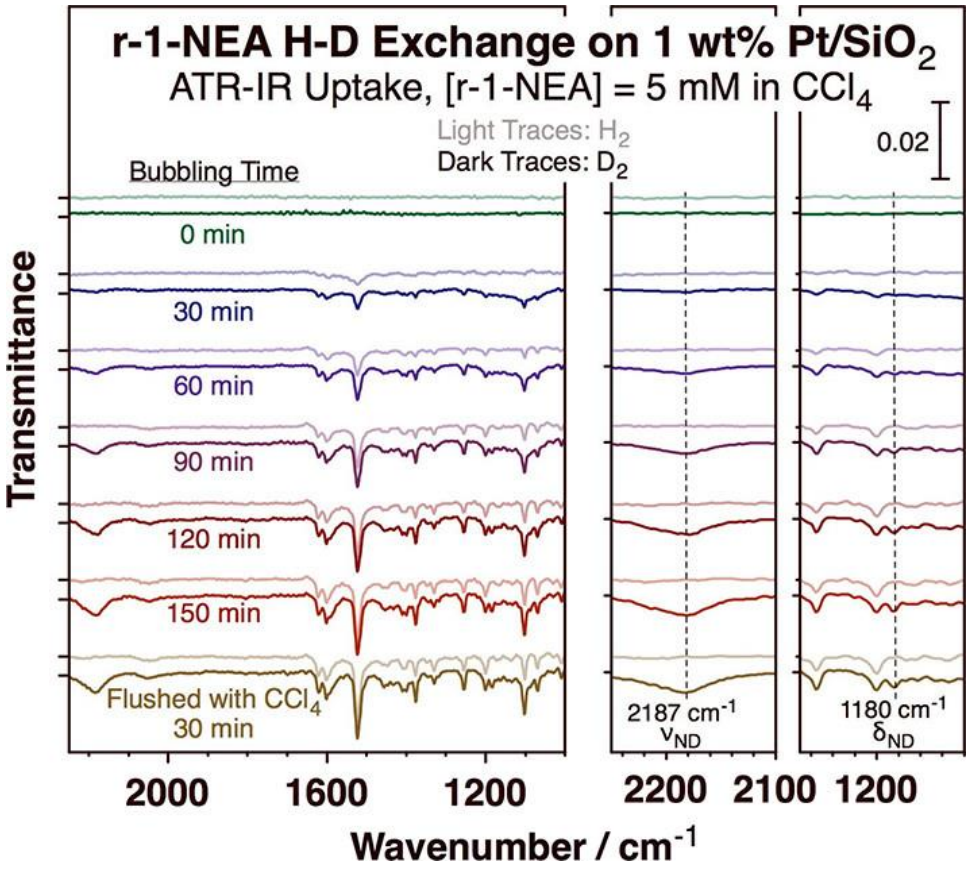

Figure 3.22 *In-situ* ATR-IR spectra obtained during the uptake of 5 mM r-1-NEA from a CCl_4 solution onto a 1 wt% Pt/SiO_2 catalyst while bubbling either H_2 (light traces) or D_2 (dark traces), plotted versus exposure time. Reprinted with permission from reference 55. Copyright 2022 American Chemical Society.

The behavior indicated in Figure 3.22 proved to be quite general. Figure 3.23, for instance, which displays the ATR-IR s-1-NEA on either Pt/SiO_2 or Pt/Al_2O_3 catalysts, indicates the incorporation of deuterium into the 1-NEA molecule in all cases: the δ_{ND} (1180-1185 cm^{-1}) and ν_{ND} (2181-2187 cm^{-1}) peaks identified above are seen in all the spectra with D_2 but not in any of the experiments with H_2.

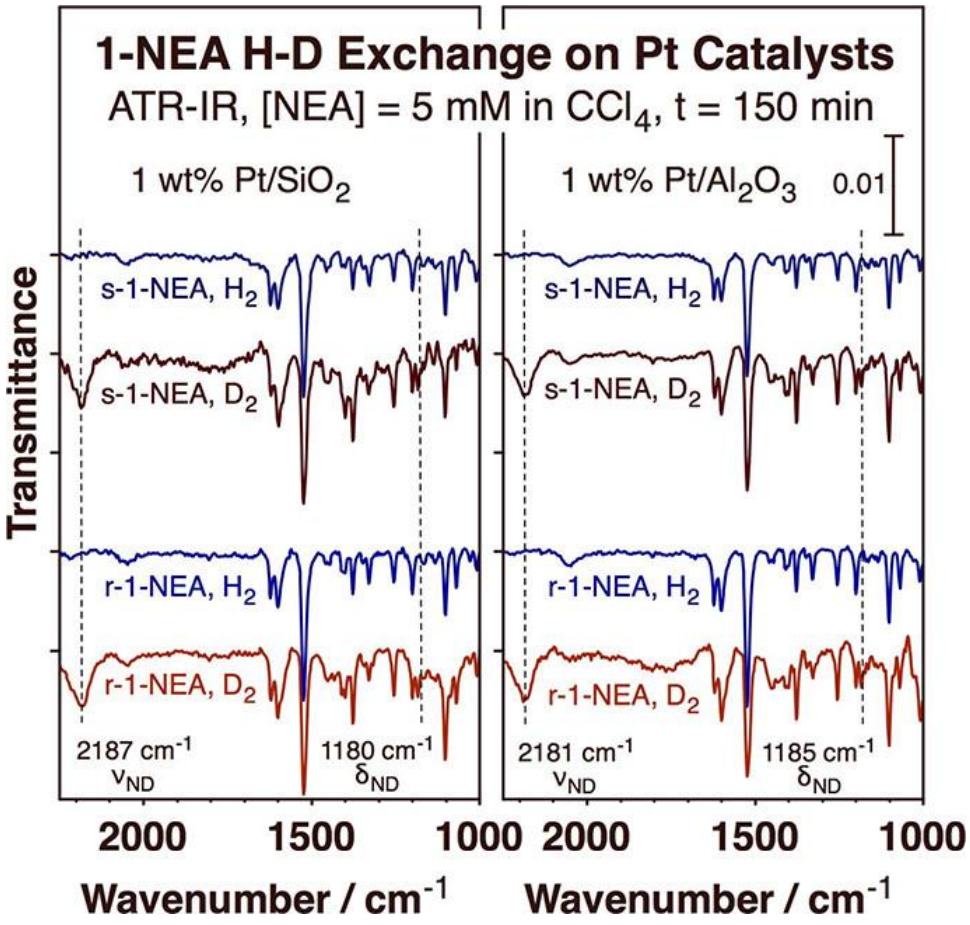

Figure 3.23 *In-situ* ATR-IR spectra obtained after 150 min of uptake of either s- (top two traces) or r- (bottom two) 1-NEA from CCl_4 solutions onto a Pt/SiO_2 (left) or a Pt/Al_2O_3 (right) catalyst while bubbling either H_2 (blue traces) or D_2 (red traces). Reprinted with permission from reference 55. Copyright 2022 American Chemical Society.

The reversibility of the H−D exchange process was also investigated, and the results are present in Figure 3.24. Initially, a solution of 1 mM r-1-NEA saturated with D_2 gas was introduced into the ATR cell, revealing two distinct features associated with the N−D bond. Subsequently, the gas was switched to H_2, and spectra were collected while bubbling H_2, as shown in the enlarged panel on the right. It is noteworthy that the relative intensity of the peak around 1184 cm^{-1} decreased significantly, indicating an irreversible H−D exchange.

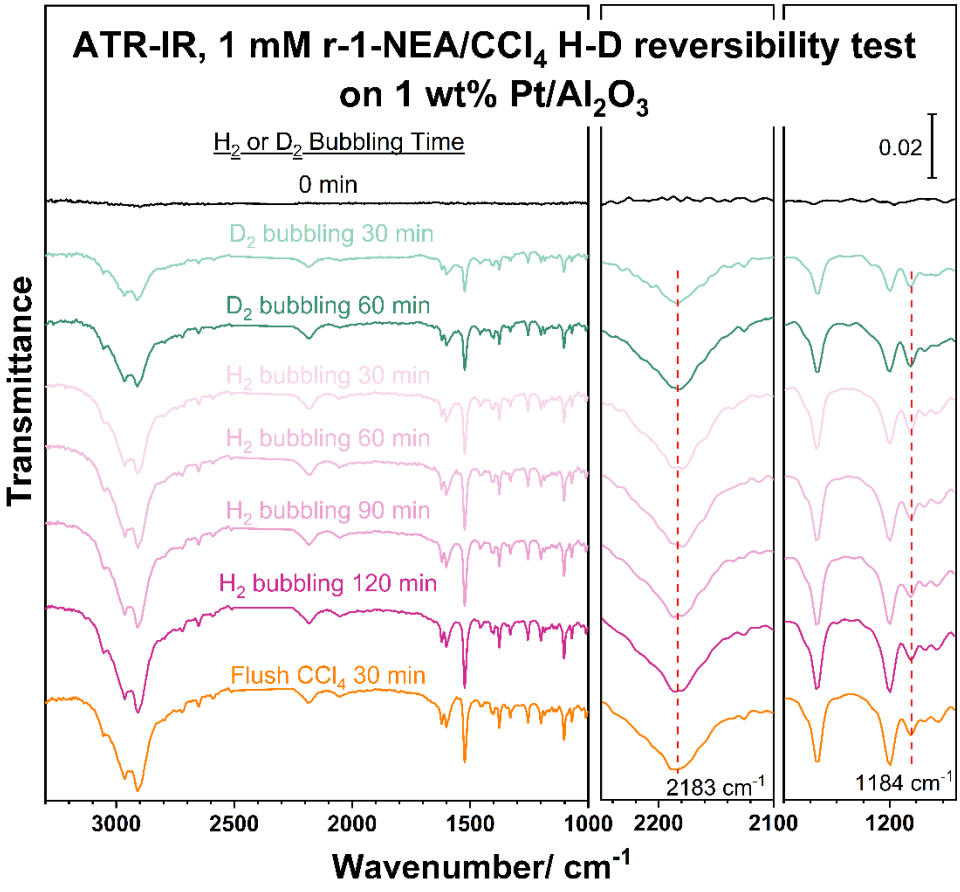

Figure 3.24 *In-situ* ATR-IR spectra obtained during the uptake of 1 mM r-1-NEA from a CCl_4 solution onto a 1 wt% Pt/Al_2O_3 catalyst while first bubbling D_2, then with H_2, plotted versus bubbling time.

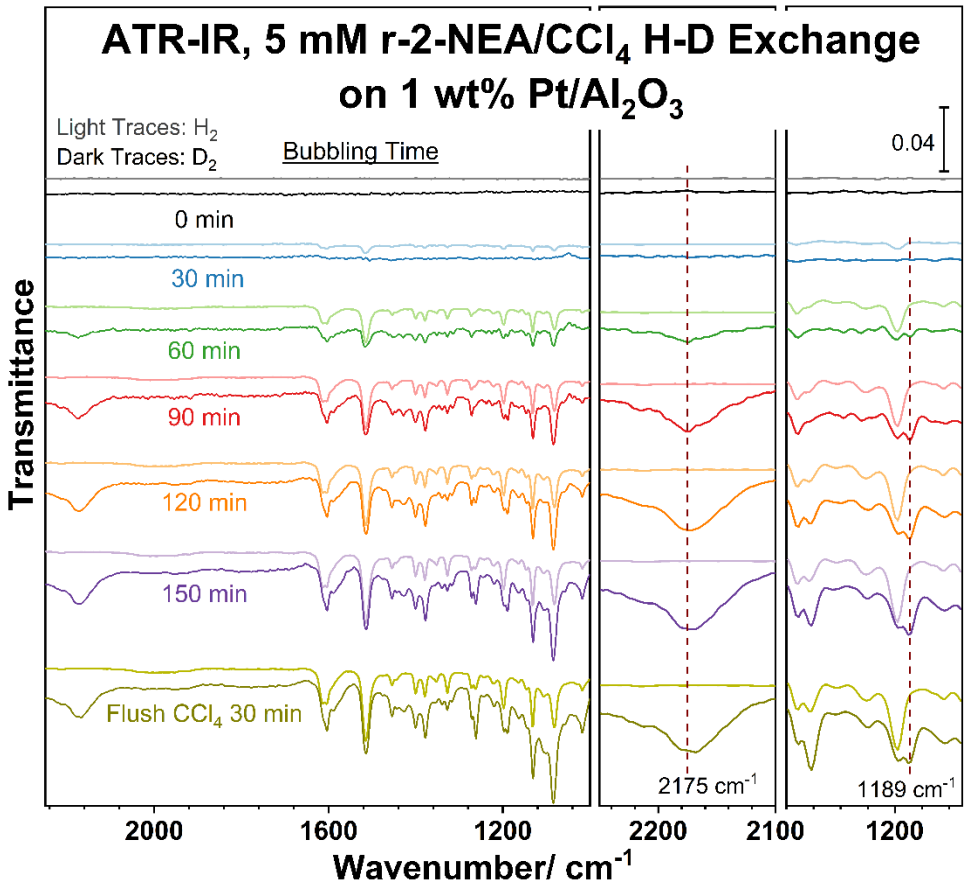

Figure 3.25 *In-situ* ATR-IR spectra obtained during the uptake of 5 mM r-2-NEA from a CCl_4 solution onto a 1 wt% Pt/Al_2O_3 catalyst while bubbling either H_2 (light traces) or D_2 (dark traces), plotted versus exposure time.

The same behavior was seen with 2-NEA as well. As shown in Figure 3.25, two features around 2175 and 1189 cm^{-1} were clearly detected in the case of 5 mM r-2-NEA in CCl_4 solution, the two features slightly shifted compared to 1-NEA molecules. Both r-2-NEA and s-2NEA showed similar behavior as indicated in Figure 3.26, which display

the ATR-IR of r- and s-2-NEA on either Pt/SiO_2 or Pt/Al_2O_3 catalysts, the features related to N−D formation was seen in all cases.

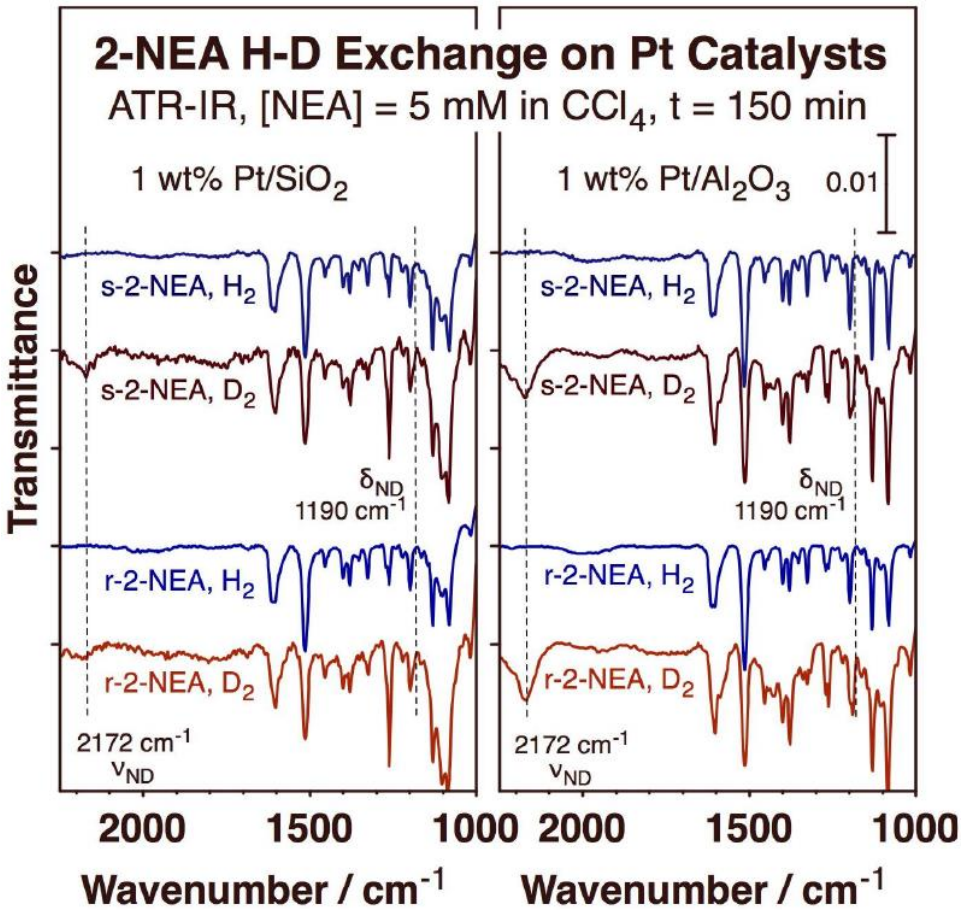

Figure 3.26 *In-situ* ATR-IR spectra obtained after 150 min of uptake of either s- (top two traces) or r- (bottom two) 2-NEA from CCl_4 solutions onto a Pt/SiO_2 (left) or a Pt/Al_2O_3 (right) catalyst while bubbling either H_2 (blue traces) or D_2 (red traces). Reprinted with permission from reference 55. Copyright 2022 American Chemical Society.

It should also be indicated that, under the conditions of these experiments, the NEA adsorption and the formation of the new surface intermediate are irreversible, a conclusion indicated by the fact that flushing with a pure solvent after the uptake results

in no changes in the positions or intensities of any of the IR peaks (bottom traces in Figure 3.22 and Figure 3.25). No desorption is observed in any of these systems.

3.3.6 ^{1}H-NMR Characterization of r-1-NEA H−D Exchange

The evidence for the interaction of the amine nitrogen atom in the NEA molecule adsorbed from solution with platinum surfaces was also obtained from reactivity studies using ^{1}H-NMR and GC-MS analysis of NEA solutions as they were allowed to react with D_2 gas. In these experiments, the mixture of chiral modifiers with Pt catalysts was bubbled with D_2 gas, then the samples at different reaction times will be collected and analyzed by both ^{1}H-NMR and GC-MS to see if there are any differences with reaction time.

Figure 3.27 below shows the ^{1}H-NMR results of a mixture of 20 mM r-1-NEA in CCl_4 with 25 mg commercial 1 wt% Pt/Al_2O_3 catalysts as a function of the time it was exposed to an atmosphere of D_2 gas. The total reaction time is 8.0 hours and the samples were collected and then analyzed every two hours. The molecule structure of r-1-NEA was inserted in the figure, and every H atom was numbered. The signals between 8.5 ppm and 7.2 ppm are assigned to H atoms from the aromatic rings (H_1-H_7); the H atom bonded to the chiral carbon (H_8) appears at 5.1 ppm. A doublet between 1.65 and 1.7 ppm is assigned to the H atoms (H_9) in the terminal methyl group, while a broad peak around 1.5 ppm is ascribed to the H atoms (H_{10}) from the amine group. The area of both peaks were seen decreasing with reaction time, indicating the H atoms were slowly exchanging with deuterium. A new peak around 1.45 ppm was observed to gradually increase with

reaction time, which could be assigned to the H atoms (H_{10}') on the newly formed R−NHD H−D exchanged amine.

The quantification of H atoms substituted by D atoms in the amine group was determined by using the areas of H_{10} (~1.5 ppm) and H_{10}' (~1.45 ppm) peaks, scaled relative to the signals for six H atoms (H_1-H_6) of the aromatic ring. The H_7 atom was not included because the signal is a little bit noisy. As indicated in the right hand side of Figure 3.27, the average number of D atoms incorporated in the r-1-NEA molecules were estimated using the data from three independent H−D exchange experiments. It is clearly seen that the extent of H−D exchange increased with reaction time. Initially, the peak area of H_{10} is 2, which means that the x value is zero. With the D_2 bubbling time increased, the x value increased from 0 to about 1.73 after about 8.0 hours. It was expected that the H atoms from the amine group would be substituted by D atoms if given sufficient time.

In addition, the peak of H_9 (a double let between 1.7 and 1.6 ppm) was seen to shift slightly with time, the slower and less extensive isotope exchange was observed at the H_9 position. However, for all other hydrogen atoms, the signal intensity incorporated at each position versus reaction time.

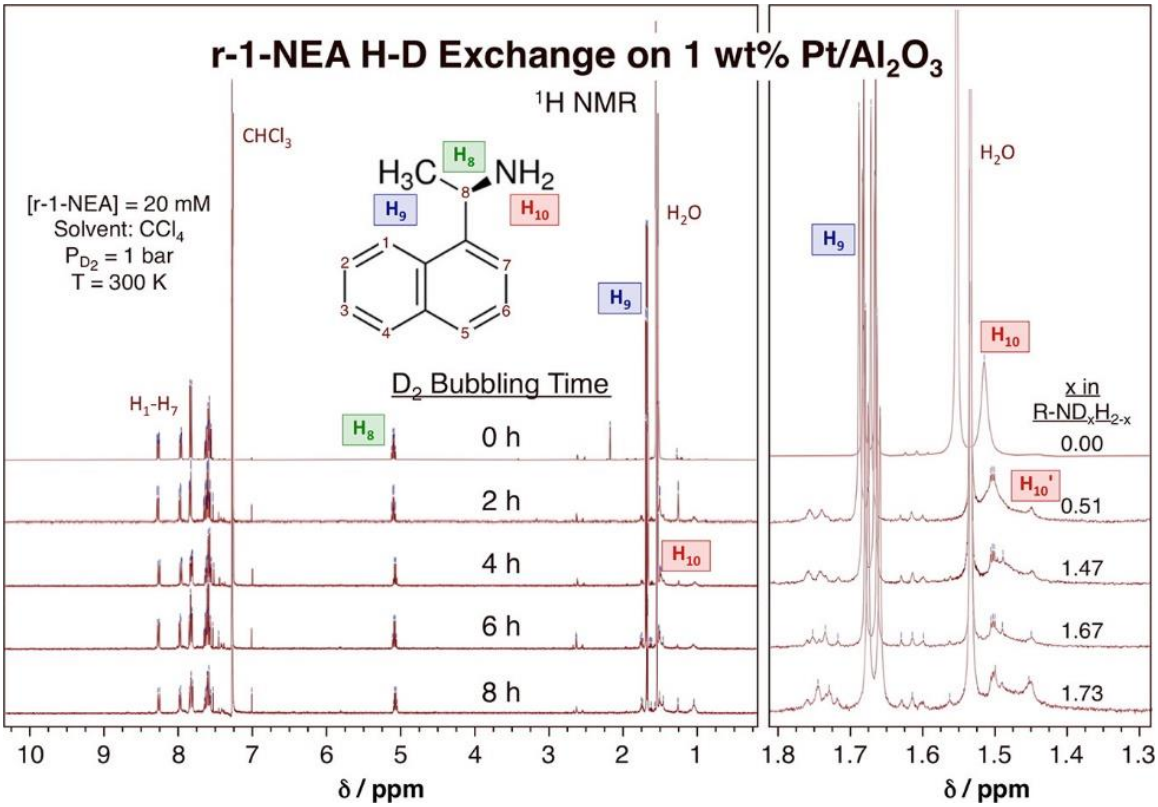

Figure 3.27 ^{1}H-NMR of an r-1-NEA solution in CCl_4 as a function of the time it was exposed to an atmosphere of D_2 while in contact with a Pt/Al_2O_3 catalyst. Reprinted with permission from reference 55. Copyright 2022 American Chemical Society.

As mentioned above, three independent kinetic experiments were performed to estimate the x values in Figure 3.27 to make sure that the observations are within the accuracy of the experiments. The Figure 3.28 shows the calculated fraction of all H atoms exchanged during the reaction time. The fraction of H_{10} and H_{10}' was clearly seen increasing with time, while the fraction of H_9 and H_7 also slowly increased.

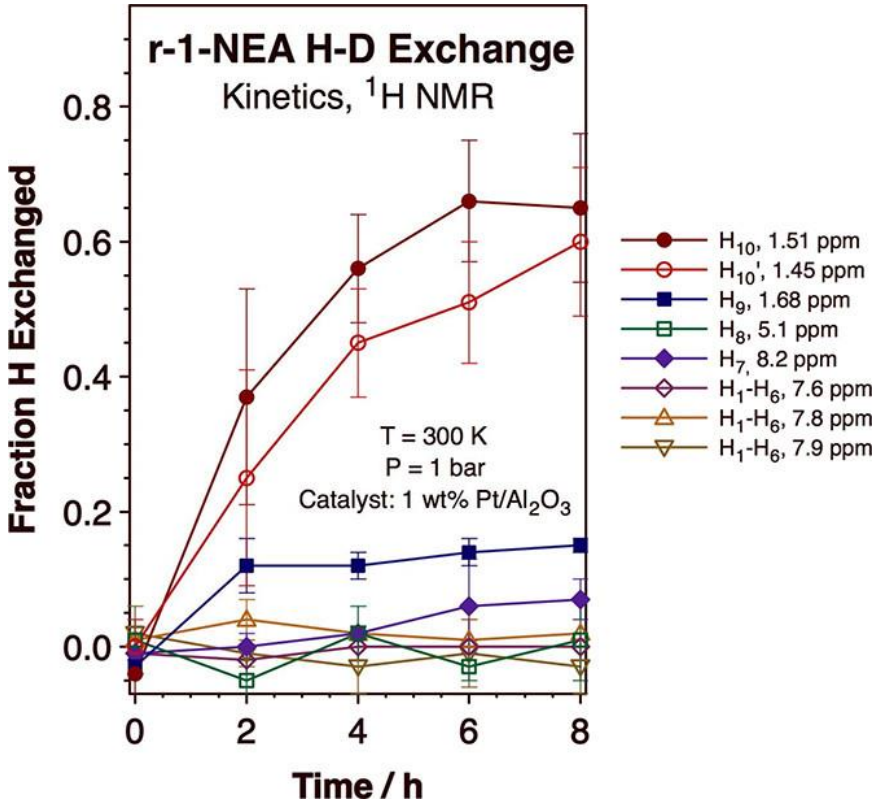

Figure 3.28 H-D exchange kinetics for r-1-NEA on Pt/Al_2O_3, measured using ^{1}H-NMR. The values and error bars were estimated using data from three independent kinetic runs. Reprinted with permission from reference 55. Copyright 2022 American Chemical Society.

The blank tests without catalysts were also carried out, the same concentration of r-1-NEA in CCl_4 was bubbled with D_2 gas without catalysts, and the samples were taken every two hours and then analyzed by ^{1}H-NMR. Figure 3.29 below shows the ^{1}H-NMR spectra of the blank test, and Table 3.2 indicates the peak integrals of all H atoms by using the peak around 8.2 ppm as a reference. As indicated in Figure 3.29, the single and broad peak around 1.5 ppm is assigned to H atoms from the amine group, which was not seen to be changing during the blank experiment. It is more straightforward to be seen in

Table 3.2, the integrals of all signals did not change significantly after bubbling D_2 for 4 hours without catalysts.

Therefore, the kinetics estimated using the signals for the H_{10} and H_{10}' peaks agree with each other within our experimental error, a fact that provides additional confirmation of the Pt-catalyzed isotope substitution at the amine group of NEA.

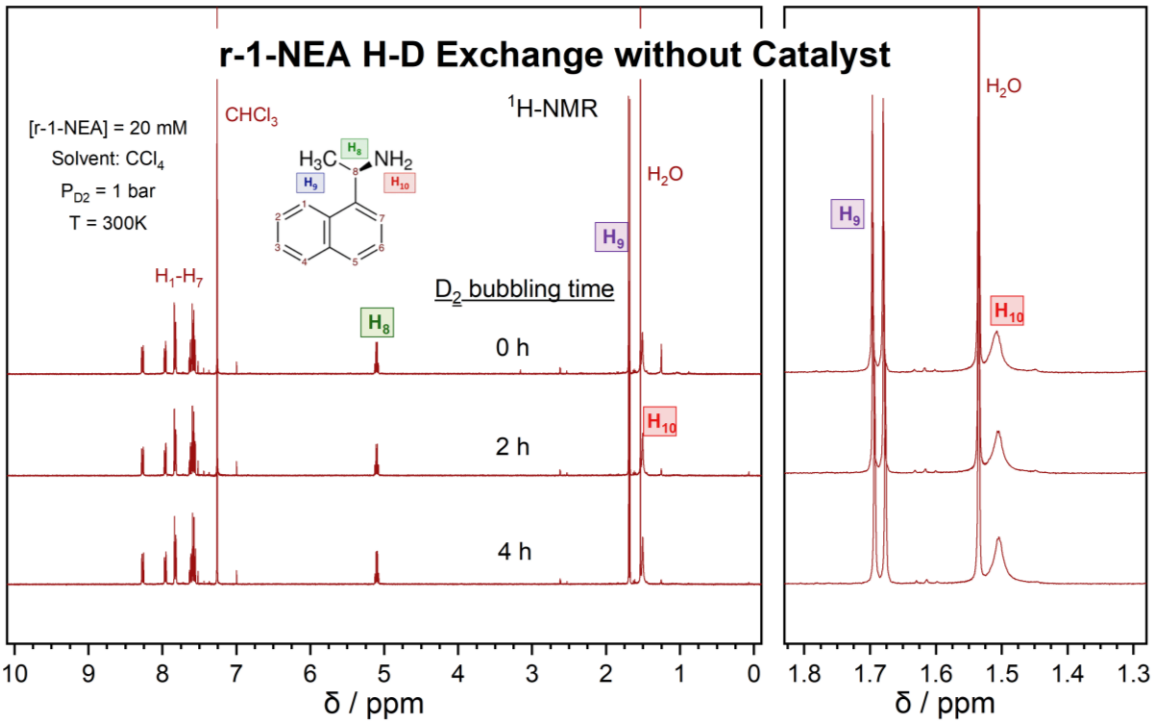

Figure 3.29 ^{1}H-NMR of an r-1-NEA solution in CCl_4 as a function of the time it was exposed to an atmosphere of D_2 without a catalyst.

Table 3.2 Kinetic experiment of r-1-NEA carried out without catalyst (referenced to the total H_1-H_6 signal, scaled to correspond to 6 H atoms).

Peak position		Pure r-1-NEA without catalyst	D_2 2.0 h without catalyst	D_2 4.0 h without catalyst
H_1-H_6	~8.2 ppm	1.00	1.00	1.00
	~7.9 ppm	1.02	1.02	1.03
	~7.8 ppm	1.95	1.96	1.95
	~7.6 ppm	3.03	3.02	3.02
H_7	~8.2 ppm	1.03	1.02	1.04
H_8	~5.1 ppm	1.10	1.09	1.08
H_9	~1.68 ppm	3.00	2.96	2.96
H_{10}	~1.51 ppm	1.98	1.98	1.95

3.3.7 GC-MS Characterization of r-1-NEA H−D Exchange

Corroborating evidence for the H−D reaction with 1-NEA was provided by results from GC-MS. One example of r-1-NEA H-D exchange on 1 wt% Pt/Al_2O_3 was provided in Figure 3.30. The left panel shows the GC traces obtained for the reaction mixture as a function of time. A large peak at retention times between approximately 7.45 and 7.6 min followed by a skewed feature extending to 8 min was seen, which is assigned to regular r-1-NEA molecules. In addition, a small but sharp new peak that develops over time at 7.60 min. The right panel shows not only the peaks expected for r-1-NEA but also a growing feature at 172 amu, the mass of molecular r-1-NEA-d_1. By taking the ratio of 172 amu (r-

1-NEA-d_1) over the 171 amu (r-1-NEA-d_0), as indicated in the right panel, the ratio does increase with time.

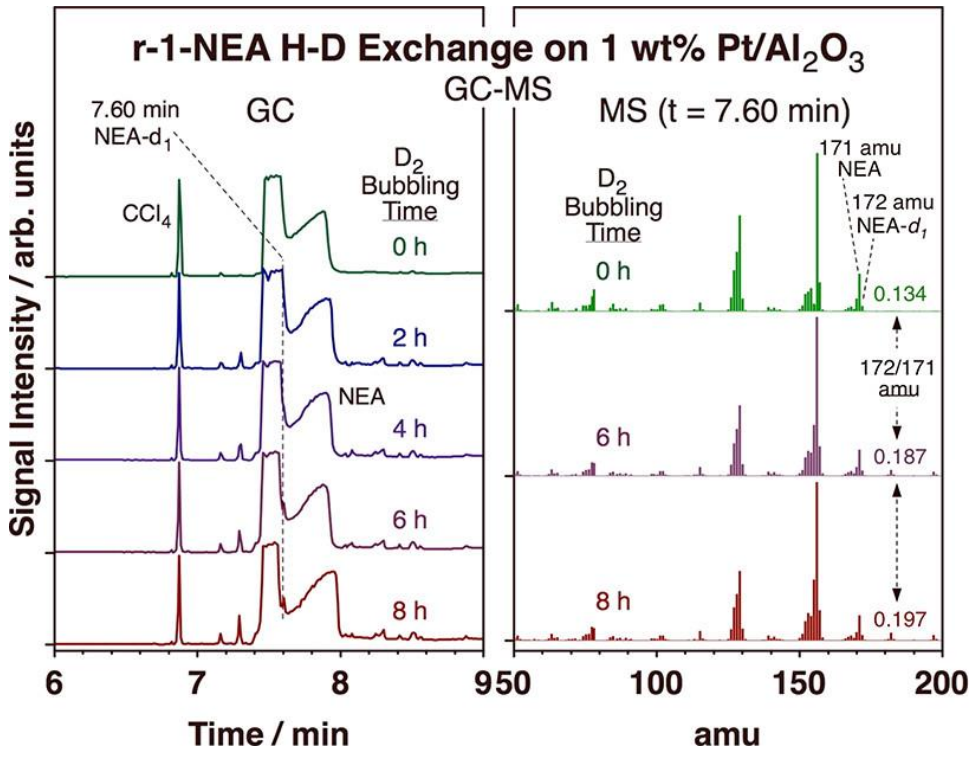

Figure 3.30 GC-MS data from the H-D exchange experiment of 20 mM r-1-NEA in CCl_4 solution mixed with 25 mg 1 wt% Pt/Al_2O_3 bubbled with D_2 gas. The samples were taken every 2 hours and the total reaction time is 8 hours. Reprinted with permission from reference 55. Copyright 2022 American Chemical Society.

In addition, two small peaks around 7.1 min and 7.3 min were seen increasing with reaction time as shown in the GC spectra (left panel) of Figure 3.30, which are actually small amount of decompositions of the r-1-NEA. The corresponding MS data is shown in Figure 3.31 and Figure 3.32. The growing peak at 7.1 min is assigned to 1-naphthyl ethane, while the peak around 7.3 min corresponds to 1-nanphthyl-1-$_D$-methane. However, both of them are minor and not relevant to the chemistry being discussed here.

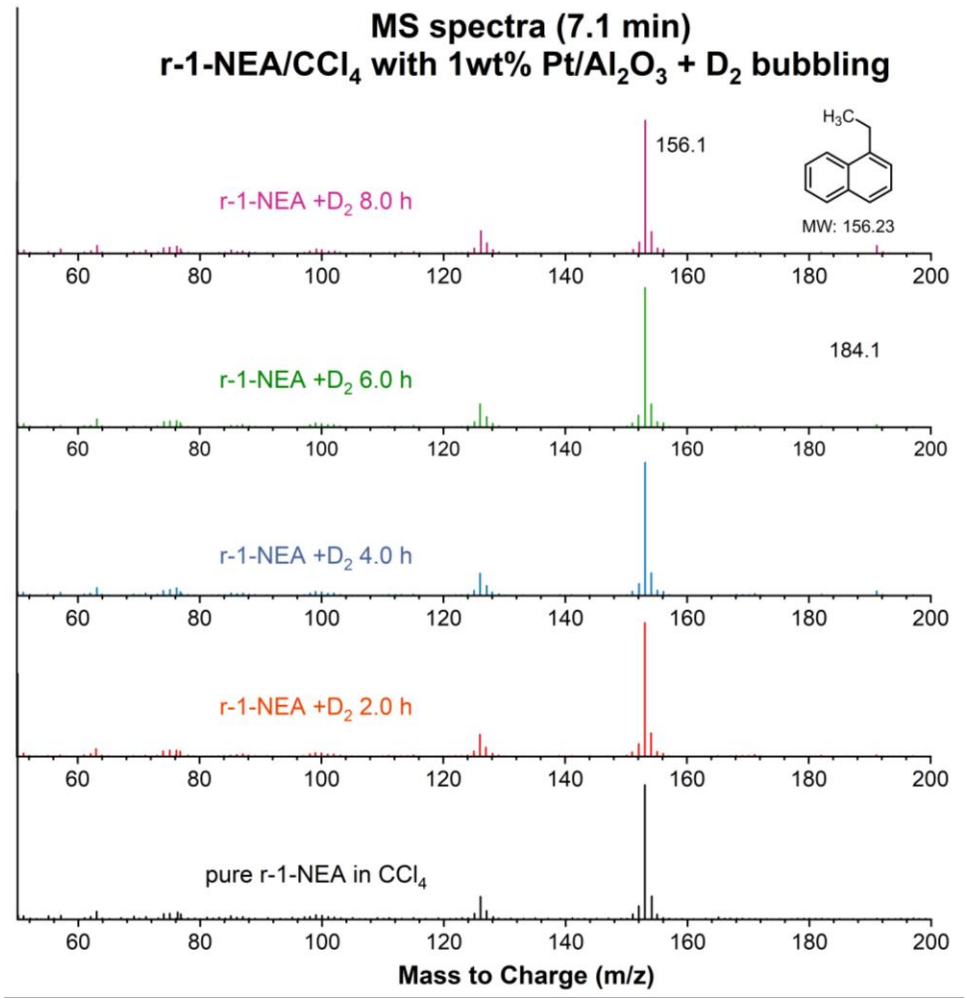

Figure 3.31 The MS of the mixture at 7.10 min elution time as indicated in the left panel of Figure 3.30.

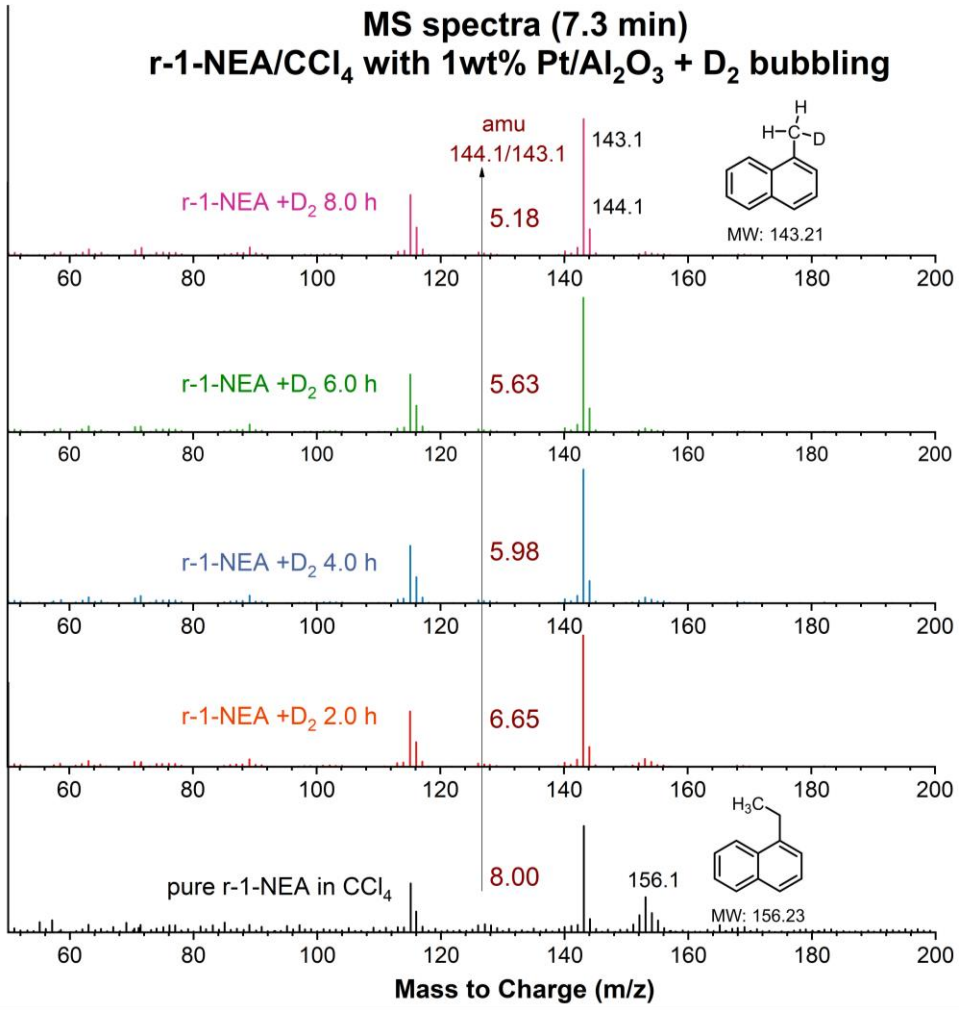

Figure 3.32 The MS of the mixture at 7.30 min elution time as indicated in the left panel of Figure 3.30.

3.3.8 The Mechanism of H−D Exchange

The next question to address here is what the mechanism may be by which the H−D exchange occurs. In this section, all of the theoretical calculations were performed by our collaborators as mentioned in the Acknowledge section. Two straightforward and simple options can be put forward, as illustrated in Figure 3.33, one pathway is involved in the initial deprotonation of 1-NEA at the amine nitrogen upon adsorption followed by

the addition of a deuterium atom from the metal surface, and the reverse deuteration of the amine position on the surface and the subsequent loss of a hydrogen atom.

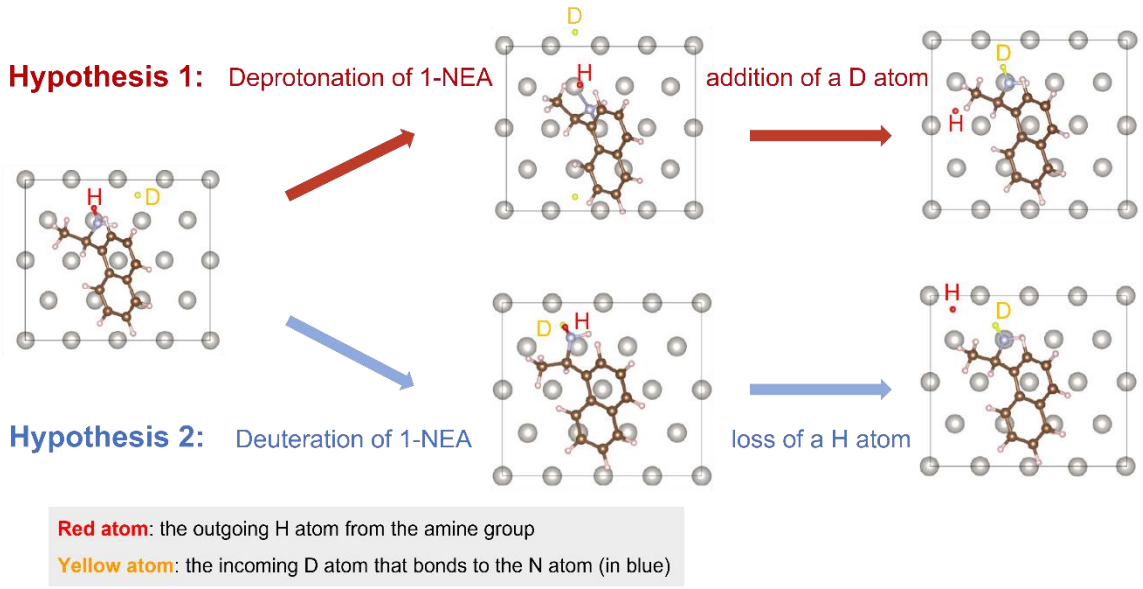

Figure 3.33 Illustration of two hypotheses of 1-NEA H−D exchange pathways. Adapted with permission from reference 55. Copyright 2022 American Chemical Society.

The energetics of these two possible reaction pathways was mapped out using DFT calculations; the results are shown in Figure 3.34, (red, top, traces for the first pathway; blue, bottom, data for the second). It is clear that, from the energy point of view, the second pathway, involving an initial protonation of the adsorbed NEA (blue trace), is favored as it requires overcoming a total energy barrier (to TS2, relative to the starting point) of only 76 kJ/mol; the first route, which involves an initial deprotonation step, displays an equivalent total barrier of 172 kJ/mol high (red trace). More details of these calculations, including drawings of the intermediate structures that form on the

surface during the incorporation and ejection of H/D atoms into/from the adsorbed 1-NEA molecule, are provided in the supporting information of our published paper.

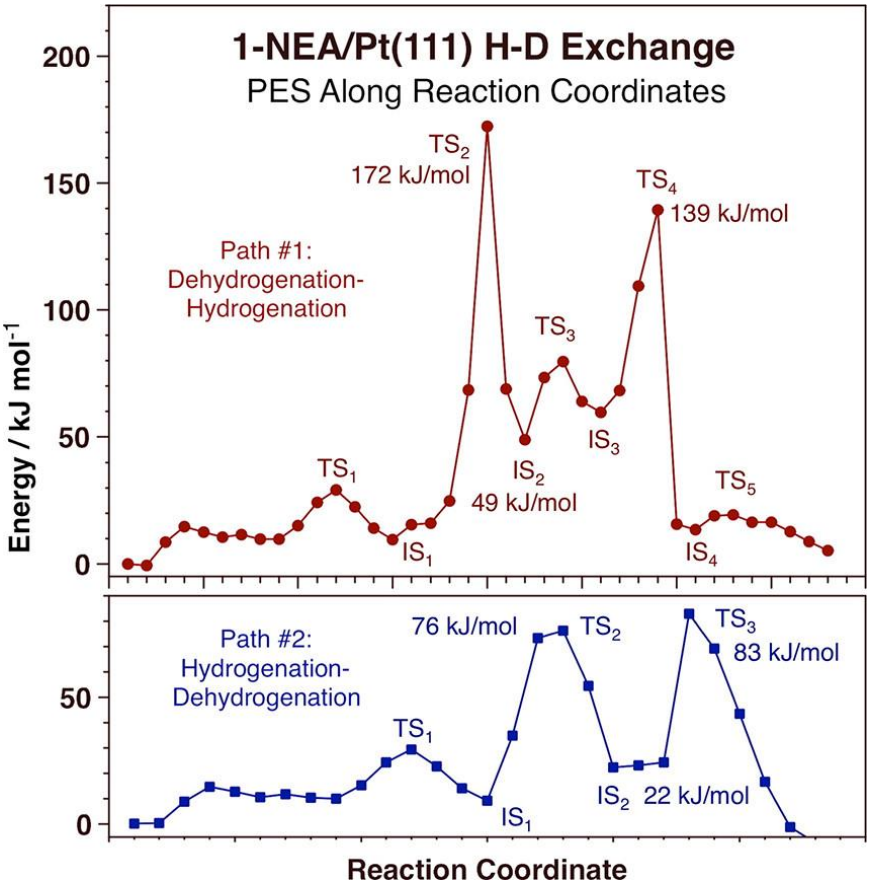

Figure 3.34 Calculated potential energy surfaces along the reaction coordinates for two possible mechanisms for the H−D exchange in 1-NEA promoted by Pt surfaces. Reprinted with permission from reference 55. Copyright 2022 American Chemical Society.

The ATR-IR data in Figure 3.22 and Figure 3.23 clearly show the formation of a new N−D bond upon the bubbling of D_2 but that does not directly address the questions related to the structure of the adsorbed NEA. This is a particularly critical aspect of the study of enantioselective catalysis aided by chiral modifiers because the *in situ* IR spectra

of the modifier adsorbed on the metal surface from liquid solutions have been shown to be very different from those acquired for the adsorbate in UHV or for the free molecules in solution[77-78]. It is clear that the presence of the liquid in contact with the catalyst affects the nature of the adsorbed molecules, but this effect cannot be fully ascribed to the solution alone. Complementary density functional theory (DFT) calculations were carried out to better understand these changes. First, the adsorption structures of pure 1-NEA and of NEA with one less or one more amine hydrogen (that is, deprotonated or protonated) were optimized, and simulated IR spectra were estimated to compare with the experimental data. The results are shown in Figure 3.35. The left panel reports the results, in the form of peak positions and peak intensities, for s-1-NEA in two different configurations, namely, adsorbed with the aromatic ring either flat or tilted with respect to the Pt surface, and for optimized adsorption geometries for the s-1-NEA molecule after either protonation or deprotonation of the amine group. It can be seen that all these options yield very different IR spectra. It should be noted, though, that the DFT IR simulations have a number of limitations and should therefore be analyzed with caution. For one, it is known that, because of the anharmonicity of the potentials around the minimum energy corresponding to the different bonds, quantum mechanics simulations miscalculate the true vibrational frequencies. This is typically addressed by scaling the frequencies in the calculated spectra using an empirical multiplicative factor[66-68]; that factor was optimized here to best fit the experimental data, as discussed later. In addition, the calculated peak intensities depend on adsorption geometries and do not account for

the free rotation of the groups around single bonds that occurs within the ethylamine moiety in 1-NEA.

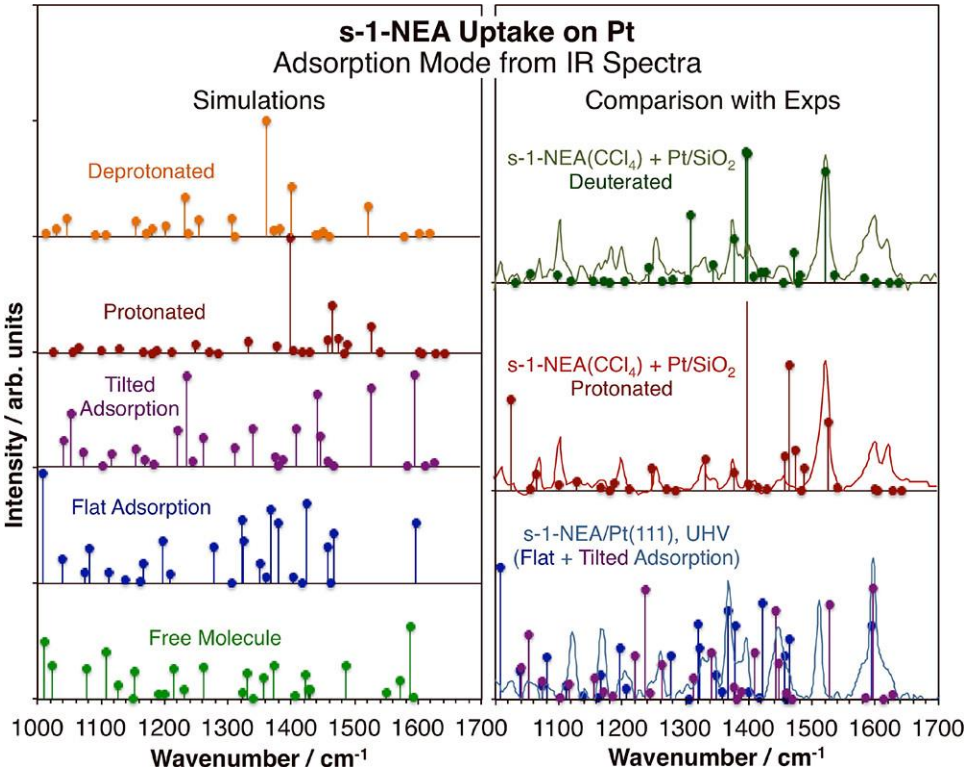

Figure 3.35 DFT-simulated IR spectra for s-1-NEA in different environments. Left: peak positions and peak intensities estimated from DFT calculations. Right: best fits to the experimental spectra for s-1-NEA adsorbed on Pt(111) in UHV and on a Pt/SiO_2 catalyst from a CCl_4 solution. Also shown are the spectrum and best fit for the latter case when D_2 instead of H_2 is bubbled through the solution. Reprinted with permission from reference 55. Copyright 2022 American Chemical Society.

In spite of these shortcomings, we have here attempted to identify the nature of the adsorbed species using simulated spectra. The key results are displayed in the right panel of Figure 3.35, and more details are provided in the supporting information of the published paper (the vibrational peak assignments are slightly different from those provided in previous reports). To decide on the simulated spectra that best interpret each

of the experimental traces, a minimum square fitting of the frequency values (experimental minus calculated) was carried out with each option as a function of the scaling factor used in the calculations, and the results with the smallest standard deviation were chosen.

Three cases are shown in Figure 3.35. In the first case (bottom, light blue trace and blue and purple bars), the spectra for s-1-NEA adsorbed on Pt (111) under UHV are interpreted in terms of a combination of flat and tilted-ring geometries; the best fit is to the tilted arrangement, but some important peaks are missed and only accounted for with a flat coadsorbate. It should be noted that most reports have concluded that NEA adsorption on bulk metal surfaces under vacuum leads to a flat geometry, but a recent IR study[79] has suggested the possibility of the formation of a tilted adsorbate at high coverages.

The second comparison is for s-1-NEA adsorbed on a Pt/SiO_2 catalyst from a CCl_4 solution (red trace and bars), and it also applies to adsorption on either a Pt foil or a Pt/Al_2O_3 catalyst since those spectra all look similar[40, 78, 80]. In this case, the best fit is to a protonated NEA adsorbate, a result that not only is consistent with the H−D exchange reaction reported above but also helps explain a number of previously unaccounted for observations. First, the IR spectrum adsorbed from solution looks completely different from those obtained for the pure compound, for the compound dissolved in a liquid solvent, or for NEA absorbed on Pt surfaces under vacuum[77-78]. It is possible that, while adsorption of NEA on the metal surface preserves the molecular stoichiometry of the chiral modifier, at a liquid-solid interface it leads to hydrogen incorporation, so the new

IR spectra correspond to adsorbed protonated 1-NEA (1-NEA + H or 1-NEA + D) instead. We speculate that the solvent may help stabilize the additional charges added to the adsorbate after protonation; according to our Bader charge calculations, the electronic charge of the N atom goes from −0.89 in deprotonated 1-NEA (1-NEA-H) to −1.04 ± 0.02 in 1-NEA and to −1.13 in 1-NEA + H, all adsorbed on Pt(111).

The second observation explained by our data is the need for hydrogen pre-conditioning of the surface to induce the efficient uptake of chiral modifiers[72, 74, 81]. In fact, it has also been shown that the addition of acids to the solution to protonate the chiral modifier helps improve the enantioselective performance of the catalyst[82]. It should also be indicated that, in our in situ ATR-IR experiments, deuterium incorporation into the adsorbed 1-NEA is only seen if the surface is exposed to D_2 prior to the addition of the chiral modifier to the solution; bubbling of D_2 after 1-NEA surface saturation does not result in the development of the new IR peaks reported above as shown in Figure 3.36. Two sets of experiments were carried out in each case, pre-treating the surface with either H_2 (top, green) or D_2 (third from top, purple) prior to the 1-NEA adsorption, and exposing the adsorbed layer to pure CCl_4 while bubbling either H_2 (second from top, blue) or D_2 (bottom, red) after 1-NEA surface saturation. The deuterium incorporation in the N atom of the r-1-NEA, indicated by the new features at 1187 and 2187 cm^{-1}, is only seen in the case of the D_2 surface preconditioning.

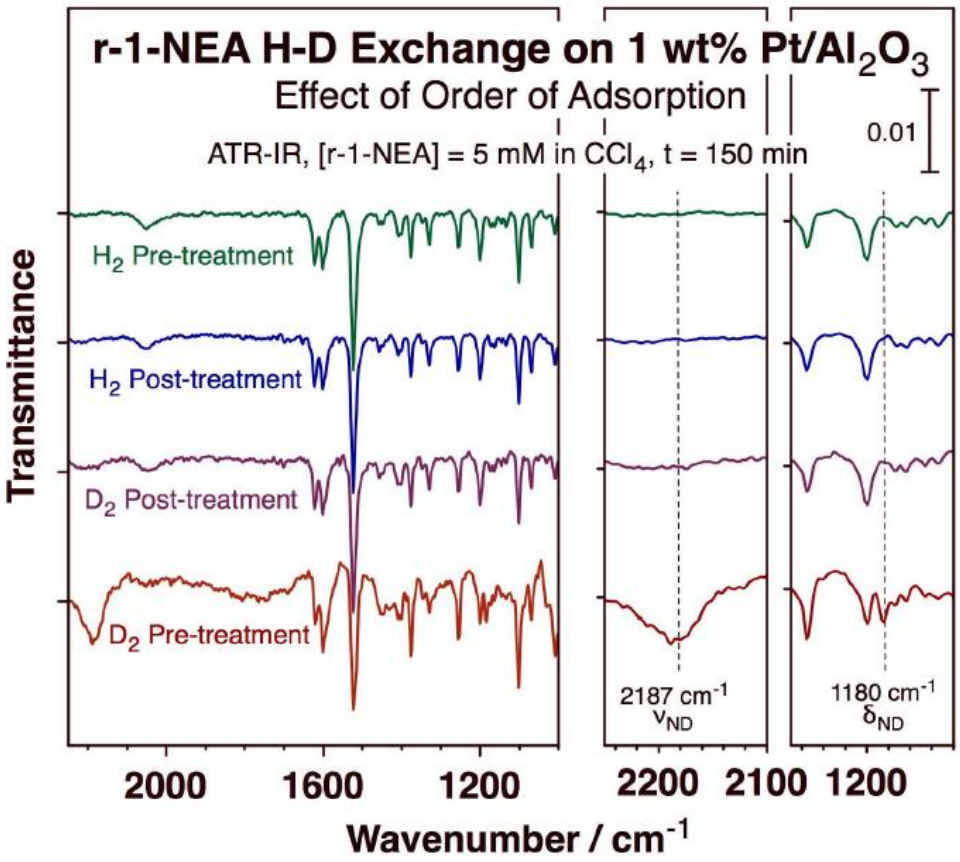

Figure 3.36 ATR-IR spectra obtained after 150 min of uptake of r-1-NEA from CCl_4 solution onto a Pt/Al_2O_3 catalyst while bubbling either H_2 (top two traces, green and blue) or D_2 (bottom two traces, purple and red). Reprinted with permission from reference 55. Copyright 2022 American Chemical Society.

The third reported case in Figure 3.35 is that of s-1-NEA adsorbed from a CCl_4 solution while bubbling D_2 instead of H_2. Again, the fit of the DFT-calculated data to the experimental results is less than ideal, but the spectra are reasonably well accounted for by a monodeuterated adsorbed amine where the amine group rotates freely around its axis. This amine protonation/deuteration seems to also be quite general: the development of the new N−D vibrational bands is seen not only in 2-NEA, as mentioned before (Figure 3.25 and Figure 3.26), but also in cinchonine (Cn), as shown in Figure 3.37.

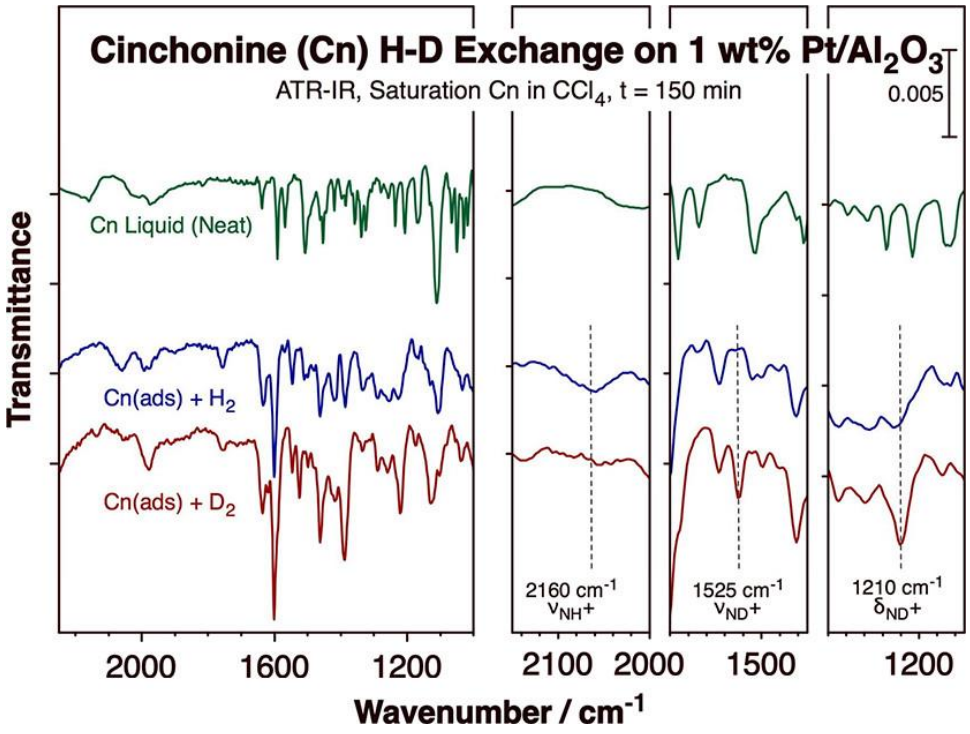

Figure 3.37 *In-situ* ATR-IR spectra obtained after 150 min of uptake of cinchonine (Cn) from a CCl_4 solution onto a Pt/Al_2O_3 catalyst while bubbling either H_2 (middle, blue, trace) or D_2 (bottom, red, trace). The spectrum of Cn in solution (top, green) is also provided for reference. Reprinted with permission from reference 55. Copyright 2022 American Chemical Society.

In this case, the two new features associated with the deformation (δ_{ND}^{+}) and stretching (ν_{ND}^{+}) modes of the N−D^+ bond that forms upon deuteration of the quinuclidine amine nitrogen are seen at 1210 and 1525 cm^{-1}, respectively. In addition, a new feature due to a ν_{NH}^{+} mode is seen at 2160 cm^{-1} in the spectrum for Cn adsorbed while bubbling H_2. Since quinuclidine is a tertiary amine, there are no N−H bonds in the free molecule, and no peaks for that vibration are seen in the spectrum for Cn dissolved in CCl_4 (top, green, trace); only upon protonation of that amine it is possible to detect a N−H^+ stretching vibration. Notice also that the ν_{NH}^{+} feature is not seen in the spectrum

recorded while bubbling D_2 either. It is important to indicate that, although the values for the stretching frequencies reported here may appear low (typical values for N−H bonds are around 3500 cm^{-1}), this is because, in our case, the amine is protonated and has a positive charge; the reported frequency range for $R{\equiv}N{-}H^+$ stretching vibrations[83] in dilute solutions is between 1800 and 2200 cm^{-1}. Protonation of the amine (quinuclidine) nitrogen in cinchona alkaloid chiral modifiers upon adsorption on Pt in the presence of H_2 gas has in fact been proposed (but not proven) before[84-85].

3.4 Summary

In this chapter, a combination of catalytic kinetic measurements, *in-situ* infrared absorption spectroscopy characterization of adsorbed species, and quantum mechanics calculations was used to probe the surface chemistry associated with the adsorption and chemical reactivity of chiral modifiers, not only 1-NEA but also 2-NEA and cinchonine, at the liquid-solid interface of the type of Pt-based supported catalysis used to promote hydrogenation reactions enantioselectivity. It was determined by using ^{1}H-NMR and GC-MS detection that, in the presence of D_2 gas and a Pt catalyst, NEA undergoes H−D exchange at the amine nitrogen atom. DFT calculations indicated that the most likely mechanism for this reaction is via the formation of a protonated (deuterated) intermediate on the surface of the metal employed as a catalyst. *In situ* IR data were used to identify this species, which displays additional vibrational modes associated with the newly formed N−D bonds. These observations proved to be fairly general, as similar results were seen with both s and r enantiomers of 1-NEA and 2-NEA as well as with cinchonine

and also with both Pt/SiO_2 and Pt/Al_2O_3 catalysts. The conclusion that NEA is protonated on the surface under reaction conditions, namely, in the presence of a solvent and as hydrogen is bubbled to the mixture, explains some observations not previously accounted for, including the unique nature of the IR spectra obtained for these adsorbed species when comparing with the free modifiers or for those adsorbed on Pt under vacuum, and also the need to precondition the surface with hydrogen for optimum adsorption and catalytic performance.

Chapter 4

Enantioselective Hydrogenation of Ethyl Pyruvate Over NEA−Pt Supported Catalyst: Effect of Silylation Agents

4.1 Brief Introduction and Hypothesis

The successful application of adding a small quantity of chiral modifier to reaction mixtures has been demonstrated in the asymmetric hydrogenation of α-keto esters modified with cinchona alkaloids. Among the catalysts, Pt-based catalysts have proven to be the most efficient heterogeneous catalysts, particularly Pt/Al_2O_3 catalyst[86]. The characteristics of the support material typically play a crucial role in catalytic performance. Our work, as well as previous research, has demonstrated that the catalytic performance of commercial 1 wt% Pt/Al_2O_3 is significantly superior to that of commercial 1 wt% Pt/SiO_2. We speculate that the acidic nature of γ-Al_2O_3 might promote reaction reactivity but could potentially compromise enantioselectivity. Consequently, we conducted modifications of Pt catalysts using various organosilanes, as illustrated in Figure 4.1. The introduction of silylation agents facilitates the formation of Si-O-Pt bonds, which have been shown to enhance catalyst performance in hydrogenation reactions. Our hypothesis is that modified Pt/Al_2O_3 catalysts with organosilanes would decrease the catalytic reactivity while increasing enantioselectivity.

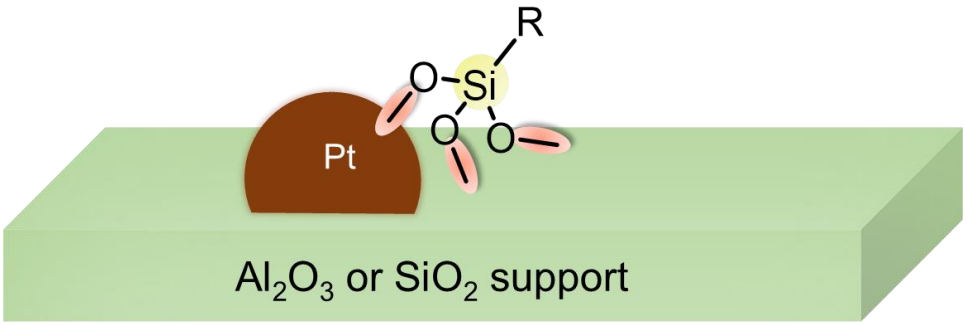

Figure 4.1 Illustration of modification of Pt supported catalysts with silylation agents.

This chapter encompasses comprehensive kinetic measurements involving different types and quantities of chiral modifiers in asymmetric hydrogenations of ethyl pyruvate (Et-Py), as depicted in Figure 4.2. Moreover, we investigated both homemade and commercial Pt catalysts, as well as the surface modification of Pt catalysts using different silylation agents, with the aim of exploring their effects on catalytic behavior in terms of reactivity and enantioselectivity.

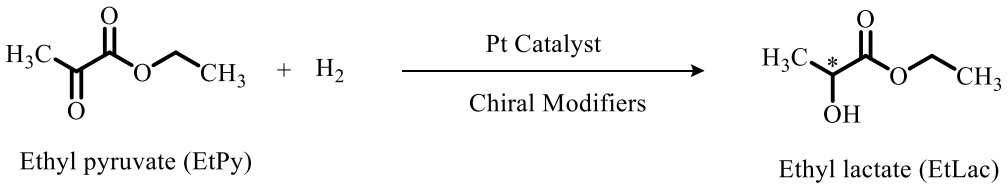

Ethyl pyruvate (EtPy) Ethyl lactate (EtLac)

Figure 4.2 Illustration of asymmetric hydrogenation of Et-Py

4.2 Experimental Details

4.2.1 Kinetic Measurements

The Et-Py hydrogenation reactions were conducted in a high pressure reactor. The typical reaction conditions are described as follows: the reactants mole ratio Pt/Et-Py/chiral modifier was determined to be 1/2000/5; the amount of Pt supported catalysts was 25 mg; the reaction pressure was 10 bar; and the toluene was used as the react solvent; reaction temperature was room temperature (approximately 298 K). The total reaction time was 3 hours, during which samples were collected every 30 minutes and analyzed using GC.

4.2.2 Silylation of Pt Supported Catalysts

The Pt-supported catalysts underwent modification using four different silylation agents: trimethoxy(octyl)silane (TMOS), 3-aminopropyltriethoxysilane (APTES), trimethoxy(propyl)silane (TMPS), and triethoxy(propyl)silane (TEPS). Figure 4.3 provides the structure and basic information of these four agents.

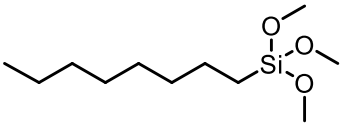

Trimethoxy(octyl)silane
(TMOS)
$C_{11}H_{26}O_3Si$
Molecular Weight: 234.41

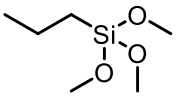

Trimethoxy(propyl)silane
(TMPS)
$C_6H_{16}O_3Si$
Molecular Weight: 164.28

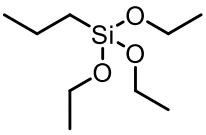

Triethoxy(propyl)silane
(TEPS)
$C_9H_{22}O_3Si$
Molecular Weight: 206.36

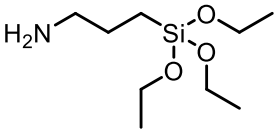

3-Aminopropyltriethoxysilane
(APTES)
$C_9H_{23}NO_3Si$
Molecular Weight: 221.37

Figure 4.3 The structure and information of all agents used for modification.

The experimental procedures for silylation of Pt/Al_2O_3 are outlined below.

1. The commercial 1 wt% Pt/Al_2O_3 catalyst was pretreated in a hydrogen flow at 400 °C for 2.0 h using a furnace tube.
2. Subsequently, the sample was cooled to room temperature in a hydrogen atmosphere and purged with Ar for 10 minutes.
3. A flask (three neck) containing 100 mg of pretreated catalysts and 20 mL pure toluene was used. The reaction was conducted under oxygen-free conditions by purging N_2 gas.
4. The silylation agent was added to the mixture at the reflux temperature (~110 °C).
5. Following a 3.0-hour reaction, the sample was cooled down and continuously stirred overnight.

6. The sample was then washed with pure toluene four times, followed by washing with pure hexane four times.
7. Lastly, the washed and filtered sample was dried under vacuum at 50 °C for 1 hour.

The surface modifications of all other Pt catalysts with different agents followed the same procedure described above.

4.2.3 Characterizations of Silylated Pt Catalysts

The silylated Pt catalysts obtained from step 7 were reactivated in a furnace tube using a hydrogen flow at 400 °C for 2.0 h. Both silylated catalysts before and after heat treatment were analyzed using transmission IR to confirm the successful modification of the agent on the Pt catalysts. Additionally, the behavior of the 1-NEA molecule on different silylated Pt catalysts was evaluated through *in-situ* ATR-IR.

4.3 Results and Discussions

4.3.1 The Catalytic Performance as a Function of Chiral Modifiers

Table 4.1 summarizes the results of testing all the 1-NEA and 2-NEA chiral modifiers, along with the traditional cinchona alkaloids, namely cinchonidine (CD) and cinchonine (CN). The conversion and *ee* values, as a function of reaction time, are presented in Figure 4.4 (for 1 wt% commercial Pt/Al_2O_3) and Figure 4.5 (for 1 wt% commercial Pt/SiO_2). Figure 4.2 illustrates that the traditional CD and CN molecules exhibited significantly higher enantioselectivity compared to all chiral NEA-related molecules.

Table 4.1 Conversion and *ee* of the Et-Py hydrogenation modified with different chiral modifiers catalyzed by Pt supported catalyst.

Catalysts	Chiral modifier	Conversion (%)	*ee* (%)
Commercial 1 wt% Pt/Al_2O_3	Without modifier	47.3	0.4
	Cinchonidine (CD)	100	58.3 (S)
	Cinchonine (CN)	100	45.4 (R)
	r-1-NEA	100	18.6 (R)
	s-1-NEA	100	17.3 (S)
	r-2-NEA	100	24.0 (R)
	s-2-NEA	100	23.8 (S)
Commercial 1 wt% Pt/SiO_2	Without modifier	22.8	0.4
	r-1-NEA	72.2	5.0 (R)
	s-1-NEA	81.0	7.2 (S)
	r-2-NEA	45.3	6.6 (R)
	s-2-NEA	54.0	8.6 (S)

Reaction conditions: t = 3.0 h, T= 298 K, $P(H_2)$=10 bar, Pt catalyst (25 mg), toluene solvent (10 mL), molar ratio of Pt:Et-Py:modifier = 1:2000:5.

In the case of commercial Pt/Al_2O_3 catalyst, the conversion was 47.3 % without the presence of chiral modifiers. However, the addition of chiral modifiers improved the reaction rate, resulting in a conversion of up to 100 % after three hours of reaction time in all cases. For the CN and CD molecules, the reaction conversion reached 100 % in approximately one hour. Moreover, the chiral 2-NEA molecules exhibited slightly higher

ee values compared to the chiral 1-NEA molecules but displayed a similar *ee* trend over time (see the right panel of Figure 4.4).

Conversely, the catalytic performance of the commercial 1 wt% was notably weaker than that of 1 wt% commercial Pt/Al_2O_3. Without chiral modifiers, the conversion with Pt/SiO_2 catalyst was only 22.8 %, approximately half of that observed with Pt/Al_2O_3. The use of chiral modifiers also did not yield results as promising as those with Pt/Al_2O_3. Additionally, the *ee* values achieved with Pt/SiO_2 were significantly lower compared to Pt/Al_2O_3. It should be noted that the reaction conditions are not yet optimized, and further exploration is required. Nonetheless, it is evident that the catalytic performance of commercial Pt/Al_2O_3 surpassed that of Pt/SiO_2.

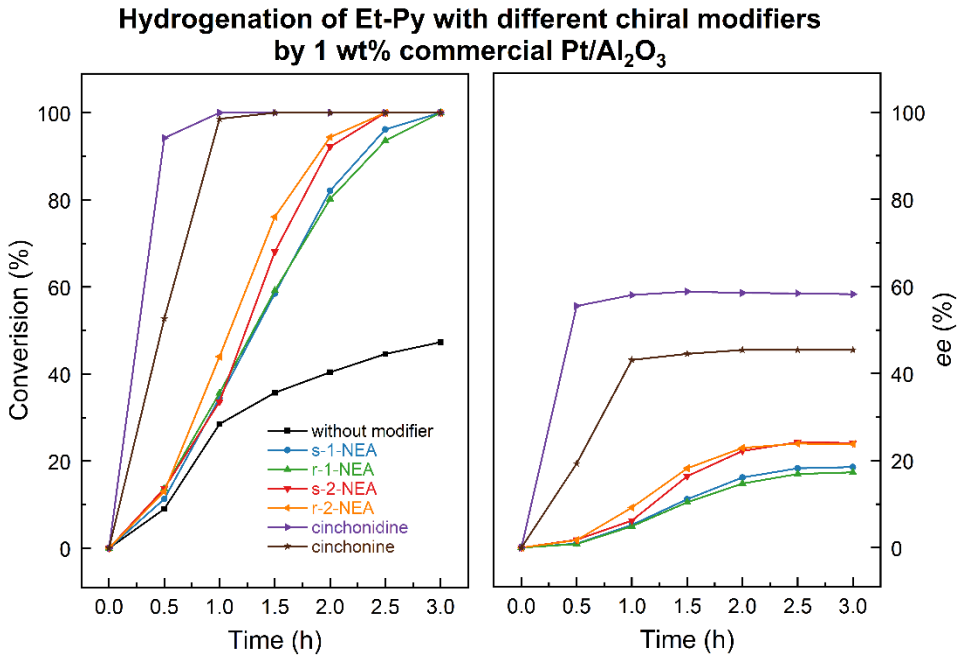

Figure 4.4 The conversion and *ee* values of Et-Py hydrogenation catalyzed by commercial 1 wt% Pt/Al_2O_3 as a function of chiral modifiers.

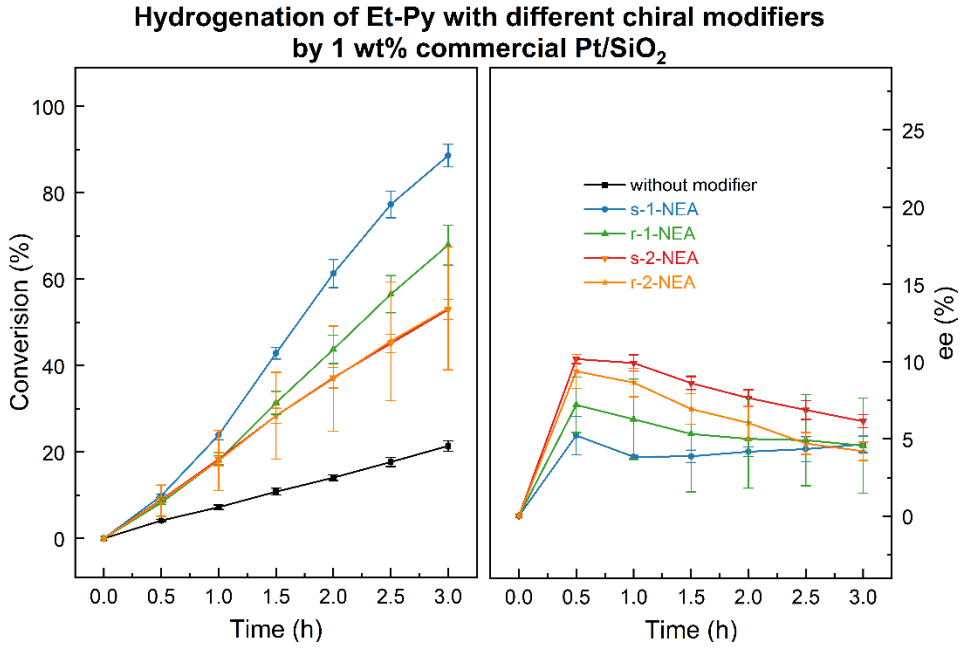

Figure 4.5 The conversion and *ee* values of Et-Py hydrogenation catalyzed by commercial 1 wt% Pt/SiO_2 as a function of chiral modifiers. The error bars were calculated based on three runs of the reactions.

4.3.2 Effect of Chiral Modifiers Amount

Additional experiments were conducted to investigate the impact of varying amounts of chiral modifiers. As previously mentioned, the reactions were carried out with a mole ratio of 1/2000/5 for Pt/Et-Py/chiral modifiers. In addition to this ratio, different quantities of s-1-NEA were introduced into the reactions, specifically labeled as 1/2000/50 and 1/2000/100, for the case of commercial Pt/Al_2O_3 (Figure 4.6) and commercial Pt/SiO_2 (Figure 4.7) catalysts, respectively.

Both Pt catalysts exhibited a similar trend, wherein an increase in the amount of chiral modifiers led to a noticeable reduction in conversion. This observation can be attributed to the fact that a higher concentration of chiral modifiers adsorbed onto the Pt surfaces would, to some extent, obstruct the active sites. Furthermore, the enantiomeric

excess (*ee*) values showed a slight decrease with an increased amount of chiral modifiers. This can be attributed to the altered chiral environment resulting from the adsorption of 1-NEA molecules, which is influenced by the surface coverage. Therefore, it can be concluded that an excessive amount of chiral modifiers negatively impacts enantioselectivity.

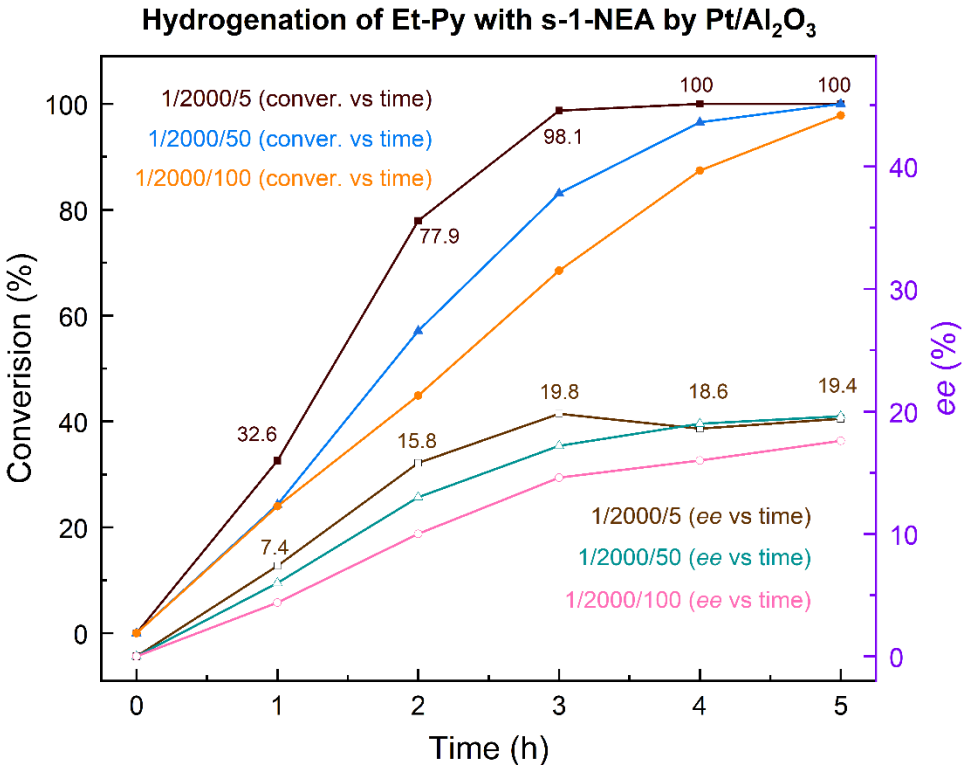

Figure 4.6 The conversion and *ee* values of Et-Py hydrogenation modified with s-1-NEA catalyzed by commercial 1 wt% Pt/Al_2O_3 as a function of chiral modifiers amount.

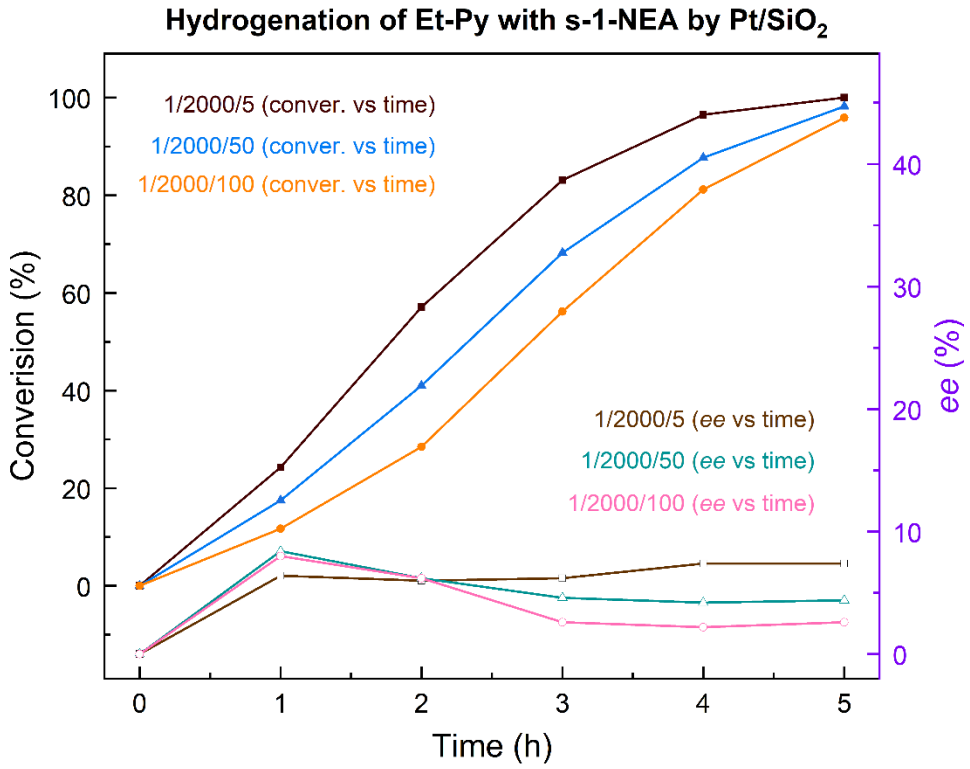

Figure 4.7 The conversion and *ee* values of Et-Py hydrogenation modified with s-1-NEA catalyzed by commercial 1 wt% Pt/SiO_2 as a function of chiral modifiers amount.

4.3.3 Comparison Between Homemade and Commercial Pt Supported Catalysts

In Chapter 2, we discussed the fabrication of homemade 1 wt% Pt/Al_2O_3 and 1 wt% Pt/SiO_2 using the simple wet-impregnation method. We also provided characterizations and discussions of these catalysts previously.

To compare the catalytic performance between the homemade and commercial Pt supported catalysts, we conducted experiments and present the results in Table 4.2 and Figure 4.8. Each Pt catalysts was tested three times, and the error bar in Figure 4.8 represent the calculated values based on these three independent runs.

Table 4.2 Conversion and *ee* of the Et-Py hydrogenation modified with s-1-NEA catalyzed by both homemade and commercial Pt supported catalysts.

Catalysts	Chiral modifier	Conversion (%)	*ee* (%)
Commercial 1 wt% Pt/Al_2O_3	s-1-NEA	100	24.0 (S)
		100	22.8 (S)
		100	24.2 (S)
Homemade 1 wt% Pt/Al_2O_3		63.2	10.4 (S)
		62.6	9.3 (S)
		60.5	10.2 (S)
Commercial 1 wt% Pt/SiO_2		85.9	16.9 (S)
		86.1	15.8 (S)
		90.0	14.4 (S)
Homemade 1 wt% Pt/SiO_2		96.2	27.8 (S)
		100	26.2 (S)
		98.7	28.6 (S)

Reaction conditions: t = 5.0 h, T= 298 K, $P(H_2)$=10 bar, Pt catalyst (25 mg), toluene solvent (10 mL), molar ratio of Pt:Et-Py:modifier = 1:2000:5.

As shown in the left panel of Figure 4.8, among the four different Pt catalysts, the commercial 1 wt% Pt/Al_2O_3 displayed the highest catalytic activity. The homemade 1 wt% Pt/SiO_2 exhibited slightly weaker activity, while the homemade 1 wt% Pt/Al_2O_3 showed the lowest activity performance. These differences can be attributed to the surface properties of the different catalysts. As discussed in Table 2.2, the surface area of homemade Pt/Al_2O_3 is only approximately 80 m^2/g, which is much smaller than other Pt

catalysts. This limited surface area results in poor catalytic behavior. On the other hand, the homemade Pt/SiO_2 catalyst has a larger surface area (~419 m^2/g). Although the surface area of commercial Pt/Al_2O_3 (~186 m^2/g) is not as large as that of Pt/SiO_2 catalysts, the pore size of commercial Pt/Al_2O_3 (~10 nm) is significantly larger than that of homemade Pt/SiO_2 (~5.9 nm). The large pore size enhances the accessibility of reactants to the active sites of the catalyst, increasing the probability of the desired reaction occurring. This could explain the superior activity performance observed with commercial Pt/Al_2O_3 catalysts.

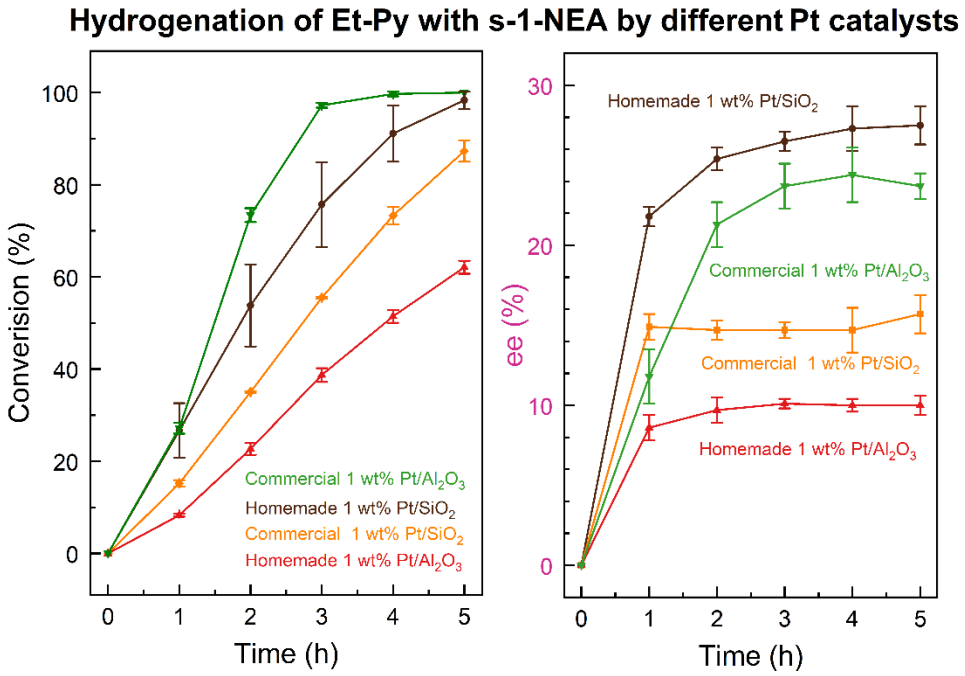

Figure 4.8 The conversion and *ee* values of Et-Py hydrogenation modified with s-1-NEA as a function of Pt catalysts. The error bars were calculated based on three runs of the reactions.

In the right panel in Figure 4.8, a similar *ee* trend with time was observed for all four Pt catalysts. The homemade Pt/SiO_2 catalyst exhibited the highest enantioselectivity, slightly surpassing the commercial Pt/Al_2O_3 catalyst. Conversely, the homemade Pt/Al_2O_3 catalyst showed the lowest enantioselectivity. The differences in properties of the Pt catalysts discussed earlier could also contribute to the observed differences in *ee*.

Overall, the results demonstrate the influence of catalyst properties on the catalytic performance and enantioselectivity, highlighting the importance of surface area and pore size in determining the activity and selectivity of the catalysts.

4.3.4 Comparisons Among Different Silylated Pt Catalysts

Table 4.1 indicates a clear difference in activity between Pt/Al_2O_3 and Pt/SiO_2 when no modifier is present. This discrepancy could be attributed to the acidity of Al_2O_3. TO investigate whether silylation of the catalysts, both Pt/Al_2O_3 and Pt/SiO_2, would affect their activity, surface silylation was performed. We hypothesized that if the acidic functionalities enhance activity but degrade enantioselectivity, silylated catalysts might exhibit reduced activity yet improved enantioselectivity.

For the silylated Pt/Al_2O_3 catalyst, transmission IR spectroscopy was utilized to confirm successful modification of the Pt catalysts by the silylation agent. Figure 4.9 summarized the comparison of the catalysts before and after silylation. The significant differences were observed around 3000 cm^{-1}, the enlarged range is provided in the right panel.

After silylation with trimethoxy(octyl)silane (TMOS), three new peaks were observed in the enlarged range at approximately 2962 cm^{-1}, 2924 cm^{-1} and 2854 cm^{-1}. These peaks likely correspond to the C−H stretching mode of silylation agent. Moreover, even after a heat-treatment (350 °C, H_2, 3.0 h), the TMOS-silylated Pt/Al_2O_3 catalysts retained these peaks, indicating the strong attachment of the agent. Although the new peaks appeared weak, this is likely due to the relatively small amount of silylation agent used.

Similarly, when trimethoxy(propyl)silane (TMPS) was employed as the silylation agent, as shown in Figure 4.9, three new peaks emerged at around 2960 cm^{-1}, 2932 cm^{-1} and 2875 cm^{-1}. However, these peaks vanished following heat treatment, suggesting that the TMPS agent could be removed from the catalysts through this thermal process.

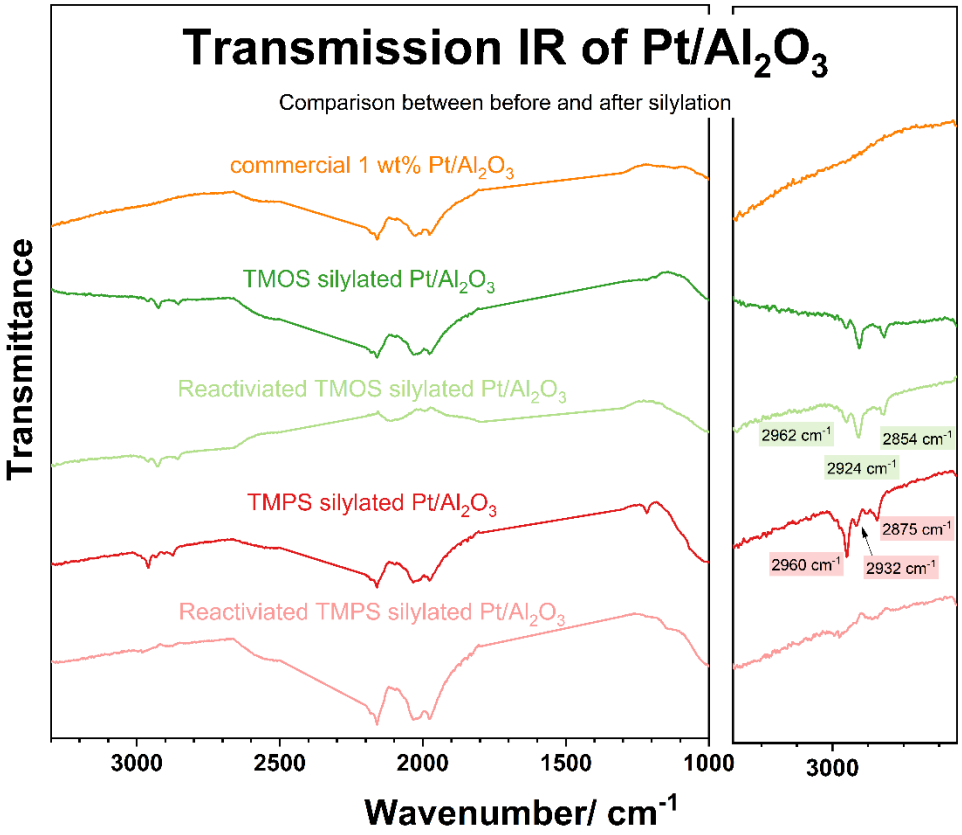

Figure 4.9 The transmission IR of Pt/Al_2O_3 before and after silylation with TMOS and TMPS.

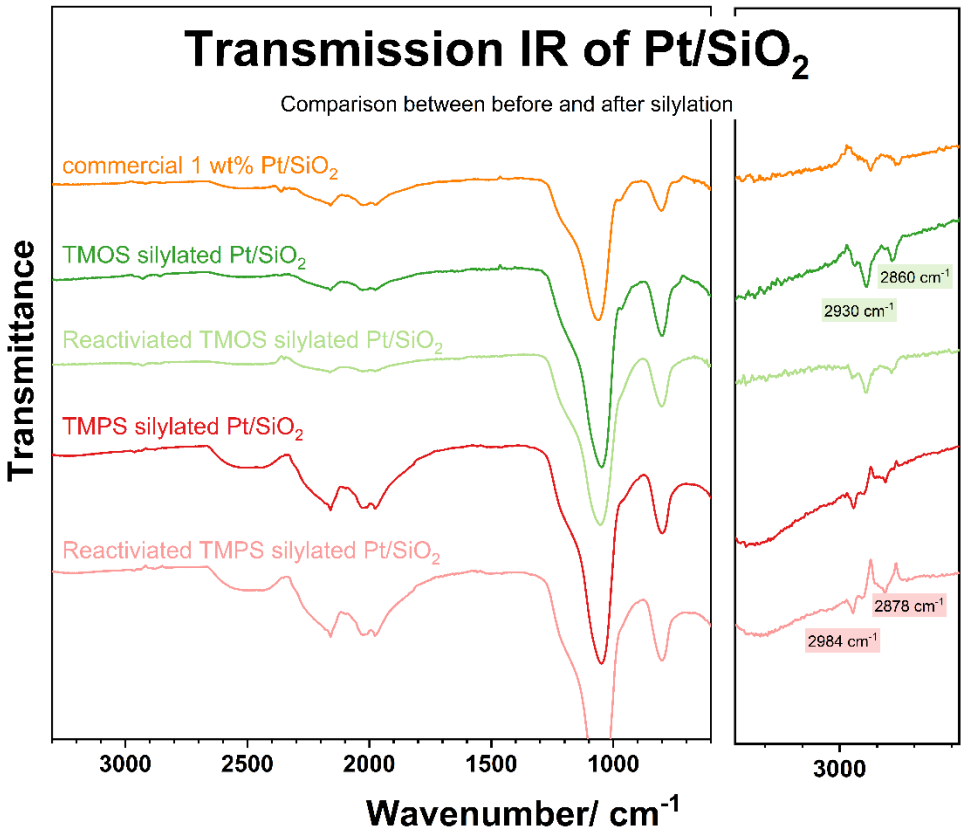

Figure 4.10 The transmission IR of Pt/SiO_2 before and after silylation with TMOS and TMPS.

Both TMOS and TMPS were utilized for silylation of Pt/SiO_2 catalyst. The silylated catalysts were analyzed by transmission IR spectroscopy, and the summarized results are presented in Figure 4.10. The top trace represents the spectrum of commercial 1 wt% Pt/SiO_2 without silylation. The full spectra did not exhibit noticeable differences, but the enlarged range around 3000 cm^{-1}, presented in the right panel, did reveal certain distinctions. Upon silylation with TMOP, two prominent peaks were detected around 2930 cm^{-1} and 2860 cm^{-1}, which can be attributed to the C−H stretching mode of the silylation agent. Even after a heat treatment (350 °C, H_2, 3.0 h), these new peaks remained. A similar behavior was observed for TMPS-silylated Pt/SiO_2, where two peaks

around 2964 cm^{-1} and 2878 cm^{-1} were detected after silylation, and they persisted after heat treatment. These results indicate the successful modification of Pt catalyst surfaces with both TMOS and TMPS, and their stability was maintained after heat treatment.

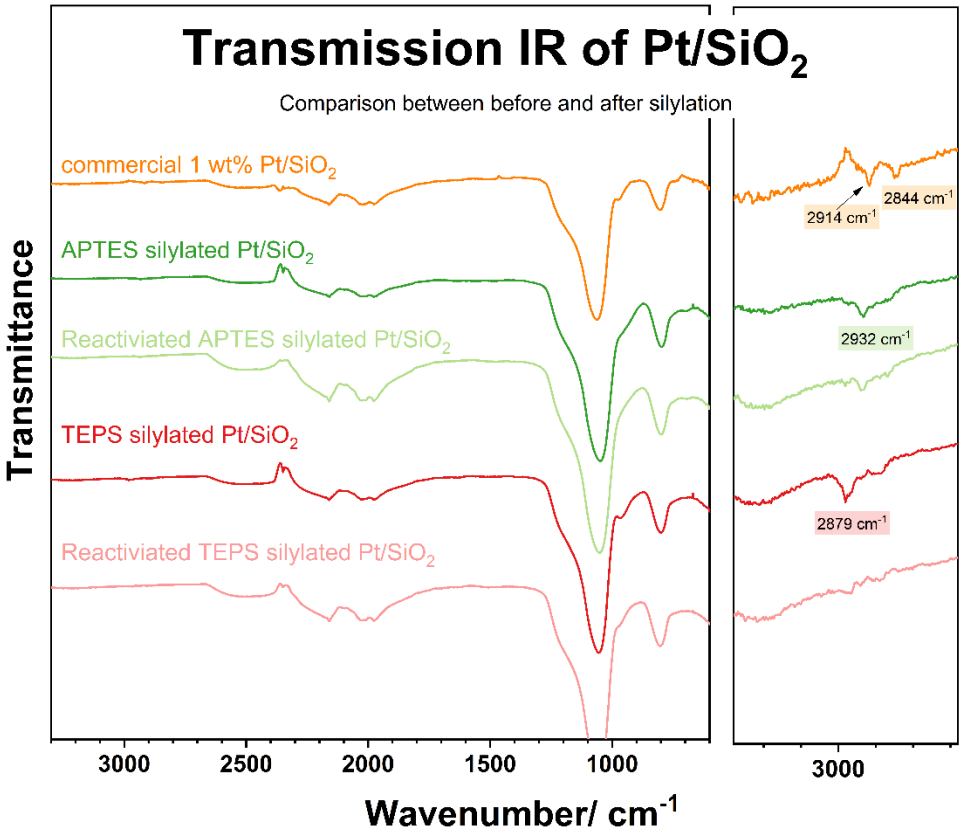

Figure 4.11 The transmission IR of Pt/SiO_2 before and after silylation with APTES and TEPS.

Furthermore, in addition to TMOS and TMPS, two other silylation agents, namely, 3-aminopropyltriethoxysilane (AMPES) and triethoxy(propyl)silane (TEPS), were investigated to assess the influence of $-NH_2$ functionality. As depicted in the right panel of Figure 4.11, two peaks around 2194 cm^{-1} and 2844 cm^{-1} were observed in the case of commercial Pt/SiO_2 catalyst, which likely correspond to the stretching mode of

C−H bonds in organic molecules adsorbed on the catalyst surfaces. APTES-silylated Pt/SiO_2 exhibited peaks before and after heat treatment, while the peaks disappeared after heat treatment in the case of TEPS-silylated Pt/SiO_2 catalysts.

Overall, transmission IR spectroscopy was employed to verify the efficacy of surface modification and assess the stability after heat treatment. For commercial Pt/Al_2O_3, both TMOS and TMPS successfully modified the catalysts; however, TMPS was removed during the heat treatment. Regarding commercial Pt/SiO_2, all four silylation agents demonstrated evidence of silylation, but only TEPS appeared likely to be eliminated by heat treatment. The transmission IR results provide valuable insights for subsequent discussion of the kinetic results.

4.3.5 *In-Situ* ATR-IR of 1-NEA Behavior on Silylated Pt Catalysts

In addition to transmission IR, the 1-NEA behavior on different silylated Pt catalysts was investigated using ATR-IR. Figure 4.12 illustrates the ATR-IR spectra of a 5mM r-1-NEA in CCl_4 solution after exposure to various silylated Pt/Al_2O_3 catalysts. The top trace represents commercial Pt/Al_2O_3 without any modifications. No noticeable differences were observed among the different silylated catalysts. One possible explanation is the minimal amount of silylation agent used. Furthermore, the silylation agents only exhibited some sample peaks around 3000 cm^{-1} due to the stretching modes of C−H bonds. Consequently, the contribution and impact of silylation agents on 1-NEA adsorption are minor and undetectable through ATR-IR.

Similar results were obtained with the silylated Pt/SiO_2 catalysts, as depicted in Figure 4.13 (TMOS and TPOS silylated Pt/SiO_2) and Figure 4.14 (APETS and TEPS silylated Pt/SiO_2). No significant differences were observed in any of the experiments. The presence of 1-NEA molecules on all the catalysts demonstrated substantial evidence of adsorption.

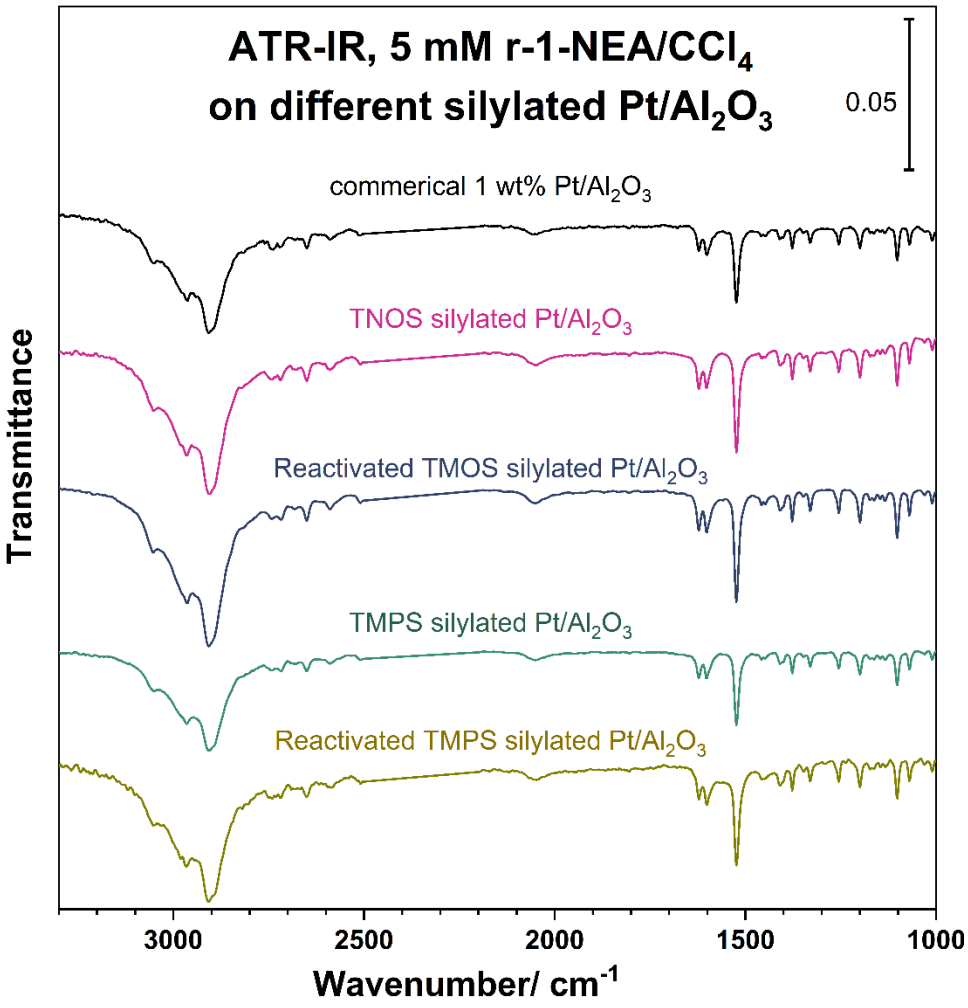

Figure 4.12 ATR-IR spectra of 5 mM r-1-NEA in CCl_4 solution adsorption on different silylated Pt/Al_2O_3 catalysts.

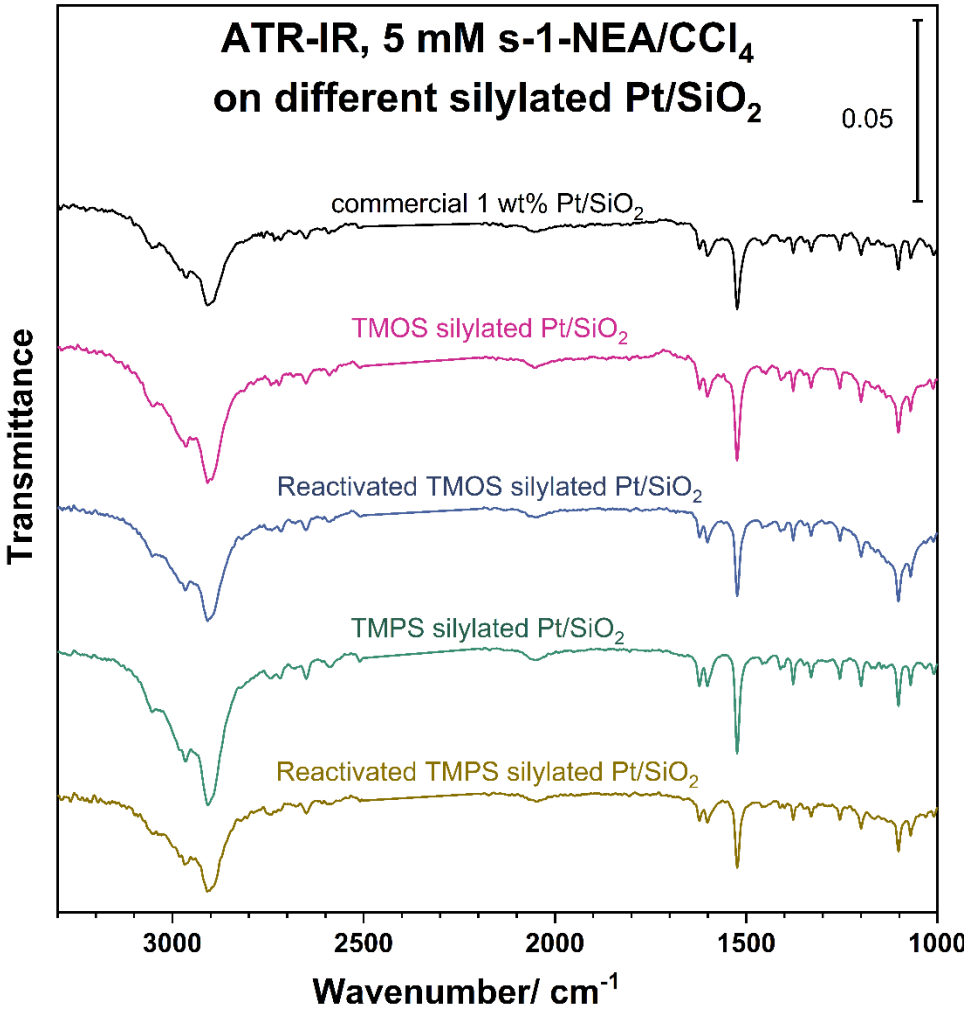

Figure 4.13 ATR-IR spectra of 5 mM s-1-NEA in CCl_4 solution adsorption on different silylated Pt/SiO_2 catalysts.

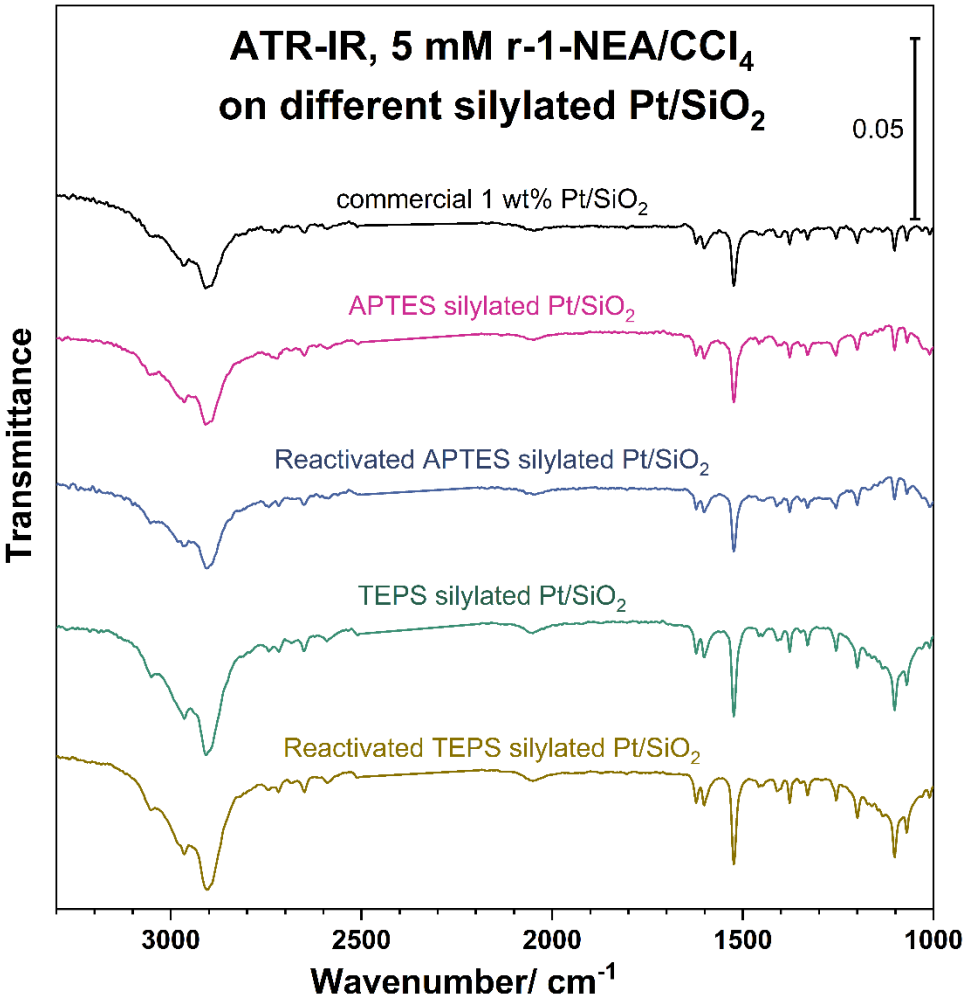

Figure 4.14 ATR-IR spectra of 5 mM r-1-NEA in CCl_4 solution adsorption on different silylated Pt/SiO_2 catalysts.

4.3.6 Catalytic Behavior of Silylated Pt Catalysts

The influence of silylated Pt catalysts on the catalytic performance was investigated. Our hypothesis was that silylation would reduce activity but potentially improve enantioselectivity.

Figure 4.15 below illustrates the hydrogenation of Et-Py reactions using various silylated Pt/Al_2O_3 catalysts modified with r-1-NEA. The left panel demonstrates the

conversion trends, showing significantly weaker activity for all silylated Pt/Al_2O_3 catalysts. This decrease in activity was expected because silylation obstructed the active Pt sites on the catalyst surface. Commercial Pt/SiO_2 catalysts also exhibited lower activity compared to commercial Pt/Al_2O_3, which could be attributed to the transmission IR results depicted in Figure 4.10 and Figure 4.11. These figures show peaks around 3000 cm^{-1}, indicating the presence of C−H stretching modes from organic molecules absorbed on the Pt/SiO_2 catalysts. The synthesis of commercial Pt/SiO_2 involved the potential introduction of organic, similar to surface modification through silylation agents mentioned earlier.

Furthermore, it was observed that commercial Pt/SiO_2 displayed similar activity to the reactivated TMPS silylated Pt/SiO_2, likely due to the removal of TMPS during the heat treatment, as indicated in Figure 4.9.

The right panel of Figure 4.15 illustrates the *ee* trends with different catalysts. Interestingly, all silylated Pt/Al_2O_3 catalysts exhibited *ee* trends that unexpectedly resembled the trend observed with commercial Pt/SiO_2. The *ee* values increased with reaction time for commercial Pt/Al_2O_3, whereas both commercial Pt/SiO_2 and all silylated Pt/Al_2O_3 catalysts showed decreasing *ee* values over time. Moreover, as shown in Figure 4.8, the *ee* trend with homemade Pt/SiO_2 differed from that of commercial Pt/SiO_2. The homemade Pt/SiO_2 catalyst was prepared using a simple wet impregnation method without any organic solvents, and no evidence of organic solvents was detected on commercial Pt/Al_2O_3 either. Therefore, the difference in *ee* trend observed with silylated Pt/Al_2O_3 catalysts was attributed to the adsorbed silylation agents on the Pt catalysts.

Additionally, the *ee* values observed in the early stages of the reaction with Pt/SiO_2 were significantly higher than those with Pt/Al_2O_3, suggesting that surface modification indeed improved enantioselectivity.

It is worth noting that a reaction using pure γ-Al_2O_3 support was conducted, which showed no catalytic activity. The contribution from the support was minimal.

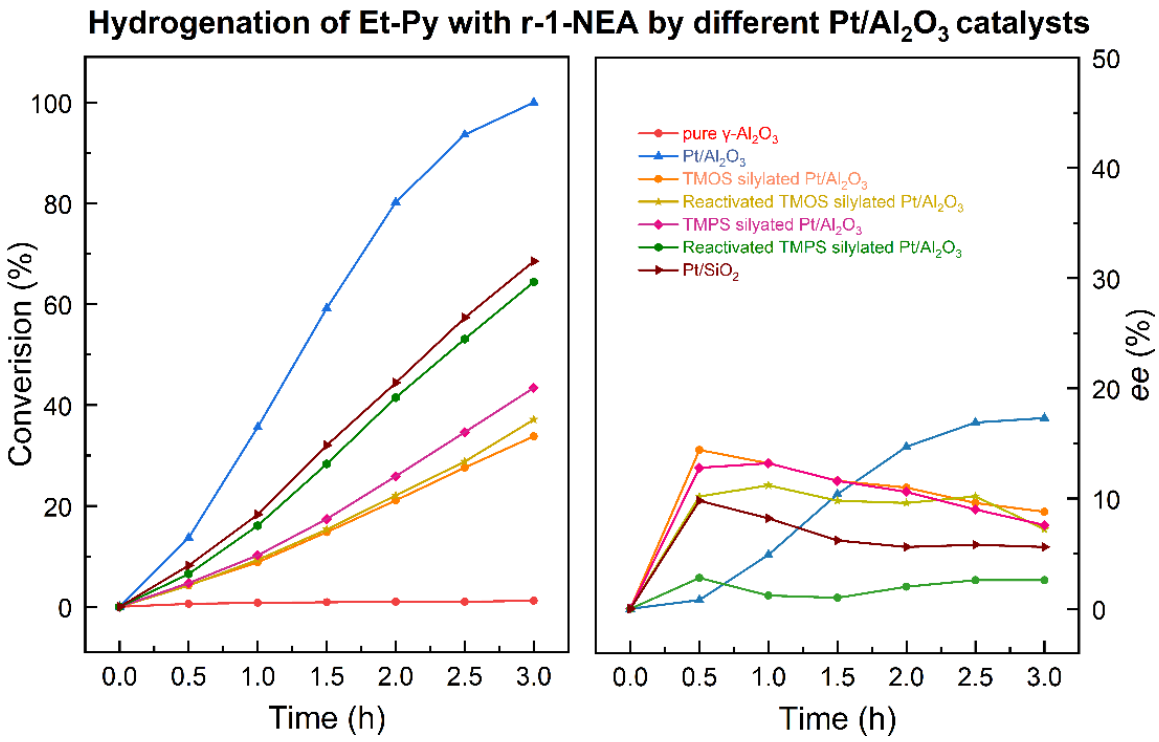

Figure 4.15 Conversion and *ee* values of Et-Py hydrogenation modified with r-1-NEA as a function of different Pt catalysts.

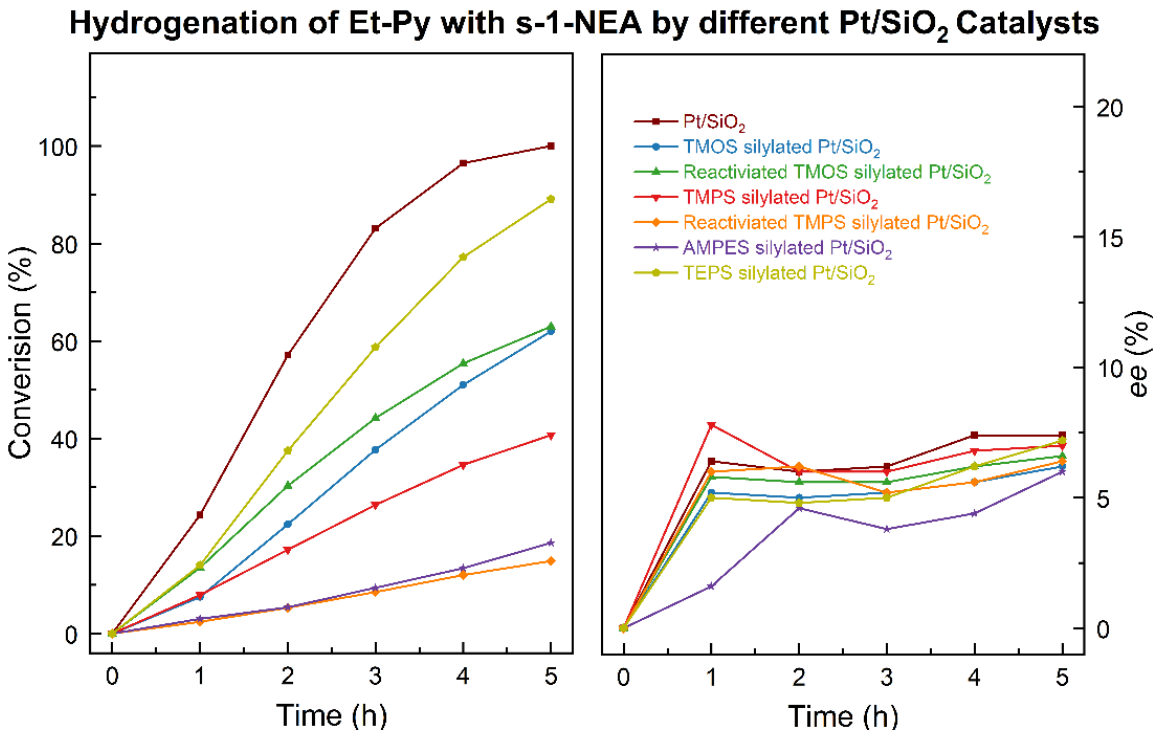

Figure 4.16 Conversion and *ee* values of Et-Py hydrogenation modified with s-1-NEA as a function of different Pt catalysts.

Figure 4.16 provides a comparison of different silylated Pt/SiO_2 catalysts. A decrease in activity was observed with all silylated catalysts compared to commercial Pt/SiO_2. However, there was no significant change in the *ee* trend, as all catalysts exhibited similar *ee* trends, as shown in the right panel of Figure 4.16.

4.4 Summary

In this chapter, we conducted a thorough investigation of the catalytic performance of various chiral NEA molecules. Our findings reveal that traditional cinchona alkaloids, such as CN and CD, exhibit superior catalytic promotion in terms of both activity and enantioselectivity compared to chiral NEA molecules. However, it is

worth noting that chiral NEA molecules still yield impressive results, considering that the reaction conditions have not been fully optimized.

Among the chiral NEA molecules, we observed slightly better catalytic performance from chiral 2-NEA molecules compared to 1-NEA molecules. This distinction may be attributed to minor differences in adsorption geometry, as discussed in Section 3.3.3 based on the ATR-IR results. Additionally, we tested various amounts of chiral modifiers and found that increasing the concentration of chiral modifiers adsorbed on Pt catalysts leads to a decrease in the number of active sites, thereby resulting in reduced catalytic activity. Furthermore, although the enantiomeric excess (*ee*) values also decreased, the decrease was not significant.

Our investigation involved both homemade and commercial Pt/Al_2O_3 and Pt/SiO_2 catalysts. The results indicate that commercial Pt/Al_2O_3 and homemade Pt/SiO_2 catalysts exhibit superior catalytic performance compared to commercial Pt/SiO_2, whereas the homemade Pt/Al_2O_3 catalyst performed the worst. The observed catalytic performance correlated with the surface properties of the different catalysts.

Another interesting phenomenon was observed in reactions without chiral modifiers, where commercial Pt/Al_2O_3 displayed significantly higher catalytic activity compared to commercial Pt/SiO_2. This behavior was initially attributed to the acidity of the γ-Al_2O_3 support. Consequently, we conducted surface modifications on both Pt/Al_2O_3 and Pt/SiO_2 catalysts. Through transmission IR analysis, we detected C−H stretching modes (typically around 3000 cm^{-1}) in successfully silylated catalysts. The behavior of

NEA adsorption on different silylated catalysts closely resembles that on commercial Pt catalysts.

However, we observed varying catalytic performances among the silylated catalysts. As anticipated, all silylated catalysts exhibited a decrease in catalytic activity due to the adsorbed silylation agents, which reduced the number of active sites on the Pt catalysts. Another intriguing observation was that all silylated Pt/Al_2O_3 catalysts exhibited a completely different *ee* trend, which, in contrast, resembled that of commercial Pt/SiO_2. Conversely, a similar *ee* trend was observed among all silylated Pt/SiO_2 catalysts compared to the commercial counterpart. The synthesis process was not provided by the vendor, we believe it involved the introduction of organic solvents, such as certain silylation agents. Moreover, the homemade Pt/SiO_2 catalyst was synthesized using a simple wet-impregnation method without the addition of organic solvents. It exhibited a similar *ee* trend to commercial Pt/Al_2O_3 but differed from commercial Pt/SiO_2, as indicated in Figure 4.8. The disparities in the *ee* trend can be attributed to the adsorbed silylated agents on Pt catalysts, which also provide an explanation for the higher activity of commercial Pt/Al_2O_3 compared to commercial Pt/SiO_2 in the absence of chiral modifiers.

Chapter 5

Compare the Role of Nitrogen- *Versus* Oxygen-Based Chiral Center Modifiers

5.1 Brief Introduction and Hypothesis

In Chapter 3 and Chapter 4 it was established that NEA molecules bind to Pt surfaces through the amine nitrogen when they are adsorbed from the solution, leading to enhanced enantioselectivity in Et-Py hydrogenation. Apart from the interactions between the amine group and Pt surfaces, it was anticipated that the hydroxyl group would also bind to Pt surfaces. The oxygen atom in the hydroxyl group can form a chemical bond with the Pt surface through its lone pair of electrons. The binding of −OH groups to Pt surfaces is of interest in several fields, including catalysis, electrochemistry, and surface science. Understanding the nature of this interaction can contribute to the development of more efficient catalysts.

This chapter proposes the investigation of several chiral modifiers with oxygen-based chiral centers, as depicted in Figure 5.1. The adsorption behavior will be examined using *in-situ* ATR-IR. To explore the impact of the hydroxyl group position, 1-(1-naphthyl) ethanol (1-NE) and 1-(2-naphthyl) ethanol (2-NE) will be studied. The molecule 1-napathaleneeathanol (NEE) is proposed to investigate the influence of alcohol type. Additionally, the effect of aromatic ring size will be explored through the study of

1-phenylethanol (PE). Furthermore, various parameters, including solvent and catalyst support, will be thoroughly examined. Our hypothesis suggests that oxygen-based chiral modifiers, such as 1-NE, will bind to the Pt metal surfaces through the hydroxyl group. The adsorption spectra on Pt surfaces are expected to exhibit different behavior compared to the free molecules in solution.

Furthermore, kinetic measurements were conducted to establish a correlation between the adsorption behavior and catalytic performance.

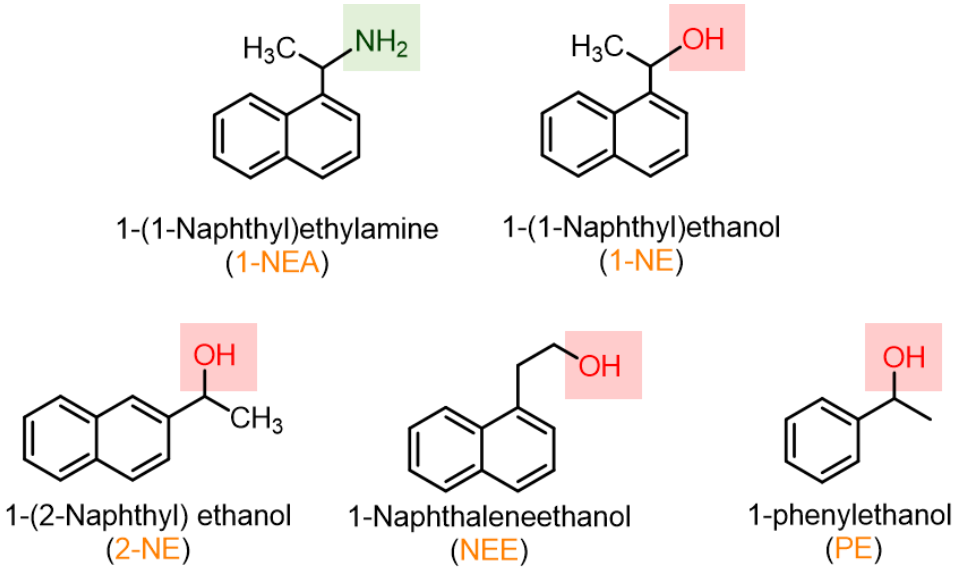

Figure 5.1 The molecular structure of 1-NEA and proposed oxygen-based molecules including 1-NE, 2-NE, NEE and PE.

5.2 Experimental Details

The adsorption tests for all chiral modifiers were conducted using *in-situ* ATR-IR, while the reference spectra of pure samples were obtained through transmission IR.

Kinetic measurements were performed using a high-pressure reactor. Chapter 2 provides comprehensive details regarding all experimental procedures.

5.3 Results and Discussions

5.3.1 *In-Situ* ATR-IR Adsorption Tests With 1-NE Molecule

The experiments commenced with 1-NE molecules, wherein the amine group was substituted with a hydroxyl group compared to 1-NEA molecules. Various concentrations of r-1-NE in CCl_4 solutions were subjected to ATR-IR analysis in the presence of 1 wt% Pt/Al_2O_3 catalysts. The summarized results are presented in Figure 5.2.

The results indicated a linear relationship between the concentration of r-1-NE solution and the intensity of the sample peaks. Most peaks were observed within the range of 1800-1000 cm^{-1}. Two peaks around 3000 cm^{-1} were identified, corresponding to the stretching modes of C−H and O−H bonds.

In the case of the 5 mM r-1-NE solution (the second trace from the top), only a few weak sample peaks were detected, while the 50 mM solution (the bottom trace) exhibited clearer and more intense sample peaks. By comparing the peaks obtained from the solution on Pt catalysts with the transmission IR of pure r-1-NE molecules (the top trace), it can be inferred that the ATR-IR spectra closely resemble the spectrum of free molecules. This similarity suggests that the sample peaks originate from the free molecules present in the solution rather than the absorbed molecules on the Pt catalysts.

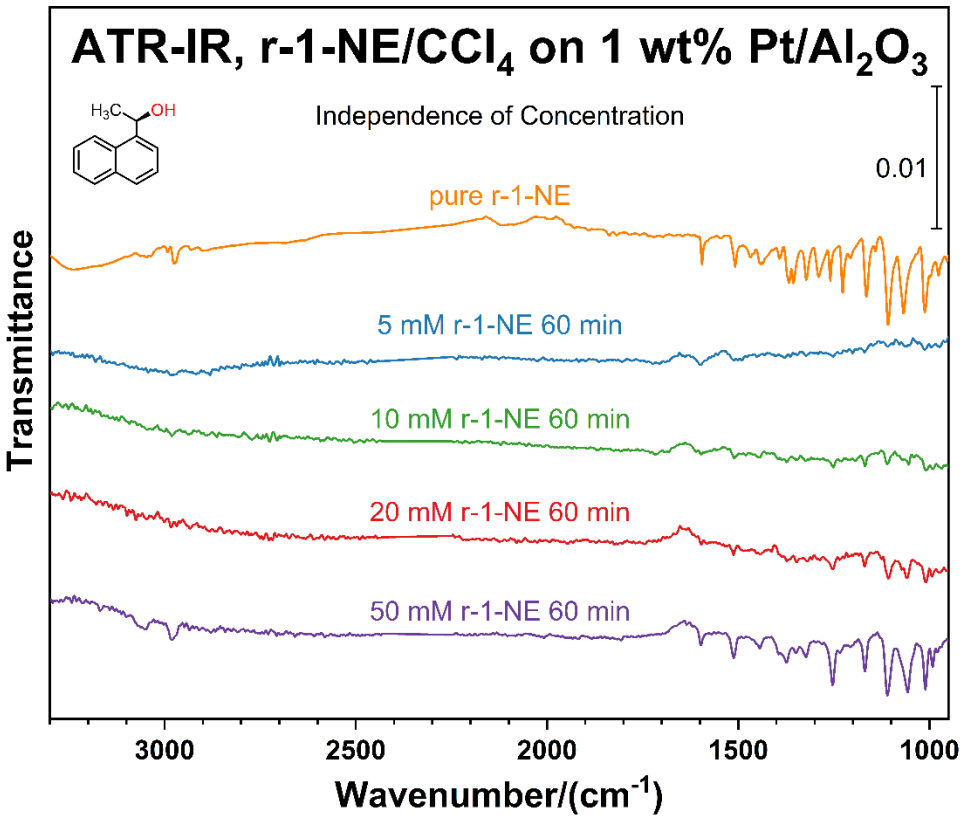

Figure 5.2 ATR-IR spectra of r-1-NE/CCl_4 on 1 wt% Pt/Al_2O_3 catalysts as function of concentration. The top one is the transmission IR spectrum of pure 1-NE.

Figure 5.3 shows an example of ATR-IR spectra for the 50 mM solution. The solid traces represent the spectra of the 50 mM 1-NE in CCl_4 solution exposed to 1 wt% Pt/Al_2O_3 catalysts as a function of exposure time, while the light traces depict the results of the blank test conducted without catalysts. As depicted in Figure 5.3, the sample peaks were clearly observed after 5 minutes of exposure, and their intensity appeared to remain relatively unchanged with further exposure up to 60 minutes. Additionally, the spectra obtained from the tests with and without catalysts exhibit similar characteristics, resembling the transmission IR of pure 1-NE molecules. These observations reinforce the

notion that the peaks originate from the free molecules in the solution rather than the molecules adsorbed on the Pt catalyst.

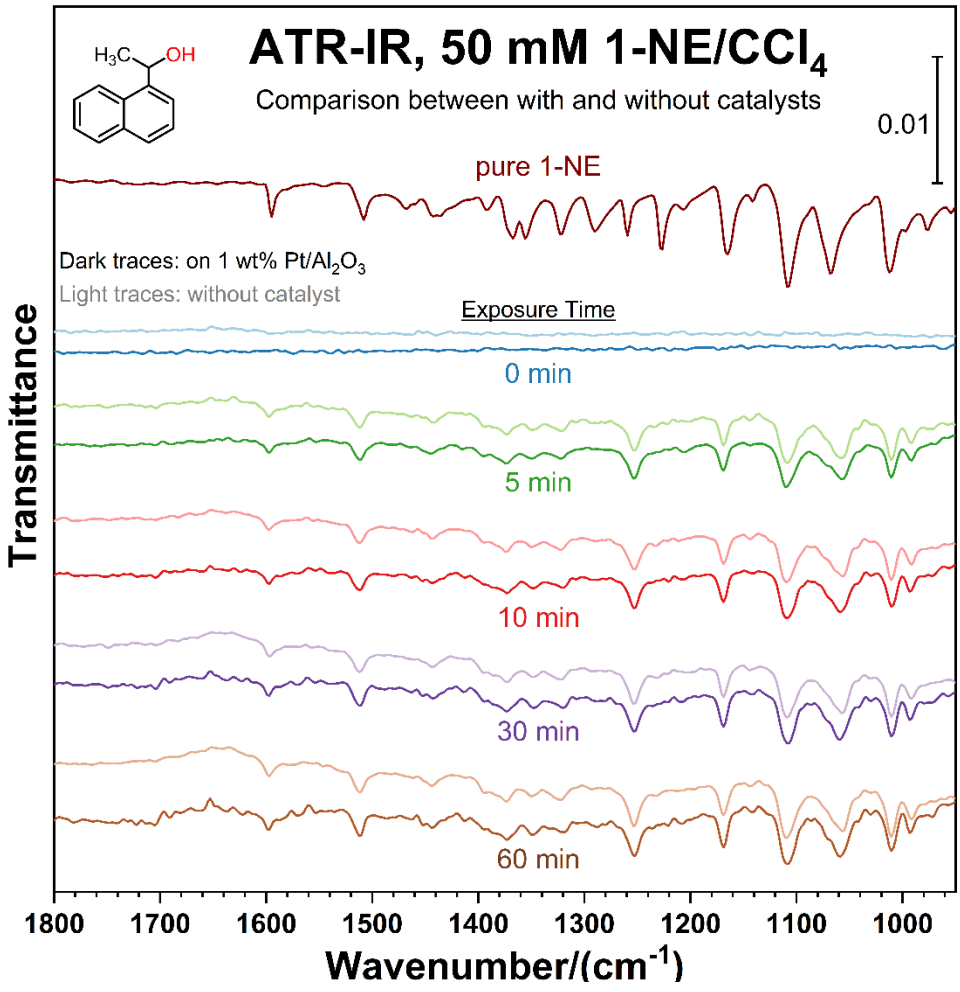

Figure 5.3 ATR-IR spectra of 50 mM 1-NE/CCl_4 with and without catalysts as function of exposure time. The dark traces are the spectra of the solution exposure to 1 wt% Pt/Al_2O_3, while the light traces are the spectra of the solution without catalyst. The top one is the transmission IR spectrum of pure 1-NE.

Further tests were conducted using both enantiomers of 1-NE (r-1-NE and s-1-NE), and the results are summarized in Figure 5.4. All three molecules were subjected to

identical ATR-IR conditions, revealing no significant differences among the various configurations of 1-NE, as indicated in Figure 5.4.

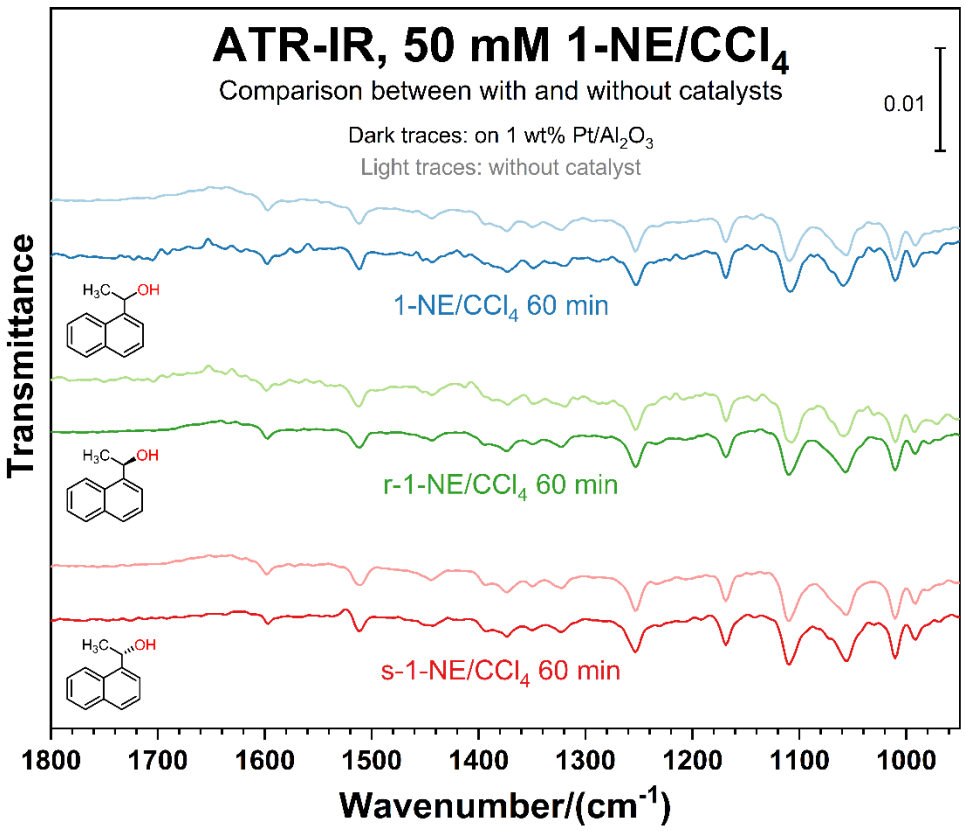

Figure 5.4 The comparison between ATR-IR spectra of 50 mM 1-NE, r-1-NE and s-1-NE in CCl_4 with and without catalysts respectively. The dark traces are the spectra of the solution exposure to 1 wt% Pt/Al_2O_3 after 60 min, while the light traces are the spectra of the solution without catalyst.

Several factors may contribute to the aforementioned results. One plausible explanation could be related to the properties of the Pt catalyst, particularly the cleanliness of its surfaces. To investigate this possibility, CO adsorption on the 1 wt% Pt/Al_2O_3 catalyst was performed using ATR-IR. This experiment aimed to eliminate any contribution resulting from the uncleanness of the Pt surfaces. The procedure involved

bubbling CO into pure CCl_4 solvent for approximately 30 minutes, followed by purging the solution into the ATR-IR cell containing evenly dispersed Pt/Al_2O_3 catalysts on the surface. The IR spectra were recorded over time, and the outcome is presented in Figure 5.5.

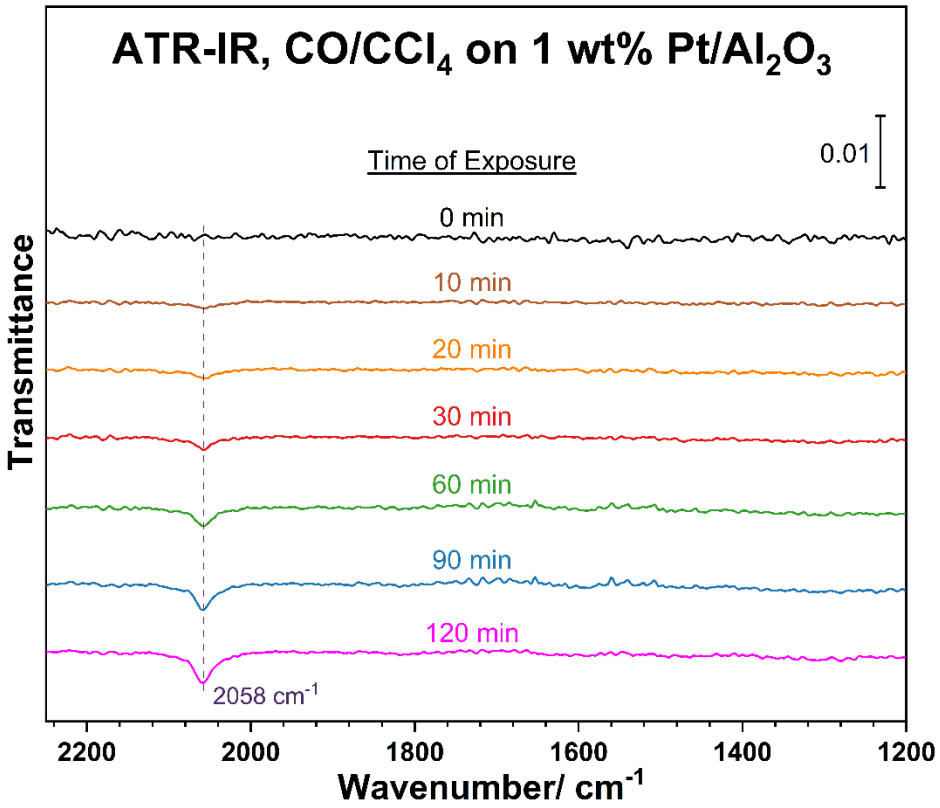

Figure 5.5 ATR-IR spectra of CO in CCl_4 adsorption on commercial 1 wt% Pt/Al_2O_3 catalysts as a function of exposure time.

A single peak at approximately 2058 cm^{-1} was observed, which corresponds to the linearly adsorbed CO on Pt atoms. Furthermore, the peak intensity showed an increase with exposure time, indicating an augmentation in CO coverage on the Pt surface. No other peaks were detected. The CO adsorption experiment confirms the cleanliness of the

Pt/Al_2O_3 surface, thus eliminating the possibility that the lack of 1-NE molecule adsorption on Pt catalysts can be attributed to surface impurities.

5.3.2 Explore the Influence of Solvent

Solvent effects play a pervasive role in organic synthesis, particularly in determining the adsorption of chiral modifiers on Pt surfaces. Thus, the following experiments were conducted to investigate the impact of solvents on the interactions between 1-NE and Pt surfaces.

Table 5.1 provides a comprehensive overview of the solvents employed in this study, including their reported empirical polarity (E_T^N)[87], dielectric constant (ϵ_r)[87], and dipole moment (μ)[88].

Table 5.1 The properties of solvents.

Solvent	Polarity (E_T^N)	Dielectric constant (ϵ_r)	Dipole moment (μ)
cyclohexane	0.006	2.02	0.00
n-pentane	0.009	1.84	0.00
n-hexane	0.009	1.88	0.00
CCl_4	0.052	2.23	0.00
CS_2	0.065	2.64	0.00
toluene	0.099	2.38	0.38
ethyl acetate	0.228	6.02	1.78
cyclohexanone	0.281	16.01	3.06
acetic acid	0.648	6.17	1.70
ethanol	0.654	24.55	1.69

Figure 5.6 illustrates the ATR-IR spectra of 5 mM r-1-NE in eight different solvents on 1 wt% Pt/Al_2O_3 catalysts. All spectra were collected after exposing the solutions to Pt catalysts for 30 minutes. The top trace represents the transmission IR of pure r-1-NE used as a reference.

For *n*-pentane, the spectrum (second trace from the top) exhibited minimal sample signals. Weak signals were observed in the case of cyclohexane (third trace from the top). In the solvent *n*-hexane (fifth trace from the top), distinct sample peaks appeared around 1750 cm^{-1}, 1450 cm^{-1}, 1370 cm^{-1}, and 1210 cm^{-1}, which can be attributed to the solvent itself. Additionally, a broad and strong peak around 1510 cm^{-1} was evident for CS_2, corresponding to the C−S stretching mode. None of these four solvents, including *n*-pentane, *n*-hexane, cyclohexane, and CS_2, revealed any additional sample peaks. One explanation is that the solubility of r-NE in these non-polar solvents is relatively low, hindering potential interactions between the chiral modifiers and Pt surfaces. Furthermore, *n*-hexane and cyclohexane exhibited significant background interferences. Although the solubility of 1-NE in CCl_4 is not high, as previously discussed in Figure 5.2, the 5 mM r-1-NE in CCl_4 also failed to exhibit significant sample signals. Nevertheless, CCl_4 proved more suitable for our studies due to its weak interference in the measurements.

Furthermore, the solubility of r-1-NE in ethyl acetate, cyclohexanone, and acetic acid is considerably higher than in non-polar solvents. However, none of these solvents exhibit distinguishable sample peaks, as depicted in Figure 5.2. The observed peaks likely originate from the solvents on the Pt surface.

In the case of toluene (the fourth trace from the top), the spectrum highlighted in the figure exhibited sample peaks similar to the transmission IR of the pure sample. The peaks around 1600 cm^{-1}, 1500 cm^{-1}, and 1260 cm^{-1} align with the top spectrum of pure r-1-NE.

Overall, the ATR-IR experiments only detect sample peaks related to r-1-NE molecules in the case of toluene. Unfortunately, for the other investigated solvents, either no sample signals were observed or the interference from the solvent was too strong, obscuring potential sample peaks.

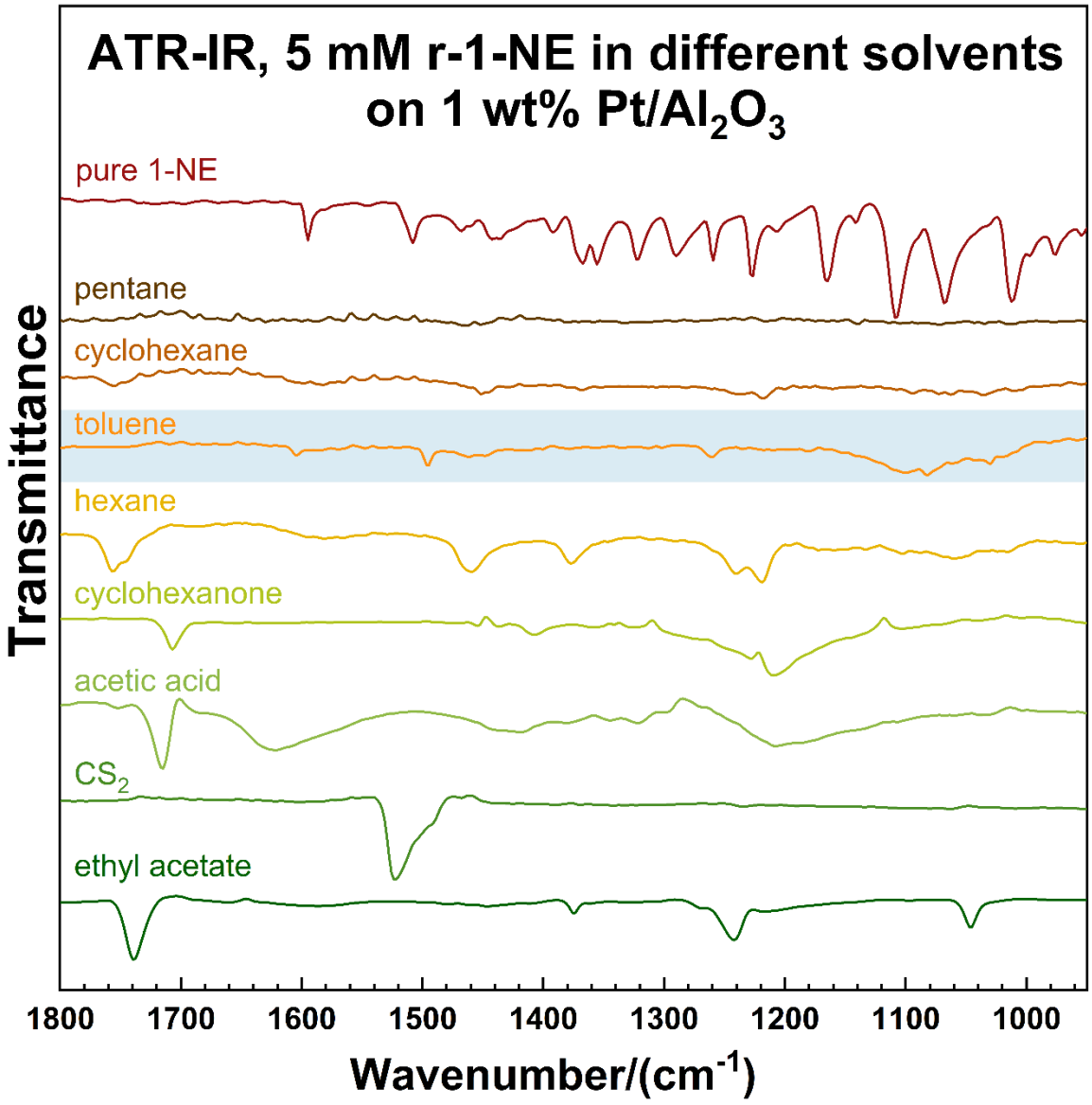

Figure 5.6 ATR-IR spectra of 5 mM r-1-NE in different solvents after exposure on 1 wt% Pt/Al_2O_3 catalysts of 30 min. The top one is the transmission IR of pure r-1-NE as a reference.

5.3.3 Explore the Solvent of Toluene

Figure 5.6 illustrates that only toluene exhibited sample peaks associated with 1-NE molecules in its spectrum. To further investigate the role of toluene as a solvent, additional experiments and comparisons were conducted.

In order to ensure that the results were not influenced by experimental procedures, the experiment was repeated. As depicted in Figure 5.7, the second trace from the top, displayed similar results to Figure 5.6. Flushing tests were also performed. Initially, after exposing the solution to Pt catalysts for 60 minutes, the cell was flushed with pure toluene. The resulting spectrum, represented by the green trace (the third one from the top), did not reveal any additional sample peaks, nor were any peaks removed by flushing. The presence of sample peaks may be attributed to toluene adsorption on the Pt surface. Subsequently, the cell was flushed with pure CCl_4, and no significant differences were observed based on the collected spectrum (the fourth trace from the top, red). These flushing tests suggest that the sample peaks likely originate from adsorbed toluene molecules on the Pt catalysts, rather than the r-1-NE molecules.

Further comparisons were made between two different concentrations. As shown in the bottom trace of Figure 5.7, the opposite direction of the peaks around 1600 cm^{-1} and 1500 cm^{-1} indicates that the peaks are actually from the toluene molecules, due to mis-cancellation from the background of the solvent, toluene. Additionally, varying amounts of Pt/Al_2O_3 catalyst were employed in the tests. The fifth trace from the top in Figure 5.7 reveals that the peaks around 1600 cm^{-1} and 1500 cm^{-1} were barely visible, with only one sharp peak around 1260 cm^{-1} being observed.

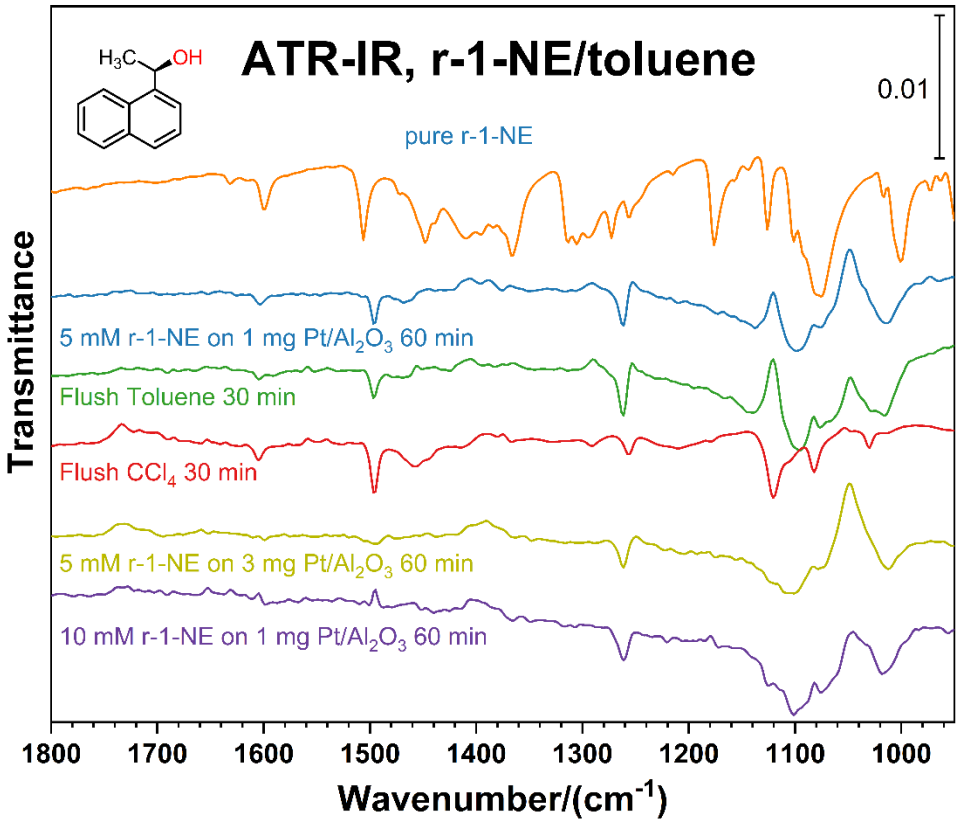

Figure 5.7 ATR-IR spectra of 5 mM r-1-NE in toluene on 1 wt% Pt/Al_2O_3 after 60 min exposure, and flushed with pure toluene 30 min and then with pure CCl_4 30 min. The compared spectra of 10 mM solution and 5 mM solution on different amounts of Pt catalyst are also provided. The top trace is the transmission IR of pure r-1-NE as a reference.

Based on these comparisons, it appears that the peaks detected in the toluene solution are not associated with the presence of 1-NE molecules, but rather with the absorbed toluene. To confirm our understanding, a blank test involving pure toluene on Pt/Al_2O_3 was conducted (top trace as shown in Figure 5.8). Furthermore, the spectra of 5 mM r-1-NE in toluene with and without catalyst are provided. The top spectrum in Figure 5.8 demonstrates the presence of two peaks around 1600 cm^{-1} and 1500 cm^{-1}, as mentioned earlier, confirming that these peaks originate from the absorbed toluene on the

Pt catalysts. The adsorption process is irreversible, as flushing with fresh solvent failed to remove the sample peaks. However, the peak observed at 1261 cm^{-1} was not present in the case of pure toluene. Nevertheless, a single peak is insufficient to indicate the presence of 1-NE molecules.

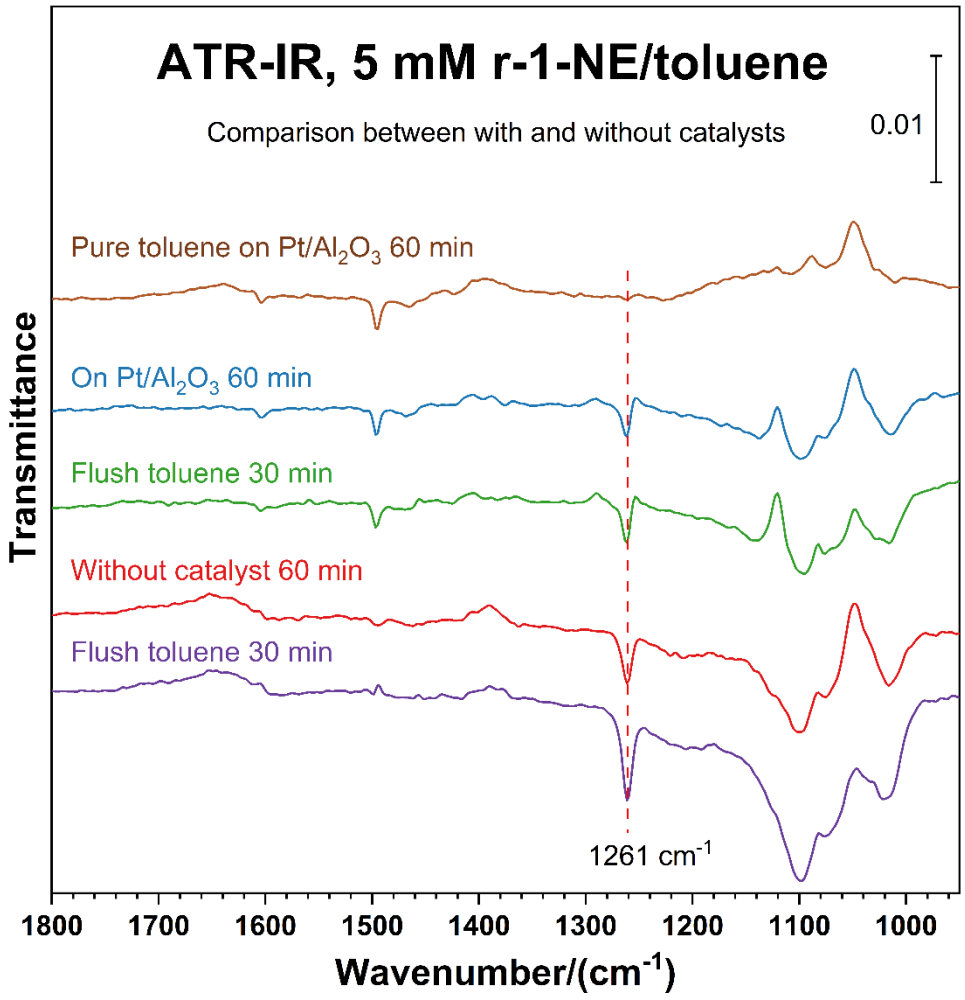

Figure 5.8 ATR-IR spectra of 5 mM r-1-NE in toluene on 1 wt% Pt/Al_2O_3 and without catalysts after 60 min exposure, and flushed with pure toluene 30 min. The top trace is the spectrum of pure toluene on Pt/Al_2O_3 catalyst after 60 min exposure.

5.3.4 Explore the Influence of Functionality Position

In order to investigate the influence of the position of the hydroxyl group, an additional molecule, 1-(2-naphthyl) ethanol (2-NE), was examined. Figure 5.9 presents an example of a 50 mM s-2-NE in CCl_4 solution exposed to a 1 wt% Pt/Al_2O_3 catalyst, demonstrating the relationship between exposure time and the resulting outcomes. The solid traces represent the spectra of 50 mM s-2-NE in CCl_4 on Pt/Al_2O_3 catalysts, while the light traces depict the collected spectra of the blank test without a catalyst.

The obtained results exhibit similarities to the case of 1-NE molecules, as illustrated in Figure 5.3. Notably, no significant differences were observed between the tests conducted with and without catalysts. Most of the peaks align with the transmission IR spectrum of pure s-2-NE (the top trace), except for the sharp peaks at 1270 cm^{-1} and 1000 cm^{-1}, which split into two doublet peaks in the CCl_4 solution. This phenomenon can be attributed to the interactions between the hydroxyl group and the CCl_4 molecules. Consequently, the results presented in Figure 5.9 do not indicate adsorption of 2-NE on Pt catalysts, at least not in the CCl_4 solution.

The solvent toluene was also employed in experiments involving 2-NE molecules. Figure 5.10 provides a summary of these experiments conducted in a toluene solution. A comparison was made between different concentrations of 2-NE in toluene (5 mM and 10 mM), represented by the fourth and bottom traces, respectively. However, no significant differences were observed. The blank test, which employed pure toluene on the Pt catalyst, was also included. The results obtained in the toluene solvent exhibit similarities to the case of 1-NE molecules. The peak at around 1261 cm^{-1} does not provide evidence

of the presence of 2-NE molecules, while the other peaks correspond to toluene molecules.

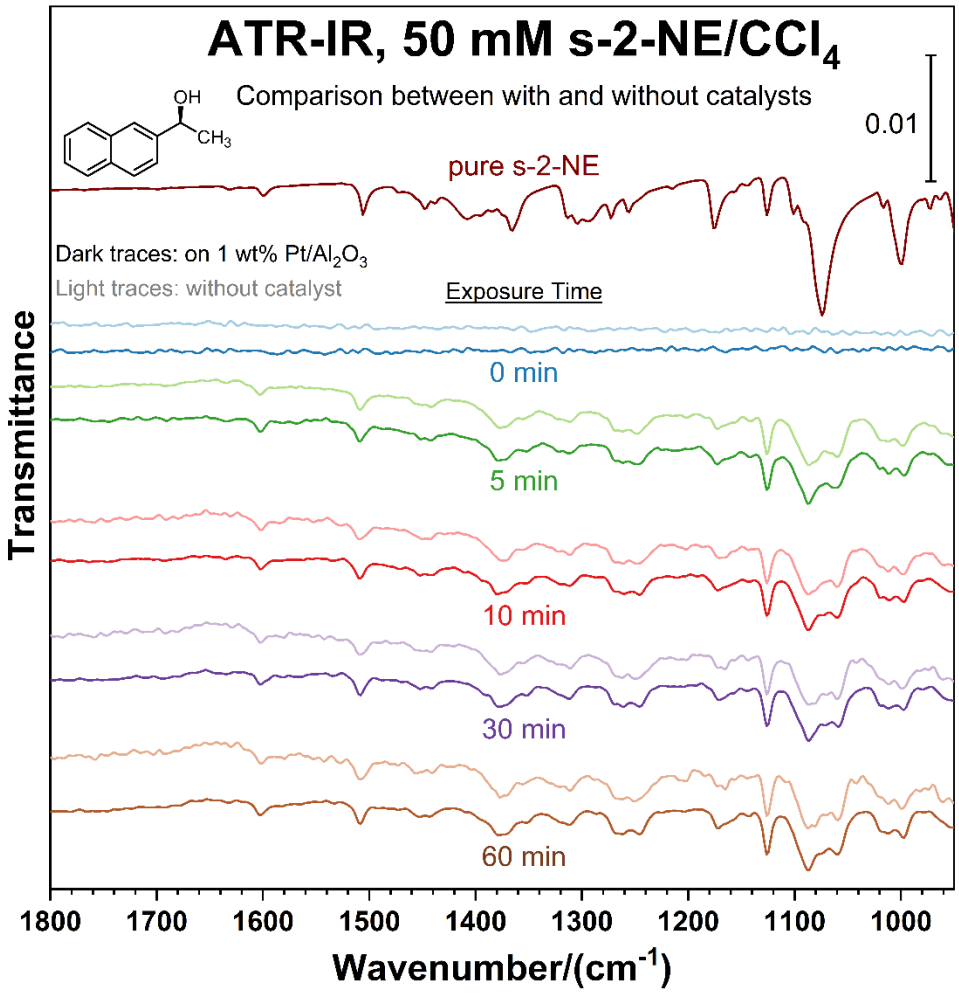

Figure 5.9 ATR-IR spectra of 50 mM s-2-NE/CCl_4 with and without catalysts as function of exposure time. The dark traces are the spectra of the solution exposure to 1 wt% Pt/Al_2O_3, while the light traces are the spectra of the solution without catalyst. The top one is the transmission IR spectrum of pure s-2-NE.

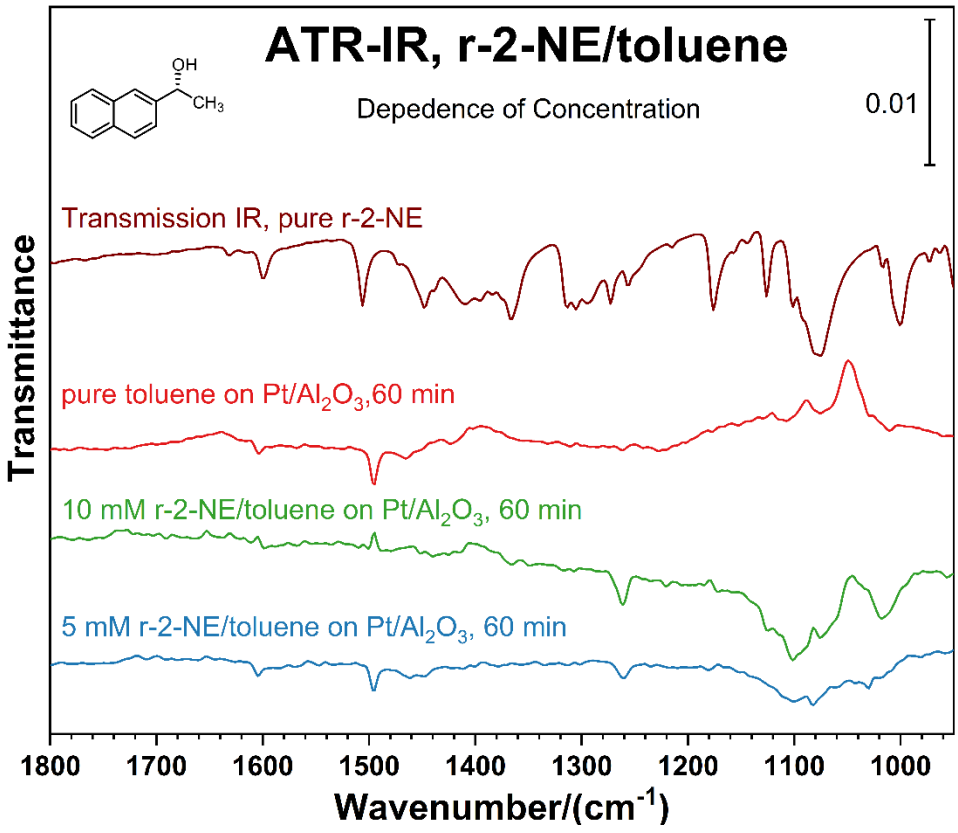

Figure 5.10 ATR-IR spectra of 5 and 10 mM r-2-NE/toluene and pure toluene on 1 wt% Pt/Al_2O_3, exposure time is 60 min. The top one is the transmission IR spectrum of pure r-2-NE.

5.3.5 Explore Influence of Aromatic Ring Size

The influence of aromatic ring size was explored by testing the molecule 1-phenylethanol (1-PE). The tests involved exposing 1-PE in CCl_4 solutions to a 1wt% Pt/Al_2O_3 catalyst at varying concentrations, while also conducting corresponding blank tests without catalysts. Figure 5.11 illustrates the results, with solid traces representing the spectra of 5 mM, 10 mM, and 20 mM 1-PE in CCl_4 on Pt/Al_2O_3 catalysts, and light traces representing the spectra of the corresponding blank tests. The top trace depicts the transmission IR spectrum of pure 1-PE for reference.

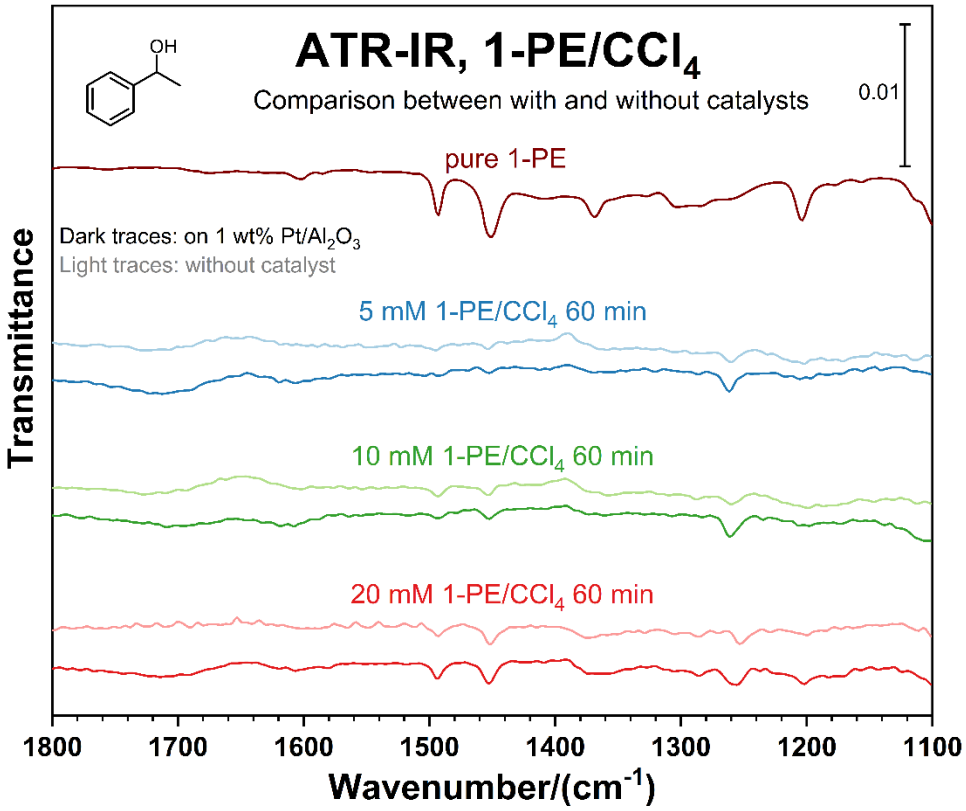

Figure 5.11 ATR-IR spectra of 1-PE in CCl_4 on 1 wt% Pt/Al_2O_3 (dark traces) and without catalyst (light traces) as a function of 1-PE concentration. The top trace is the transmission IR spectrum of pure 1-PE for reference.

In the top spectrum, a prominent peak is observed around 1450 cm^{-1}, accompanied by two sharp and strong peaks around 1490 cm^{-1} and 1200 cm^{-1}. When CCl_4 solutions are used, the intensity of these peaks increases with higher concentration. In the case of a 20 mM 1-PE solution, the spectrum resembles the top spectrum, albeit with the near absence of the peak around 1200 cm^{-1} and the emergence of a new peak around 1260 cm^{-1}, which can be attributed to the C−O stretching mode of the secondary

alcohol. This new peak potentially indicates interactions between Pt and the C−O group, although these interactions are not particularly strong.

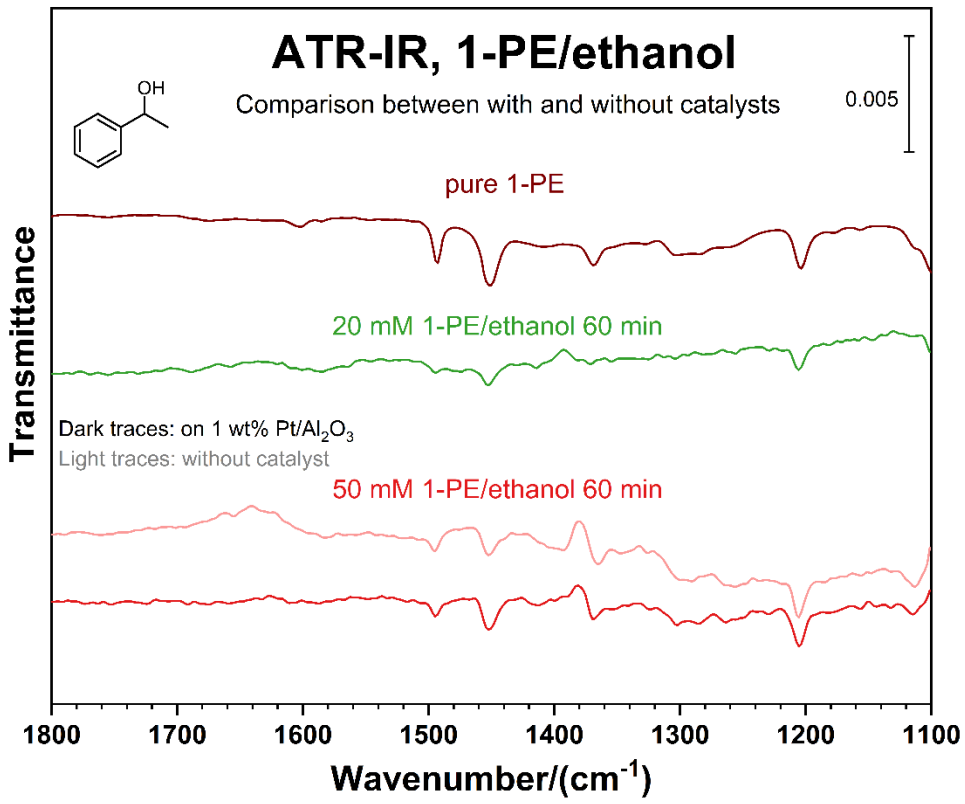

Figure 5.12 ATR-IR spectra of 1-PE in ethanol on 1 wt% Pt/Al_2O_3 (dark traces) and without catalyst (light traces) as a function of 1-PE concentration. The top trace is the transmission IR spectrum of pure 1-PE for reference.

Regarding ethanol, as depicted in Figure 5.12, spectra were collected for 20 mM and 50 mM 1-PE in ethanol on Pt/Al_2O_3 catalysts. The spectrum of the 50 mM solution (the solid red trace, bottom one) exhibits significantly stronger peak signals compared to the spectrum of the 20 mM solution. Furthermore, the spectrum obtained from the blank test of the 50 mM solution without catalysts closely matches the test conducted on Pt

catalysts. However, unlike in the case of CCl_4, the peak around 1250 cm^{-1} does not appear when ethanol is used as the solvent. Therefore, in the presence of ethanol, the 1-PE molecules tend to prefer dissolution in ethanol rather than absorption on Pt catalysts.

5.3.6 Explore the Type of Alcohol

Additional tests were conducted using a different alcohol molecule, 1-naphthaleneethanol (1-NEE). Figure 5.13 displays the ATR-IR spectra 50 mM and 100 mM 1-NEE in CCl_4 with and without catalysts. The solid traces are the spectra collected after exposing to 1 wt% Pt/Al_2O_3 catalyst for 60 minutes, while the light traces correspond to the spectra of the corresponding blank tests without a catalyst. The collected spectra reveal several sample peaks, with the most prominent peak occurring around 1040 cm^{-1}, which could be attributed to the C−O stretching mode. The transmission IR spectrum of pure 1-NEE exhibits the C−O stretching mode at approximately 1030 cm^{-1}. The peak shift may be attributed to the interaction between the hydroxyl group and the solvent. The other sample signals detected in the 1600-1350 cm^{-1} range closely resemble the transmission IR spectrum (the top trace).

Furthermore, similar behavior was observed in the blank tests without catalysts (the light traces), indicating that 1-NEE does not bind to Pt catalysts. Additionally, the intensity of the peaks does not significantly increase in more concentrated solutions.

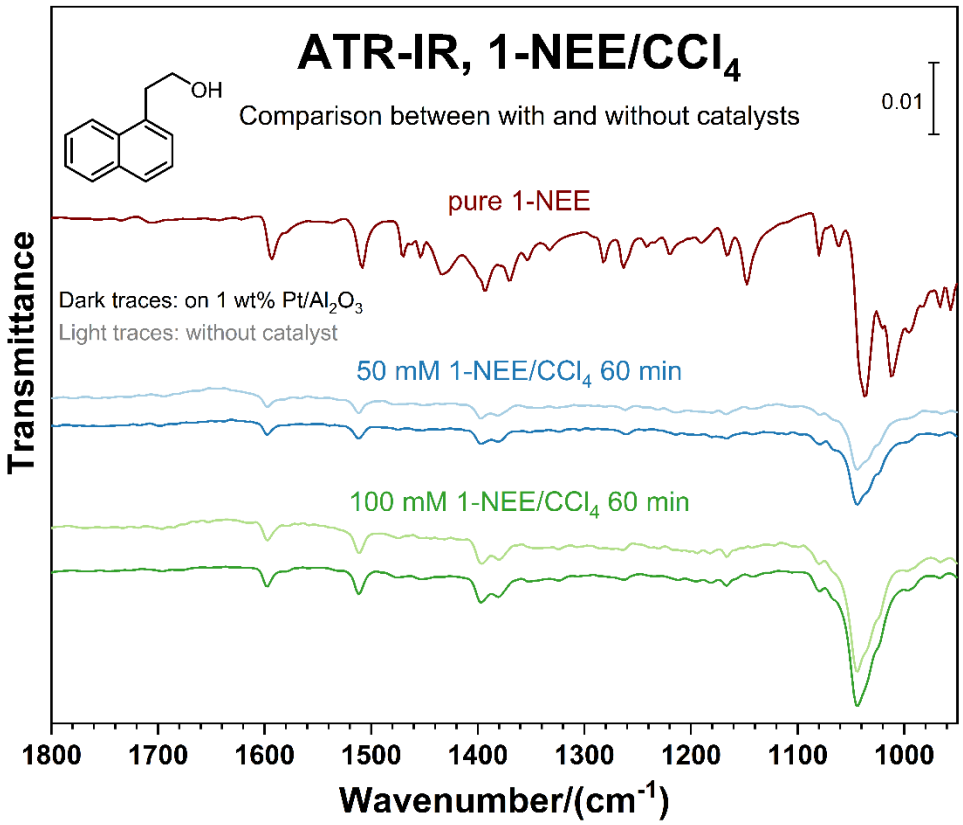

Figure 5.13 ATR-IR spectra of 1-NEE in CCl_4 on 1 wt% Pt/Al_2O_3 (dark traces) and without catalyst (light traces) as a function of 1-NEE concentration. The top trace is the transmission IR spectrum of pure 1-NEE for reference.

5.3.7 Kinetic Measurements with NE Modifiers

Kinetic measurements were conducted using the Et-Py hydrogenation modified with chiral 1-NE and 2-NE molecules. The kinetic data is summarized in Table 5.2, with the corresponding reaction conditions noted below the table. No evident enantioselectivity was detected with any of the chiral 1-NE and 2-NE modifiers. However, under the same conditions, the chiral NEA molecules exhibited much higher conversion and *ee* values. Based on adsorption studies involving nitrogen- and oxygen-based molecules, it was observed that none of the oxygen-based molecules exhibited any

signs of adsorption on Pt catalysts, while both 1-NEA and 2-NEA molecules showed binding to Pt surfaces. Therefore, the chiral modifiers bound to Pt surfaces likely created a chiral environment, contributing to the observed enantioselectivity. However, the NE-related molecules did not bind to the Pt surface, as indicated by the ATR-IR studies. Consequently, the reactions modified with chiral NE molecules did not exhibit significant *ee* values.

Table 5.2 Conversion and ee of the Et-Py hydrogenation catalyzed by a 1 wt% Pt/Al_2O_3 catalyst as a function of the modifier used.

Modifier	**Mole ratio of reactants Pt/Et-Py/modifier**	**Conversion (%)**	***ee* (%)**
No modifier	1/2000/none	47.3	0.4
r-1-NEA	1/2000/5	100	18.6 (R)
s-1-NEA	1/2000/5	100	17.3 (S)
r-2-NEA	1/2000/5	100	24.0 (R)
s-2-NEA	1/2000/5	100	23.8 (S)
r-1-NE	1/2000/5	60.4	1.2
s-1-NE	1/2000/5	29.4	0.2
r-2-NE	1/2000/5	58.2	0.9
s-2-NE	1/2000/5	37.1	0.2

Reaction conditions: t = 3.0 h, T= 298 K, $P(H_2)$=10 bar, Pt catalyst (25 mg), toluene solvent (10 mL), molar ratio of Pt:Et-Py:modifier = 1:2000:5.

5.4 Summary

In this chapter, we investigated various types of chiral modifiers featuring oxygen-based centers, as illustrated in Figure 5.14 below. Regrettably, no evidence of adsorption was observed for any of the molecules in solution, despite examining the effects of solvent, catalyst support, position of the alcohol group, size of the aromatic ring, and the type of alcohol.

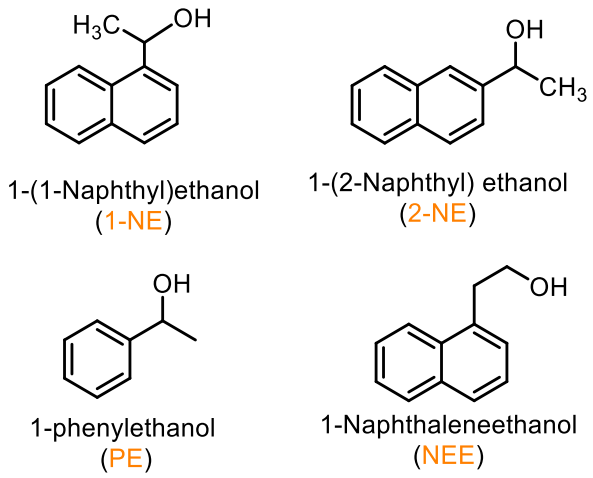

Figure 5.14 The structure of oxygen-based molecules investigated in this chapter.

It appears that achieving high coverage on the Pt surface proved challenging, as the oxygen-based molecules exhibited a preference for dissolving in solvents rather than binding to Pt catalysts. The molecules demonstrated stronger interactions with the solvent compared to the Pt catalysts. Conversely, kinetic studies using chiral NE molecules revealed no significant enantioselectivity when compared to chiral NEA molecules.

Chapter 6

Adsorption of 3-(1-Naphthyl)-L-alanine (1-NLA) on Pt Surfaces in Heterogeneous Catalysis

6.1 Brief Introduction and Hypothesis

As stated in the Introduction section, one successful instance of chiral molecule-modified heterogeneous catalysis is the hydrogenation of β-keto esters facilitated by nickel catalysts modified with tartaric acid. The carboxylic groups in tartaric acid contribute to the enantioselectivity of the reaction. In our study, we observed that the amine groups also exhibit the ability to promote enantioselectivity. Hence, we proposed that a combination of both amines and carboxylic groups would yield the maximum chiral effects.

Amino acids are organic molecules that possess both an amino group ($-NH_2$) and a carboxylic acid group ($-COOH$). They serve as fundamental constituents of proteins and play a vital role in the structure and functioning of all living organisms. Amino acids are additionally employed as chiral modifiers in asymmetric catalysis due to their capacity to enhance the enantioselectivity of the reactions in which they participate. To expand the repertoire of amino acids, we propose the investigation of 3-(1-naphthyl)-L-alanine (1-NLA) and related compounds, as depicted in Figure 6.1.

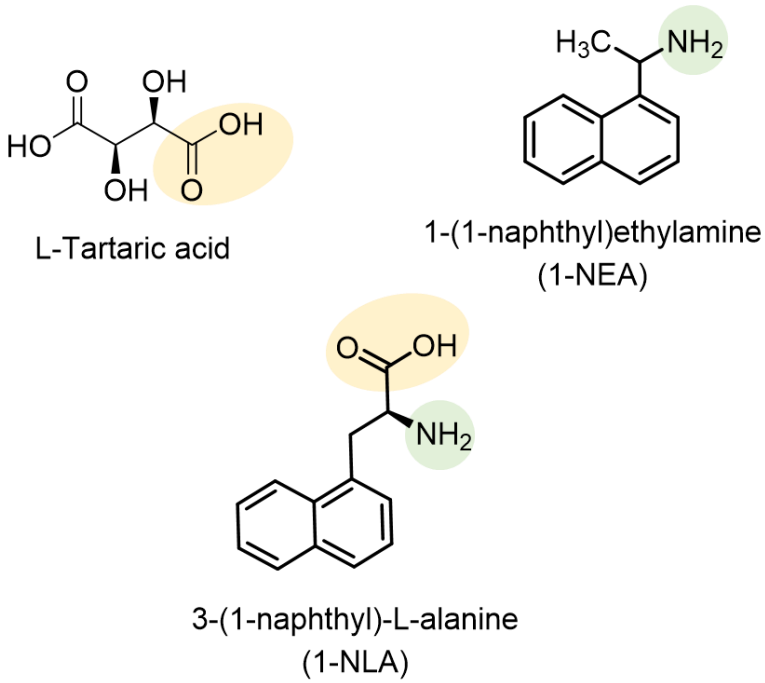

Figure 6.1 Molecular structure of L-tartaric acid, 1-NEA and 1-NLA.

This chapter aims to examine the adsorption behavior of amino acids onto Pt catalysts from liquid solutions using our *in-situ* ATR-IR instrument. Furthermore, we investigate the effects of catalyst support, solvent, and the position of the amino acid group. Additionally, kinetic measurements were conducted.

6.2 Experimental Details

The adsorption tests for all the chiral modifiers were conducted using *in-situ* ATR-IR, while the reference spectra of pure samples were obtained through transmission IR spectroscopy. Kinetic measurements were performed using high-pressure reactors. For

a comprehensive understanding of the experimental procedures, please refer to Chapter 2, where all the experimental details are provided.

6.3 Results and Discussions

6.3.1 *In-Situ* ATR-IR Adsorption Studies of 1-NLA on Pt Surfaces

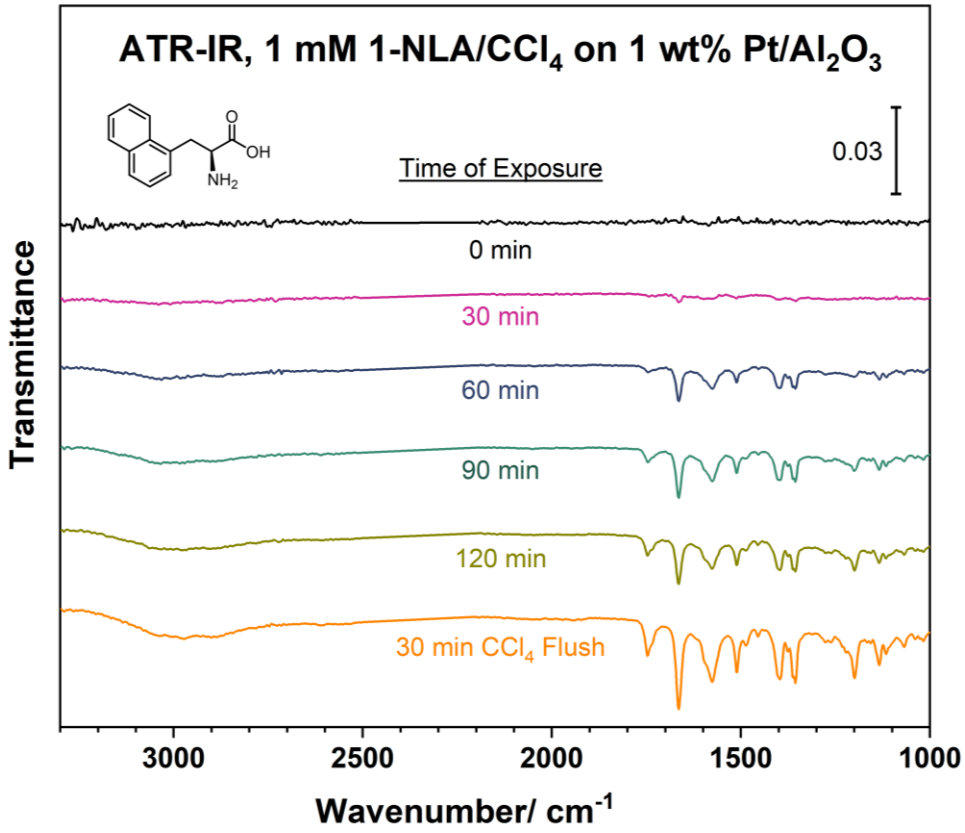

Figure 6.2 ATR-IR spectra of 1 mM 1-NLA in CCl_4 adsorption on 1 wt% Pt/Al_2O_3 catalysts as a function of time exposure.

The experiments commenced by utilizing an amino acid known as 3-(1-naphthyl)-L-alanine (1-NLA). Figure 6.2 illustrates the ATR-IR spectra of a 1 mM 1-NLA solution in CCl_4 when exposed to 1 wt% Pt/Al_2O_3, with exposure time serving as the independent

variable. Following a 30-minute exposure, certain faint peaks became apparent, and subsequently, a progressive increase in peak intensity was observed over time. After a duration of 2.0 hours, the system was purged with pure solvent (CCl_4). Notably, all sample peaks persisted after a 30-minute flushing period. This phenomenon potentially suggests the binding of 1-NLA to Pt catalysts. To reach a definitive conclusion, additional tests, such as control experiments without catalysts, must be conducted.

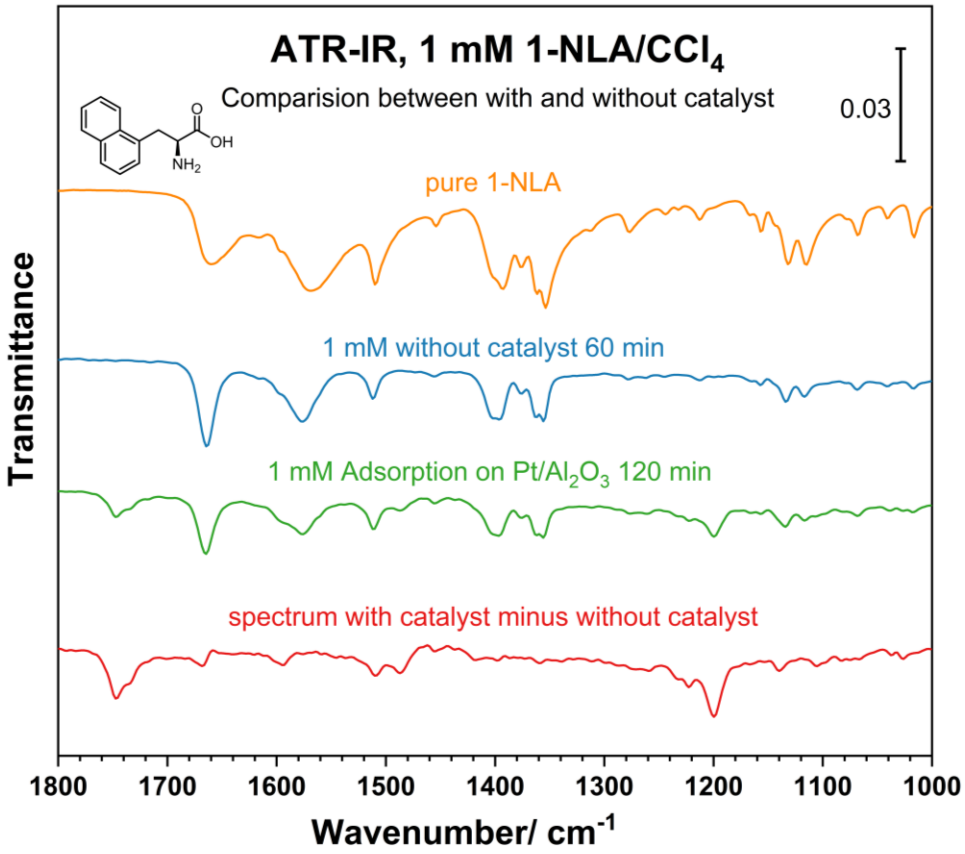

Figure 6.3 The comparison between the ATR-IR spectra of 1 mM 1-NLA in CCl_4 adsorption on 1 wt% Pt/Al_2O_3 and without catalysts. The top one is the transmission IR of pure 1-NLA. And the bottom one is the spectrum after subtracting the scaled spectrum without catalyst (blue trace) from the spectrum on catalyst (green trace).

Figure 6.3 presents a comparison between tests performed with and without catalysts. The uppermost trace represents the transmission IR spectrum of 1 mM 1-NLA, serving as the reference. As illustrated in Figure 6.3, the ATR-IR spectrum of a 1 mM 1-NLA solution without a catalyst (second trace from the top) closely resembles the transmission IR spectrum of the pure sample (uppermost trace). However, minor discrepancies exist. For instance, the broad peak centered around 1660 cm^{-1} becomes narrower and slightly shifts to a higher wavenumber. This peak can be attributed to the N−H bending of the amine group. The observed peak shift and increased sharpness in the CCl_4 solution might result from weakened hydrogen bonding among the 1-NLA molecules due to their dilution in the solvent.

Regarding the spectrum obtained in the presence of Pt catalysts (green trace, third from the top), novel peaks emerge over time, particularly two peaks at approximately 1740 cm^{-1} and 1200 cm^{-1}. Hence, we propose that the spectrum of the 1 mM 1-NLA on Pt catalysts represents a combination of free molecules in the solution and absorbed molecules on the Pt surface. The appearance of the new peaks could be attributed to the amine group binding to the Pt surface. To eliminate the contribution from free molecules in the solution, we subtracted the scaled spectrum obtained without the catalyst from the spectrum collected on the Pt/Al_2O_3 catalyst. The resulting subtracted spectrum is depicted in the bottom trace. Despite the subtraction, some distinct peaks persist. Apart from the two prominent peaks mentioned earlier, there are additional, less intense peaks around 1500 cm^{-1} and 1600 cm^{-1}. We believe these remaining peaks can be assigned to the absorbed 1-NLA on Pt surfaces.

6.3.2 Effect of Catalyst Support on 1-NLA Adsorption

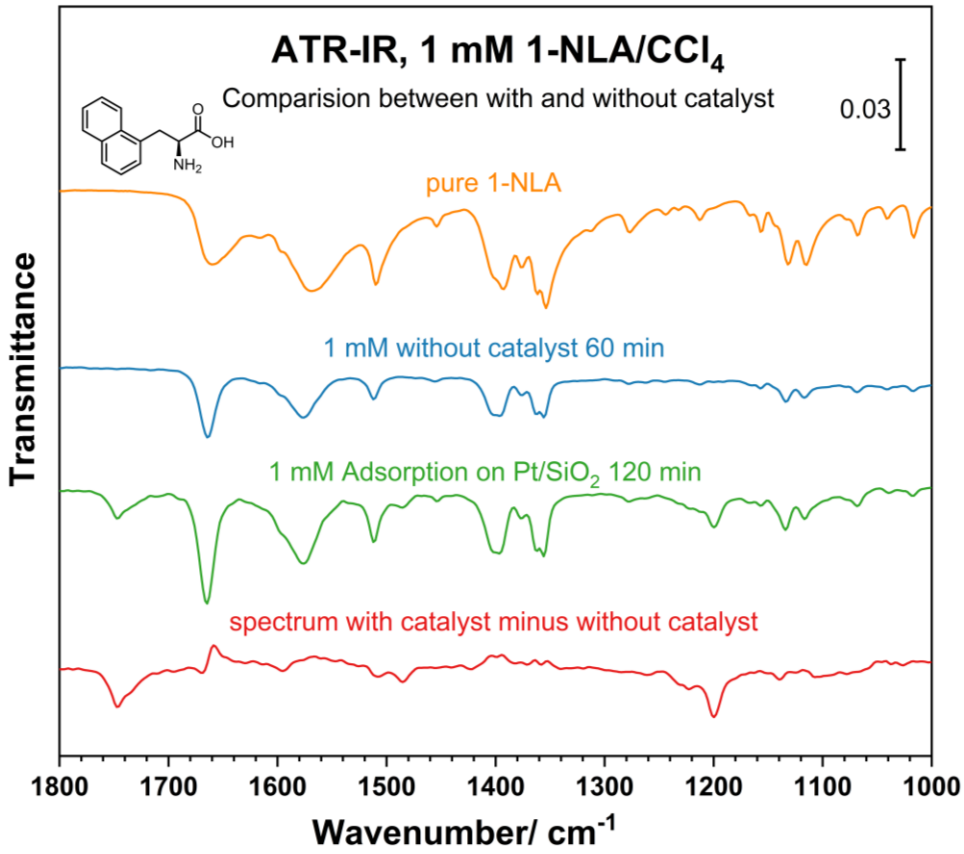

Figure 6.4 The comparison between the ATR-IR spectra of 1 mM 1-NLA in CCl_4 adsorption on 1 wt% Pt/SiO_2 and without catalysts. The top one is the transmission IR of pure 1-NLA. And the bottom one is the spectrum after subtracting the scaled spectrum without catalyst (blue trace) from the spectrum on catalyst (green trace).

As previously discussed, the Pt/Al_2O_3 catalysts exhibited the appearance of new peaks when exposed to 1 mM 1-NLA in CCl_4. To further explore the influence of the catalyst support, we conducted the same tests on 1 wt% Pt/SiO_2 catalysts. Figure 6.4 illustrates that the Pt/SiO2 catalyst displayed a similar behavior.

6.3.3 Effect of Solvent on 1-NLA Adsorption

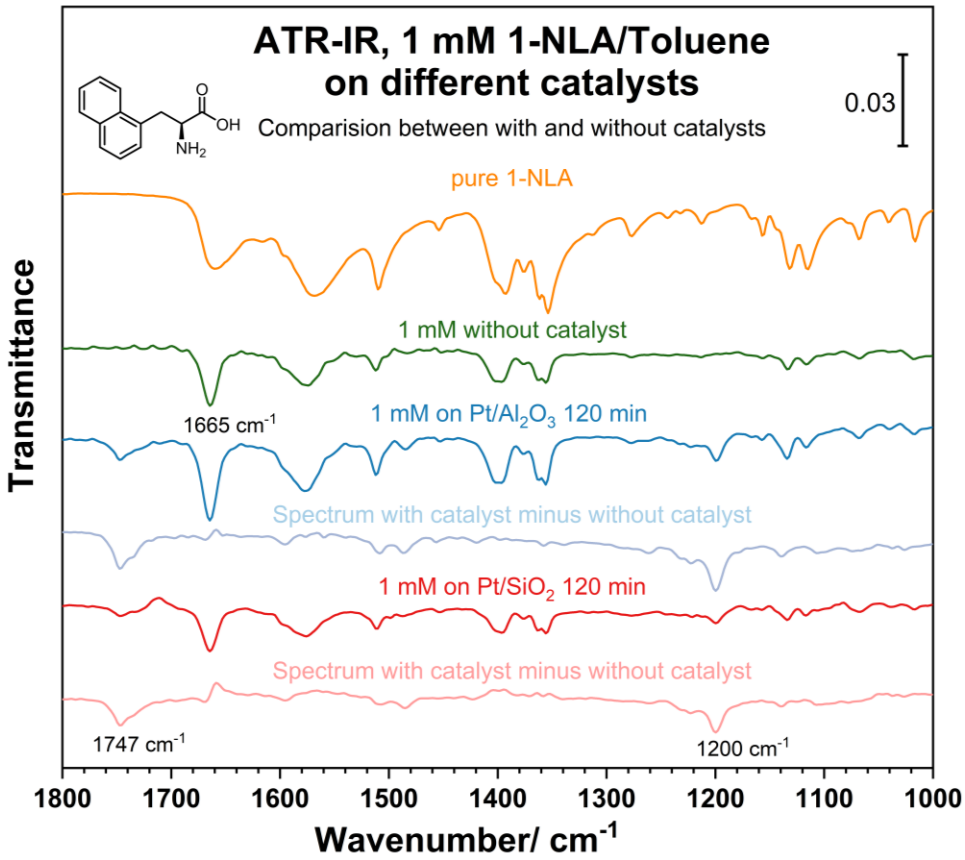

Figure 6.5 ATR-IR spectra of 1 mM 1-NLA in toluene adsorption on different catalysts. The top one is the transmission IR of pure 1-NLA. The dark traces are the IR spectra of 1mM 1-NLA in toluene without catalyst and exposed to 1 wt% Pt/Al_2O_3, 1 wt% Pt/SiO_2 respectively. And the light traces are the spectra after subtracting the scaled spectrum without catalyst from the spectrum on catalyst.

The influence of solvents on the behavior of chiral modifiers in solution when exposed to the Pt surface was discussed in Chapter 5. In addition to the solvents previously mentioned, namely CCl_4, three more solvents were tested in the 1-NLA adsorption studies: toluene, acetic acid, and ethanol.

Figure 6.5 presents a comparison between the 1 mM 1-NLA in toluene, with and without Pt catalysts. Both 1 wt% Pt/Al_2O_3 and 1 wt% Pt/SiO_2 catalysts were tested. The light traces represent the subtracted spectrum obtained by subtracting the spectrum without catalyst from the one with catalyst. The results are consistent with those discussed in Figure 6.3 and Figure 6.4 for the case of CCl_4. In the blank test, the dominant peak appears around 1665 cm^{-1}, which can be attributed to the N−H bending of the amine group. Additionally, two new peaks, particularly around 1747 cm^{-1} and 1200 cm^{-1}, were observed.

To facilitate a better comparison between CCl_4 and toluene, Figure 6.6 illustrates the results obtained with both solvents. As depicted in the figure, there is no significant difference in terms of peak position. However, it appears that the intensity of the peaks in the toluene sample is slightly higher than that of the CCl_4 sample. Usually, peak intensity is related to surface coverage, suggesting that toluene may enhance the 1-NEA adsorption to a greater extent.

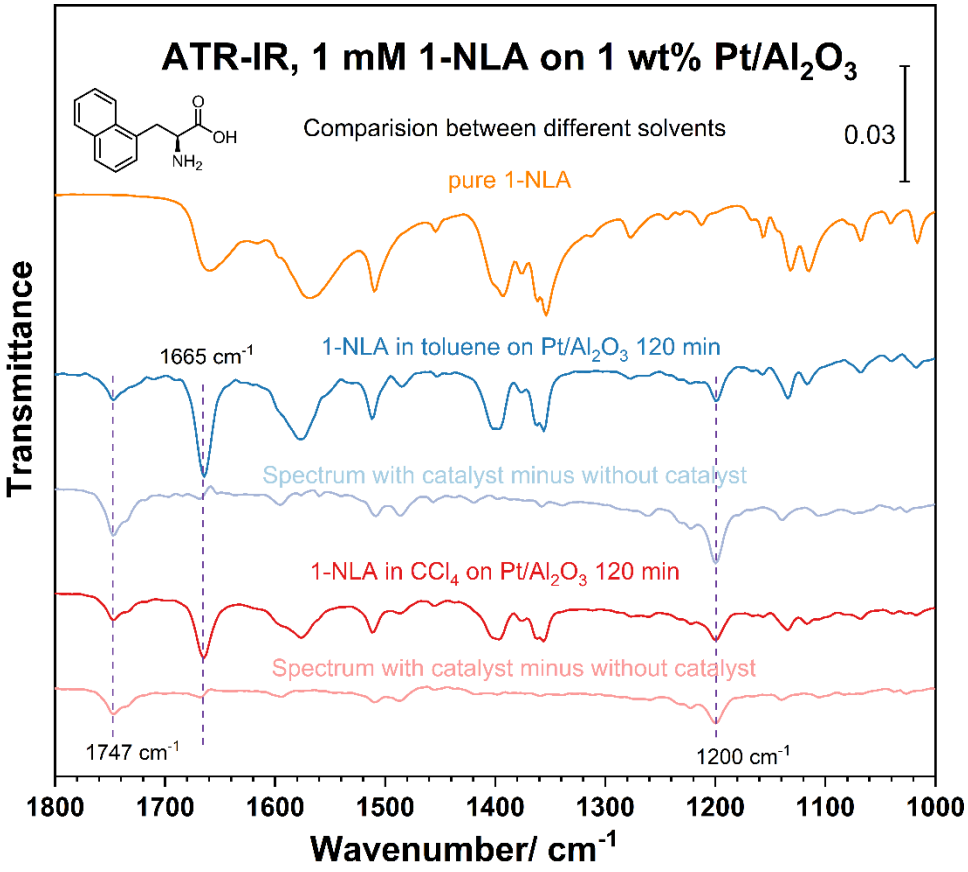

Figure 6.6 The comparison between ATR-IR spectra of 1 mM 1-NLA in toluene and in CCl_4 solutions adsorption on 1 wt% Pt/Al_2O_3 catalysts. The top one is the transmission IR of pure 1-NLA. And the light traces are the spectra after subtracting the scaled spectrum without catalyst from the spectrum on catalyst.

Another solvent, acetic acid, was also utilized for the experiments, and the results obtained for various catalysts are presented in Figure 6.7 above. The tests were conducted both with Pt-supported catalysts and without any catalysts. Additionally, a comparison was made by performing ATR-IR analysis on pure acetic acid without a catalyst. The figure below illustrates the obtained spectrum, showing two prominent peaks at approximately 1715 cm^{-1} and 1290 cm^{-1} in the case of the Pt catalyst. Interestingly, the spectrum acquired from the 1 mM solution without a catalyst closely resembles the

spectrum of pure acetic acid analyzed by ATR-IR. Consequently, these two strong peaks can be attributed to acetic acid molecules rather than 1-NLA molecules. Due to the significantly higher solubility of 1-NLA in acetic acid, the molecular interactions between 1-NLA and acetic acid are considerably stronger. This, in turn, results in a higher preference for 1-NLA to be dissolved in acetic acid rather than being bound to the Pt surface.

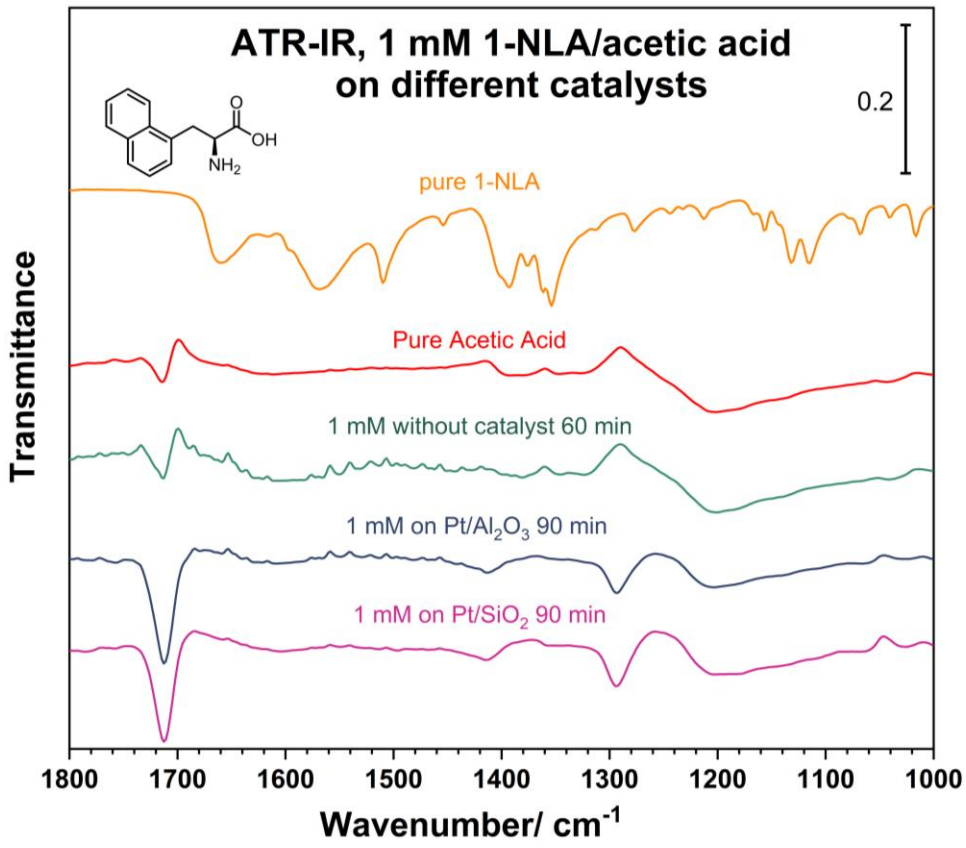

Figure 6.7 The ATR-IR spectra of 1 mM 1-NLA in acetic acid adsorption on different catalysts. The top one is the transmission IR of pure 1-NLA. The second one from the top is the IR spectrum of pure acetic acid without catalyst. The following traces are the spectra of 1mM 1-NLA in acetic acid without catalyst and exposed to 1 wt% Pt/Al_2O_3, 1 wt% Pt/SiO_2 catalysts respectively.

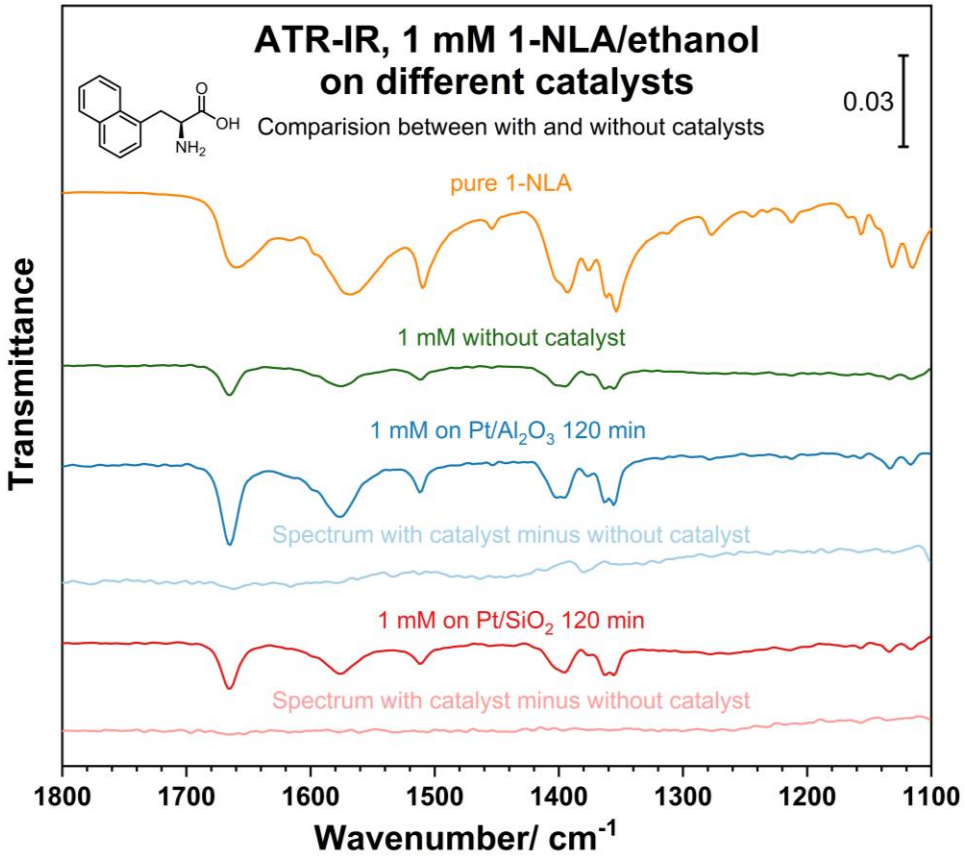

Figure 6.8 ATR-IR spectra of 1 mM 1-NLA in ethanol adsorption on different catalysts. The top one is the transmission IR of pure 1-NLA. The dark traces are the IR spectra of 1mM 1-NLA in ethanol without catalyst and exposed to 1 wt% Pt/Al_2O_3, 1 wt% Pt/SiO_2 respectively. And the light traces are the spectra after subtracting the scaled spectrum without catalyst from the spectrum on catalyst.

To investigate the adsorption of 1-NLA, ethanol was also employed as a solvent, and the corresponding results are summarized in Figure 6.8 and Figure 6.9.

Figure 6.8 provides a comparison between the spectra obtained from 1 mM 1-NLA solutions in ethanol with and without catalysts. Both tests exhibit similar spectra, and upon performing subtraction as previously done, no significant peaks were observed. Furthermore, tests were conducted using a lower concentration (0.5 mM) of 1-NLA

solutions under the same conditions, and the results are summarized in Figure 6.9. In this case, no noteworthy differences were observed.

The case of ethanol shares some similarities with acetic acid as a solvent. Both solvents are polar and possess high dielectric constants, particularly ethanol. In such solvent types, molecules tend to prefer dissolution due to the strong interaction between the molecules and the solvents.

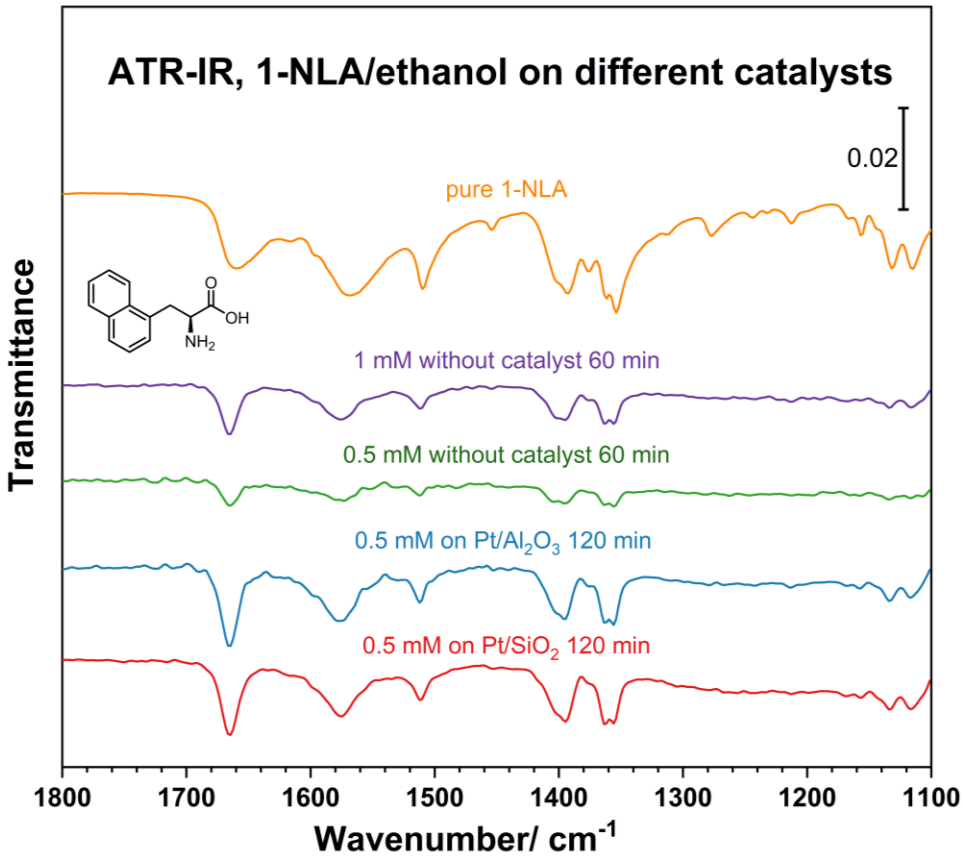

Figure 6.9 ATR-IR spectra of 0.5 mM 1-NLA in ethanol adsorption on different catalysts. The top one is the transmission IR of pure 1-NLA. The second one from the top is the spectrum of 1 mM 1-NLA in ethanol without catalyst. The following traces are the IR spectra of 0.5 mM 1-NLA in ethanol without catalyst and exposed to 1 wt% Pt/Al_2O_3, 1 wt% Pt/SiO_2 respectively.

6.3.4 Comparison Between 1-NLA and 1-NDA

The other configuration of 1-NLA, 3-(1-napthyl)-D-alanine, referred to as 1-NDA in this paper, was also tested. The structures of both molecules are depicted in Figure 6.10.

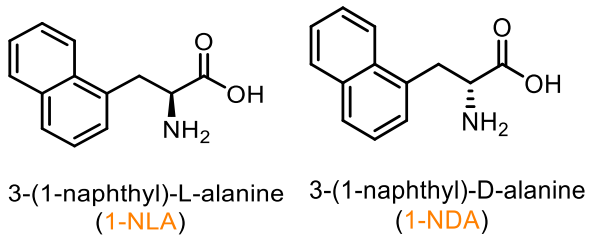

Figure 6.10 The structure of 1-NLA and 1-NDA.

Since enantiomers possess identical physical and chemical properties, it would be anticipated that both enantiomers, 1-NLA and 1-NDA, would exhibit similar behavior in the ATR-IR tests. However, the results indicate that 1-NDA does not behave in the same manner as 1-NLA molecules.

Figure 6.11 displays spectra collected as function of exposure time using a 1 mM 1-NDA in CCl_4 solution on 1 wt% Pt/Al_2O_3 catalysts. Despite the increasing intensity of the sample peaks over time, all the sample signals resemble the top spectrum (transmission IR of pure 1-NLA), and the appearance of new peaks observed in the case of 1-NLA (depicted in Figure 6.2) is absent here. This phenomenon presents a challenging explanation. Moreover, the data concerning 1-NLA molecules in the previous sections are reproducible. To ensure that this result is not attributable to experimental errors, further tests were conducted.

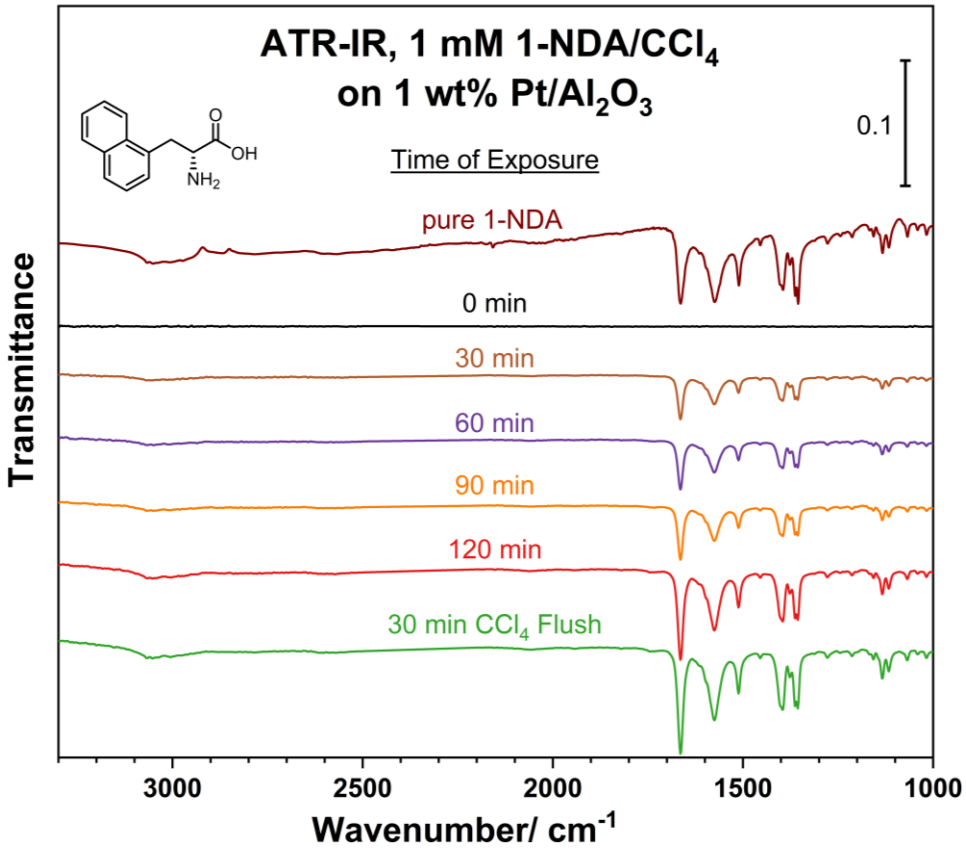

Figure 6.11 ATR-IR spectra of 1 mM 1-NDA in CCl_4 adsorption on 1 wt% Pt/Al_2O_3 catalysts as a function of time exposure to the surface. The top trace is the transmission IR of pure 1-NDA.

Firstly, a less concentrated solution (0.5 mM) was tested under identical conditions. Additionally, a blank test without a catalyst was performed. Figure 6.12 illustrates that the only distinction between the 0.5 mM and 1.0 mM solutions is the peak intensity. Furthermore, the blank test of the 0.5 mM solution aligns with the spectrum of the 0.5 mM solution on Pt catalysts. The subtracted spectrum (the bottom trace) exhibits minimal significant signals.

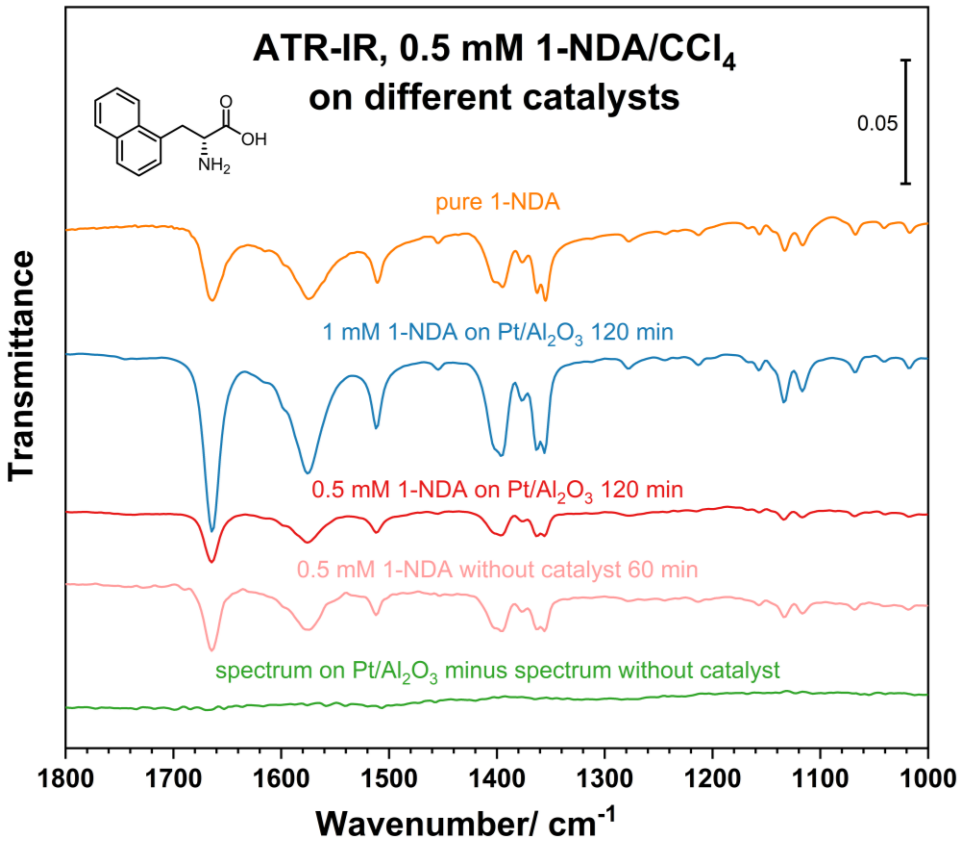

Figure 6.12 ATR-IR spectra of 0.5 mM 1-NDA in CCl_4 adsorption on different catalysts. The top one is the transmission IR of pure 1-NDA. The second one from the top is the spectrum of 1 mM 1-NDA in CCl_4 without catalyst. The following dark and light red traces are the ATR-IR spectra of 0.5 mM 1-NDA in CCl_4 without catalyst and exposed to 1 wt% Pt/Al_2O_3 respectively. The bottom one is the spectrum after subtracting the scaled spectrum without catalyst from the spectrum on catalyst.

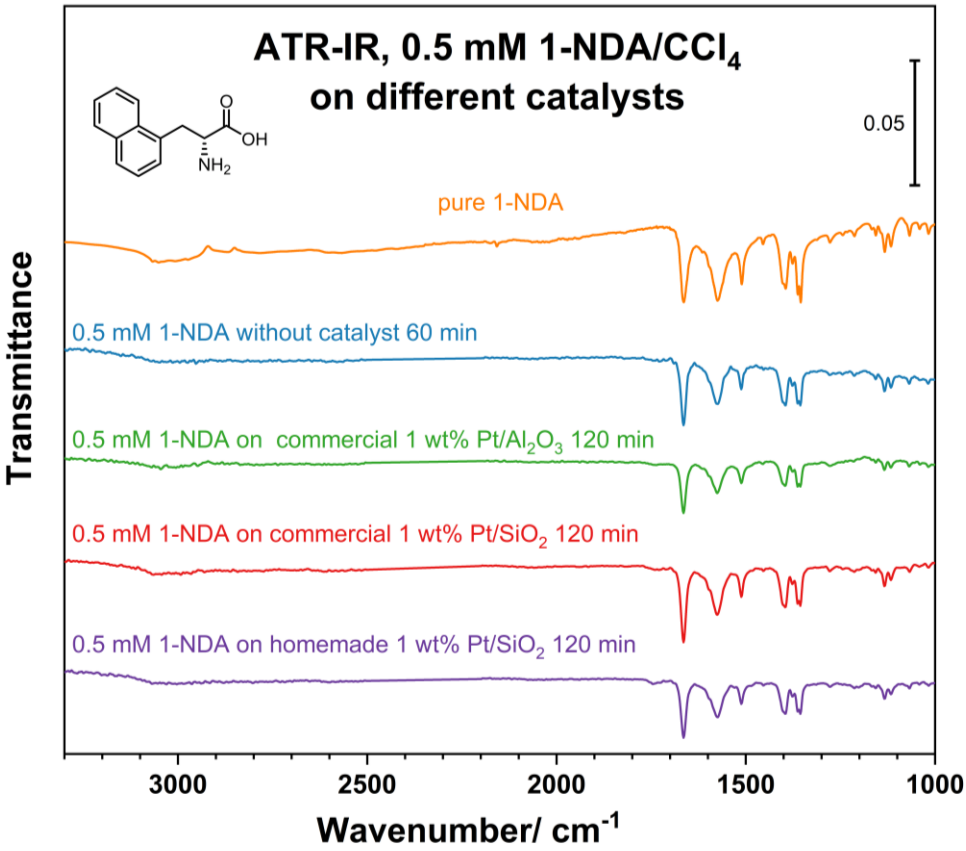

Figure 6.13 The ATR-IR spectra of 0.5 mM 1-NDA in CCl_4 adsorption on different catalysts. The top one is the transmission IR of pure 1-NDA. The following traces are the ATR-IR spectra of 0.5 mM 1-NDA in CCl_4 without catalyst and exposed to 1 wt% commercial Pt/Al_2O_3, 1 wt% commercial Pt/SiO_2 and 1 wt% homemade Pt/SiO_2 catalysts respectively.

In order to ensure that the phenomenon was not specific to Pt/Al_2O_3 catalysts, additional tests were conducted using different Pt catalysts. Three catalysts were tried: commercial 1 wt% Pt/Al_2O_3, commercial 1 wt% Pt/SiO_2, and homemade 1 wt% Pt/SiO_2. The results of the comparisons are summarized in Figure 6.13.

As depicted in Figure 6.13, the behavior of 0.5 mM 1-NDA in CCl_4 was consistent across all catalysts, showing no appearance of additional peaks in any of the cases. The distinction between 1-NLA and 2-NDA is more pronounced in Figure 6.14.

Notably, the subtracted spectrum exhibited no significant peaks for 1-NDA molecules. These observations were repeated multiple times, suggesting that the sample quality might be a contributing factor. Although the precise reasons behind this peculiar behavior have yet to be determined, it may be worthwhile to test a new molecule before proceeding further in this area.

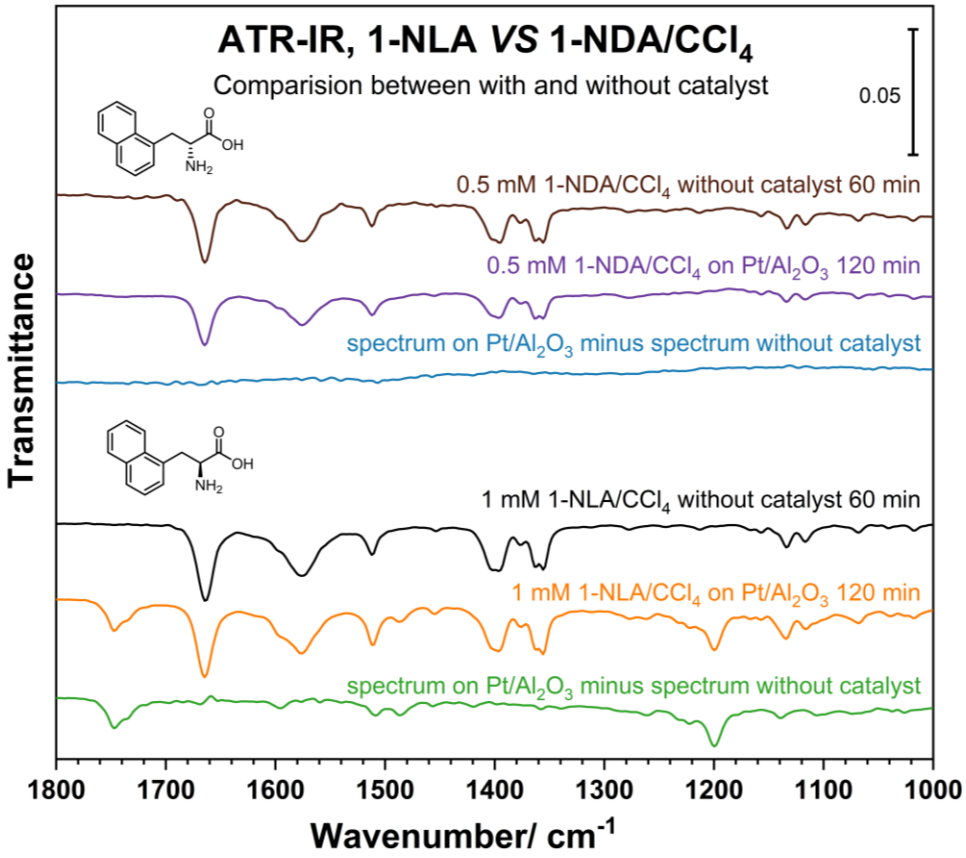

Figure 6.14 The comparison between the ATR-IR spectra of 1 mM 1-NDA and 1-NLA in CCl_4 adsorption on 1 wt% Pt/Al_2O_3 and without catalysts. And the third from the top and the bottom traces are the spectra after subtracting the scaled spectrum without catalyst from the spectrum on catalyst.

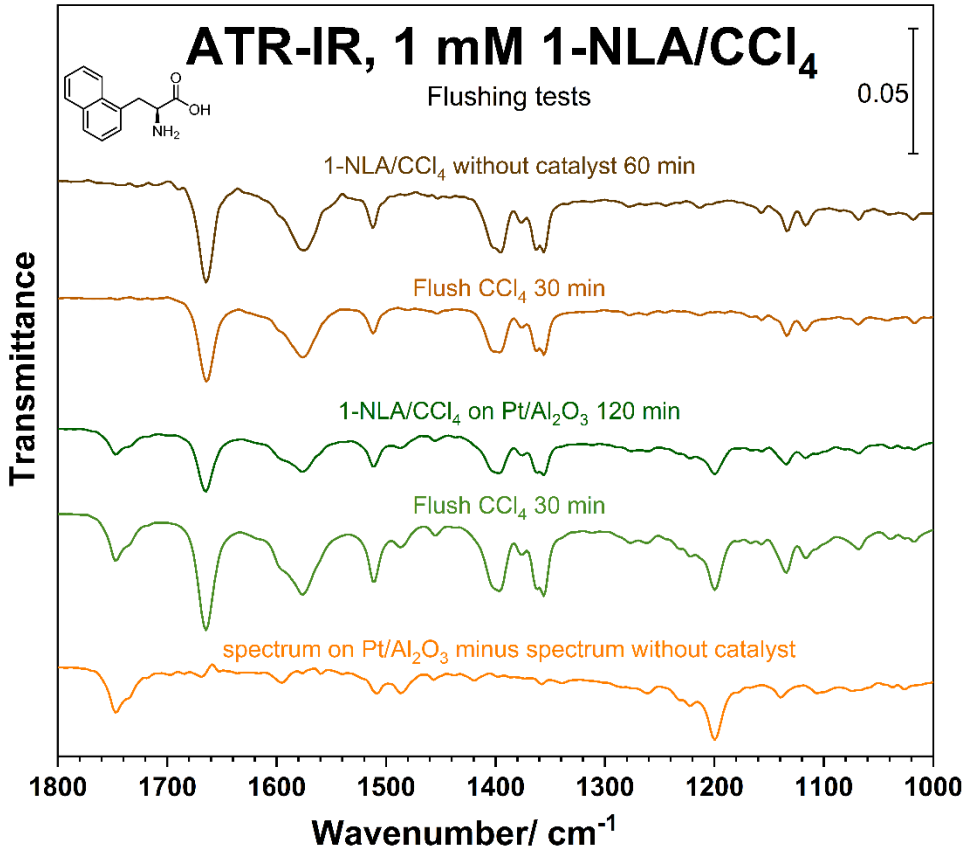

Figure 6.15 ATR-IR spectra of 1 mM NLA in CCl_4 solution after exposing to Pt/Al_2O_3 catalysts or without catalysts for 60 min, then the spectra were taken after flushing the cell with pure CCl_4 for 30 min. The bottom trace is the spectrum after subtracting the scaled spectrum without catalyst from the spectrum on catalyst.

Furthermore, flushing tests were conducted, yielding intriguing results that warrant discussion. As previously hypothesized, the sample spectra of 1-NLA on Pt catalysts should comprise a combination of free molecules in solution and adsorbed molecules on Pt surfaces. Consequently, if the cell was flushed with pure CCl_4 solvent, the peaks corresponding to free molecules should be eliminated or at least considerably weakened. To validate this hypothesis, flushing tests were performed on the Pt catalysts. Figure 6.15 illustrates the results, with the light green trace (fourth trace from the top)

representing the spectrum collected after flushing the ATR-IR cell for 30 minutes. Surprisingly, the sample peaks did not weaken; in fact, they became even stronger.

More intriguing findings emerged from the flushing tests conducted without a catalyst as a control. As depicted in the top two spectra of Figure 6.15, it was discovered that the sample peaks from the free molecules were not removed by the CCl_4 solvent in the absence of a catalyst. Hence, we postulate that 1-NLA molecules could condense on the crystal surface of the ATR-IR, making them difficult to remove even with a nonpolar solvent like CCl_4. It is important to note that the solubility of 1-NLA in CCl_4 is not high, and although we have not determined its exact solubility, the concentration of the 1 mM solution exceeds saturation conditions. Taking all these factors into consideration, we conclude that the spectra collected on the Pt catalysts consist of both free molecules condensed on the ATR-IR cell and adsorbed molecules on the Pt catalysts. However, the majority of the peaks originate from the free molecules, indicating that the adsorption of 1-NLA molecules on Pt catalysts is not very strong.

6.3.5 *In-Situ* ATR-IR Adsorption Studies of 2-NDA

The influence of the position of the amino acid group was also investigated in this study. Two additional molecules, namely 3-(2-naphthyl)-L-alanine (2-NLA) and 3-(2-naphthyl)-D-alanine (2-NDA), as shown in Figure 6.16 were examined. Similar experiments were conducted to study the effects of catalyst support and solvent.

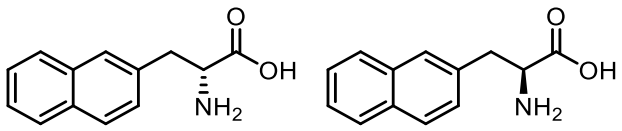

3-(2-naphthyl)-L-alanine (2-NLA) 3-(2-naphthyl)-D-alanine (2-NDA)

Figure 6.16 The structure of 2-NLA and 2-NDA.

The investigation involving 2-NDA molecules began with the ATR-IR test of a 1 mM solution of 2-NDA in CCl_4, which was exposed to 1 wt% Pt/Al_2O_3 catalysts. Figure 6.17 illustrates the spectra as a function of exposure time.

Initially, distinct peaks were observed, with their intensity increasing over time. A comparison with the transmission IR spectrum of pure 2-NDA (the top trace) revealed the presence of new peaks. Within the range of 1800-1000 cm^{-1}, a sharp peak at around 1740 cm^{-1} was clearly evident, along with a peak around 1480 cm^{-1} and a triplet peak around 1220 cm^{-1}, which differed from the transmission IR spectrum of pure 2-NDA molecules. However, some weak peaks, such as those at 1554 and 1310 cm^{-1}, matched the top spectrum and could be attributed to free molecules in the solution.

Moreover, there were peaks at higher wavenumbers, approximately 3000 cm^{-1}. Although a broad peak was present, certain peaks became more distinct. These peaks around 3000 cm^{-1} are characteristic of C–H stretches in aromatic compounds. The stretching of O–H from the acid group was not observed at higher wavenumbers. The sharpening of some peaks in the solution might be attributed to a reduction in hydrogen bonding due to molecular interactions.

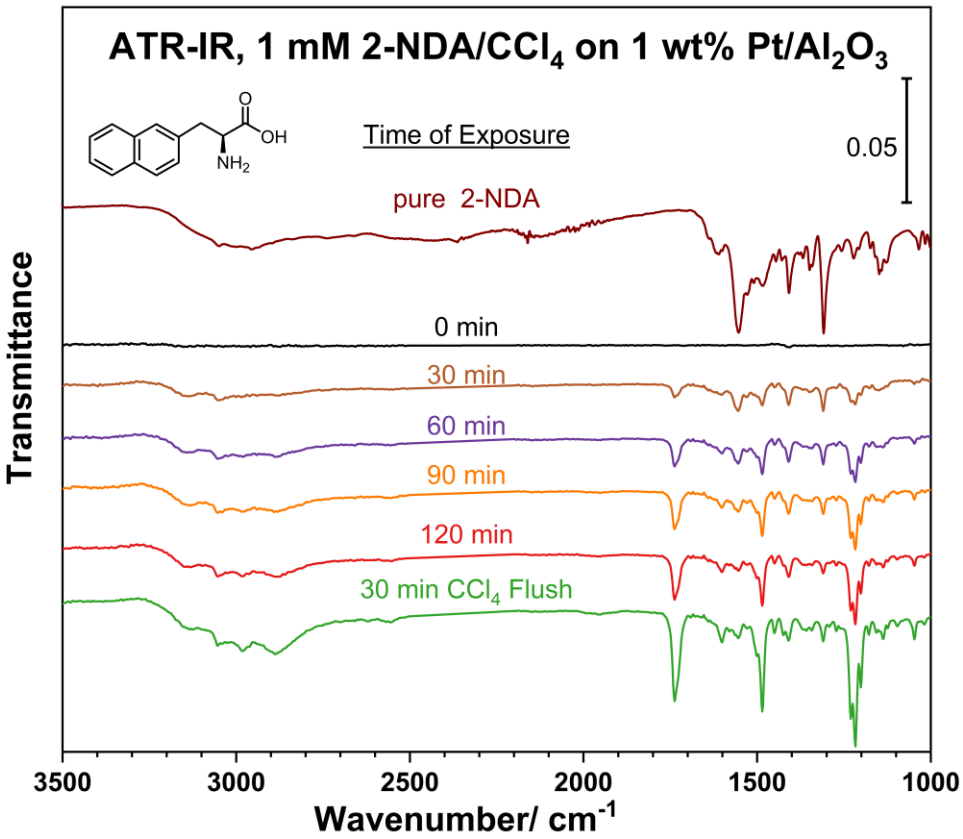

Figure 6.17 ATR-IR spectra of 1 mM 2-NDA in CCl_4 adsorption on 1 wt% Pt/Al_2O_3 catalysts as a function of time exposure to the surface. The top one is the transmission IR of pure 2-NDA.

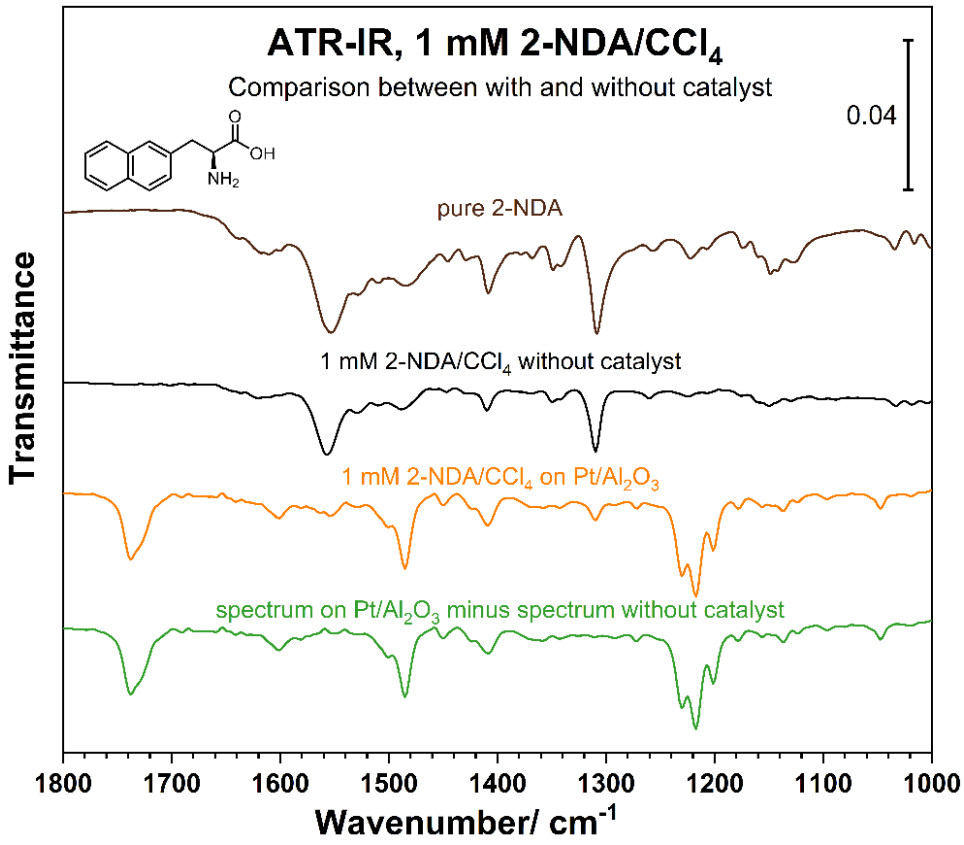

Figure 6.18 The comparison between the ATR-IR spectra of 1 mM 2-NDA in CCl_4 adsorption on 1 wt% Pt/Al_2O_3 and without catalysts. The top one is the transmission IR of pure 2-NDA. And the bottom one is the spectrum after subtracting the scaled spectrum without catalyst from the spectrum on catalyst.

Furthermore, a blank test was conducted using a 1 mM 2-NDA solution in CCl_4 without a catalyst. The resulting spectrum, presented in Figure 6.18 as the second trace, clearly corresponds to the transmission IR spectrum of pure 2-NDA, indicating that it represents the presence of free 2-NDA molecules in the CCl_4 solution. Upon examining the spectrum obtained from the Pt catalysts, it was observed that certain peaks attributed to free 2-NDA molecules were still present, similar to the 1-NLA molecules. Consequently, we hypothesize that the spectrum obtained from the Pt catalysts may arise from a combination of free molecules in the solution and 2-NDA molecules adsorbed

onto the Pt surfaces. To ascertain the validity of this hypothesis, we performed a subtraction method to eliminate the potential contribution from the free 2-NDA molecules. By subtracting the appropriately scaled spectrum obtained without a catalyst from the spectrum collected on the Pt catalysts, we derived the processed spectrum, depicted as the bottom green trace in Figure 6.18. It is reasonable to attribute the peaks on the left side of the spectrum to the absorbed 2-NDA species on the Pt/Al_2O_3 catalyst.

6.3.6 Effect of Catalyst Support on 2-NDA Adsorption

To investigate the behavior of 2-NDA on various Pt catalysts, additional tests were conducted using both commercial and homemade 1 wt% Pt/SiO_2 catalysts. The findings, along with the results of flushing tests, are summarized in Figure 6.19.

The figure demonstrates that similar behavior was observed for both the commercial and homemade 1 wt% Pt/SiO_2 catalysts. However, there are noteworthy differences that warrant discussion. Although the peak positions are quite similar across the different catalysts, there are variations in peak intensity. Notably, the peaks are considerably weaker in the case of the commercial Pt/SiO_2, as indicated by the middle two traces in the figure. The spectrum is dominated by two peaks at approximately 1554 and 1310 cm^{-1}, which likely originate from free 2-NDA molecules present in the solution, as discussed previously. Conversely, the contribution from free 2-NDA molecules is significantly smaller in the case of commercial Pt/SiO_2 and Pt/Al_2O_3. Additionally, the intensity of the peaks is highest for Pt/Al_2O_3, suggesting that commercial Pt/Al_2O_3 is more favorable for 2-NDA adsorption. Comparatively, homemade Pt/SiO_2 exhibits

greater favorability for 2-NDA adsorption than commercial Pt/SiO_2. As mentioned in Chapter 2, the commercial and homemade Pt/SiO_2 catalysts differ in their SiO_2 support, which indicates that the support material of the Pt catalyst influences the adsorption of 2-NDA.

Furthermore, flushing tests were conducted, as depicted in Figure 6.19. In each experiment, the cell was flushed with pure CCl_4 solvent, and the spectra were collected after a 30-minute period. In all three cases, the peaks corresponding to the samples remained, indicating that the adsorption of 2-NDA on the Pt surface is irreversible.

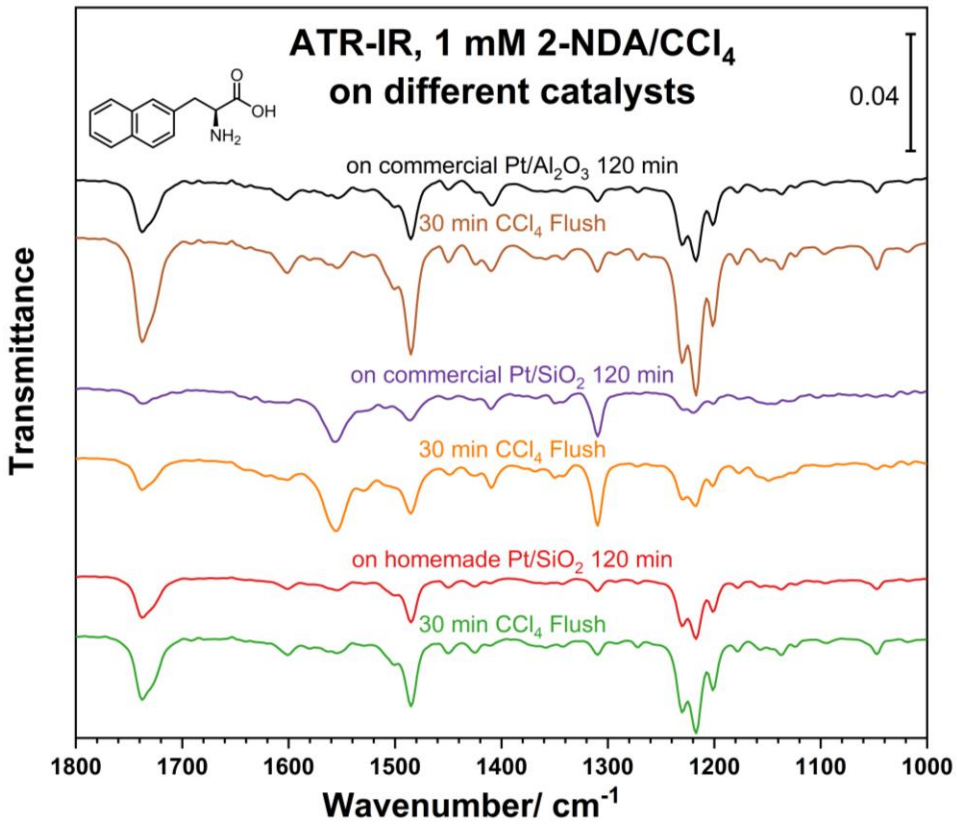

Figure 6.19 ATR-IR spectra of 1 mM 2-NDA in CCl_4 adsorption on different catalysts including 1 wt% commercial Pt/Al_2O_3, 1 wt% commercial Pt/SiO_2 and 1 wt% homemade Pt/SiO_2. The corresponding spectra of flushing test with pure CCl_4 were also shown below the adsorption spectra.

6.3.7 Effect of Solvent on 2-NDA Adsorption

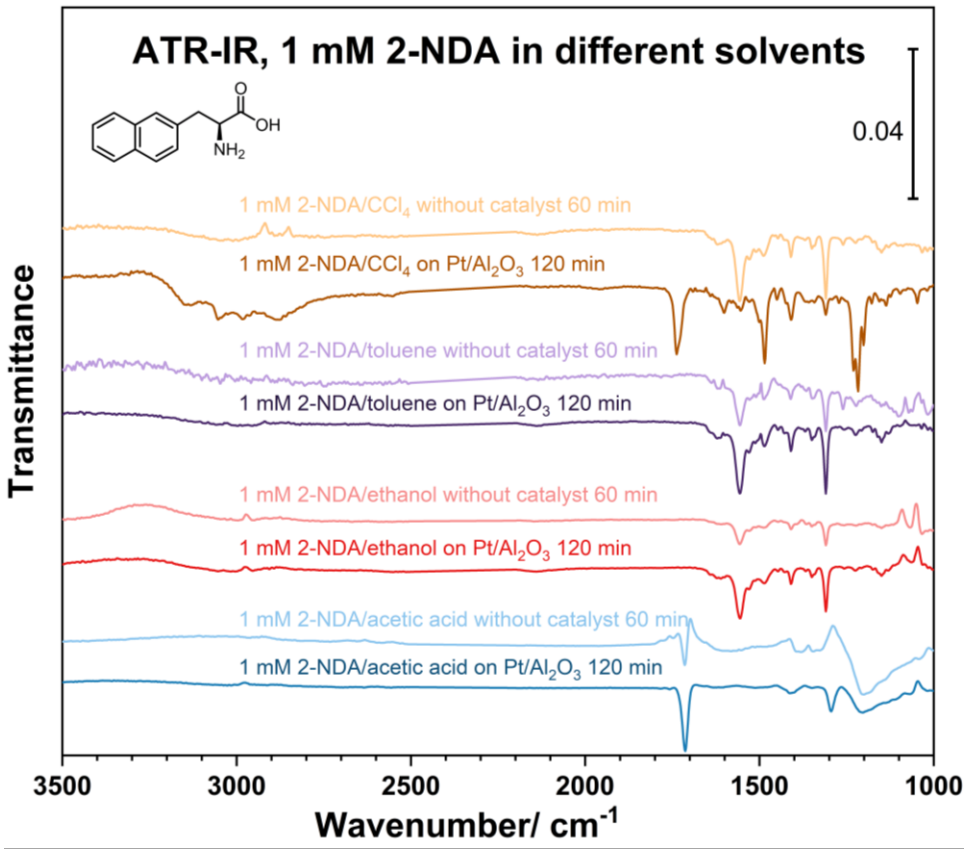

Figure 6.20 ATR-IR spectra of 1 mM 2-NDA in different solvents including CCl_4, toluene, ethanol and acetic acid. The dark traces are the spectra of 1 mM 2-NDA adsorption on 1 wt% Pt/Al_2O_3 while the light traces are the spectra without catalyst.

The effect of solvents was investigated by studying four different solvents: carbon tetrachloride, toluene, ethanol, and acetic acid. Figure 6.20 presents a comparison among these solvents, and corresponding blank tests without catalysts were also conducted, with the collected spectra provided in the figure.

In the case of toluene as the solvent, no signs of adsorption were observed, which differs from the results obtained with 1-NLA in toluene. Regarding 2-NDA molecules, the spectrum collected with the catalyst resembled the blank test without catalyst. No sample signals were observed, as was the case with CCl_4 as the solvent.

With ethanol as the solvent, the solubility of 2-NDA in ethanol was significantly higher, resulting in the collected spectrum being associated with free molecules in ethanol. Conversely, in the case of acetic acid, the solvent interference had a notable impact, as depicted in the above figure. Although there are several peaks around 1700 and 1300 cm^{-1}, these peaks are attributed to acetic acid rather than significant 2-NDA molecule peaks.

Therefore, only in the solvent of CCl_4 was the adsorption of 2-NDA observed.

6.3.8 ATR-IR Adsorption Studies of 2-NLA

The other configuration of 2-NDA, 2-NLA was also investigated. We performed the same set of experiments on 2-NLA molecules. Figure 6.21 illustrates the ATR-IR spectra obtained from a 1 mM solution of 2-NLA in CCl_4, both with and without catalysts. A similar trend was observed in the case of the 2-NLA solution. The subtraction spectrum reveals prominent peaks, which we attribute to the absorption of 2-NLA molecules on Pt catalysts.

Furthermore, three different Pt catalysts, including commercial 1 wt% Pt/Al_2O_3, commercial and homemade 1 wt% Pt/SiO_2, were tested. The corresponding results are presented in Figure 6.22. No significant variations were observed among the three Pt

catalysts. Additionally, the flushing tests using pure CCl_4 failed to eliminate the sample peaks, indicating the irreversible adsorption of 2-NLA on the Pt surface.

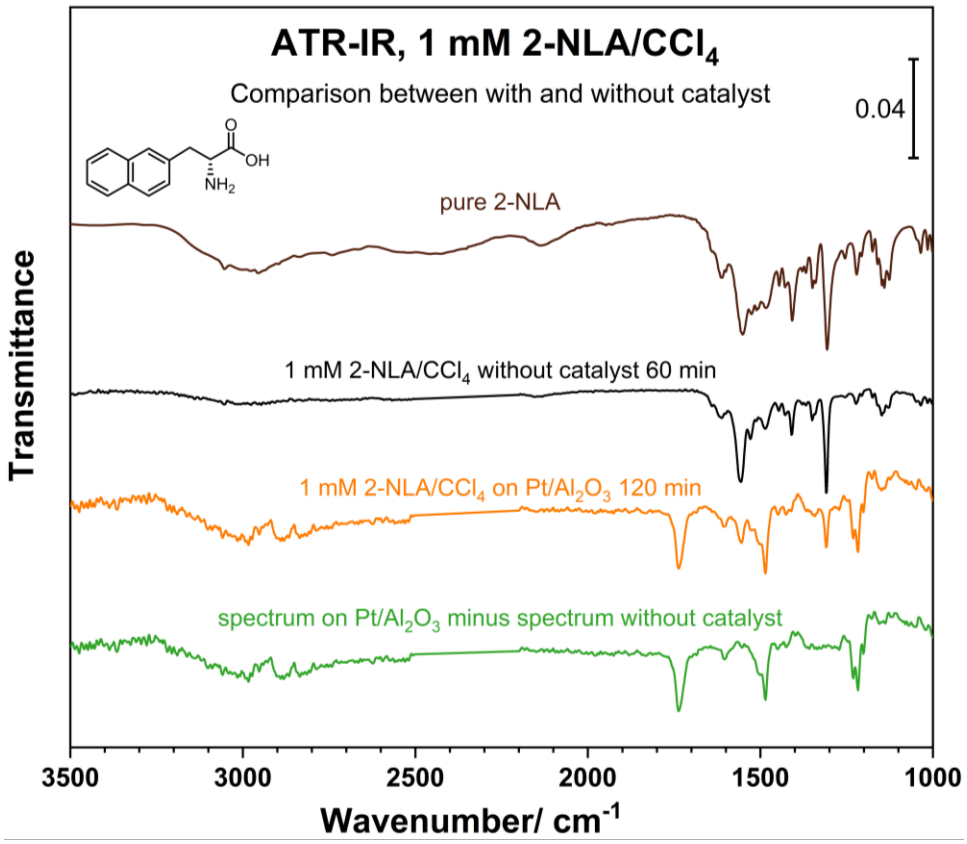

Figure 6.21 The comparison between the ATR-IR spectra of 1 mM 2-NLA in CCl_4 adsorption on 1 wt% Pt/Al_2O_3 and without catalysts. The top one is the transmission IR of pure 2-NLA. And the bottom one is the spectrum after subtracting the scaled spectrum without catalyst from the spectrum on catalyst.

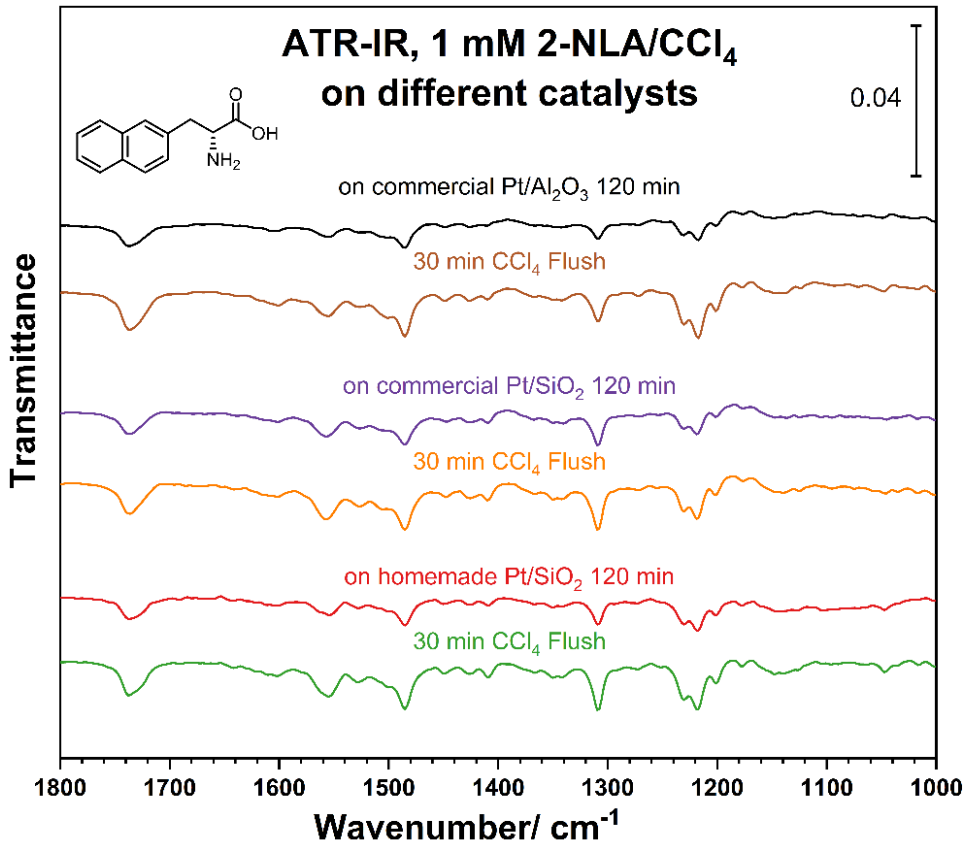

Figure 6.22 ATR-IR spectra of 1 mM 2-NLA in CCl_4 adsorption on different catalysts including 1 wt% commercial Pt/Al_2O_3, 1 wt% commercial Pt/SiO_2 and 1 wt% homemade Pt/SiO_2. The corresponding spectra of flushing test with pure CCl_4 were also shown below the adsorption spectra.

6.3.9 Comparison Between 2-NLA and 2-NDA

The comparison between 2-NLA and 2-NDA was conducted, as illustrated in Figure 6.23 below. As anticipated, both enantiomers exhibited identical behavior on Pt catalysts. Additionally, certain weak peaks corresponded well with the spectrum obtained without a catalyst, indicating the detection of free molecules in the solution. Regarding the blank test conducted without a catalyst, the spectrum obtained after flushing the cell with pure solvent for 30 minutes still displayed the same signals, suggesting that some

molecules would condense on the ATR-IR cell, making it difficult to remove them by flushing with CCl_4 solvent.

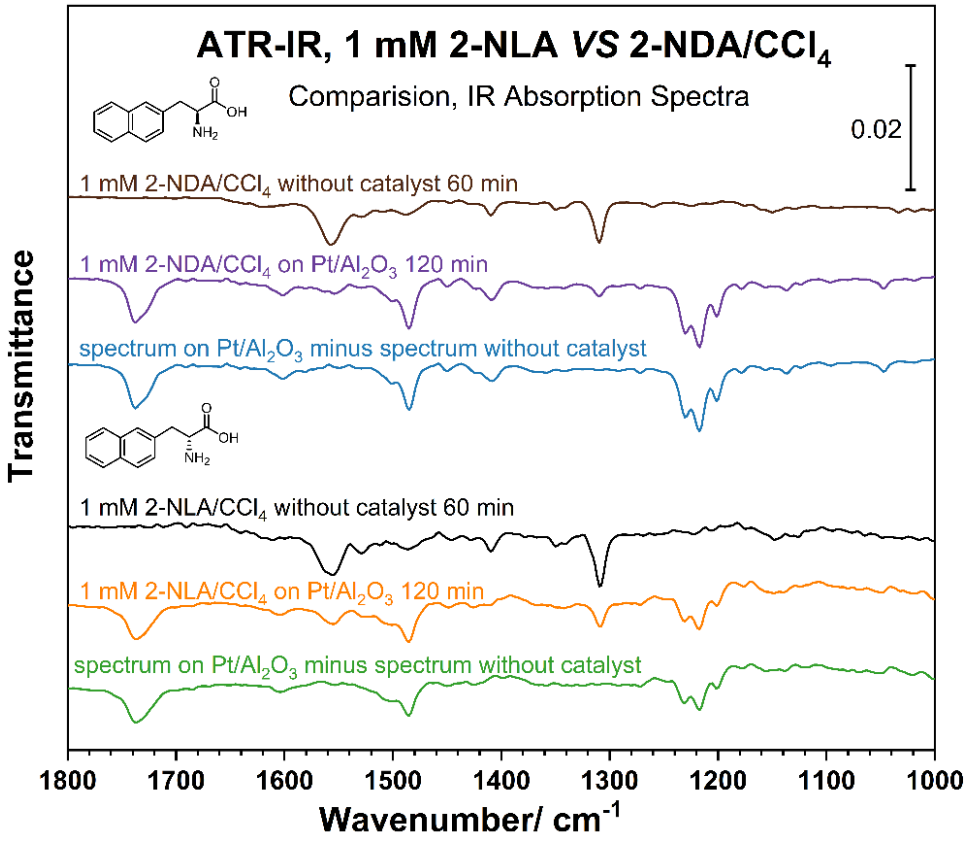

Figure 6.23 The comparison between the ATR-IR spectra of 1 mM 2-NDA and 2-NLA in CCl_4 adsorption on 1 wt% Pt/Al_2O_3 and without catalysts. And the third from the top and the bottom traces are the spectra after subtracting the scaled spectrum without catalyst from the spectrum on catalyst.

Based on the ATR-IR studies, while 1-NDA did not exhibit any signs of adsorption, which we expected it would, all 1-NLA, 2-NDA, and 2-NLA exhibited significant signs of adsorption. The detected spectra could be a combination of free molecules condensed on the ATR-IR cell and adsorbed molecules on the Pt surfaces. Moreover, the contribution from free molecules in the case of 2-NDA and 2-NLA was

much weaker compared to 1-NLA. The IR spectra clearly indicate that the peaks corresponding to free 2-NDA or 2-NLA are weak, whereas they appear to be dominant in the case of 1-NLA. Consequently, the adsorption of 2-NDA and 2-NLA is significantly stronger than that of 1-NLA. The positioning of the amino acid group indeed has a substantial influence on adsorption.

6.3.10 The Peak Assignment of 2-NDA Adsorption on 1 wt% Pt/Al_2O_3

As previously discussed, 2-NDA and 2-NLA exhibited more significant adsorption on Pt surfaces. These compounds possess both an amino group ($-NH_2$) and a carboxyl group ($-COOH$), suggesting the possibility of zwitterionic formation during the adsorption process. In the zwitterionic form of an amino acid, the amino group is protonated while the carboxyl group is deprotonated, resulting in an overall neutral molecule carrying both positive and negative charges.

The zwitterionic state of an amino acid is known to be pH-dependent. Under low pH conditions, the amino acid is predominantly protonated and positively charged, whereas at high pH, it tends to be deprotonated and negatively charged. However, at the isoelectric point, which corresponds to the pH at which the molecule has no net charge, the amino acid exists exclusively in the zwitterionic form, with both the amino and carboxyl groups ionized.

Based on ATR-IR studies, the adsorption of 2-NDA and 2-NLA (which we expect to occur) was solely observed in the solvent CCl_4, a neutral medium. This observation led us to propose that the zwitterionic form of 2-NDA or 2-NLA might be present during the

adsorption process. We have also found that the NEA molecule becomes protonated during adsorption. It is likely that the amine group of 2-NDA and 2-NLA molecules undergoes protonation, resulting in the formation of NH_3^+. The zwitterionic form is favored in the CCl_4 solution environment. Based on this hypothesis, we attempted to assign the observed peaks of 2-NDA in different environments.

Figure 6.24 displays the full spectra between 3500 and 1000 cm^{-1}, while Figure 6.25 shows the specific range between 1800 and 1000 cm^{-1}.

Firstly, in the transmission IR spectrum of pure 2-NDA (top trace) and the ATR-IR spectrum of 1 mM 2-NDA in CCl_4 without catalyst (second from the top), two prominent peaks at approximately 1555 cm^{-1} and 1308 cm^{-1} can be attributed to the stretching vibration of the C=O (carbonyl group). These peaks were also observed in the case of Pt/Al_2O_3 but were completely eliminated after subtraction. In the presence of Pt/Al_2O_3 catalyst, a new peak emerges at around 1735 cm^{-1}, corresponding to the stretching mode of COO^-.

Additionally, the peaks around 3000 cm^{-1} represent C–H stretches in aromatic compounds and could also indicate the stretching mode of N−H from amine salt. Consequently, the peak at 2877 cm^{-1} may be assigned to the stretching mode of NH_3^+. The small, broad peak at around 1485 cm^{-1} is likely the bending mode of NH_2 in the case of solid 2-NDA molecules.

Table 6.1 Assignment of IR peaks for 2-NDA species in different chemical environments.

Mode	1mM 2-NDA/CCl_4 on Pt/Al_2O_3	1 mM 2-NDA/CCl_4 without catalysts	Solid
$\delta_{oop}(CH)_{ring}$	1047		
$\delta_{ip}(CH)_{ring}$	1136	1148	1148
$\delta_{ip}(CH)_{ring}$	1201, 1216, 1228	1224	1222
$\nu(C\text{-}O)_{carbonyl}$		1308	1308
$\delta_{asym}(CH_3)$amine	1408	1408	1408
δ (NH_2)	1485	1485	1485
$\nu(C{=}O)_{carbonyl}$		1557	1553
$\nu_{ip}(CC)_{ring}$	1602	1617	1617
ν(COO-)	1735		
$\nu(NH_3^+)$	2877		
$\delta(CH)_{ring}$	2980, 3049, 3148		3049

Figure 6.24 ATR-IR spectra (3500-1000 cm^{-1}) of 1 mM 2-NDA in CCl_4 with and without Pt catalysts. The bottom one is the subtracted spectrum by using the spectrum collected on Pt catalysts minus the spectrum without catalysts. The top one is the transmission IR of pure 2-NDA.

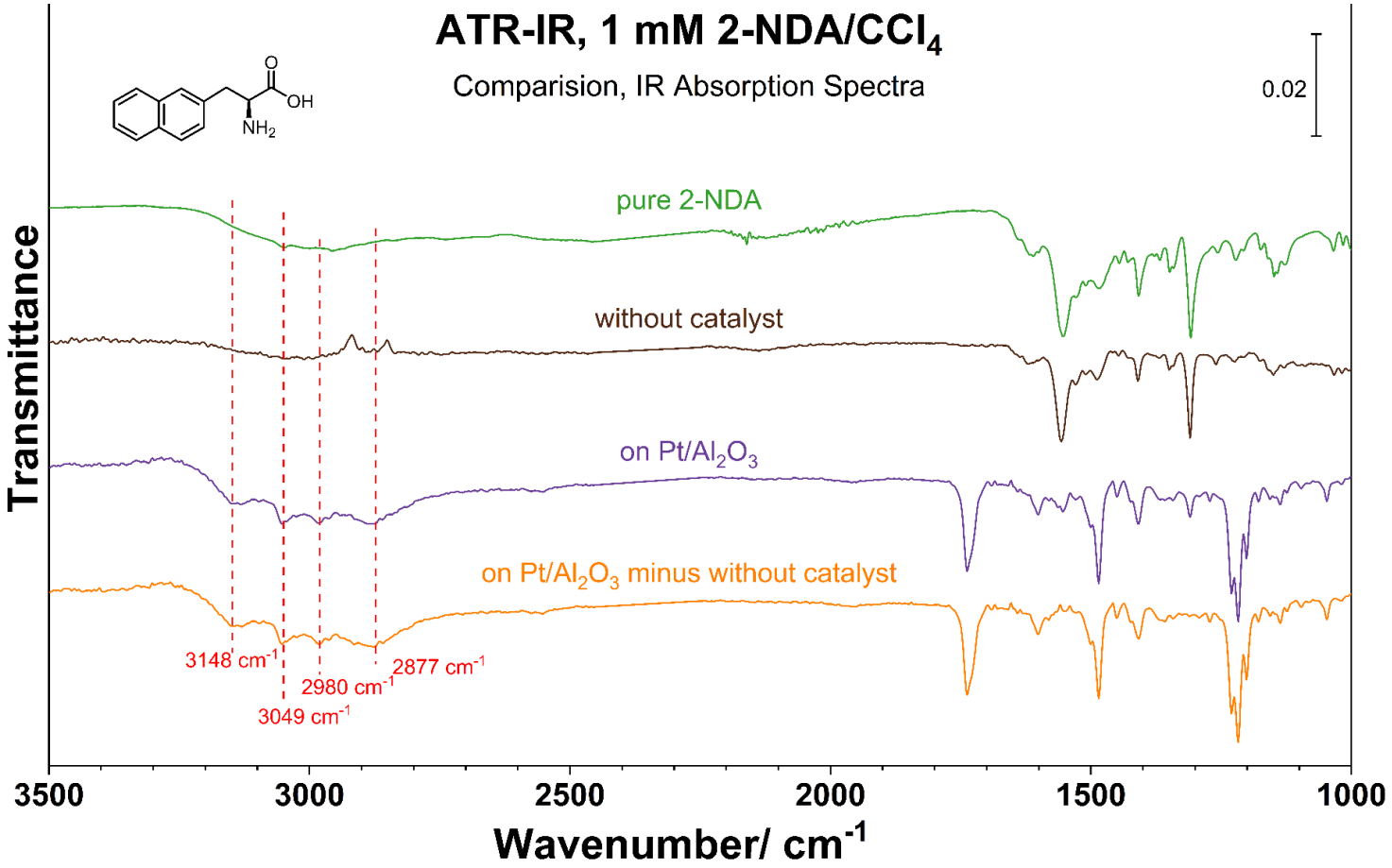

Figure 6.25 ATR-IR spectra (1800-1000 cm^{-1}) of 1 mM 2-NDA in CCl_4 with and without Pt catalysts. The bottom one is the subtracted spectrum by using the spectrum collected on Pt catalysts minus the spectrum without catalysts. The top one is the transmission IR of pure 2-NDA

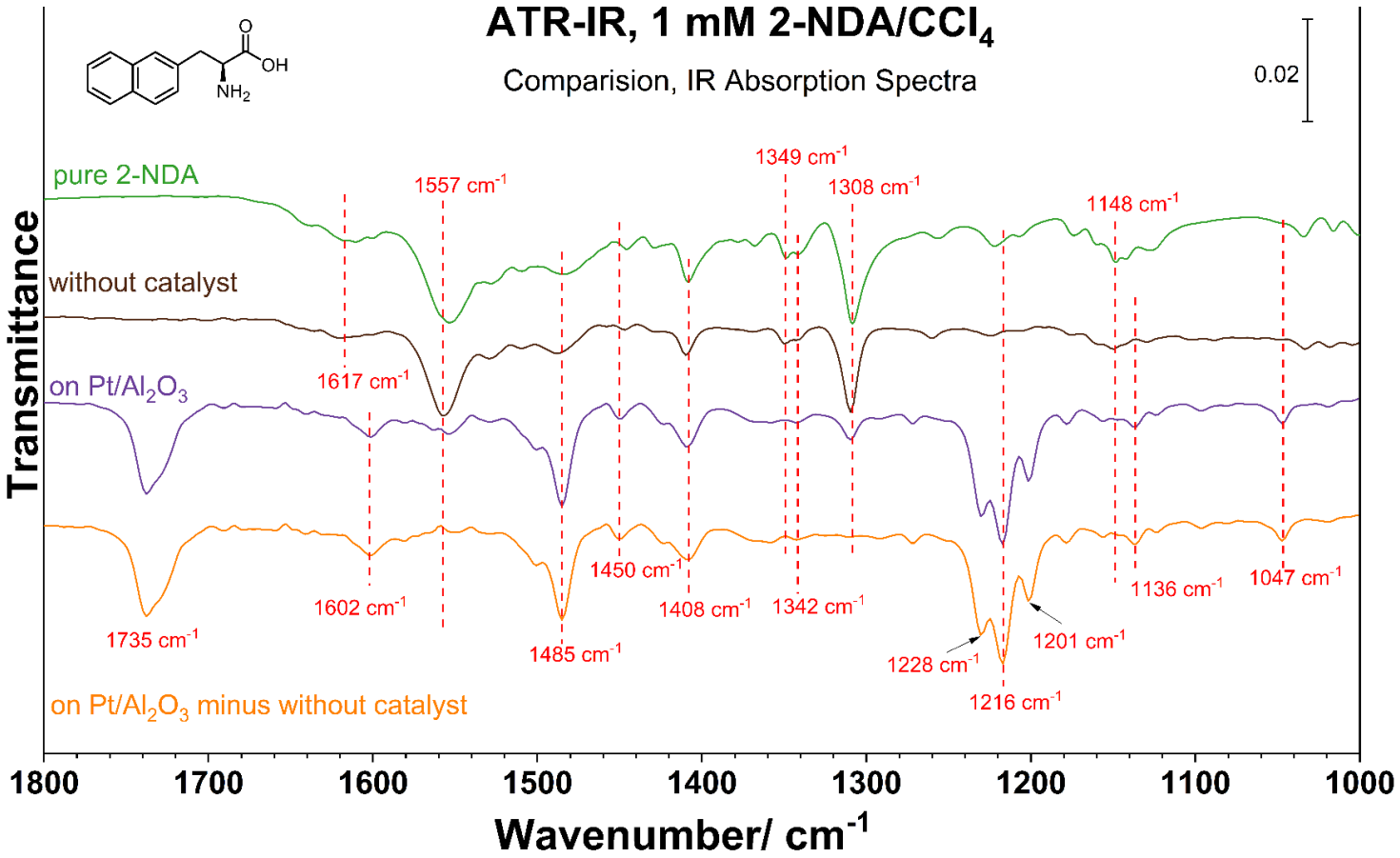

6.3.11 Kinetic Measurements with 1-NLA and 2-NDA

The hydrogenation of Et-Py reactions modified with 1-NLA, catalyzed by commercial Pt/Al_2O_3 and Pt/SiO_2, were studied using both toluene and acetic acid as the reaction solvent. The results are summarized in Table 6.2, and the trends of conversion and *ee* values with time are shown in Figure 6.26. Each reaction, with the presence of modifiers and catalysts, was performed three times. Therefore, the error bars in Figure 6.26 represent the range across the three different runs.

Table 6.2 Conversion and ee of the Et-Py hydrogenation modified with 1-NLA.

Catalyst	Modifier	Solvent	Conversion (%)	ee (%)
Pt/Al_2O_3	No modifier	Toluene	47.3	0.4
	1-NLA		64.8	2.6 (R)
Pt/SiO_2	No modifier		22.8	0.2
	1-NLA		74.2	4.5 (R)
No catalyst	No modifier		1.1	0.6
	1-NLA		1.2	0.8
Pt/Al_2O_3	No modifier	Acetic acid	36.3	2.0
	1-NLA		60.7	13.9 (R)
Pt/SiO_2	No modifier		31.7	1.8
	1-NLA		55.7	16.1 (R)
No catalyst	No modifier		1.1	0.2
	1-NLA		1.0	0.6

Reaction conditions: t = 3.0 h, T= 298 K, $P(H_2)$=10 bar, Pt catalyst (25 mg), solvent (10 mL), molar ratio of Pt:Et-Py:modifier = 1:2000:5.

When toluene was used as the solvent, the Et-Py hydrogenation reaction in the absence of catalyst showed negligible activity, with conversions of only 1.1% (no modifier) and 1.2% (with 1-NLA) after a 3.0-hour reaction. However, the reactions with catalysts exhibited significantly improved catalytic performance, even without chiral modifiers. The conversion reached up to 47.3% for the reaction catalyzed by Pt/Al_2O_3 and 22.8% for Pt/SiO_2 in the absence of chiral modifiers. Thus, the catalysts contributed to enhancing the reaction rate.

The addition of a small quantity of 1-NLA to the reactions resulted in increased conversion and *ee* values, indicating that the chiral modifier not only improved enantioselectivity but also promoted catalytic activity. However, the enantioselectivity of 1-NLA in toluene-based reactions was limited. As depicted in Figure 6.26, the the ee values were approximately 2.6% for Pt/Al_2O_3 and 4.5% for Pt/SiO_2, which is less ideal compared to NEA modifiers.

In acetic acid, significantly improved catalytic enantioselectivity was observed, albeit with lower activity. The right panel of Figure 6.26 illustrates the more impressive *ee* values obtained. The *ee* value calculated for Pt/Al_2O_3 was 13.9%, while it was 16.1% for the reaction catalyzed by Pt/SiO_2. The reaction activity in acetic acid was not as good as in toluene, resulting in a decrease in conversion. Nevertheless, the addition of 1-NLA in the reaction mixture in acetic acid solvent promoted the reaction activity compared to the reactions without 1-NLA.

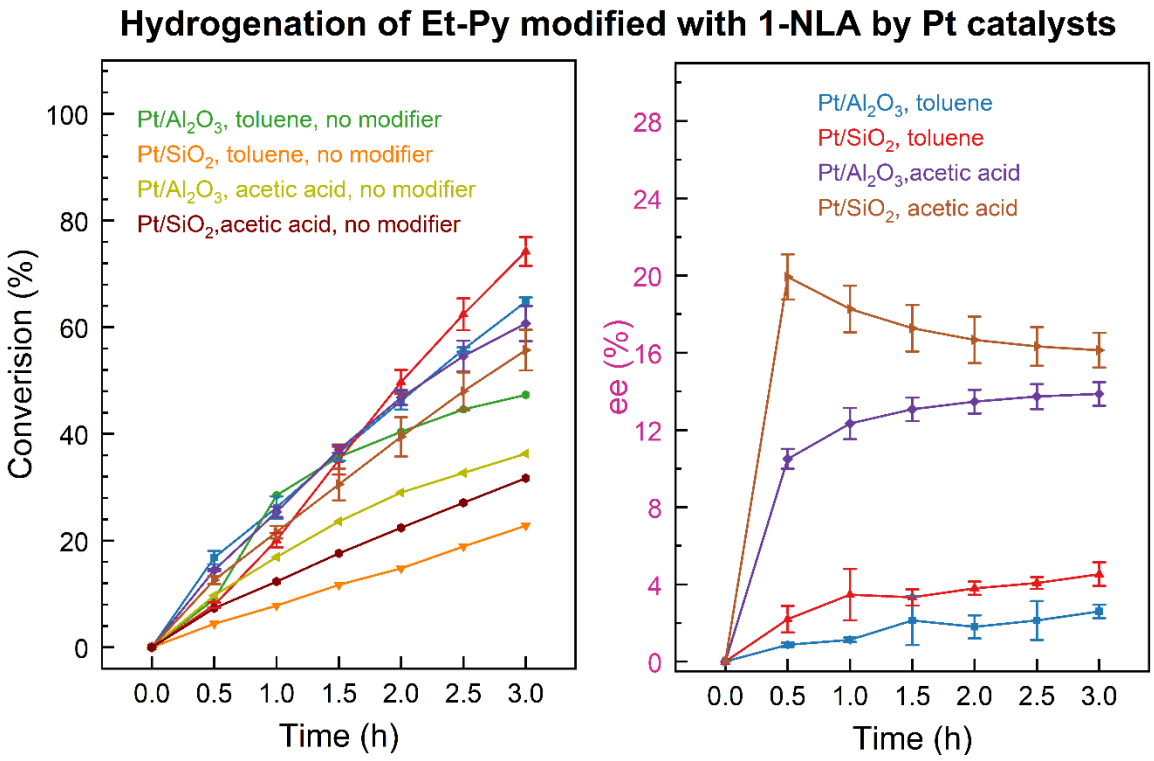

Figure 6.26 Conversion (left panel) and *ee* (right panel) with reaction time of the Et-Py hydrogenation modified with 1-NLA catalyzed by different Pt catalysts and in different solvents.

Overall, the addition of 1-NLA in both toluene and acetic acid solvents improved enantioselectivity and reaction activity. However, the enantioselectivity observed in toluene solutions was limited compared to that in acetic acid solutions. One possible explanation is the difference in solubility. 1-NLA is more soluble in acetic acid than in toluene, leading to more efficient interactions among the reactants and better catalytic performance.

In addition to 1-NLA, the chiral modifier 2-NDA was also applied to the reaction. ATR-IR data provided more convincing evidence of the adsorption of 2-NDA on Pt surfaces compared to 1-NLA. Kinetic comparisons were conducted using three different

solvents: toluene, acetic acid, and ethanol, with three different Pt catalysts: commercial Pt/Al_2O_3, commercial Pt/SiO_2, and homemade Pt/SiO_2. The results are presented in Table 6.3, and the conversion and *ee* trends with time are plotted in Figure 6.27.

Table 6.3 Conversion and ee of the Et-Py hydrogenation modified with 2-NDA.

Catalyst	Solvent	Conversion (%)	ee (%)
Commercial Pt/Al_2O_3	Toluene	92.7	17.0 (S)
Commercial Pt/SiO_2		44.4	10.8 (S)
Homemade Pt/SiO_2		60.9	13.4 (S)
Commercial Pt/Al_2O_3	Acetic acid	38.0	4.4 (S)
Commercial Pt/SiO_2		49.4	10.2 (S)
Homemade Pt/SiO_2		67.0	9.4 (S)
Commercial Pt/Al_2O_3	Ethanol	13.0	1.6 (S)
Commercial Pt/SiO_2		3.7	3.7 (S)
Homemade Pt/SiO_2		2.8	1.8 (S)

Reaction conditions: t = 5.0 h, T= 298 K, $P(H_2)$=10 bar, Pt catalyst (25 mg), solvent (10 mL), molar ratio of Pt:Et-Py:modifier = 1:2000:5.

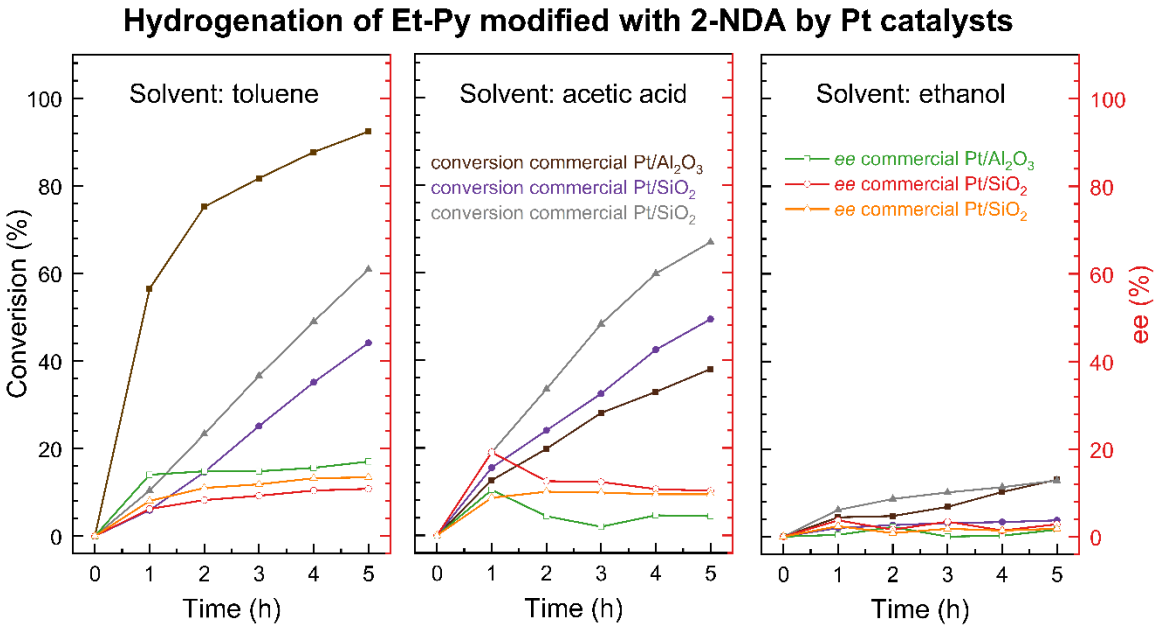

Figure 6.27 Conversion and *ee* with reaction time of the Et-Py hydrogenation modified with 2-NDA in different solvents, including toluene (left panel), acetic acid (middle panel) and ethanol (right panel) catalyzed by different Pt catalysts.

Among the three solvents tested, toluene solutions exhibited superior catalytic performance in terms of both activity and selectivity. Among the three Pt catalysts examined, the commercial Pt/Al_2O_3 demonstrated the highest effectiveness. However, when acetic acid was used as the solvent, the catalytic behavior of Pt/SiO_2 outperformed that of the commercial Pt/Al_2O_3. Ethanol, on the other hand, proved to be the least favorable choice for the reactions, as it did not exhibit any significant catalytic ability.

The kinetic results obtained with different solvents and Pt catalysts indicate that the interactions among the reactants play a crucial role in determining the catalytic performance. Therefore, it is essential to devote more effort to future studies in this direction. The current data, although valuable, is insufficient to establish correlations among the parameters.

6.4 Summary

In this chapter, we conducted a thorough investigation of the adsorption behavior of 1-NLA and 1-NDA on Pt surfaces. The ATR-IR spectra revealed a combination of both free molecules in solution and adsorbed 1-NLA on the Pt surfaces. This conclusion was drawn after subtracting the spectrum collected without catalysts from the spectrum collected with catalysts. Flushing tests demonstrated that 1-NLA molecules would condense on the surface, which was difficult to remove using non-polar solvents, such as CCl_4. Thus, we believe that while some 1-NLA molecules in the solution would bind to Pt surfaces, the majority of them would condense on the ATR-IR crystal. However, the behavior of 1-NDA was unexpectedly different, as there was no evidence of adsorption. We suspect that this discrepancy could be attributed to the quality of the commercial 1-NDA used in the experiment.

Similar trends were observed with 2-NLA and 2-NDA molecules. However, in this case, more adsorbed sample peaks were detected, indicating that only a small portion of the 2-NDA would condense on the ATR-IR crystal, while the majority of it would adhere to the Pt surfaces. Furthermore, the adsorption process appeared to be irreversible. This suggests that the adsorption energy of 2-NDA and 2-NLA molecules is higher than that of 1-NLA.

Additionally, we hypothesized the occurrence of the zwitterionic form when the amino acid binds to Pt surfaces, based on the detection of unique IR signals distinct from those of the pure sample. To support this hypothesis, further experiments and theoretical calculations are required to confirm the peak assignment.

We also investigated the kinetic measurements with 1-NLA and 2-NDA, exploring the influence of the solvent and the type of Pt catalysts used. In the case of 1-NLA, the catalytic performance in terms of enantioselectivity was higher in acetic acid compared to toluene. This difference in performance may be attributed to the varying solubility of 1-NLA in the two solvents.

On the other hand, preliminary kinetic data was obtained for 2-NDA molecules, indicating that toluene was more suitable for the 2-NDA molecules compared to acetic acid and ethanol solvents. However, further experiments are required to establish a correlation between the adsorption behavior on Pt surfaces and catalytic performance.

Chapter 7

Adsorption and Reactivity of Axially Chiral Compounds on Pt Surfaces in Heterogeneous Catalysis

7.1 Brief Introduction and Hypothesis

Previous studies conducted by our group and others have demonstrated that chiral modifiers, including cinchona alkaloids and NEA chiral modifiers, are primarily adsorbed on noble metal surfaces. Figure 7.1 illustrates some models for heterogeneous chiral catalysis. The interactions between these chiral modifiers and metals can induce chirality, thereby enhancing enantioselectivity in asymmetric hydrogenations.

In a recent publication[89], it was reported that the chiral modifier NOBIN exhibited a unique interaction at the interface of Ir and CeO_2. This interaction involved the coordination bonds between the Ir metal and the NH_2 group, as well as between CeO_2 and the OH group (shown in the right bottom of Figure 7.1). Consequently, NIBON demonstrated moderate enantiomeric excess in the hydrogenation of acetophenone to 1-phenylethanol. This paper drew our attention to chiral biaryl compounds.

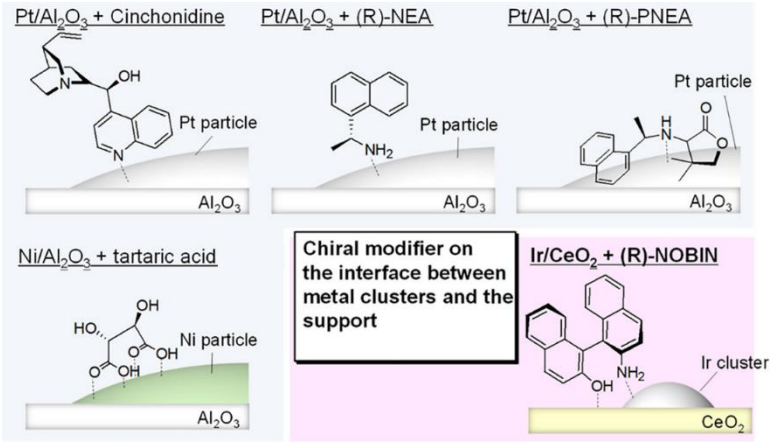

Figure 7.1 Different models for heterogeneous chiral catalysts. Adapted with permission from reference 89, Copyright 2022 American Chemical Society.

Biaryl compounds, which consist of two aromatic rings connected by a single bond, are a class of organic compounds commonly employed as ligands in organometallics for homogeneous chiral catalysis[90]. Unlike the chiral molecules with chiral centers, biaryl compounds possess chiral axes that can introduce axial chirality. The rotation around the bond connecting the aromatic rings generates enantiomers. Examples of s-BINOL, s-BINAM, and s-NOBIN are depicted in Figure 7.2.

Interestingly, chiral biaryl compounds are not extensively used in the asymmetric hydrogenation of α-keto esters catalyzed by Pt catalysts. Therefore, it is crucial to investigate their behavior on noble Pt surfaces and their catalytic performance. This exploration could potentially bridge the gap between homogeneous and heterogeneous catalysis and facilitate the rational testing of other families of ligands in the future. Based on the findings presented in this paper, both the amine group and the naphthyl ring are necessary for adsorption on Pt surfaces. Consequently, we hypothesized that s-BINAM

and s-NOBIN would bind to Pt surfaces, whereas s-BINOL would not. It is important to note that the high cost of NOBIN samples precluded its study in this chapter.

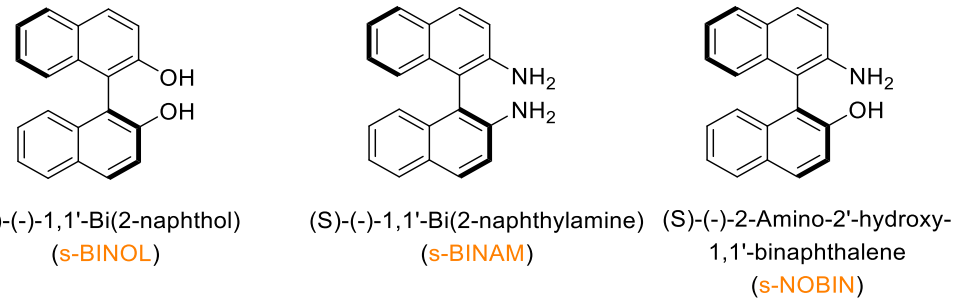

(S)-(-)-1,1'-Bi(2-naphthol) (s-BINOL)

(S)-(-)-1,1'-Bi(2-naphthylamine) (s-BINAM)

(S)-(-)-2-Amino-2'-hydroxy-1,1'-binaphthalene (s-NOBIN)

Figure 7.2 Molecular structure of s-BINOL, s-BINAM and s-NOBIN.

7.2 Experimental Details

The adsorption tests of each chiral modifier were conducted using *in-situ* ATR-IR, while the reference spectra of pure samples were obtained through transmission IR spectroscopy. Kinetic measurements were carried out using high-pressure reactors. Detailed information regarding the experimental procedures can be found in Chapter 2.

7.3 Results and Discussions

7.3.1 *In-Situ* ATR-IR Studies of s-BINOL and s-BINAM

The experimental process commenced with an ATR-IR test of a 1 mM s-BINAM solution in CCl_4, upon exposure to a 1 wt% Pt/Al_2O_3 catalyst. As illustrated in Figure 7.3, the second trace from the top displays the spectrum obtained after a 120-minute exposure

to Pt catalysts. Notably, it exhibits relatively weak signals related to the s-BINAM molecules compared to the transmission IR of pure s-BINAM (the top trace).

In contrast, the third trace from the top represents the spectrum collected from a 5 mM solution, which demonstrates markedly stronger and more credible IR signals, significantly deviating from the spectrum of unbound molecules. Additionally, a control test was conducted with a 5 mM solution in the absence of any catalyst, and the resulting spectrum is presented in Figure 7.3 (the bottom trace). Despite some sample signals appearing in the spectrum obtained without a catalyst, the relatively weak signals align with the spectrum of pure s-BINAM molecules. A comparison between the spectra collected with and without catalysts highlights numerous discrepancies, as denoted in Figure 7.3.

Primarily, the emergence of a robust peak around 1690 cm^{-1} was observed, with its intensity incrementally increasing with exposure time, as delineated in Figure 7.4 (this figure depicts the ATR-IR spectra of 5 mM s-BINAM in a CCl_4 solution, exposed to 1 wt% Pt/Al_2O_3, over a duration of time). It is conjectured that this new peak can be attributed to N−H bending from the amine group bound to Pt surfaces. Upon binding of the amine group to Pt surfaces, the N−H bending mode is shifted to a higher wavenumber due to alterations in the molecule's bonding geometry and electronic structure, induced by adsorption to the Pt surface.

Another noticeable discrepancy was perceived around 1620 cm^{-1}. The spectrum of pure s-BINAM (top trace) predominately showcases a medium and broad peak around 1620 cm^{-1}, identifiable as N−H bending from the amine group. This peak was also

detected in both 5 mM solutions, with and without catalysts. However, in the presence of the catalyst, the peak was amplified and sharper, which we attribute to diminished hydrogen bonding amongst the s-BINAM molecules within the CCl_4 solution.

Furthermore, the relative intensity of the peaks, spanning from 1800 cm^{-1} to 1400 cm^{-1} in the presence of Pt catalysts, surpassed that of the unbound molecules. This implies a stronger interaction between the s-BINAM molecules and Pt surfaces.

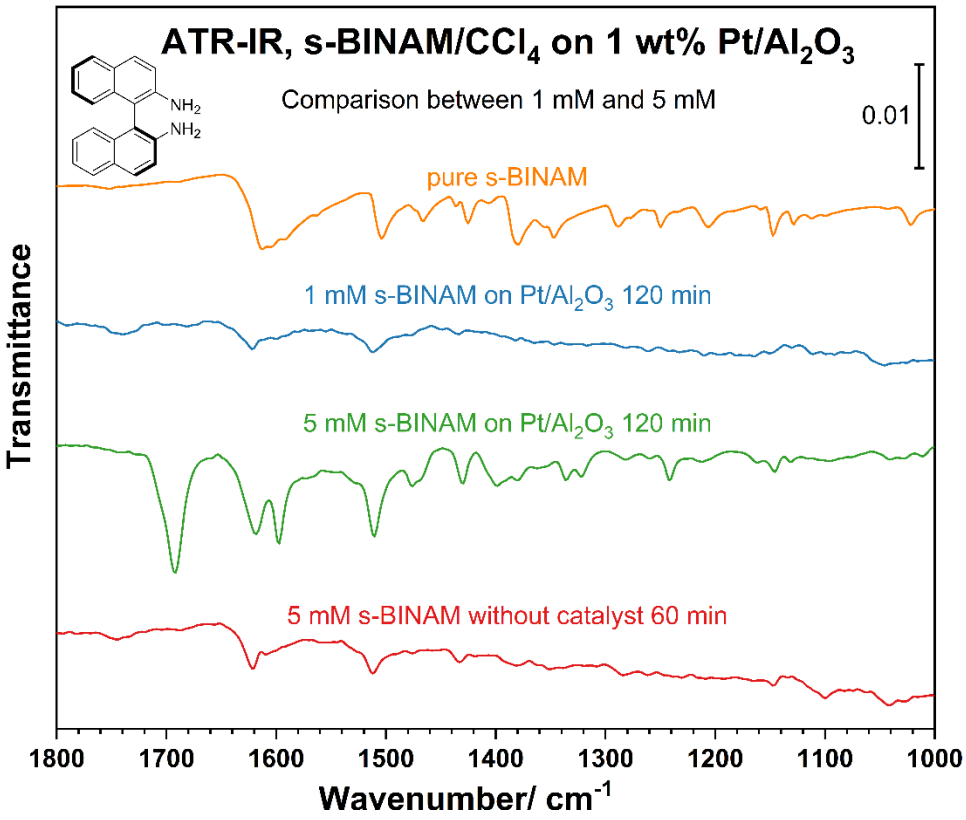

Figure 7.3 ATR-IR spectra of 1 mM and 5 mM s-BINAM in CCl_4 adsorption tests on 1 wt% Pt/Al_2O_3 catalyst. The bottom one is the blank test of 5 mM s-BINAM in CCl_4 without catalyst. The top trace is the transmission IR spectrum of pure s-BINAM.

Given the observed disparities between the spectra acquired with catalysts in the solution and the spectrum of pure s-BINAM molecules, it is inferred that s-BINAM molecules are likely to bind to the Pt/Al_2O_3 catalyst in the CCl_4 solution. A novel peak, noticed around 1690 cm^{-1}, was hypothesized to result from the adsorption of the amine group on Pt surfaces. However, this was not definitively established. As delineated in Figure 7.4, following a thorough flush of the ATR-IR cell with pure CCl_4, a spectrum was obtained post a 30-minute flush, as presented in the bottom trace. The fact that the flushing of CCl_4 after 30 minutes did not eliminate any sample peaks implies the irreversible adsorption process of s-BINAM.

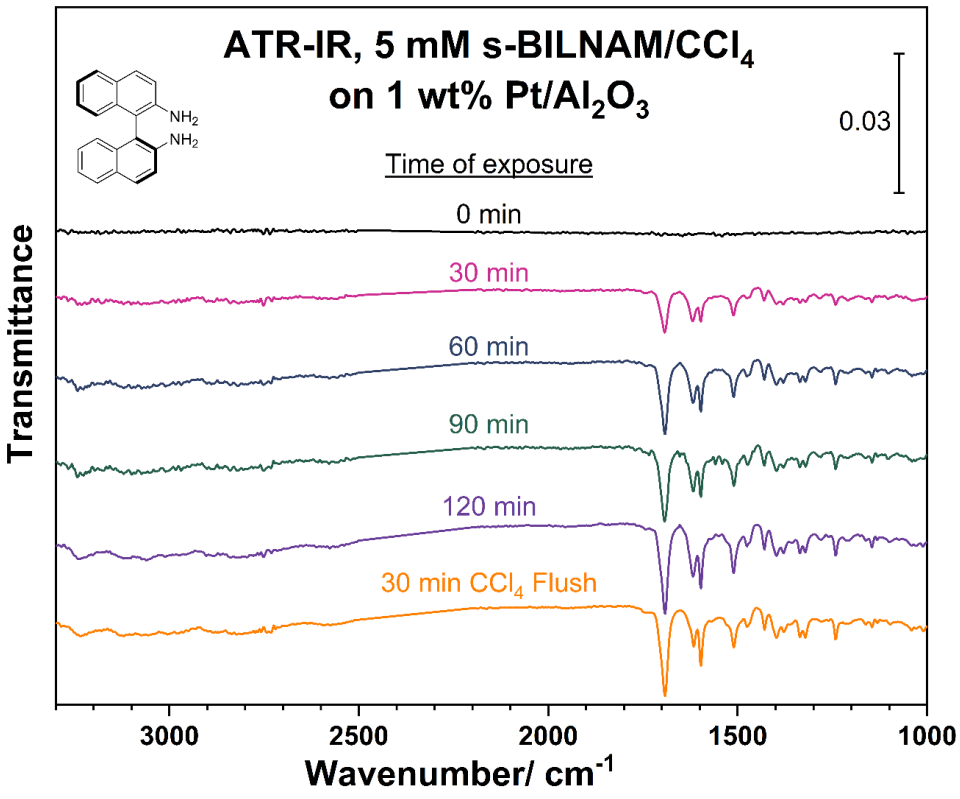

Figure 7.4 ATR-IR spectra of 5 mM s-BINAM in CCl_4 adsorption on 1 wt% Pt/Al_2O_3 as a function of exposure time.

To validate the repeatability of the results discussed previously, two more tests were conducted under identical conditions. These results are demonstrated in Figure 7.5 below. Trials 1, 2, and 3, as labeled in the figure, signify the three individual ATR-IR tests under uniform conditions. As the figure reveals, all three trials exhibited the same pattern, with the pure CCl_4 flush not removing any peak signals in all cases. The consistency of these results, coupled with the evidence provided in Figure 7.3, supports the notion that s-BINAM in CCl_4 is likely to bind to the Pt/Al_2O_3 catalyst.

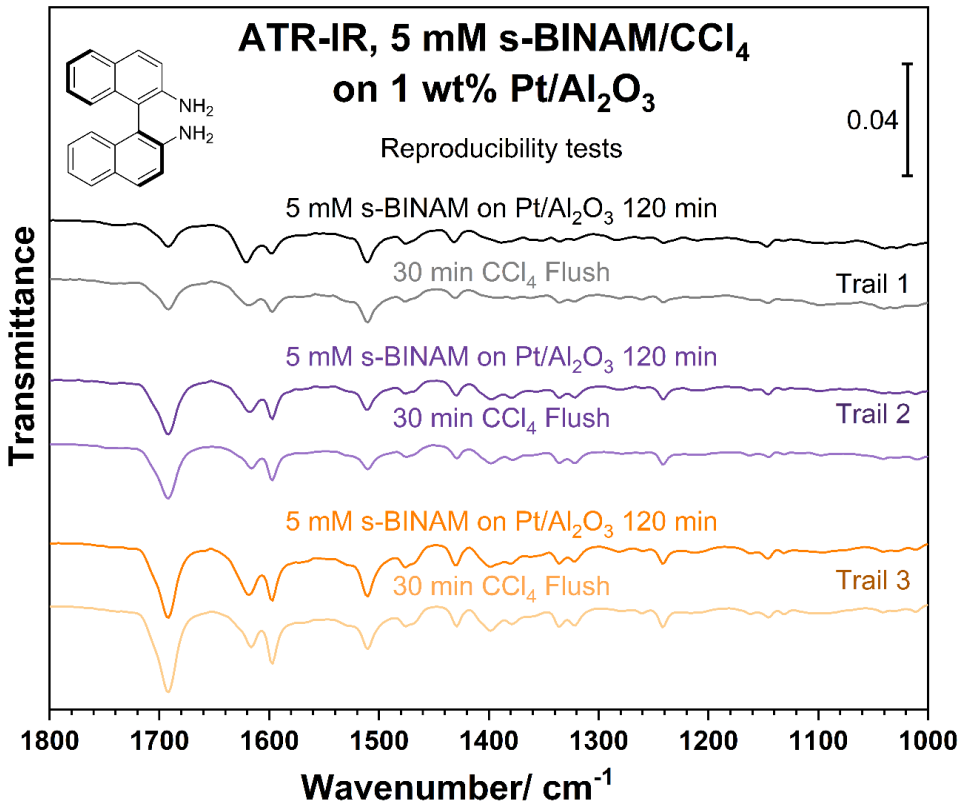

Figure 7.5 ATR-IR spectra of 5 mM s-BINAM in CCl_4 adsorption on 1 wt% Pt/Al_2O_3 catalyst at the exposure time of 120 min and then flushed with pure CCl_4 for 30 min. The trail 1, 2 and 3 means that the tests were performed three times under identical conditions to check the reproducibility.

s-BINOL molecules were also tested using *in-situ* ATR-IR, in addition to s-BINAM. Figure 7.6 showcases an instance of 5 mM s-BINOL in CCl_4 with 1 wt% Pt/Al_2O_3 catalyst over time. The upper trace represents the transmission IR of pure s-BINOL for reference.

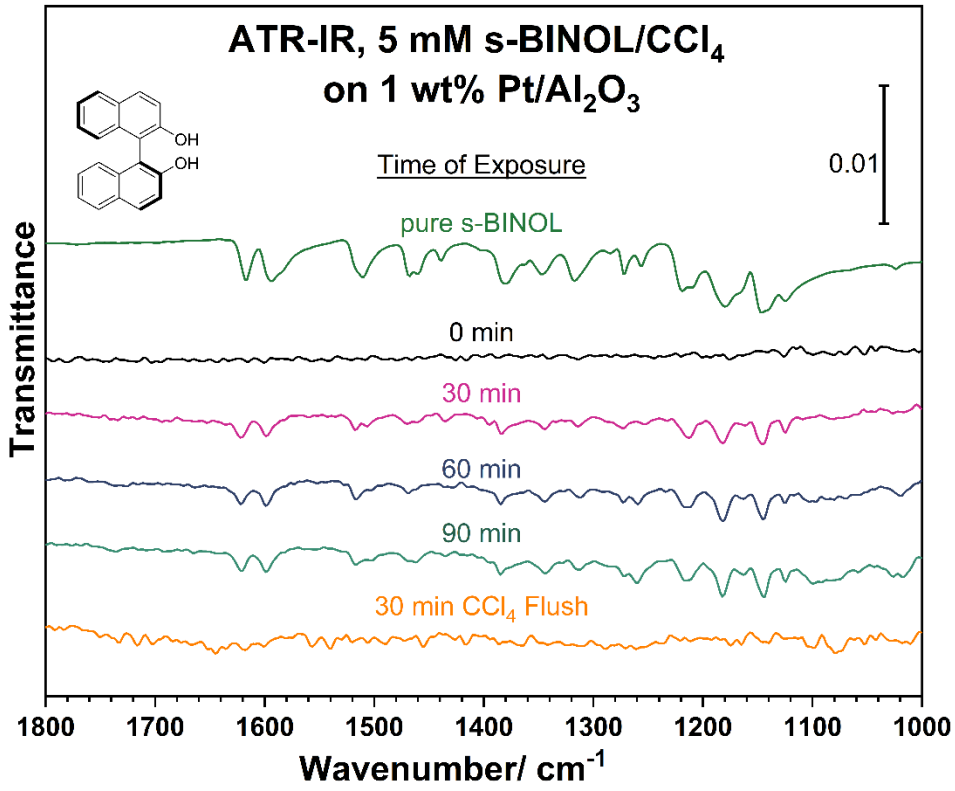

Figure 7.6 ATR-IR spectra of 5 mM s-BINOL in CCl_4 adsorption on 1 wt% Pt/Al_2O_3 as a function of exposure time. The top trace is the transmission IR of pure s-BINOL.

As suggested in Figure 7.6, a few sample peaks were initially noticed, and these peaks did not significantly alter with increased exposure time. Comparatively, most peaks are congruent with each other, barring the relative intensity of a few peaks. This variation in relative intensity may be attributed to the presence of solvent. Nevertheless, no

evidence was found suggesting the binding of s-BINOL to Pt surfaces. Furthermore, the concluding flushing test revealed that almost all sample peaks vanished post a 30-minute CCl_4 flush, as visible in the bottom trace. Consequently, the sample peaks might originate from free molecules in the solution, rather than adsorbed molecules on Pt surfaces.

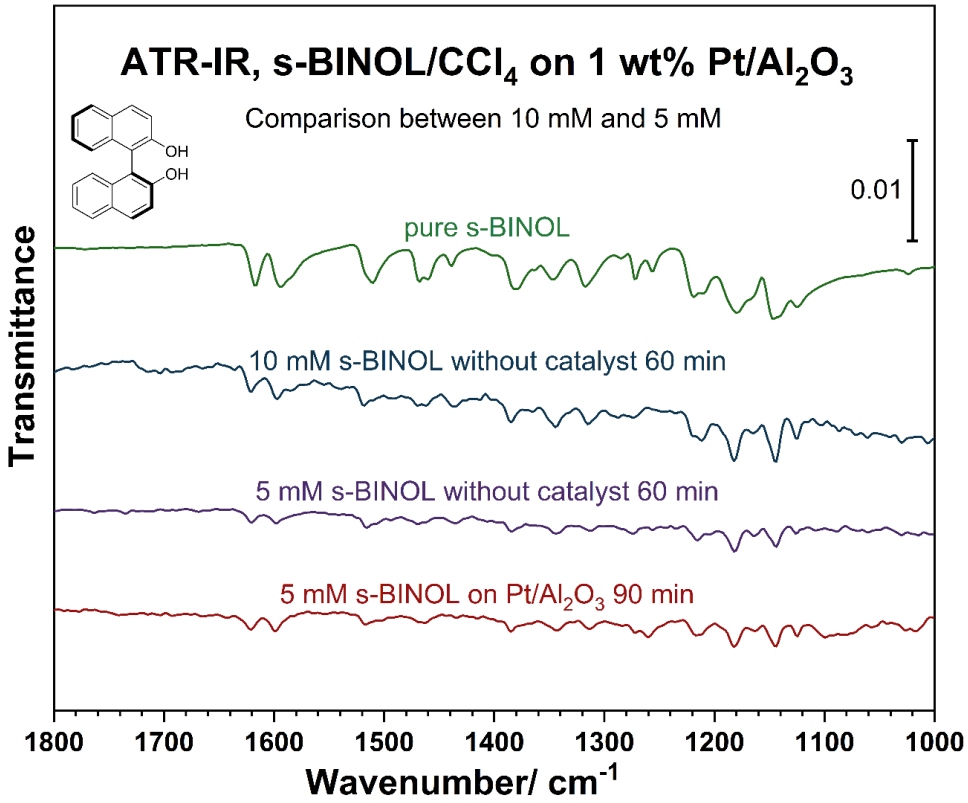

Figure 7.7 ATR-IR of s-BINOL in CCl_4 on 1 wt% Pt/Al_2O_3 and without catalysts. Comparisons were made between 5 mM s-BINOL with and without catalyst, and 5 mM and 20 mM s-BINOL without catalyst. The top trace is the transmission IR of pure s-BINOL.

An additional control test of 5 mM s-BINOL in CCl_4 without catalyst was executed, the spectrum obtained post a 60-minute period is presented in Figure 7.7 above, the third trace from the top. There are no discernable disparities between the spectra with

and without Pt catalysts, indicating that the sample peaks result from free molecules in the solution. Additionally, a higher concentration of 10 mM s-BINOL in CCl_4 solution was also tested without catalyst, as shown in the second trace from the top in Figure 7.7. The intensity of the peaks linearly increased with concentration, without any shift in peak position or relative intensity as compared to the spectrum collected with a 5 mM solution in the absence of Pt catalyst. This suggests that the sample peaks actually originate from free s-BINOL molecules, with no evidence of adsorption observed.

7.3.2 Effects of Solvent on s-BINAM and s-BINOL Adsorption

In the case of CCl_4, it is evident that s-BINAM binds to Pt/Al_2O_3 catalysts, while there is no supporting evidence that suggests s-BINOL adheres to Pt catalysts. The effect of solvent on s-BINAM or s-BINAM adsorption was explored in this study to observe its behavior in varying solvent environments.

Two additional solvents, toluene and ethanol, were tested for the s-BINAM molecules. Figure 7.8 illustrates the spectra captured with a 5 mM s-BINAM in a toluene solution when exposed to the Pt/Al_2O_3 catalyst (the second trace from the top), and without catalysts (the third trace from the top).

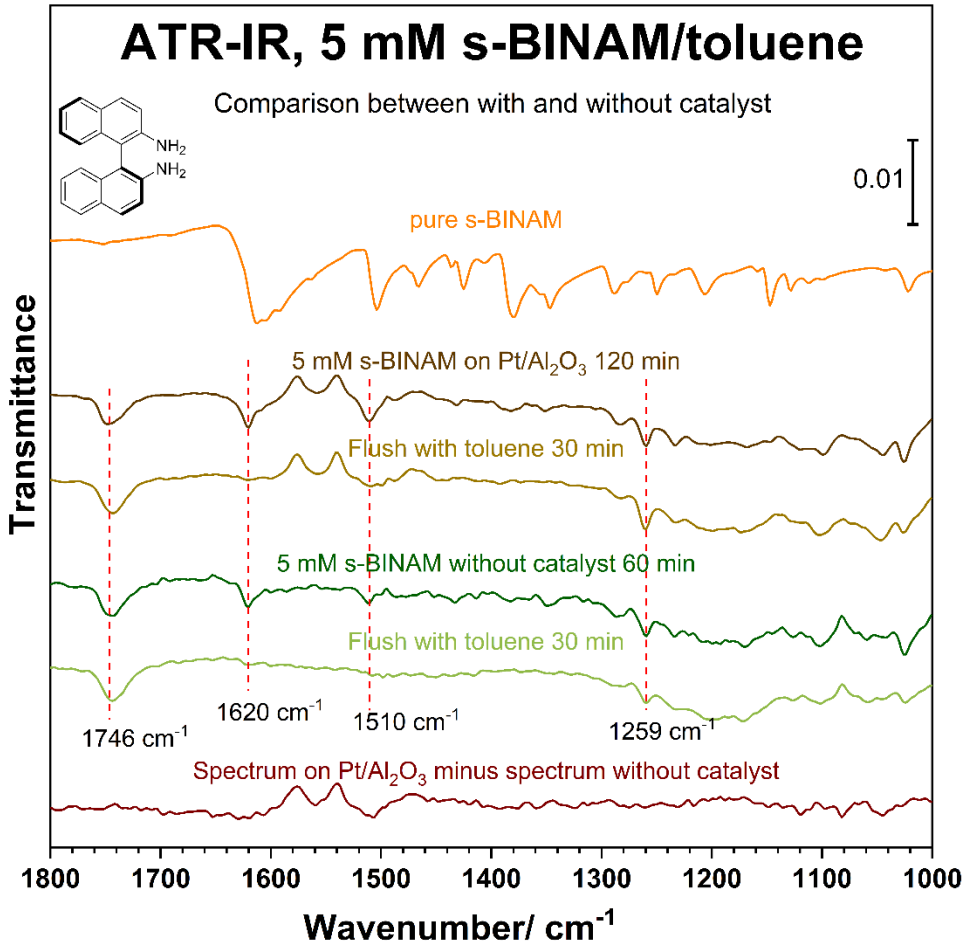

Figure 7.8 ATR-IR spectra of 5 mM s-BINAM in toluene adsorption on 1 wt% Pt/Al_2O_3 and without catalyst and after flushing with pure toluene at the end. The bottom trace is the spectrum on Pt/Al_2O_3 catalyst minus spectrum without catalyst. The top one is the transmission IR of pure s-BINAM.

The spectrum collected in the presence of Pt catalysts in toluene revealed noticeable differences in comparison to the transmission IR spectrum of pure s-BINAM. Specifically, a new peak around 1746 cm^{-1} emerged. When s-BINAM was placed in CCl_4 with Pt catalysts, another new peak around 1690 cm^{-1} was observed, believed to be a result of the amine group binding to Pt surfaces. However, the presence of this peak in toluene, even without Pt catalysts (as indicated in the second trace from the top in the

figure below), and its persistence after flushing the ATR-IR with pure toluene, suggests an alternative scenario.

Additionally, two peaks at around 1620 and 1510 cm^{-1} mirror the transmission IR spectrum of pure s-BINAM. Both peaks disappeared after flushing the cell with pure toluene, suggesting that the peaks may be attributed to free s-BINAM molecules in solution. Another peak at approximately 1259 cm^{-1} persisted, which might be assigned to toluene. As such, no evidence of adsorption was observed in the case of toluene. The remaining peaks post-flush are likely due to the toluene molecules.

Ethanol was another solvent tested. Results for 5 mM s-BINAM in ethanol solutions, with and without catalysts, are presented in Figure 7.9. Weak sample signals were observed in both cases, and the spectra were similar, displaying only two distinct peaks at around 1623 and 1513 cm^{-1}, matching the transmission IR spectrum of pure s-BINAM molecules. All sample peaks vanished after flushing with fresh ethanol, suggesting that s-BINAM does not bind to Pt catalysts in an ethanol solution. Increased solubility of s-BINAM in ethanol may complicate achieving high surface coverage of modifiers on Pt surfaces.

In conclusion, no evidence of adsorption was observed for s-BINAM molecules in either toluene or ethanol. The sample peaks are hypothesized to originate from free molecules in the solutions.

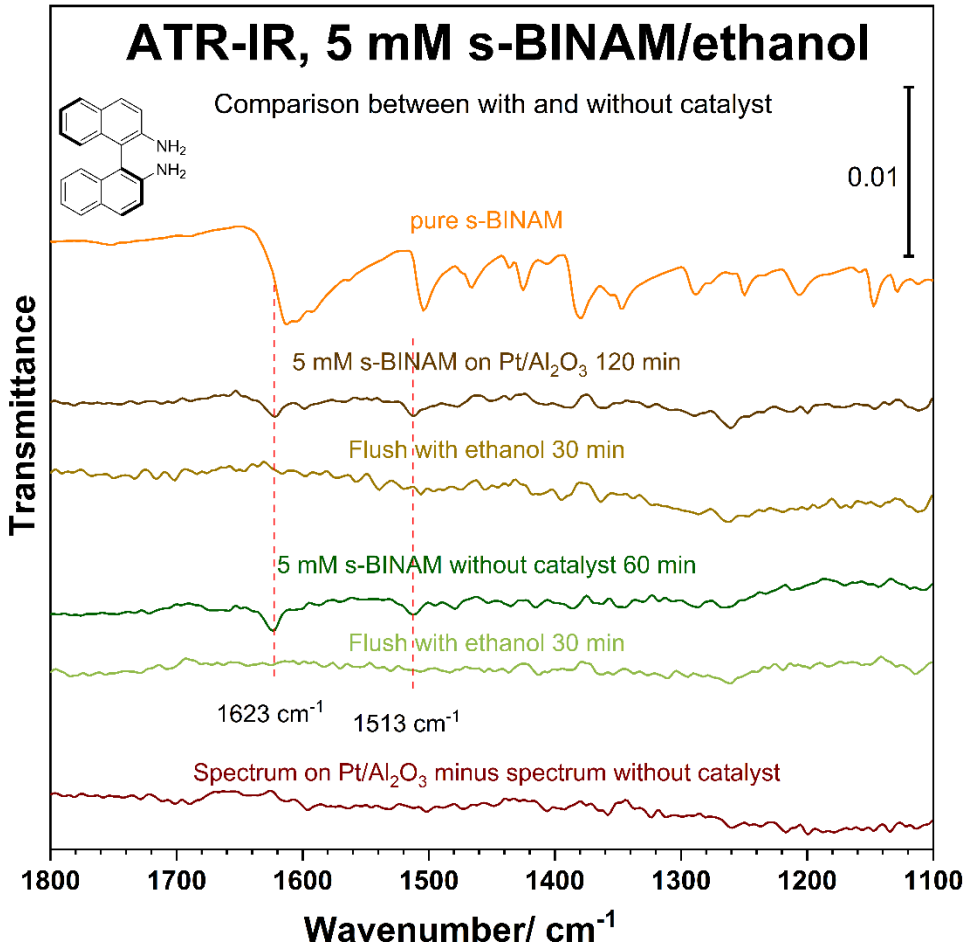

Figure 7.9 ATR-IR spectra of 5 mM s-BINAM in ethanol adsorption on 1 wt% Pt/Al_2O_3 and without catalyst and after flushing with pure ethanol at the end. The bottom trace is the spectrum on Pt/Al_2O_3 catalyst minus spectrum without catalyst. The top one is the transmission IR of pure s-BINAM.

Similar investigations were conducted for the s-BINOL molecules, using toluene and ethanol as solvents. The gathered spectra are compared in Figure 7.10 below. Regrettably, no evidence of adsorption was found, regardless of the varied concentrations tested. In the case of CCl_4, as shown in Figure 7.7, a similar behavior was observed in the case of Pt/SiO_2 as indicated in Figure 7.10, s-BINOL did not bind to Pt/Al_2O_3 catalysts, a behavior mirrored in the case of Pt/SiO_2, as seen in the second trace from the top in

Figure 7.10. Subsequent tests with 10 mM s-BINOL in toluene solution, and 10 mM and 20 mM s-BINOL in ethanol solutions, revealed that all spectra mirrored the transmission IR of pure s-BINOL.

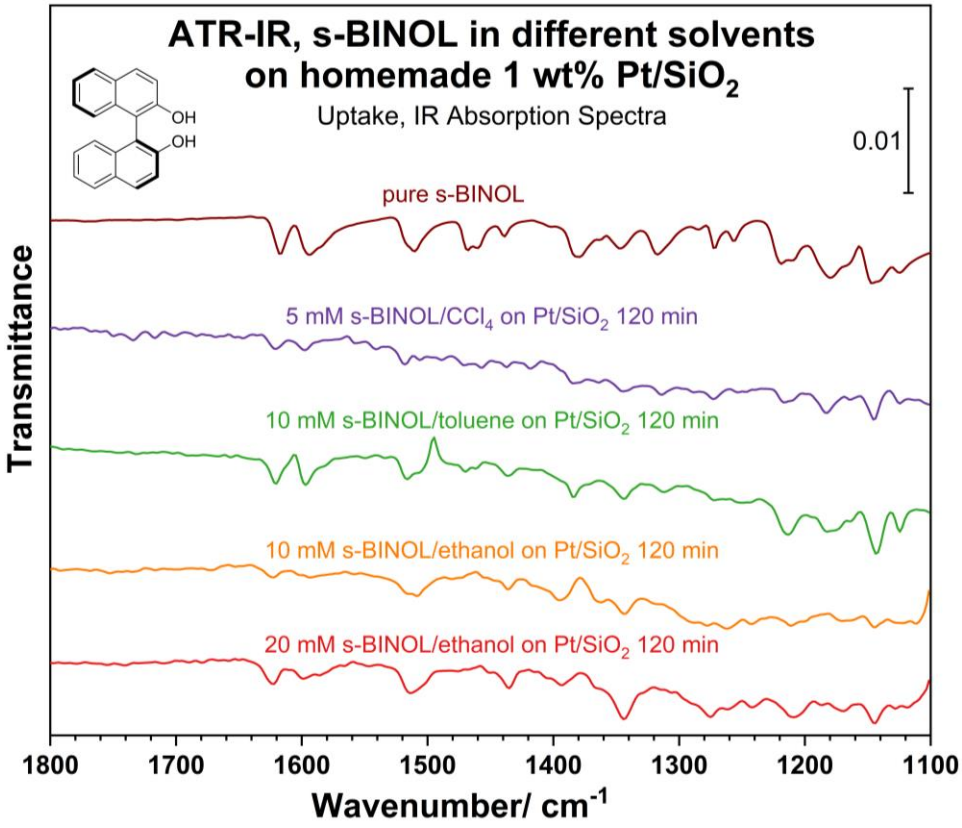

Figure 7.10 ATR-IR of s-BINOL in different solvents including CCl_4, toluene and ethanol adsorption on 1 wt% Pt/SiO_2. The top one is the transmission IR of pure s-BINOL.

7.3.3 Effect of Catalysts on s-BINAM and s-BINAM Adsorption

The ATR-IR spectra of a 5 mM s-BINAM solution in CCl_4, interacting with a 1 wt% Pt/Al_2O_3 catalyst, provided compelling evidence of molecular binding to Pt catalyst. To eliminate potential interference from the Al_2O_3 support, a control test was conducted

with a 5 mM solution on pure γ-Al_2O_3. The resultant spectrum, obtained after 120-minute exposure to pure γ-Al_2O_3, is presented in Figure 7.11. A distinct difference is apparent between the spectra obtained in the presence of γ-Al_2O_3 and Pt/Al_2O_3, the latter of which bears significant similarity to the blank test conducted without a catalyst. This observation infers that s-BINAM tends to adhere to Pt surfaces, while largely ignoring the γ-Al_2O_3 support.

Further investigation into the effect of catalyst support material was conducted using both commercial and homemade 1 wt% Pt/SiO_2 catalysts. Contrary to expectations, s-BINAM in CCl_4 did not bind to either of the Pt/SiO_2 catalysts, as illustrated in Figure 7.11. The spectra obtained from both Pt/SiO_2 catalysts closely resembled those taken without a catalyst, with the sample peaks indicative of unbound molecules in the solution. This unexpected outcome suggests that γ-Al_2O_3 support may contribute to the adsorption process, potentially due to its inherent acidity. The primary contrast between γ-Al_2O_3 and SiO_2 supports lies in their acidity levels; SiO_2 is regarded as a mildly acidic oxide, whereas γ-Al_2O_3 possesses a higher density of acid sites owing to the presence of Lewis acid sites on its surface.

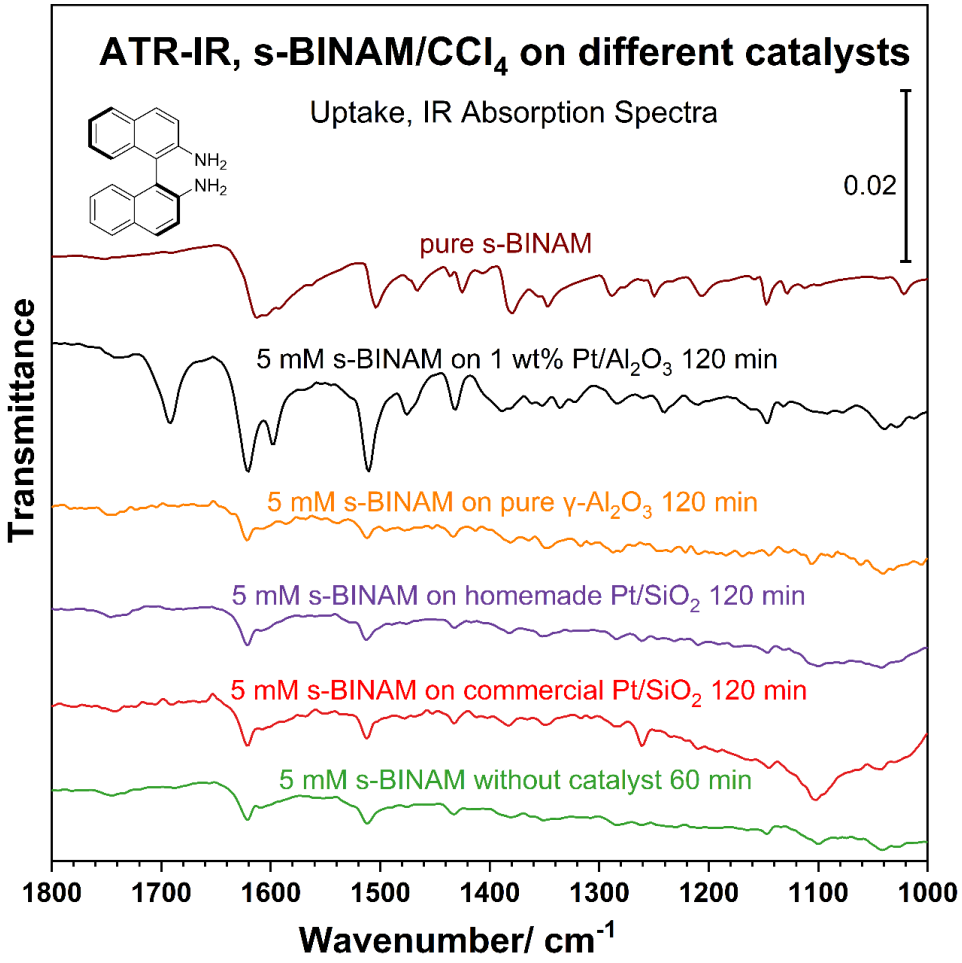

Figure 7.11 ATR-IR of 5 mM s-BINAM in CCl_4 adsorption on different catalysts, from the second to the bottom are 1 wt% Pt/Al_2O_3, pure γ-Al_2O_3, homemade 1 wt% Pt/SiO_2, commercial 1 wt% Pt/SiO_2 and without catalyst. The top one is the transmission IR of pure s-BINAM.

The impact of the Pt catalyst support on s-BINOL was also examined. Both commercial Pt/Al_2O_3 and homemade Pt/SiO_2 catalysts were tested, with the outcomes consolidated in Figure 7.12. No conspicuous differences were discerned between the tests conducted with and without a Pt catalyst.

Moreover, Cu supported on SBA-15 catalysts were evaluated. As indicated in Figure 7.12, s-BINOL in CCl_4 exhibited no tendency to bind to either Cu or oxidized Cu (CuO_x, as denoted in the figure) surfaces.

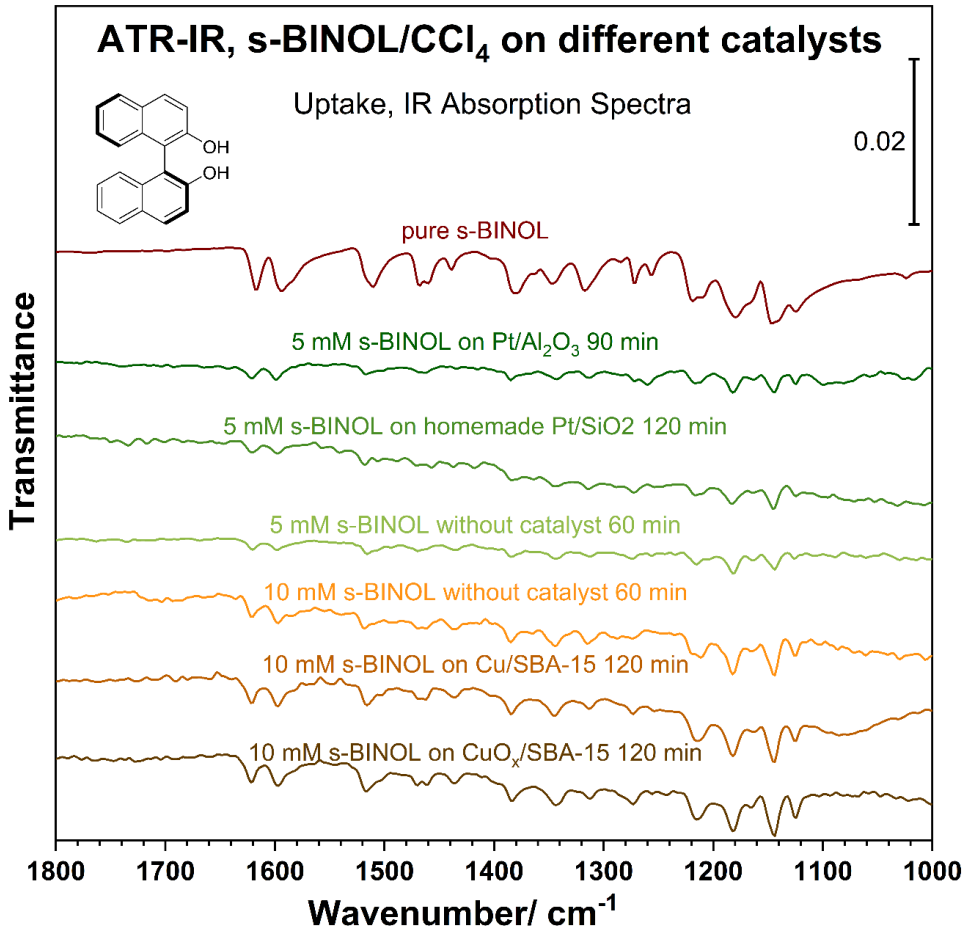

Figure 7.12 ATR-IR of 5 mM and 10 mM s-BINOL in CCl_4 adsorption on different catalysts, from the second to the bottom are 5 mM s-BINOL on 1 wt% Pt/Al_2O_3, homemade 1 wt% Pt/SiO_2 and without catalyst; 10 mM s-BINOL without catalyst, on Cu/SBA-15 and CuO_x/SBA-15. The top one is the transmission IR of pure s-BINOL.

7.3.4 Kinetic Measurements with s-BINAM and s-BINOL

Kinetic measurements were conducted utilizing both s-BINAM and s-BINOL. Strong adsorption of s-BINAM on Pt surfaces was observed, contrasting with the lack of discernible adsorption for s-BINOL. Consequently, the catalytic behavior of these two molecules was anticipated to vary.

The study also investigated a commercial Pt/Al_2O_3 catalyst in three different solvents: toluene, acetic acid, and ethanol. As depicted in the left panel of Figure 7.13, toluene demonstrated superior catalytic activity compared to ethanol, with acetic acid showing the least ideal performance. Both s-BINOL and s-BINAM exhibited similar reaction rates in toluene. However, in ethanol, s-BINOL displayed a significantly higher reaction rate than s-BINAM, potentially attributable to more efficient reactant interactions due to a greater solubility of s-BINOL in ethanol.

The enantiomeric excess (*ee*) values, as indicated in the right panel of Figure 7.13, revealed a surprising similarity between s-BINAM and s-BINOL in terms of enantioselectivity within the same solvent. Given our adsorption studies showing no evidence of s-BINOL adsorption, it suggests that the enantioselectivity promotion mechanisms of s-BINOL and s-BINAM differ from those of cinchona alkaloids and NEA modifiers. Furthermore, enantioselectivity varied among different solvents, with ethanol yielding the highest levels despite similar results in toluene.

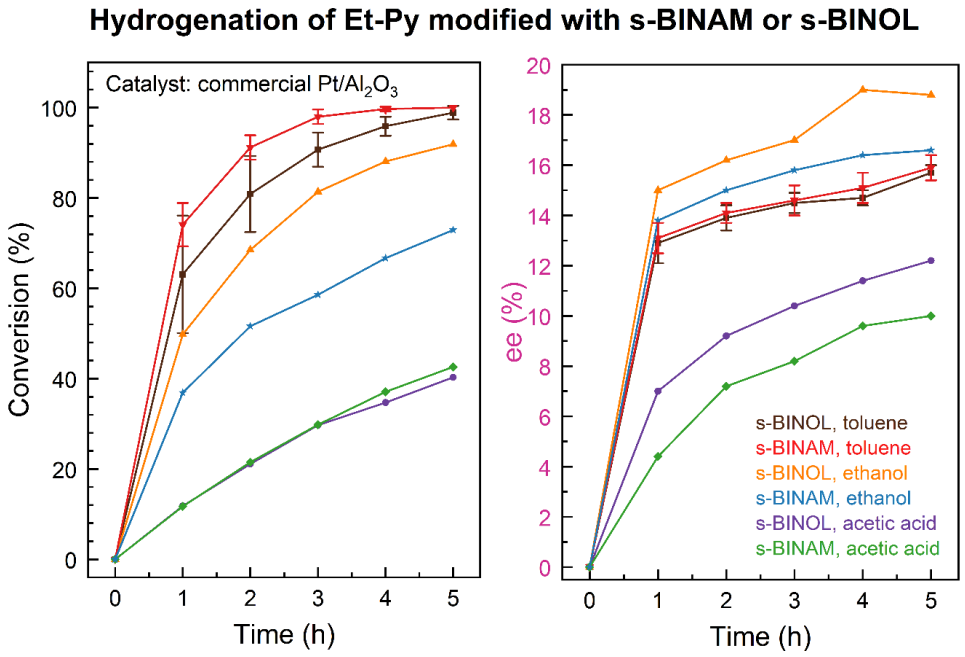

Figure 7.13 The conversion (left panel) and ee (right panel) with time of Et-Py hydrogenation modified with either s-BINAM or s-BINOL catalyzed by commercial Pt/Al_2O_3 catalyst in different solvents.

Experiments with reactions modified by s-BINAM or s-BINOL were additionally catalyzed using homemade or commercial Pt/SiO_2. Results, as illustrated in Figure 7.14 (homemade Pt/SiO_2) and Figure 7.15 (commercial Pt/SiO_2), initially appear perplexing but clearly suggest that Pt/SiO_2 is less effective as a catalyst than Pt/Al_2O_3. Regarding homemade Pt/SiO_2, the data seems to suggest a trend of increasing ee values with reaction time across all solvents. However, no consistent correlation was identified. This may suggest a distinct enantioselectivity enhancement mechanism that necessitates further exploration in future research.

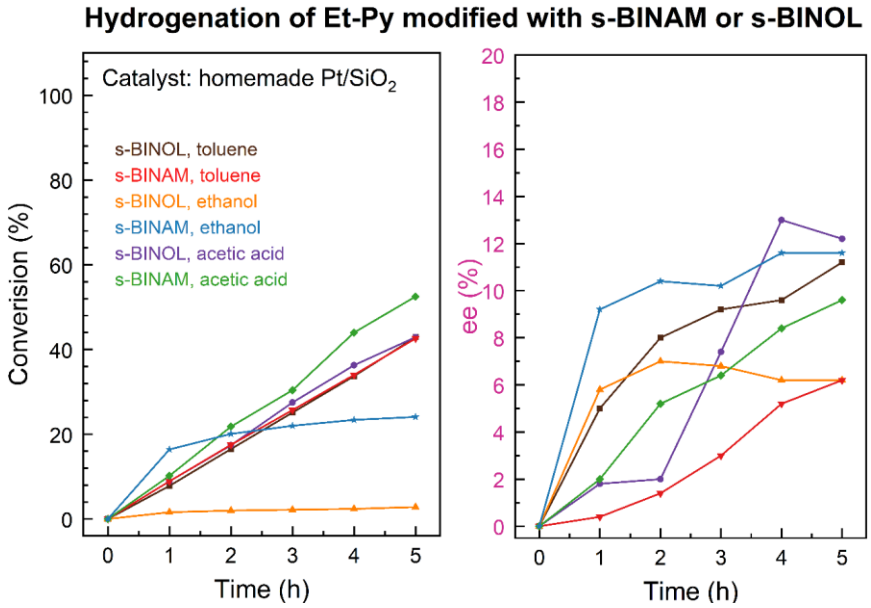

Figure 7.14 The conversion (left panel) and ee (right panel) with time of Et-Py hydrogenation modified with either s-BINAM or s-BINOL catalyzed by homemade Pt/SiO_2 catalyst in different solvents.

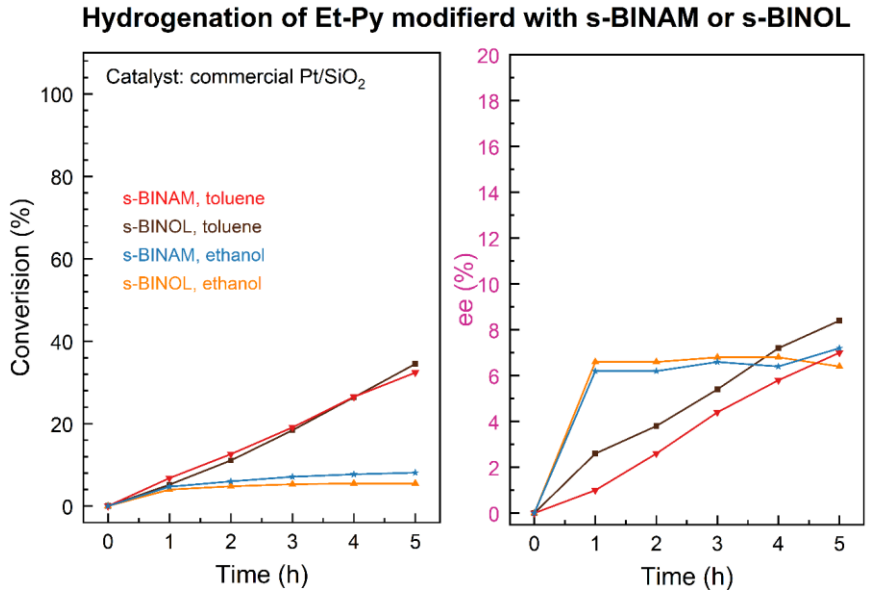

Figure 7.15 The conversion (left panel) and ee (right panel) with time of Et-Py hydrogenation modified with either s-BINAM or s-BINOL catalyzed by commercial Pt/SiO_2 catalyst in different solvents.

7.4 Summary

In conclusion, adsorption studies were undertaken with s-BINOL and s-BINAM to discern the effects of solvents and catalysts. These studies revealed that in CCl_4 solutions, s-BINAM could bind to Pt/Al_2O_3 catalysts but would not adhere to Pt/SiO_2 catalysts. Furthermore, no adsorption was observed when toluene or ethanol were used as solvents. Similarly, no evidence of adsorption was detected with s-BINOL in solutions on Pt or Cu supported catalysts.

Analyzing the kinetic results, no correlation was identified between adsorption behavior and catalytic performance, despite the fact that both modifiers could enhance the enantioselectivity. Overall, Pt/Al_2O_3 catalysts demonstrated superior catalytic performance compared to Pt/SiO_2 catalysts. It is postulated that s-BINAM or s-BINOL may contribute to enantioselectivity in a distinctive manner, deviating from the original hypothesis with cinchona alkaloids, or NEA molecules. Future research will endeavor to delve further into this catalytic behavior.

Chapter 8

Behavior of Terpinen-4-ol on Pt Surfaces in Heterogeneous Catalysis

8.1 Brief Introduction and Hypothesis

Thus far, investigations into chiral modifiers have demonstrated their ability to enhance the enantioselectivity of hydrogenation reactions. An alternate approach involves the hydrogenation of double bonds on a molecule with an inherent chiral center that could guide the enantioselectivity.

Terpinen-4-ol, depicted in Figure 8.1, is a naturally occurring organic compound classified as a monoterpene. Its wide application in fragrance and flavor industries is primarily due to its appealing scent. It is typically sourced from the essential oils of various plants, encompassing vegetables, eucalyptus, and cardamom.

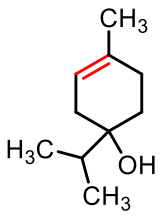

Terpinen-4-ol

Figure 8.1 Structure of terpinen-4-ol.

Apart from its agreeable fragrance, terpinen-4-ol is notable for its enantioselectivity. This compound has been identified as exhibiting direct enantioselectivity, implying it can preferentially interact with one enantiomer over the other. This trait is likely a result of its chiral structure. The direct enantioselectivity of terpinen-4-ol has undergone extensive study in recent years and has shown potential for use in diverse fields such as catalysis, organic synthesis, and medicinal chemistry[92-93].

This chapter explores the adsorption behavior of terpinen-4-ol on metal surfaces, using *in-situ* ATR-IR, and examine its catalytic performance in Et-Py hydrogenation.

8.2 Experimental Details

The adsorption tests for all chiral modifiers were conducted using in-situ ATR-IR, and reference spectra of pure samples were obtained through transmission IR. Kinetic measurements were conducted using a high-pressure reactor. The experimental details are provided in Chapter 2.

8.3 Results and Discussions

8.3.1 *In-Situ* ATR-IR Studies of Terpinen-4-ol

The investigation began with ATR-IR examinations of varying concentrations of (s)-terpinen-4-ol in CCl_4 solutions using 1 wt% Pt/Al_2O_3 catalysts, the results of which are displayed in Figure 8.2 below.

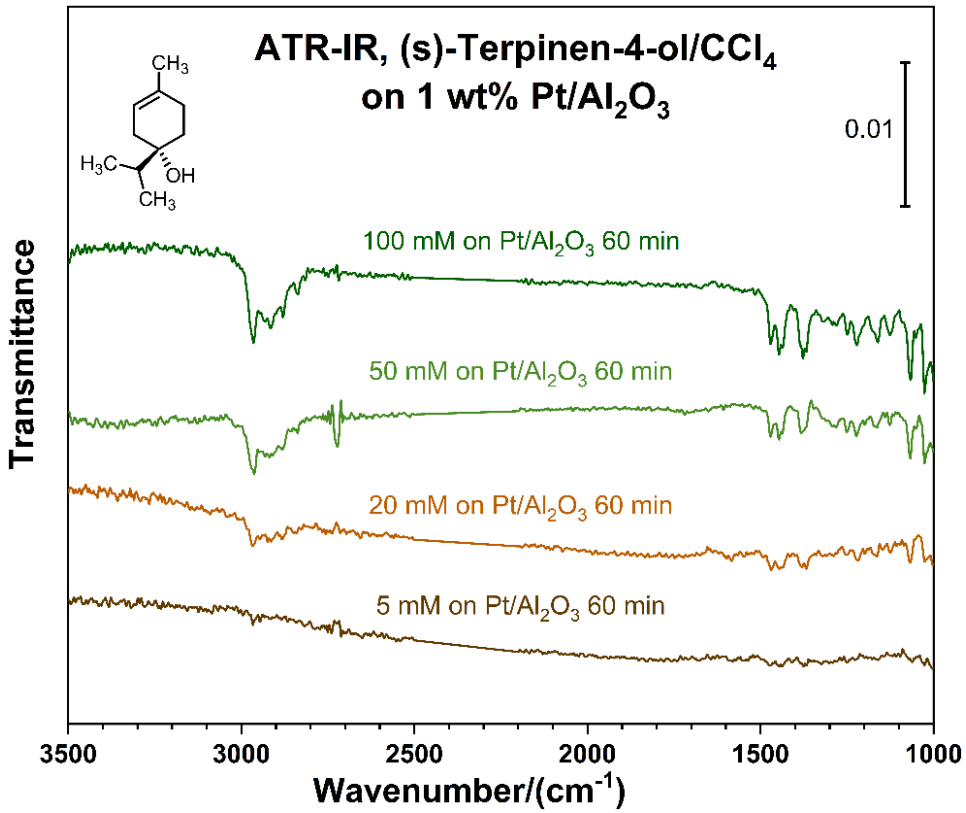

Figure 8.2 ATR-IR spectra of (s)-Terpinen-4-ol in CCl_4 exposed to a 1 wt% Pt/Al_2O_3 catalyst after 60 min as a function of concentration.

It was noted that the intensity of the sample peaks exhibited a linear relationship with concentration. In the spectrum of the 5 mM solution (the lowest one), no significant sample signals were discernible. However, with increasing concentration, the sample signals became more defined and robust.

Given that the 100 mM concentration presented more compelling sample signals, further ATR-IR tests of 100 mM in CCl_4 solution, without the use of catalysts, were undertaken. The findings and comparative data are demonstrated in Figure 8.3. The

figure also includes the transmission IR of pure (s)-terpinen-4-ol, depicted in the top trace.

Despite the inconspicuous differences between the transmission IR spectrum and the ATR-IR spectrum of 100 mM (s)-terpinen-4-ol in CCl_4 solution, the shift and relative intensity of specific sample signals merit discussion. For instance, the broad dual peaks ranging between 1480 cm^{-1} and 1400 cm^{-1} became more defined post exposure to the Pt catalyst in the CCl_4 solution. This pattern was similarly apparent for peaks at higher wavenumbers, around 3000 cm^{-1}. As hydrogen bonding is anticipated among the (s)-terpinen-4-ol molecules, the sharpening of peaks could be attributed to the weakening of hydrogen bonding in the presence of the CCl_4 solvent. Furthermore, the two peaks around 1200 cm^{-1} and 1220 cm^{-1} shifted slightly towards higher wavenumbers, and the peak around 1120 cm^{-1} was considerably diminished.

Figure 8.3 also includes a control test without a catalyst, represented in the bottom trace. The spectrum bears resemblance to the spectrum (middle trace) obtained in the case of Pt catalysts, indicating that (s)-terpinen-4-ol does not readily bind to Pt catalysts. The sample signals, therefore, originate from free molecules in solution.

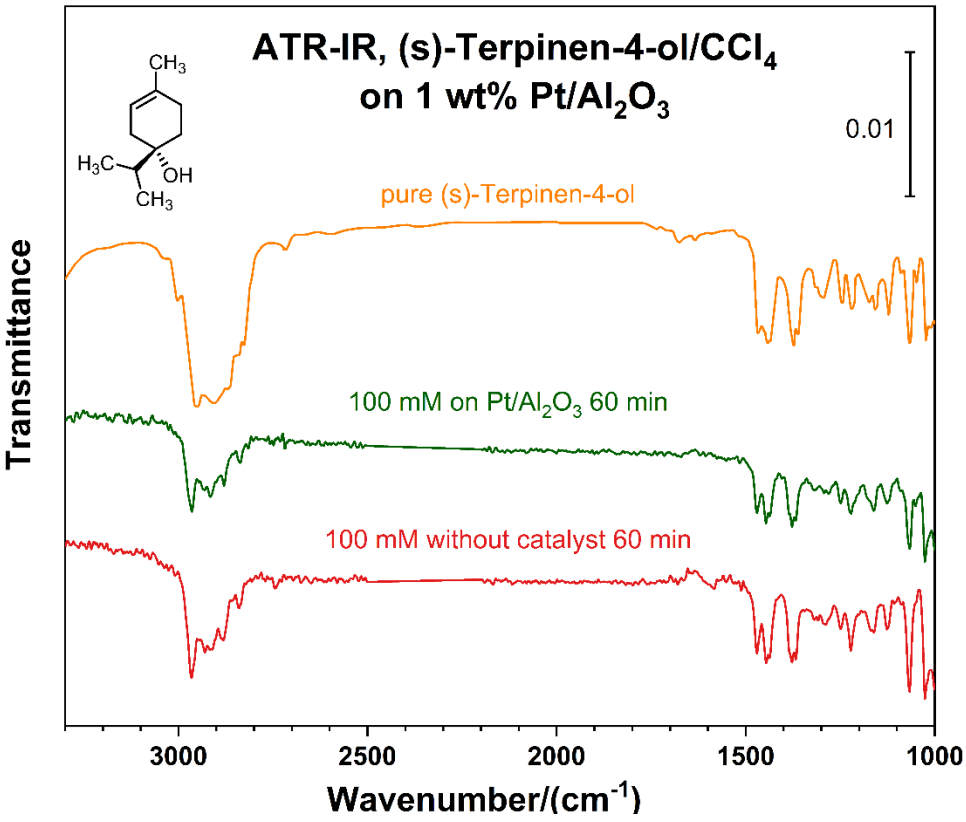

Figure 8.3 ATR-IR spectra of (s)-terpinen-4-ol in CCl_4 exposed to a 1 wt% Pt/Al_2O_3 catalyst after 60 min as a function of concentration. The top trace is the transmission IR of pure (s)-terpinen-4-ol for reference.

8.3.2 Effect of Catalyst on Terpinen-4-ol Adsorption

The impact of catalysts was examined through experiments utilizing both Pt and Cu supported catalysts. Various supports for Pt catalysts, including Al_2O_3, SiO_2 and SBA-15, were explored. Additionally, both Cu and Pt supported on SBA-15 catalysts were studied, along with further investigations into the alloy of Cu-Pt, and Cu-Pd supported on SBA-15 catalysts. Figure 8.4 summarizes the results. Spectra were collected from a 100 mM (r)-terpinen-4-ol solution in CCl_4 after exposure to a catalyst for a

duration of 60 minutes. The transmission IR spectrum of pure (r)-terpinen-4-ol is also included for comparison purposes.

A consistent behavior was observed across all catalysts, as indicated in the figure. A blank test without the use of any catalyst yielded similar results, demonstrating the absence of detectable adsorption with any catalysts.

Additionally, after flushing the ATR-IR cell with pure CCl_4, the collected spectra did not present any significant remaining signals. Figure 8.5 displays two examples of flushing tests with Pt/Al_2O_3 and Pt/SBA-15 catalysts. Nearly all sample peaks vanished after the application of pure solvent, leading to the conclusion that the sample peaks originated from free molecules in the solution.

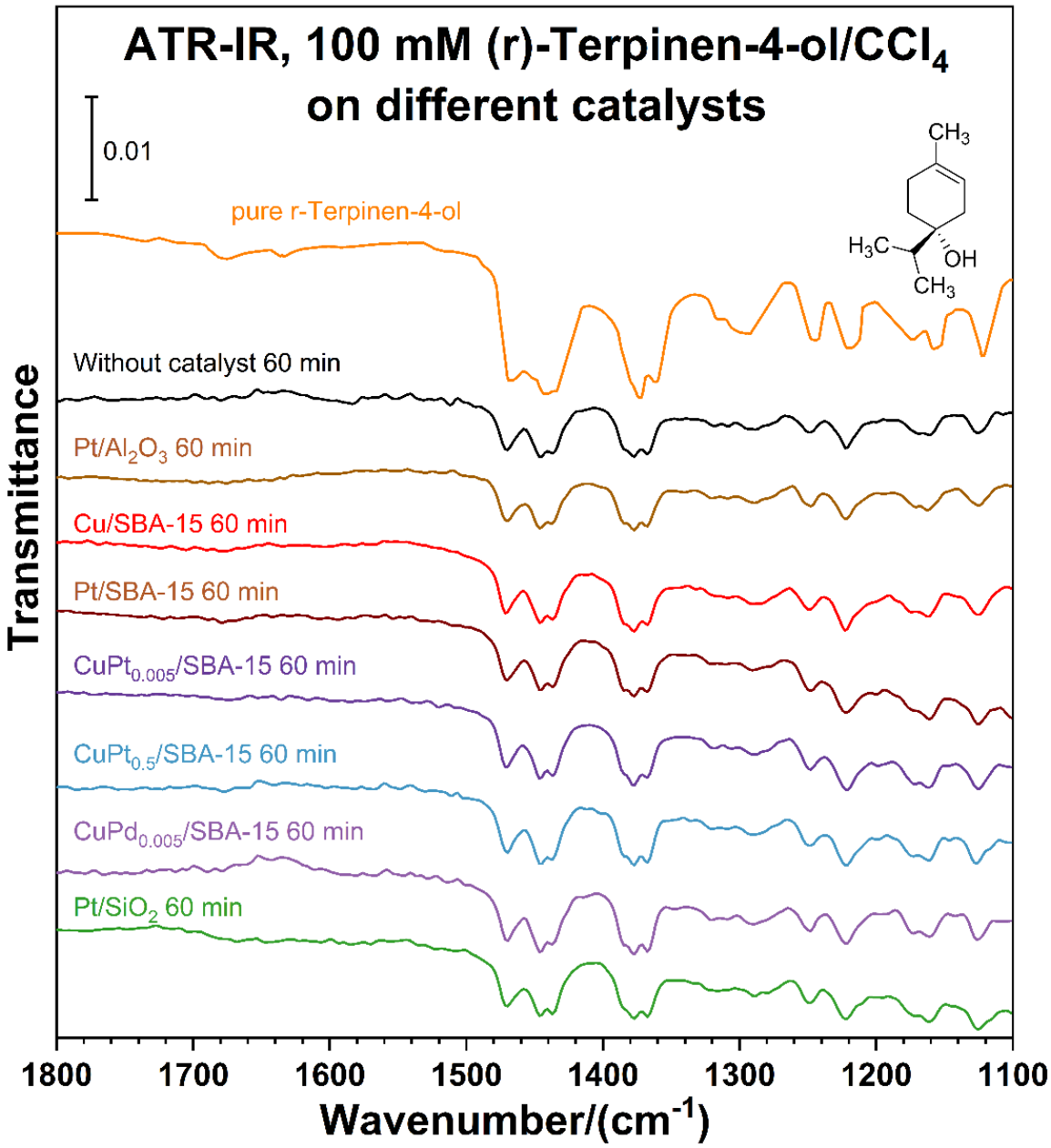

Figure 8.4 ATR-IR spectra of 100 mM (r)-terpinen-4-ol in CCl_4 on different catalysts. The top trace is the transmission IR of pure (r)-terpinen-4-ol for reference.

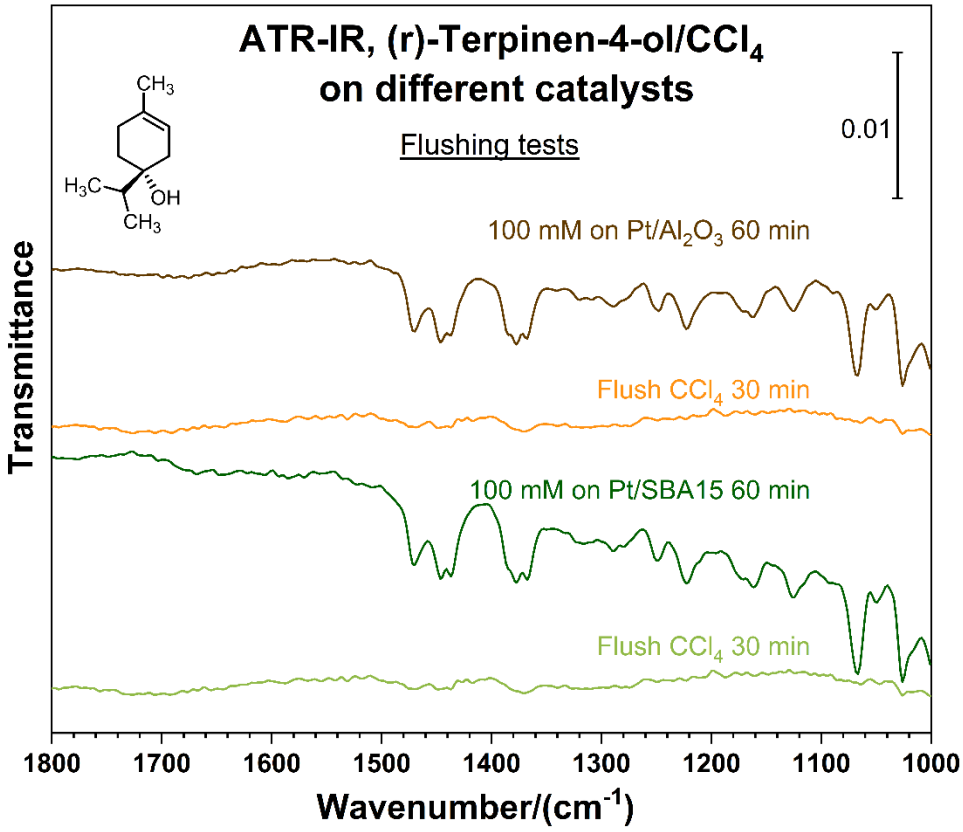

Figure 8.5 ATR-IR spectra of 100 mM (r)-terpinen-4-ol in CCl_4 solution collected after exposing to Pt catalysts for 60 min and then flushing with pure CCl_4 for 30 min.

8.3.3 Effect of Solvent on Terpinen-4-ol Adsorption

Toluene, an alternative solvent, was also tested. Three sets of ATR-IR experiments were conducted, consisting of a 100 mM (r)-terpinen-4-ol solution in toluene exposed to Pt/Al_2O_3 and Pt/SBA-15 catalysts, and a blank test without any catalyst. As depicted in Figure 8.6, despite the appearance of some sample peaks corresponding to (r)-terpinen-4-ol molecules, no evidence of adsorption was detected.

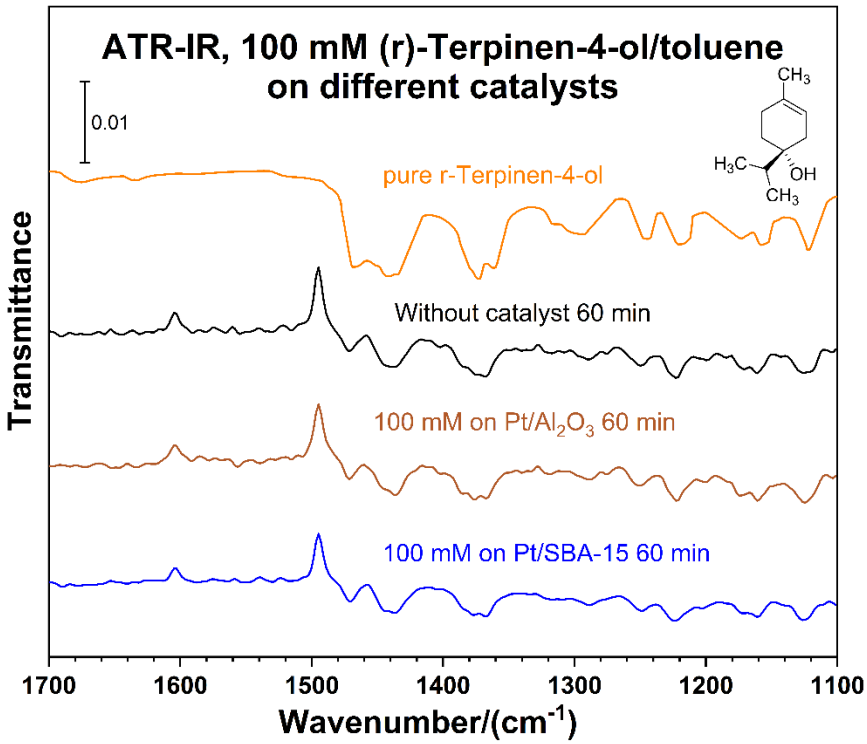

Figure 8.6 ATR-IR spectra of 100 mM (r)-terpinen-4-ol in toluene on different catalysts. The top trace is the transmission IR of pure (r)-terpinen-4-ol for reference.

8.3.4 Kinetic Measurements with Terpinen-4-ol

Kinetic measurements were conducted on Et-Py hydrogenation modified with terpinen-4-ol. Unlike the usual reactions with NEA-related modifiers, terpinen-4-ol itself undergoes hydrogenation, as demonstrated in Figure 8.7. The corresponding kinetic data is outlined in Table 8.1.

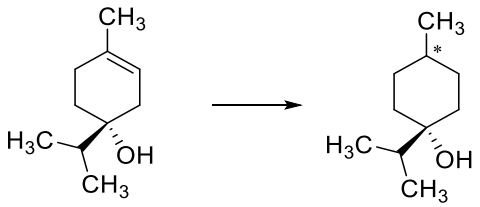

Figure 8.7 Illustration of hydrogenation of terpinen-4-ol reaction.

Table 8.1 Activity and *ee* for the hydrogenation of Et-Py modified with chiral terpinen-4-ol

Modifier	**Catalyst**	**Mole ratio Pt/Et-Py/modifier**	**Et-Py Conversion (%)**	***ee* (%)**
No modifier	No catalyst	1/2000/na	0	0
No modifier	Pt/Al_2O_3	1/2000/na	47.3	0.4
(s)-terpinen-4-ol	Pt/Al_2O_3	1/2000/50	35.4	3.1 (R)
	Pt/SiO_2	1/2000/50	21.9	1.2 (R)
	Pt/SBA-15	1/2000/50	86.6	2.8 (R)
	$CuPt_{0.5}$/SBA-15	1/2000/50	0	0
	$CuPt_{0.75}$/SBA-15	1/2000/50	1.2	0.4
	$CuPd_{0.005}$/SBA-15	1/2000/50	0	0
	No catalyst	1/2000/50	0	0
(r)-terpinen-4-ol	Pt/Al_2O_3	1/2000/50	32.5	2.0 (R)
		1/2000/100	31.7	1.8 (R)
		1/2000/200	33.1	3.4 (R)

Reaction conditions: t = 3.0 h, T= 298 K, $P(H_2)$=10 bar, catalyst (25 mg), toluene solvent (10 mL).

When examining (s)-terpinen-4-ol, conversion and enantiomeric excess (*ee*) values corresponding to reaction time are illustrated in Figure 8.8. Notably, all Cu-based

catalysts failed to exhibit catalytic activity for Et-Py hydrogenations. Conversely, Pt-based catalysts demonstrated activity, albeit with remarkably low *ee* values.

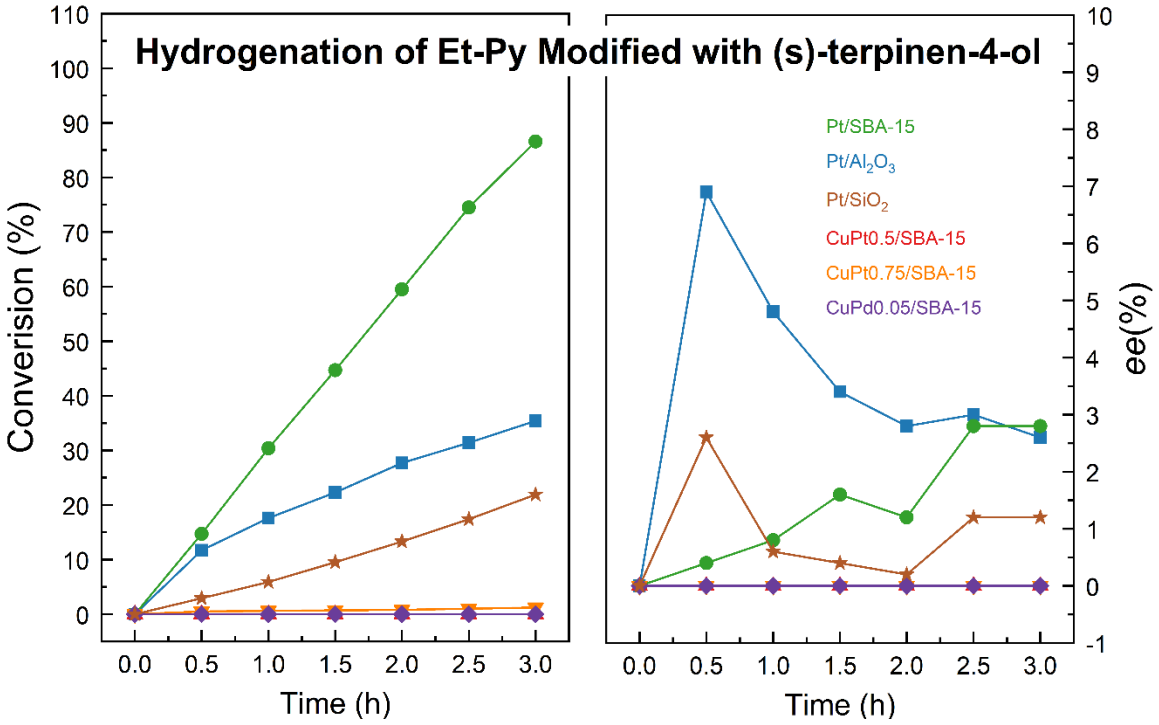

Figure 8.8 Conversion and *ee* values of hydrogenation of Et-Py modified with (s)-terpinen-4-ol catalyzed by different catalysts.

Interestingly, the reaction catalyzed by Pt/Al_2O_3, with added (s)-terpinen-4-ol, resulted in an Et-Py conversion of 35.4%. This is lower than the conversion (~47.3%) achieved in reactions without the modifier. As previously stated, terpinen-4-ol contains a double bond which can also be hydrogenated. These kinetic results were further corroborated by gas chromatography, as displayed in Figure 8.8. The left panel shows that the activity of Cu-based catalysts was substantially weaker than that of platinum-based catalysts, akin to the Et-Py hydrogenations illustrated in Figure 8.9. The catalysts

$CuPt_{0.75}$/SBA-15 and $CuPt_{0.5}$/SBA-15 yielded much higher *ee* values for the hydrogenated (s)-terpinen-4-ol than all other instances. Regrettably, these catalysts did not demonstrate capacity for Et-Py hydrogenations.

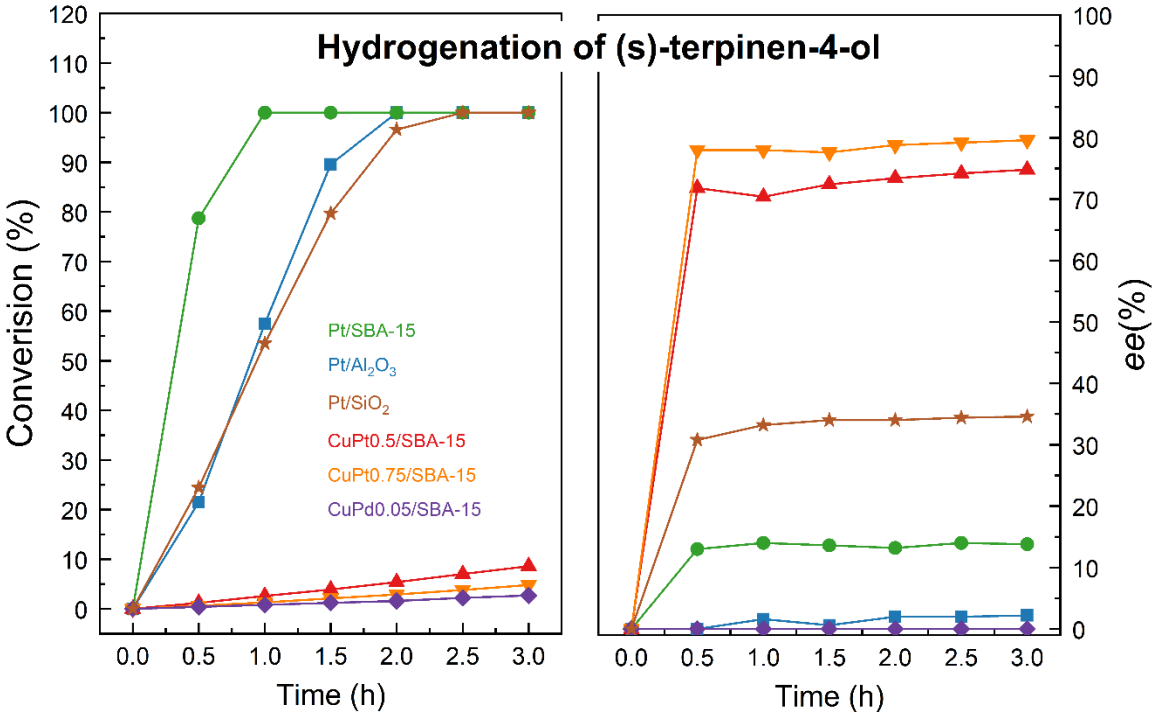

Figure 8.9 Conversion and *ee* values of hydrogenation of (s)-terpinen-4-ol catalyzed by different catalysts.

Further studies were conducted with (r)-terpinen-4-ol, and the influence of the modifier amount was investigated. As depicted in Figure 8.10, there were no discernible differences in conversion or *ee* values with varying quantities of (r)-terpinen-4-ol incorporated into the reactions.

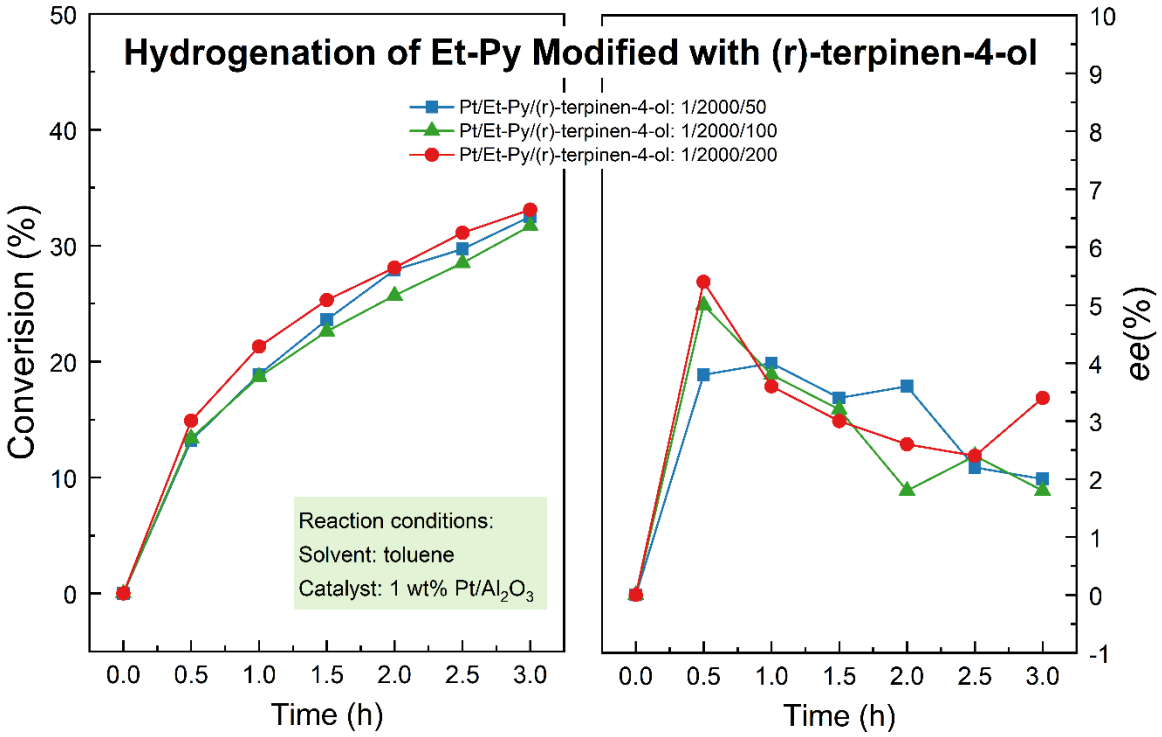

Figure 8.10 Conversion and *ee* values of hydrogenation of Et-Py modified with (r)-terpinen-4-ol catalyzed by Pt/Al_2O_3 catalysts as a function of (r)-terpinen-4-ol amount.

8.4 Summary

This chapter focuses on the exploration of terpinen-4-ol molecules, which, as per the existing literature, have demonstrated the capacity for directing enantioselectivity. However, *in-situ* ATR-IR characterizations have not suggested that terpinen-4-ol in CCl_4 or toluene solutions readily bonds to metal surfaces. A range of catalysts, encompassing those based on Pt, Cu, and mixed Cu-Pt or Cu-Pd, were examined, but regrettably, no tangible evidence of adsorption was discerned.

The behavior of terpinen-4-ol in ethyl pyruvate (Et-Py) hydrogenations proved to be more intricate, primarily because terpinen-4-ol also undergoes hydrogenation during

the reaction process. Cu-based catalysts failed to exhibit proficiency in Et-Py hydrogenations but showed a moderate capacity for terpinen-4-ol hydrogenation. The enantiomeric excess (*ee*) values of the hydrogenated terpinen-4-ol were notably high. In contrast, Pt-supported catalysts, while showcasing impressive catalytic activity, rendered relatively low *ee* values.

Chapter 9

Conclusion and Prospective Directions for Future

9.1 Conclusion

The characterization of adsorption and reactivity with NEA molecules, along with quantum mechanics calculations, revealed that NEA molecules become protonated on the surface under specific reaction conditions. These conditions involve the presence of a solvent and the introduction of hydrogen into the mixture. This accounts for several previously unexplained observations, including the distinctive nature of the IR spectra for these adsorbed species when compared to unbound modifiers.

The *in-situ* ATR-IR adsorption studies using various modifiers, as depicted in Figure 9.1, conclude that the naphthyl ring and amine group are essential prerequisites for adsorption on Pt surfaces from liquid solutions.

The left panel of Figure 9.1 shows no evidence of adsorption in either polar or non-polar solvents. In contrast, the right panel indicates that certain molecules bind to Pt surfaces in CCl_4 solutions, with the exceptions being 1-NEA and 2-NEA, which exhibit signs of adsorption in toluene.

There was no observable adsorption of any molecules containing a hydroxyl group, with the exception of amino acids 1-NLA and 2-NLA. This behavior could be attributed to strong molecular interactions, particularly hydrogen bonding among

molecules containing an alcohol group. These molecules exhibit a preference for dissolving in solutions rather than adsorbing onto Pt surfaces.

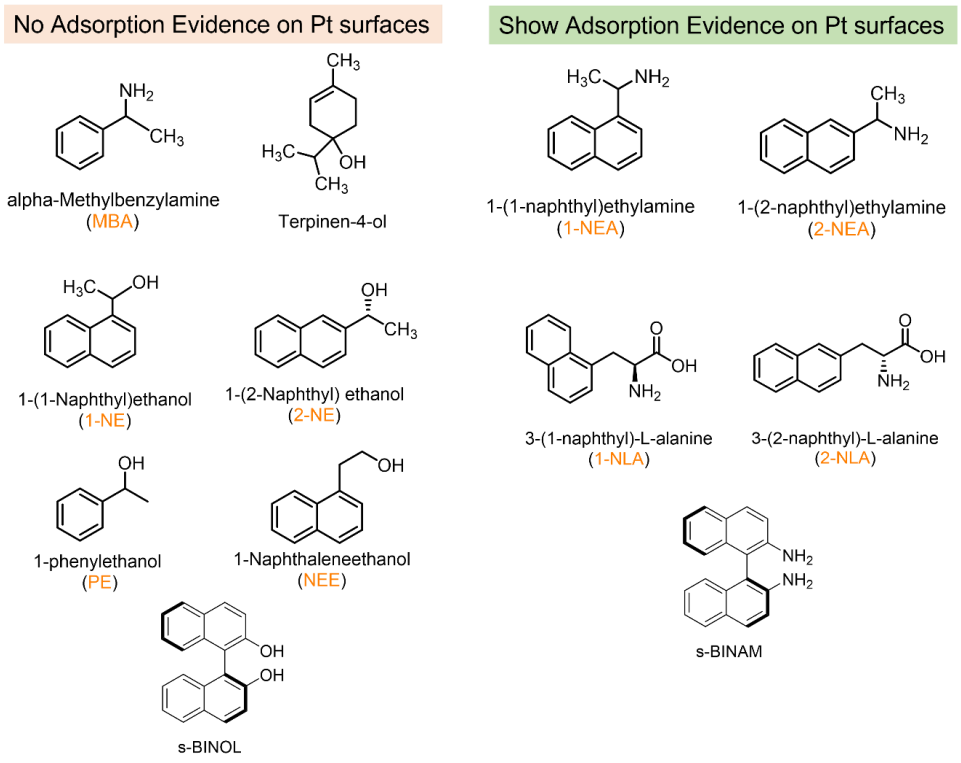

Figure 9.1 Molecules have been studied in this paper.

In kinetic measurements, the commercial Pt/Al_2O_3 catalyst demonstrated superior catalytic performance in comparison to the commercial Pt/SiO_2 catalyst, absent a chiral modifier. This disparity is not exclusively attributable to the intrinsic properties of the support. The unidentified organic molecules, detected on the surface of commercial Pt/SiO_2 catalysts via transmission IR, might be responsible for its inferior catalytic activity. While the modification of Pt catalysts with silylation agents resulted in less activity, it did not offer a substantial improvement in enantioselectivity as predicted.

Although the chiral NEA molecules did not achieve enantioselectivity on par with traditional cinchona alkaloids, their simpler structure is noteworthy. Moreover, the reaction conditions have been optimized. The chiral 1-NE or 2-NE did not exhibit any enantioselectivity, thereby supporting the hypothesis that the addition of chiral modifiers may co-adsorb with reactants on Pt surfaces to enhance enantioselectivity.

The kinetic behavior associated with terpinen-4-ol was more intricate due to its hydrogenation during the Et-Py hydrogenation process. No evident enantiomeric excess of hydrogenated Et-Py was observed when modified with terpinen-4-ol. However, the enantioselectivity of hydrogenated terpinen-4-ol catalyzed with Cu supported SBA-15 catalysts was noteworthy.

The kinetic data of amino acids, 1-NLA or 2-NDA, suggested a significant role of the solvent in the reactions. Surprisingly, both s-BINAM and s-BINOL demonstrated comparable catalytic performance in terms of activity and enantioselectivity, despite the absence of adsorption evidence for s-BINOL on Pt surfaces. This suggests that chiral biaryl compounds might facilitate enantioselectivity differently from cinchona alkaloids and NEA modifiers.

9.2 Prospective Directions

Further research should aim to design a novel IR cell anticipated to facilitate continuous flow for *operando* studies as depicted in Figure 9.2. This advancement is premised on the capability of executing simultaneous IR characterization of adsorbed species and kinetic measurements. One key challenge lies in distinguishing the adsorbed

chiral modifiers from the adsorbed reactants and the solvent. Therefore, an in-depth understanding of the competitive adsorption between the chiral modifiers and reactants becomes imperative. Some preliminary experiments have been undertaken to examine the competitive adsorption between 1-NEA and Et-Py.

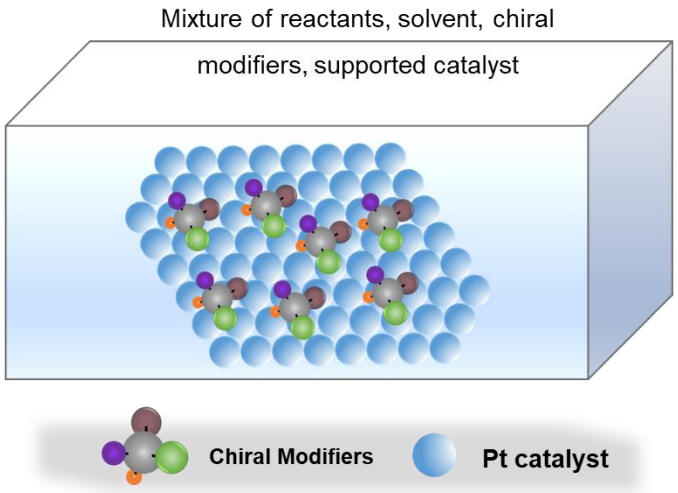

Figure 9.2 Illustration of *operando* study in the presence of all reactants in realistic environments.

In order to elucidate the competitive adsorption between 1-NEA and Et-Py on Pt surfaces, two distinctive types of experiments were conducted. The first experiment entailed saturating the Pt surfaces with s-1-NEA initially, followed by the addition of Et-Py. As depicted in Figure 9.3, the experiment commenced with a 1 mM s-1-NEA (3.4 μL in 20 mL CCl_4 solution) in the presence of a 10 mg Pt/Al_2O_3 catalyst. The spectrum collected after 90 minutes distinctly showed the adsorption of s-1-NEA on Pt surfaces. Upon adding 34 μL of Et-Py to the mixture, which was followed by two further additions of 34 μL fresh Et-Py, the collected spectra exhibited conspicuous peaks around 1730,

1300 and 1140 cm^{-1}. These peaks were attributed to Et-Py molecules, as indicated by a comparison with the ATR-IR spectrum of pure Et-Py without the catalyst. The ATR-IR cell was subsequently flushed with pure CCl_4, which almost entirely removed the peaks from Et-Py. This demonstrated that Et-Py would not bind to Pt surfaces in CCl_4 solutions, thereby not influencing the adsorbed s-1-NEA species on the Pt catalysts.

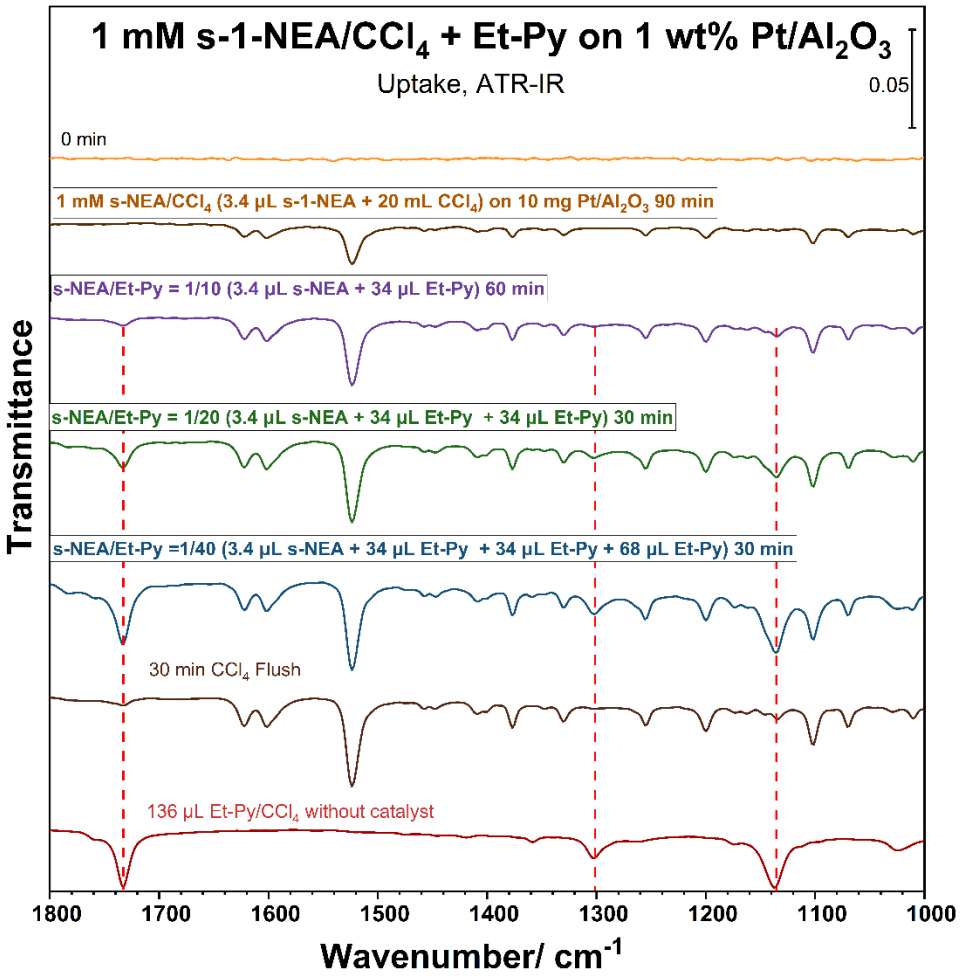

Figure 9.3 ATR-IR spectra of 1 mM s-1-NEA and Et-Py in CCl_4 adsorption on Pt/Al_2O_3 catalyst. The test started with the adsorption test of 1 mM s-NEA in CCl_4, then with addition of different amounts of Et-Py to the mixture, finally the ATR-IR was flushed with pure CCl_4. The bottom one is the spectrum of pure Et-Py in CCl_4 without catalyst.

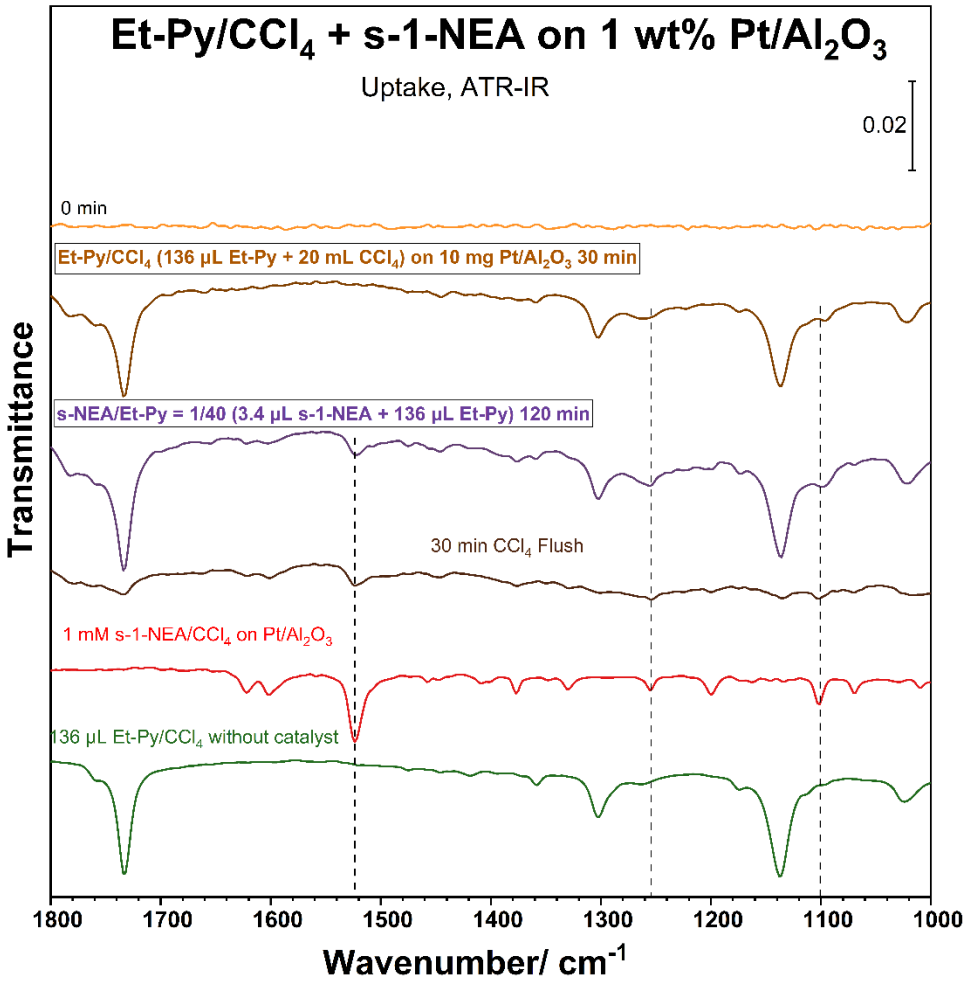

Figure 9.4 ATR-IR of 1 mM s-1-NEA and Et-Py in CCl_4 adsorption on Pt/Al_2O_3 catalyst. The test started with the adsorption test of Et-Py in CCl_4, then added s-NEA to the mixture, finally the ATR-IR was flushed with pure CCl_4. The second trace from the bottom is the spectrum of 1 mM s-1-NEA in CCl_4 adsorption on 10 mg Pt/Al_2O_3 catalyst, while the bottom one is the spectrum of pure Et-Py in CCl_4 without catalyst. Both are added for reference.

The alternative experiment commenced with an Et-Py (136 µL) in a 20 mL CCl_4 solution without a catalyst. The observation of three new peaks around 1140, 1300 and 1730 cm^{-1}, as shown in Figure 9.4, confirmed the presence of free Et-Py molecules in the solution. The subsequent addition of an equivalent amount of s-1-NEA (3.4 µL) to the

mixture did not yield any significant adsorbed s-1-NEA signals, suggesting that the pre-existing Et-Py might inhibit s-1-NEA uptake. After flushing the cell with pure solvent, some weak peaks attributable to adsorbed s-1-NEA molecules were detected. However, the observed spectrum was different from the one recorded in the absence of Et-Py.

A further experiment, which exposed a mixture of s-1-NEA and Et-Py in CCl_4 solution to Pt catalysts simultaneously, yielded results consistent with the second experiment, as demonstrated in Figure 9.5. This implies that Et-Py inhibits s-1-NEA uptake when added either prior to or alongside s-1-NEA. Consequently, an effective method for enhancing the enantioselectivity with chiral 1-NEA molecules may involve pre-conditioning the chiral modifiers in the solution before introducing Et-Py.

In subsequent research, it is critical to invest more effort into characterizing adsorbed species during the hydrogenation process. This is necessary to establish the correlation between adsorption behavior and catalytic performance.

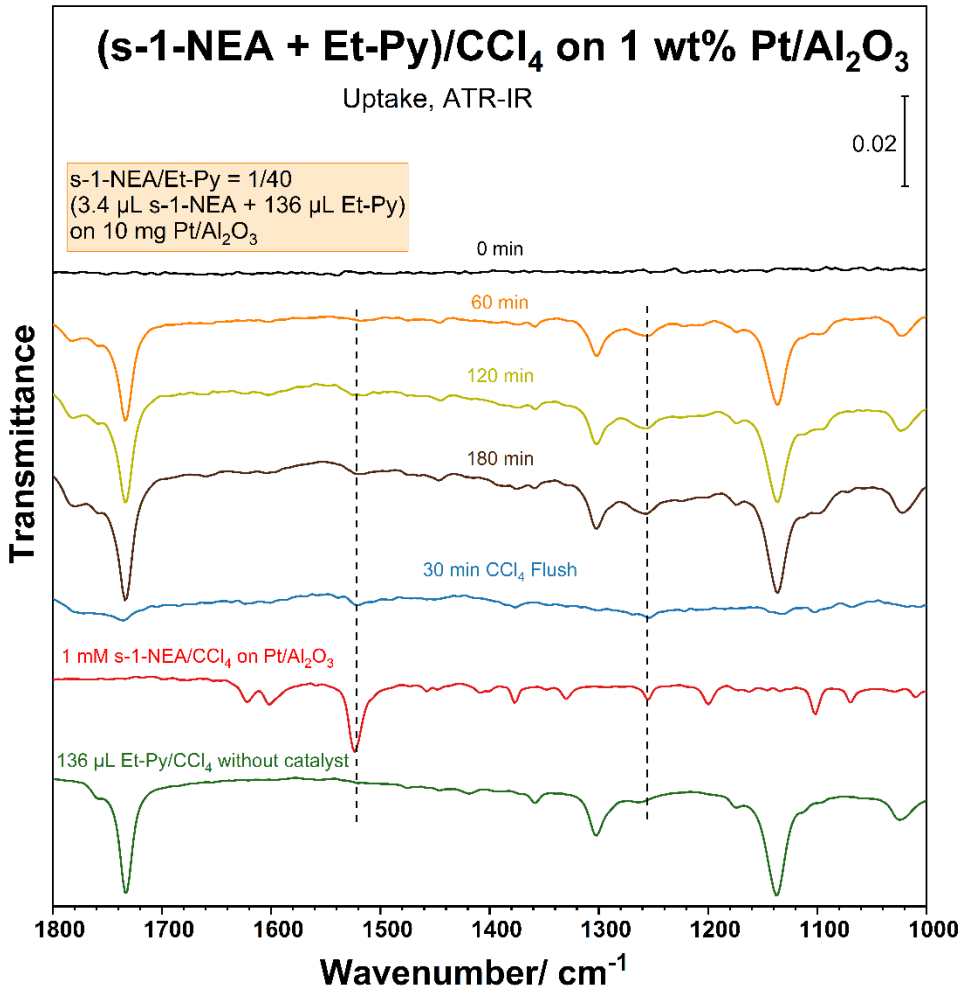

Figure 9.5 ATR-IR spectra of a mixture of 3.4 µL s-1-NEA and 136 µL Et-Py in 20 mL CCl_4 adsorption on Pt/Al_2O_3 catalyst. The second trace from the bottom is the spectrum of 1 mM s-1-NEA in CCl_4 adsorption on 10 mg Pt/Al_2O_3 catalyst, while the bottom one is the spectrum of pure Et-Py in CCl_4 without catalyst. Both are added for reference.

References

1. Barron, L., Symmetry and molecular chirality. *Chemical Society Reviews* **1986,** *15* (2), 189-223.

2. Kelvin, W. T. B., *The molecular tactics of a crystal*. Clarendon Press: **1894**.

3. Flack, H., Louis Pasteur's discovery of molecular chirality and spontaneous resolution in 1848, together with a complete review of his crystallographic and chemical work. *Acta Crystallographica Section A: Foundations of Crystallography* **2009,** *65* (5), 371-389.

4. Kasprzyk-Hordern, B., Pharmacologically active compounds in the environment and their chirality. *Chemical Society Reviews* **2010,** *39* (11), 4466-4503.

5. Moreno Ríos, A. L.; Gutierrez-Suarez, K.; Carmona, Z.; Ramos, C. G.; Silva Oliveira, L. F., Pharmaceuticals as emerging pollutants: Case naproxen an overview. *Chemosphere* **2022,** *291*, 132822.

6. Murakami, H., From Racemates to Single Enantiomers – Chiral Synthetic Drugs over the last20 Years. In *Novel Optical Resolution Technologies*, Sakai, K.; Hirayama, N.; Tamura, R., Eds. Springer Berlin Heidelberg: Berlin, Heidelberg, **2007**; pp 273-299.

7. Lorenz, H.; Seidel-Morgenstern, A., Processes to separate enantiomers. *Angewandte Chemie International Edition* **2014,** *53* (5), 1218-1250.

8. Bernardo-Bermejo, S.; Sanchez-Lopez, E.; Castro-Puyana, M.; Marina, M. L., Chiral capillary electrophoresis. *TrAC Trends in Analytical Chemistry* **2020,** *124*, 115807.

9. Tarafder, A.; Miller, L., Chiral chromatography method screening strategies: Past, present and future. *Journal of Chromatography A* **2021,** *1638*, 461878.

10. Francotte, E., Enantioselective Chromatography: From its Emergence to its Successful Implementation in the Pharmaceutical Environment. *CHIMIA* **2009,** *63* (12), 867.

11. Maier, N. M.; Franco, P.; Lindner, W., Separation of enantiomers: needs, challenges, perspectives. *Journal of Chromatography A* **2001,** *906* (1), 3-33.

12. Wandrey, C.; Liese, A.; Kihumbu, D., Industrial Biocatalysis: Past, Present, and Future. *Organic Process Research & Development* **2000,** *4* (4), 286-290.

13. Bell, E. L.; Finnigan, W.; France, S. P.; Green, A. P.; Hayes, M. A.; Hepworth, L. J.; Lovelock, S. L.; Niikura, H.; Osuna, S.; Romero, E.; Ryan, K. S.; Turner, N. J.; Flitsch, S. L., Biocatalysis. *Nature Reviews Methods Primers* **2021,** *1* (1), 46.

14. Chenault, H. K.; Dahmer, J.; Whitesides, G. M., Kinetic resolution of unnatural and rarely occurring amino acids: enantioselective hydrolysis of N-acyl amino acids catalyzed by acylase I. *Journal of the American Chemical Society* **1989,** *111* (16), 6354-6364.

15. Koeller, K. M.; Wong, C.-H., Enzymes for chemical synthesis. *Nature* **2001,** *409* (6817), 232-240.

16. Johannes G. de Vries, D. C. J. E., Frontmatter. In *The Handbook of Homogeneous Hydrogenation*, **2006**; pp I-XXXII.

17. Wen, J.; Wang, F.; Zhang, X., Asymmetric hydrogenation catalyzed by first-row transition metal complexes. *Chemical Society Reviews* **2021,** *50* (5), 3211-3237.

18. Knowles, W. S., Asymmetric Hydrogenations (Nobel Lecture). *Angewandte Chemie International Edition* **2002,** *41* (12), 1998-2007.

19. Wang, D.-S.; Chen, Q.-A.; Lu, S.-M.; Zhou, Y.-G., Asymmetric hydrogenation of heteroarenes and arenes. *Chemical reviews* **2012,** *112* (4), 2557-2590.

20. Zhao, D.; Glorius, F., Enantioselective hydrogenation of isoquinolines. *Angewandte Chemie International Edition* **2013,** *52* (37), 9616-9618.

21. Weng, Z.; Zaera, F., Increase in Activity and Selectivity in Catalysis via Surface Modification with Self-Assembled Monolayers. *The Journal of Physical Chemistry C* **2014,** *118* (7), 3672-3679.

22. Nakanishi, T.; Yamakawa, N.; Asahi, T.; Osaka, T.; Ohtani, B.; Uosaki, K., Enantioselective Adsorption of Phenylalanine onto Self-Assembled Monolayers of 1,1‘-Binaphthalene-2,2‘-dithiol on Gold. *Journal of the American Chemical Society* **2002,** *124* (5), 740-741.

23. Forster, M.; Dyer, M. S.; Persson, M.; Raval, R., Tailoring Homochirality at Surfaces: Going Beyond Molecular Handedness. *Journal of the American Chemical Society* **2011,** *133* (40), 15992-16000.

24. Barlow, S. M.; Raval, R., Complex organic molecules at metal surfaces: bonding, organisation and chirality. *Surface Science Reports* **2003,** *50* (6), 201-341.

25. Zhang, S.; Zhang, B.; Liang, H.; Liu, Y.; Qiao, Y.; Qin, Y., Encapsulation of Homogeneous Catalysts in Mesoporous Materials Using Diffusion-Limited

Atomic Layer Deposition. *Angewandte Chemie International Edition* **2018,** *57* (4), 1091-1095.

26. Motoyama, Y.; Mitsui, K.; Ishida, T.; Nagashima, H., Self-Encapsulation of Homogeneous Catalyst Species into Polymer Gel Leading to a Facile and Efficient Separation System of Amine Products in the Ru-Catalyzed Reduction of Carboxamides with Polymethylhydrosiloxane (PMHS). *Journal of the American Chemical Society* **2005,** *127* (38), 13150-13151.

27. Hong, J.; Zaera, F., Interference of the Surface of the Solid on the Performance of Tethered Molecular Catalysts. *Journal of the American Chemical Society* **2012,** *134* (31), 13056-13065.

28. Hong, J.; Lee, I.; Zaera, F., Correlated bifunctionality in heterogeneous catalysts: selective tethering of cinchonidine next to supported Pt nanoparticles. *Catalysis Science & Technology* **2015,** *5* (2), 680-689.

29. Caplan, N. A.; Hancock, F. E.; Bulman Page, P. C.; Hutchings, G. J., Heterogeneous Enantioselective Catalyzed Carbonyl- and Imino-Ene Reactions using Copper Bis(Oxazoline) Zeolite Y. *Angewandte Chemie International Edition* **2004,** *43* (13), 1685-1688.

30. Zaera, F., Surface chemistry at the liquid/solid interface. *Surface Science* **2011,** *605* (13), 1141-1145.

31. Zaera, F., Probing Liquid/Solid Interfaces at the Molecular Level. *Chemical Reviews* **2012,** *112* (5), 2920-2986.

32. Zaera, F., New advances in the use of infrared absorption spectroscopy for the characterization of heterogeneous catalytic reactions. *Chemical Society Reviews* **2014,** *43* (22), 7624-7663.

33. Ni, Y.; Gordon, A. D.; Tanicala, F.; Zaera, F., Correlation between chiral modifier adsorption and enantioselectivity in hydrogenation catalysis. *Angewandte Chemie* **2017,** *129* (27), 8071-8074.

34. Gordon, A. D.; Zaera, F., Adsorption of 1-(1-Naphthyl) ethylamine from Solution onto Platinum Surfaces: Implications for the Chiral Modification of Heterogeneous Catalysts. *Angewandte Chemie International Edition* **2013,** *12* (52), 3453-3456.

35. Osawa, T.; Harada, T.; Tai, A., Enantio-differentiating Hydrogenation of 2-Alkanones over asymmetrically modified nickel catalyst and its application to the preparation of optically pure 2-alkanols. *Journal of Catalysis* **1990,** *121* (1), 7-17.

36. Osawa, T.; Sakai, S.; Deguchi, K.; Harada, T.; Takayasu, O., High durability of asymmetrically modified nickel catalysts prepared by in situ modification. *Journal of Molecular Catalysis A: Chemical* **2002,** *185* (1), 65-69.

37. LeBlond, C.; Wang, J.; Andrews, A. T.; Sun, Y. K., Establishment and maintenance of an optimal chiral surface in cinchona-modified 1% Pt/Al2O3 for enantioselective hydrogenation of α-keto esters. *Topics in Catalysis* **2000,** *13* (3), 169-174.

38. Blaser, H.-U.; Studer, M., Cinchona-Modified Platinum Catalysts: From Ligand Acceleration to Technical Processes. *Accounts of Chemical Research* **2007,** *40* (12), 1348-1356.

39. Blaser, H. U.; Jalett, H. P.; Lottenbach, W.; Studer, M., Heterogeneous Enantioselective Hydrogenation of Ethyl Pyruvate Catalyzed by Cinchona-Modified Pt Catalysts: Effect of Modifier Structure. *Journal of the American Chemical Society* **2000,** *122* (51), 12675-12682.

40. Ni, Y.; Gordon, A. D.; Tanicala, F.; Zaera, F., Correlation between Chiral Modifier Adsorption and Enantioselectivity in Hydrogenation Catalysis. *Angewandte Chemie International Edition* **2017,** *56* (27), 7963-7966.

41. Andanson, J.-M.; Baiker, A., Exploring catalytic solid/liquid interfaces by in situ attenuated total reflection infrared spectroscopy. *Chemical Society Reviews* **2010,** *39* (12), 4571-4584.

42. Kubota, J.; Ma, Z.; Zaera, F., In situ characterization of adsorbates in solid− liquid interfaces by reflection− absorption infrared spectroscopy. *Langmuir* **2003,** *19* (8), 3371-3376.

43. Zhang, J.; Zhao, B.; Liang, W.; Zhou, G.; Liang, Z.; Wang, Y.; Qu, J.; Sun, Y.; Jiang, L., Three-Phase Electrolysis by Gold Nanoparticle on Hydrophobic Interface for Enhanced Electrochemical Nitrogen Reduction Reaction. *Advanced Science* **2020,** *7* (22), 2002630.

44. Hutter, E.; Fendler, J. H., Exploitation of Localized Surface Plasmon Resonance. *Advanced Materials* **2004,** *16* (19), 1685-1706.

45. Mujahid, A.; Afzal, A.; Dickert, F. L., An Overview of High Frequency Acoustic Sensors—QCMs, SAWs and FBARs—Chemical and Biochemical Applications. *Sensors* **2019,** *19* (20), 4395.

46. Song, W.; Guo, X.; Sun, W.; Yin, W.; He, P.; Yang, X.; Zhang, X., Target-triggering multiple-cycle signal amplification strategy for ultrasensitive detection of DNA based on QCM and SPR. *Analytical Biochemistry* **2018,** *553*, 57-61.

47. Sedigh Rahimabadi, P.; Khodaei, M.; Koswattage, K. R., Review on applications of synchrotron-based X-ray techniques in materials characterization. *X-Ray Spectrometry* **2020,** *49* (3), 348-373.

48. Tahara, K.; Okuhata, S.; Adisoejoso, J.; Lei, S.; Fujita, T.; Feyter, S. D.; Tobe, Y., 2D networks of rhombic-shaped fused dehydrobenzo [12] annulenes: structural variations under concentration control. *Journal of the American Chemical Society* **2009,** *131* (48), 17583-17590.

49. Lei, S.; Tahara, K.; De Schryver, F. C.; Van der Auweraer, M.; Tobe, Y.; De Feyter, S., One building block, two different supramolecular surface-confined patterns: concentration in control at the solid–liquid interface. *Angewandte Chemie* **2008,** *120* (16), 3006-3010.

50. Vayner, G.; Houk, K.; Sun, Y.-K., Origins of enantioselectivity in reductions of ketones on cinchona alkaloid modified platinum. *Journal of the American Chemical Society* **2004,** *126* (1), 199-203.

51. Demers-Carpentier, V.; Goubert, G.; Masini, F.; Lafleur-Lambert, R.; Dong, Y.; Lavoie, S.; Mahieu, G.; Boukouvalas, J.; Gao, H.; Rasmussen, A. M., Direct observation of molecular preorganization for chirality transfer on a catalyst surface. *Science* **2011,** *334* (6057), 776-780.

52. Meemken, F.; Steiger, T.; Holland, M. C.; Gilmour, R.; Hungerbühler, K.; Baiker, A., Adsorption and stability of chiral modifiers based on 1-(1-naphthyl)-ethylamine for Pt catalysed heterogeneous asymmetric hydrogenations. *Catalysis Science & Technology* **2015,** *5* (2), 705-715.

53. Bhambhani, M.; Cutting, P.; Sing, K.; Turk, D., Analysis of nitrogen adsorption isotherms on porous and nonporous silicas by the BET and αs methods. *Journal of Colloid and Interface Science* **1972,** *38* (1), 109-117.

54. Sing, K. S. W., Reporting physisorption data for gas/solid systems with special reference to the determination of surface area and porosity (Recommendations 1984). *Pure and Applied Chemistry* **1985,** *57* (4), 603-619.

55. Wang, Z.; Fernández-Escamilla, H. N.; Guerrero-Sánchez, J.; Takeuchi, N.; Zaera, F., Adsorption and Reactivity of Chiral Modifiers in Heterogeneous Catalysis: 1-(1-Naphthyl)ethylamine on Pt Surfaces. *ACS Catalysis* **2022,** *12* (17), 10514-10521.

56. Schwalm, O.; Minder, B.; Weber, J.; Baiker, A., Enantioselective hydrogenation of α-ketoesters over Pt/alumina modified with cinchonidine: theoretical investigation of the substrate-modifier interaction. *Catalysis letters* **1994,** *23*, 271-279.

57. Baiker, A., Progress in asymmetric heterogeneous catalysis: Design of novel chirally modified platinum metal catalysts. *Journal of Molecular Catalysis A: Chemical* **1997,** *115* (3), 473-493.

58. Diezi, S.; Mallat, T.; Szabo, A.; Baiker, A., Fine tuning the "chiral sites" on solid enantioselective catalysts. *Journal of Catalysis* **2004,** *228* (1), 162-173.

59. Baiker, A., Crucial aspects in the design of chirally modified noble metal catalysts for asymmetric hydrogenation of activated ketones. *Chemical Society Reviews* **2015,** *44* (21), 7449-7464.

60. Zaera, F., Designing Sites in Heterogeneous Catalysis: Are We Reaching Selectivities Competitive With Those of Homogeneous Catalysts? *Chemical Reviews* **2022,** *122* (9), 8594-8757.

61. Kozlov, A. N.-E. S. M.; Viñes, F.; Illas, F., Electronic-structure-based chemical descriptors:(in) dependence on self-interaction and Hartree-Fock exchange. *Phys. Rev. B* **1996,** *54*, 11169-11186.

62. Blöchl, P. E., Projector augmented-wave method. *Physical review B* **1994,** *50* (24), 17953.

63. Perdew, J. P.; Burke, K.; Ernzerhof, M., Generalized gradient approximation made simple. *Physical review letters* **1996,** *77* (18), 3865.

64. Grimme, S.; Antony, J.; Ehrlich, S.; Krieg, H., A consistent and accurate ab initio parametrization of density functional dispersion correction (DFT-D) for the 94 elements H-Pu. *The Journal of chemical physics* **2010,** *132* (15), 154104.

65. Baroni, S.; De Gironcoli, S.; Dal Corso, A.; Giannozzi, P., Phonons and related crystal properties from density-functional perturbation theory. *Reviews of modern Physics* **2001,** *73* (2), 515.

66. Alecu, I.; Zheng, J.; Zhao, Y.; Truhlar, D. G., Computational thermochemistry: scale factor databases and scale factors for vibrational frequencies obtained from electronic model chemistries. *Journal of chemical theory and computation* **2010,** *6* (9), 2872-2887.

67. Laury, M. L.; Carlson, M. J.; Wilson, A. K., Vibrational frequency scale factors for density functional theory and the polarization consistent basis sets. *Journal of computational chemistry* **2012,** *33* (30), 2380-2387.

68. Kesharwani, M. K.; Brauer, B.; Martin, J. M., Frequency and zero-point vibrational energy scale factors for double-hybrid density functionals (and other

selected methods): can anharmonic force fields be avoided? *The Journal of Physical Chemistry A* **2015,** *119* (9), 1701-1714.

69. Henkelman, G.; Uberuaga, B. P.; Jónsson, H., A climbing image nudged elastic band method for finding saddle points and minimum energy paths. *The Journal of chemical physics* **2000,** *113* (22), 9901-9904.

70. Henkelman, G.; Jónsson, H., Improved tangent estimate in the nudged elastic band method for finding minimum energy paths and saddle points. *The Journal of chemical physics* **2000,** *113* (22), 9978-9985.

71. Goubert, G.; Rasmussen, A. M.; Dong, Y.; Groves, M. N.; McBreen, P. H.; Hammer, B., Walking-like diffusion of two-footed asymmetric aromatic adsorbates on Pt (111). *Surface science* **2014,** *629*, 123-131.

72. Ma, Z.; Kubota, J.; Zaera, F., The influence of dissolved gases on the adsorption of cinchonidine from solution onto Pt surfaces: an in situ infrared study. *Journal of Catalysis* **2003,** *219* (2), 404-416.

73. LeBlanc, R. J.; Chu, W.; Williams, C. T., Surface Raman characterization of cinchonidine-modified platinum in ethanol: effects of liquid-phase concentration and co-adsorbed hydrogen. *Journal of Molecular Catalysis A: Chemical* **2004,** *212* (1), 277-289.

74. Motobayashi, K.; Tomioka, R.; Uchida, T.; Osawa, M., Effect of Hydrogen on the Orientation of Cinchonidine Adsorbed on Platinum: An ATR-SEIRAS Study. *Chemistry Letters* **2015,** *44* (6), 770-772.

75. Ni, Y.; Wang, Z.; Lee, I.; Zaera, F., Adsorption of chiral modifiers from solution onto supported platinum catalysts: The effect of the solvent, other coadsorbates, and the support. *The Journal of Physical Chemistry C* **2020,** *124* (14), 7903-7913.

76. Gordon, A. D.; Karakalos, S.; Zaera, F., Dependence of the adsorption of chiral compounds on their enantiomeric composition. *Surface Science* **2014,** *629*, 3-10.

77. Ma, Z.; Lee, I.; Zaera, F., Factors controlling adsorption equilibria from solution onto solid surfaces: the uptake of cinchona alkaloids on platinum surfaces. *Journal of the American Chemical Society* **2007,** *129* (51), 16083-16090.

78. Zaera, F., Infrared absorption spectroscopy characterization of liquid–solid interfaces: The case of chiral modification of catalysts. *Surface Science* **2018,** *669*, 16-24.

79. Attia, S.; Spadafora, E. J.; Schmidt, M. C.; Schröder, C.; Baumann, A.-K.; Schauermann, S., Adsorption geometry and self-assembling of chiral modifier

(R)-(+)-1-(1-naphthylethylamine) on Pt (111). *Physical Chemistry Chemical Physics* **2020,** *22* (27), 15696-15706.

80. Lee, I.; Ma, Z.; Kaneko, S.; Zaera, F., 1-(1-Naphthyl) ethylamine adsorption on platinum surfaces: On the mechanism of chiral modification in catalysis. *Journal of the American Chemical Society* **2008,** *130* (44), 14597-14604.

81. LeBlanc, R. J.; Chu, W.; Williams, C. T., Surface Raman characterization of cinchonidine-modified platinum in ethanol: effects of liquid-phase concentration and co-adsorbed hydrogen. *Journal of Molecular Catalysis A: Chemical* **2004,** *212* (1-2), 277-289.

82. Blaser, H.; Jalett, H.; Wiehl, J., Enantioselective hydrogenation of α-ketoesters with cinchona-modified platinum catalysts: Effect of acidic and basic solvents and additives. *Journal of molecular catalysis* **1991,** *68* (2), 215-222.

83. Socrates, G., Infrared characteristic group frequencies, Tables and charts. *Journal of the American Chemical Society* **1995,** *117* (5), 1671-1671.

84. Vargas, A.; Ferri, D.; Baiker, A., DFT and ATR-IR insight into the conformational flexibility of cinchonidine adsorbed on platinum: Proton exchange with metal. *Journal of Catalysis* **2005,** *236* (1), 1-8.

85. Olsen, R. A.; Borchardt, D.; Mink, L.; Agarwal, A.; Mueller, L. J.; Zaera, F., Effect of Protonation on the Conformation of Cinchonidine. *Journal of the American Chemical Society* **2006,** *128* (49), 15594-15595.

86. Meemken, F.; Baiker, A., Recent Progress in Heterogeneous Asymmetric Hydrogenation of C═O and C═C Bonds on Supported Noble Metal Catalysts. *Chemical Reviews* **2017,** *117* (17), 11522-11569.

87. Makitra, R. G., Reichardt, C., Solvents and Solvent Effects in Organic Chemistry, Weinheim: Wiley-VCH, 2003, 630 p. *Russian Journal of General Chemistry* **2005,** *75* (4), 664-664.

88. Ma, Z.; Zaera, F., Role of the Solvent in the Adsorption−Desorption Equilibrium of Cinchona Alkaloids between Solution and a Platinum Surface: Correlations among Solvent Polarity, Cinchona Solubility, and Catalytic Performance. *The Journal of Physical Chemistry B* **2005,** *109* (1), 406-414.

89. Tamura, M.; Hayashigami, N.; Nakayama, A.; Nakagawa, Y.; Tomishige, K., Heterogeneous Enantioselective Hydrogenation of Ketones by 2-Amino-2′-hydroxy-1,1′-binaphthyl-Modified CeO2-Supported Ir Nanoclusters. *ACS Catalysis* **2022,** *12* (2), 868-876.

90. Wang, Y.-B.; Tan, B., Construction of Axially Chiral Compounds via Asymmetric Organocatalysis. *Accounts of Chemical Research* **2018,** *51* (2), 534-547.

91. Shumski, A. J.; Swann, W. A.; Escorcia, N. J.; Li, C. W., Heterogeneous Hydroxyl-Directed Hydrogenation: Control of Diastereoselectivity through Bimetallic Surface Composition. *ACS Catalysis* **2021,** *11* (10), 6128-6134.

92. Morello, G. R.; Zhong, H.; Chirik, P. J.; Hopmann, K. H., Cobalt-catalysed alkene hydrogenation: a metallacycle can explain the hydroxyl activating effect and the diastereoselectivity. *Chemical Science* **2018,** *9* (22), 4977-4982.

93. Friedfeld, M. R.; Margulieux, G. W.; Schaefer, B. A.; Chirik, P. J., Bis(phosphine)cobalt Dialkyl Complexes for Directed Catalytic Alkene Hydrogenation. *Journal of the American Chemical Society* **2014,** *136* (38), 13178-13181.